The Pennsylvania State University

The Graduate School

College of Engineering

ADVANCED HYBRID ROCKET MOTOR PROPULSION UNIT FOR CUBESATS

A Thesis in

Mechanical Engineering

by

Brendan R. McKnight

Submitted in Partial Fulfillment
of the Requirements
for the Degree of

Master of Science

August 2015

The thesis of Brendan R. McKnight was reviewed and approved* by the following:

Richard A. Yetter
Professor of Mechanical Engineering
Thesis Advisor

Jacqueline O'Connor
Assistant Professor of Mechanical Engineering

Karen A. Thole
Professor of Mechanical Engineering
Department Head of Mechanical and Nuclear Engineering

*Signatures are on file in the Graduate School.

ABSTRACT

CubeSats continue to become popular for universities and businesses to affordably conduct research in low Earth orbit. Falling within the nanosatellite category, CubeSats typically consist of a 1U, 1.5U, 2U, or 3U standard configuration. A 1U CubeSat is a 10 cm x 10 cm x 10 cm cube, while 1.5U, 2U, and 3U CubeSats consist of stacked U(s) with a 10 cm x 10 cm square footprint. More recently, 6U CubeSats have been developed in both 6U x 1U and 3U x 2U configurations. Larger CubeSats will continue to be developed as dispenser systems become larger to accommodate the satellites during launch and deployment. To date, CubeSats have been limited by the orbit into which they are deployed, either as an auxiliary payload on a rocket carrying a primary payload to its required orbit or from the International Space Station. With the development of a safe and reliable propulsion system, CubeSats will be capable of performing orbital control maneuvers, such as orbit raising to extend the lifespan of the satellite and provide onboard instruments with additional data collection time. The propulsion unit in the current work was developed in collaboration with The Aerospace Corporation to provide a 6U CubeSat with this ability. The 1U propulsion unit consists of an additively manufactured carbon-filled polyamide structure and integrated nitrous oxide tank with a cartridge-loaded, 3D-printed solid fuel grain of ABS or paraffin/acrylic composition and performance enhancing geometry. Strength testing of the structure material characterized its properties as-received and after exposure to nitrous oxide. A significant plasticizing effect was observed for the material exposed to nitrous oxide. Ultimate tensile strength decreased by over 20% and modulus of elasticity decreased by over 40%, while elongation to break was increased. For this reason, future work will investigate an additively manufactured metal propulsion unit of similar design. Hot-fire testing of various solid fuel grain compositions and geometries was conducted at the

Pennsylvania State University's High Pressure Combustion Laboratory using the Long-Grain Center-Perforated hybrid rocket motor with nitrous oxide. The results of the test series revealed interesting behavior for the additively manufactured paraffin, paraffin/acrylic, ABS, and Windform XT 2.0 fuel grains. Carbon-filled polyamide, Windform XT 2.0, fuel grains exhibited very slow regression rates, as was expected. ABS fuel grains with star-swirl port geometry were found to have increased regression rate over straight port ABS fuel grains, similar to what was found from previous oxygen testing of star-swirl geometry acrylic fuel grains. However, interesting to note was an observed increase in regression rate for white and black colored ABS fuel grains over pure ABS. This could be the result of increased radiation absorption with the added pigments, but due to a lack of provided information from the manufacture about the pigments this cannot be directly concluded. Combustion efficiency results show a decrease for star-swirl geometry fuel grains compared to straight port fuel grains for all ABS samples, while star-swirl geometry appeared to increase combustion efficiency for Windform XT 2.0 fuel grains. Increased regression rate was also observed for paraffin/acrylic diaphragm fuel grains over straight port paraffin. Examination of fired paraffin/acrylic 0.050" diaphragm fuel grains showed chipping of the acrylic diaphragms and resulting uneven regression in the downstream paraffin sections. The paraffin/acrylic 0.100" diaphragm fuel grains better maintained uniform regression due to the increased acrylic diaphragm thickness, however, combustion efficiency decreased significantly compared to that of pure paraffin. An iteration on the diaphragm fuel grain design included one 0.100" acrylic diaphragm with an acrylic mixing section downstream of the diaphragm. This particular fuel grain design was shown to increase combustion efficiency over the original paraffin/acrylic diaphragm fuel grain design and pure paraffin fuel grains.

TABLE OF CONTENTS

LIST OF FIGURES

LIST OF TABLES

NOMENCLATURE

a	Fuel Specific Regression Rate Coefficient
A^*	Nozzle Throat Area
A_0	Average Initial Cross-Sectional Area of the Gage Section
A_p	Initial Port Area
ABS	Acrylonitrile Butadiene Styrene
AM	Additive Manufacturing
c*	Characteristic Velocity
c^*_{ideal}	Ideal Characteristic Velocity
Cal Poly SLO	California Polytechnic State University, San Luis Obispo
CAT	CubeSat Ambipolar Thruster
CFD	Computational Fluid Dynamics
COTS	Commercial Off-the-Shelf
CSD	Canisterized Satellite Dispenser
CSLI	CubeSat Launch Initiative
D_c	Characteristic Regressed Distance
D_r	Regressed Distance of Ridges
D_v	Regressed Distance of Valleys
delta V or ΔV	Change in Velocity
DMLS	Direct Metal Laser Sintering
E	Modulus of Elasticity
ϵ_{break}	Tensile Strain at Break

ϵ_{yield}	Tensile Strain at Yield
f_c	Regression Rate Correction Factor for Non-Circular Port Geometry
F_{max}	Maximum Load
FEA	Finite Element Analysis
FDM	Fused Deposition Modeling
FOS	Factor of Safety
G_{ox}	Oxidizer Mass Flux
$\bar{G}_{ox}$	Time Averaged Oxidizer Mass Flux
HAN	Hydroxylammonium Nitrate
HPCL	High Pressure Combustion Laboratory
HTPB	Hydroxyl-terminated Polybutadiene
$I_{sp,vac}$	Vacuum Specific Impulse
iEPS	ion Electrospray Propulsion System
I.D.	Inner Diameter
ISIS	Innovative Solutions in Space
ISS	International Space Station
J-SSOD	Japanese Experiment Module Small Satellite Orbital Deployer
LEO	Low Earth Orbit
LGCP	Long-Grain Center-Perforated Hybrid Rocket Motor
LV	Launch Vehicle
M_f	Final Fuel Grain Mass

$\overline{\dot{m}}_f$	Time Averaged Fuel Mass Flow Rate
M_i	Initial Fuel Grain Mass
$\overline{\dot{m}}_{ox}$	Time Averaged Oxidizer Mass Flow Rate
MDP	Maximum Design Pressure
MEOP	Maximum Expected Operating Pressure
n	Fuel Specific Regression Rate Power Law Exponent
η_{c^*}	c* Combustion Efficiency
NASA CEA2	NASA Chemical Equilibrium with Applications Version 2
NLAS	Nanosatellite Launch Adapter System
NRCSD	NanoRacks CubeSat Deployer
O.D.	Outer Diameter
O/F Ratio	Oxidizer to Fuel Ratio
$\overline{P}_c$	Time Averaged Chamber Pressure
PMMA	Poly-methyl Methacrylate
P-POD	Poly-Picosatellite Orbital Deployer
PSU	Pennsylvania State University
PUC	Propulsion Unit for CubeSats
$\dot{r}$	Regression Rate
$\bar{\dot{r}}$	Time Averaged Regression Rate
r_f	Final Port Radius
r_i	Initial Port Radius
σ_{UTS}	Ultimate Tensile Strength

SLS	Space Launch System
SLS	Selective Laser Sintering
SP	Straight Port
SPUG	Secondary Payload User's Guide
SSDL	Stanford University's Space Systems Development Laboratory
ST-SW	Star-Swirl Port
t_b	Burn Duration
tpi	Turn Per Inch
UTS	Ultimate Tensile Strength
wt%	Percentage by Weight

ACKNOWLEDGEMENTS

I would first like to thank my thesis advisor, Dr. Richard Yetter, for his continued support and guidance during this research program. In addition, I would like to thank Dr. Eric Boyer for his role as a mentor and for providing extensive technical knowledge that made completing this work possible. Additional thanks to Dr. Andrew Cortopassi for his work on the propulsion unit design and finite element analysis and for his assistance with the oxidizer tank and structure material strength testing aspect of this program.

I would like to thank graduate student Paige Nardozzo and undergraduate student Skylar Schirtzinger for their assistance in conducting hybrid rocket motor tests for this work. I would also like to thank Paige for her work in optimizing the propulsion unit design and Skylar for his assistance in conducting strength testing of the propulsion unit oxidizer tank and structure material.

Special thanks to Dr. John DeSain, Dr. Brian Brady, Dr. Andrea Hsu-Schouten, Mr. Jerry Fuller, and Dr. Thomas Curtiss of The Aerospace Corporation for their work on the propulsion unit design and for supplying the printed unit and solid fuel grains tested in this work. I would also like to thank them for their support and guidance throughout the duration of the program.

This work was performed under NASA Contract NNJ11HB94C; prime contract to The Aerospace Corporation with subcontract to the Pennsylvania State University. I would like to thank Mr. George Story of NASA-MSFC for serving as the technical monitor on this work.

CHAPTER 1. Introduction

1.1 Background

1.1.1 The CubeSat Standard

In recent years, CubeSats have become widely popular for relatively inexpensive experimentation in low Earth orbit (LEO). The idea for a standard picosatellite design was originally developed by Prof. Jordi Puig-Suari of the California Polytechnic State University, San Luis Obispo (Cal Poly SLO) and Prof. Bob Twiggs at Stanford University's Space Systems Development Laboratory (SSDL).[1] The concept focused on creating a standard that would reduce the cost and development time normally associated with satellite design and increase accessibility to space.[2] With standard size and mass constraints, anyone with the ability to design and build a CubeSat meeting the requirements can be considered for launch, without specialized considerations typically needed for individual satellite shapes, sizes, and masses. This idea has since become an international reality with the CubeSat Project now consisting of over 100 universities, high schools, and private firms.[1]

The detailed requirements for standard CubeSat configurations are given in the CubeSat Design Specification Rev. 13 report from Cal Poly SLO's CubeSat Program.[1] The report defines a 1U CubeSat as a 10 cm x 10 cm x 10 cm cube, with a mass no more than 1.33 kg. Subsequent configurations of 1.5U, 2U, and 3U satellites consist of stacked U(s) with a 10 cm x 10 cm square footprint and are given mass requirements of 2.00 kg, 2.66 kg, and 4.00 kg, respectively. Drawings of 1U, 1.5U, 2U, 3U, and 3U+ configurations from the report are provided in Appendix A. A 1U CubeSat falls at the upper end of the picosatellite classification and the lower end for nanosatellites, while larger configuration CubeSats are within the nanosatellite category.[3] For the purpose of consistency, nanosatellite will be used to refer to the size class for CubeSats.

NASA's Small Spacecraft Technology State of the Art 2014 document summarizes the state of small satellites including propulsion, structures, thermal control, communications, and launch and deployment of the satellites.[4] The information presented in this section will touch upon various aspects discussed from this report with a focus on deployment and the current state of propulsion systems applicable to CubeSats. The report serves as a useful reference tool for additional information and details regarding the technology development in these areas.

The NASA CubeSat Launch Initiative (CSLI) makes it possible for CubeSats to be launched into orbit as auxiliary payloads on missions with extra space and mass available. The Poly-Picosatellite Orbital Deployer (P-POD), developed by Cal Poly SLO, is used to eject the CubeSats from the launch vehicle (LV).[5] Six 1U CubeSats and two P-PODs are shown in Figure 1.1. A rendering and view of the inside of the P-POD is given in Figure 1.2. Innovative Solutions in Space (ISIS) has also developed a launch adapter similar to the P-POD, called the ISIPOD, for deploying CubeSats up to 3U with their ISILaunch Services program.[6] Based on the initial design of the ISIPOD, Andrews Space makes a 3U deployment system for ISIS called the EZPOD.[7]

Figure 1.1 Six 1U CubeSats with Two P-PODs[1]

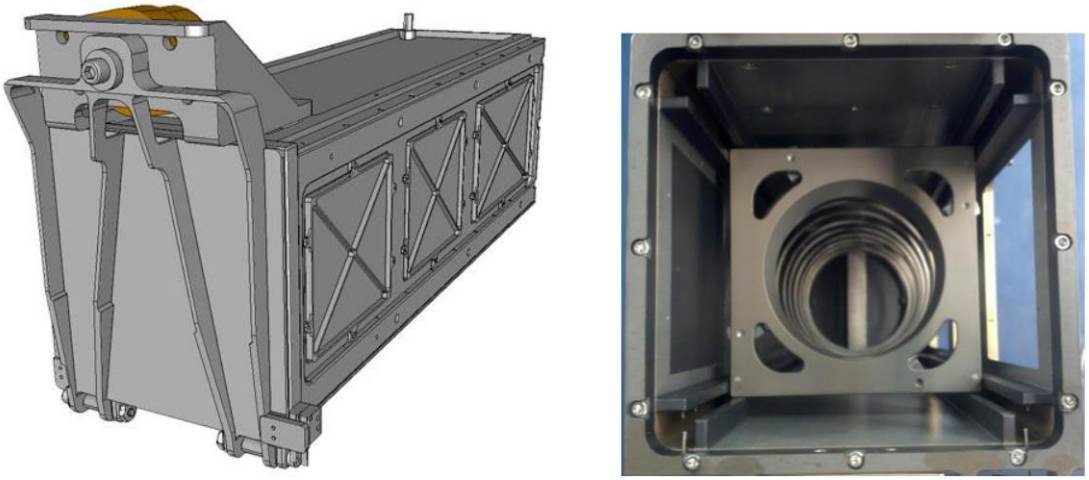

Figure 1.2 P-POD CubeSat Deployment System[1]

The P-POD CubeSat deployment system is spring-loaded and capable of deploying three 1U CubeSats, a combination of 1U, 1.5U, and 2U CubeSats, or a single 3U CubeSat.[8,9] While this system allows for various size configurations, it is limited to a maximum size of 3U. Because of this limitation, NASA Ames Research Center has been working in collaboration with the Operationally Responsive Space office at Kirtland Air Force Base to develop a Nanosatellite Launch Adapter System (NLAS) to allow CubeSats up to 6U (3U x 2U) to be deployed, in addition to those capable by the P-POD system.[10] Planetary Systems Corporation has also developed a 6U capable deployment system called the Canisterized Satellite Dispenser (CSD).[11]

The NLAS consists of an adapter structure and sequencer with CubeSat dispensers, such as the NLAS dispenser or the P-POD. The NLAS was created based on the CubeSat form factor and the first configuration considered was the 6U (3U x 2U). The 6U dispenser is basically two P-PODs joined together, with or without a separating wall down the center, and allows for configurations up to a single 6U CubeSat. The 6U (3U x 2U) CubeSat is deployed as two 3U CubeSats joined together. A 3D rendering of the NLAS mounted on a LV with NLAS and P-

POD dispensers is shown in Figure 1.3. A photograph of the NLAS dispenser is shown in Figure 1.4. The NLAS was first successfully flown on November 19, 2013.[12]

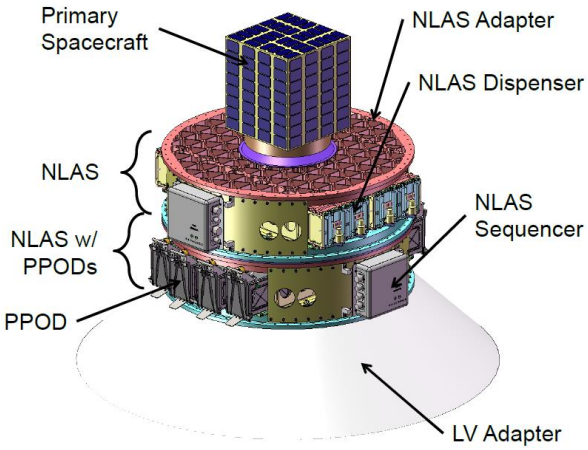

Figure 1.3 3D Rendering of NLAS Configuration for Launching CubeSats[12]

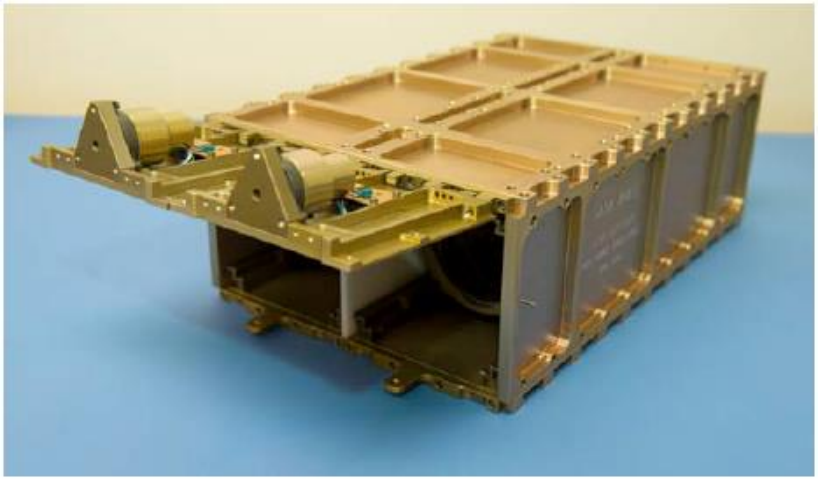

Figure 1.4 Photograph of NLAS CubeSat Dispenser[12]

In addition to being deployed directly from a launch vehicle using a P-POD, EZPOD, NLAS, or CSD, some CubeSats are launched to the International Space Station (ISS) and deployed using the NanoRacks CubeSat Deployer (NRCSD)[13] or the Japanese Experiment Module Small Satellite Orbital Deployer (J-SSOD)[14]. The NRCSD and J-SSOD designs are

similar to that of the P-POD, but the NRCSD system is capable of deploying a 6U (6U x 1U) CubeSat. A rendering of the NRCSD is shown in Figure 1.5. Figure 1.6 is a photograph of the NRCSD, attached to the Japanese robotic arm on the ISS, releasing a set of CubeSats into LEO.

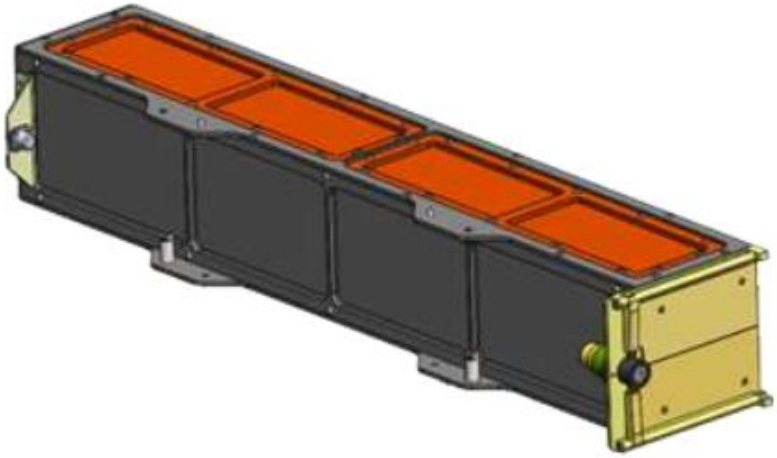

Figure 1.5 3D Rendering of NRCSD[13]

Figure 1.6 CubeSats Released from a NanoRacks Deployer on the ISS[15]

With the creation of a standard CubeSat form factor, the complexity of nanosatellite design and flight has been significantly reduced. The standard eliminates the need for specialized flight requirements for each nanosatellite design and enables the development of various CubeSat dispensers that fit the standard CubeSat sizes. The various dispensers open up the possibility of deploying the nanosatellites directly from a launch vehicle or from the ISS in configurations ranging from 1U to 6U. The NLAS, CSD, and NRCSD enable flying 6U CubeSats (3U x 2U and 6U x 1U, respectively) and expand beyond the original 3U limitation. With the ability to house and deploy 6U CubeSats from launch vehicles and the ISS confirmed, these larger CubeSats can be designed and fabricated for future flight opportunities.

NASA's Space Launch System (SLS) will be capable of carrying secondary payloads in 6U (10 x 20 x 30 cm) and 12U (20 x 20 x 30 cm) deployers according to the SLS Secondary Payload User's Guide (SPUG).[16] The SPUG also provides critical information for designing CubeSats that will meet the size, mass, center of mass, and factor of safety requirements for flight as a secondary payload on the SLS. These guidelines include proof and ultimate factors of safety for designing pressurized fluid systems. In addition, storage and handling conditions that the payload may experience during integration, rollout, and on the launch pad are provided.

1.1.2 CubeSat Propulsion

The growing popularity of CubeSats has resulted in research and development in many new areas of small-scale satellite components. One area of interest is propulsion systems capable of performing attitude and orbital control maneuvers. The NASA Small Spacecraft Technology State of the Art 2014 report is a useful summary of the development of CubeSat propulsion systems.[4] In addition, the thesis work by Liam J. Cheney at Cal Poly SLO summarizes safety standards for CubeSat propulsion systems and is a valuable guide in developing such a unit.[17]

Large satellites have systems capable of completing precise maneuvers to control the orientation and orbit of a satellite. These systems are critical for orienting cameras and instruments and maintaining a stable orbit for successful mission operation. For CubeSats, the nanosatellite form factor limits the implementation of such systems. The strict size and mass constraints present difficulties in designing a propulsion system that can meet the CubeSat requirements and provide adequate performance for the satellite.

CubeSats are often an auxiliary payload and are placed into an orbit during ascent to the primary payload's target orbit, while some may be placed into orbit directly from the ISS. For this reason, CubeSats may be placed into an undesirable orbit and with little or no control over satellite orientation. The ability for a CubeSat to stabilize or raise its orbit creates new opportunities for the small satellite. By imparting a change in velocity on the satellite (delta V), the orbit can be adjusted to increase the duration of data collection and prolong the orbital decay process that will eventually result in reentry to the Earth's atmosphere and end the mission. This is a driving force for innovation in the area of small-scale propulsion systems applicable to the CubeSat standard.

A large number of companies and universities, including Aerojet Rocketdyne, Busek, Clyde Space, The University of Michigan, Massachusetts Institute of Technology, and The Aerospace Corporation, have been involved in developing various types of propulsion systems capable of providing CubeSats with this added ability. A thorough review of propulsion systems for CubeSats was completed in 2010 by Mueller, et al.[18] In this review, currently available and in development propulsion systems of all types from chemical to electric are examined and presented in a concise manner. The area of CubeSat propulsion has drawn research from across the globe. With this in mind, only a select few of these systems will be discussed in detail.

The comparison of various Moog and Marotta cold gas thrusters from Mueller et al. is particularly useful. This is provided in Table 1.1. The performance of various cold gas thrusters is presented. These thrusters all use nitrogen gas as a propellant, and generally provide low thrust levels. Cold gas propulsion is extremely simple, which is favorable for nanosatellite propulsion, but the performance of the current thrusters are inadequate for performing maneuvers beyond minor attitude control to orient instruments. The lack in ability for these systems to perform significant orbit raising maneuvers leaves an area to be addressed.

Table 1.1 Summary of Cold Gas Thruster Performance[18]

	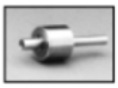			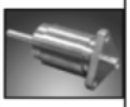		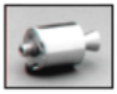	
Manufacturer	Moog	Moog	Moog	Moog	Marotta	Moog	Moog
Model	58X125A	58E143 58E144 58E145 58E146	58E142	58E151	Cold Gas Micro-Thruster	58-118	50-820
Propellant	N2	N2	N2	N2	N2	N2	N2
Thrust (N)	0.0044	0.016 - 0.040	0.12	0.12	0.05 - 2.36	3.6	52-105
Mass (g)	9	40	16	70	<70	23	430
Size (mm)	11.9x34.7	13.97x57.2	14x20.3	19.05x 40.87		6.6x25.4	98.2x104.1
Valve Power (Open) (W)	10	10	<35	10.5	<1	30	47
Valve Power (Hold) (W)		1					
Isp (sec)	65	>60	>57	65	65	65	65
Operat. Pressure (psia)	0-50	0-36	50-300	0-400	100-2240	230	215-2515
Proof Pressure (psia)	300	290	600	1015	3360	1115	3765
Burst Pressure (psia)		508	1200	1615	5600		6265
Response (Open) (ms)	2.5	2.5	3.5	5	5	<4	<10
Response (Close) (ms)	2.5	2.5	3.5	3	5		<10
Minimum Ibit (mNs)					<44		
Life (No. of Cycles)	>15,000	500,000 - 2,000,000	20,000	1,000,000		>10,000	>6,000
Status	Flight Qual	Flight Qual	Flight Qual	Flight Qual	Flight Qual	Flight Qual	Flight Qual
Comments	Brilliant Pebbles, SAFER, Pluto Fast Flyby	CHAMP, GRACE	SIRTF	SIRTF	Developped for GSFC Nanosats, ST-5	SCIT, SAFER, Pluto Fast Fly-by	COMET, Pegasus Cluster of 3 thrusters: 2 @ 52N, 1 @ 105N

Aerojet Rocketdyne has been developing a product line of modular propulsion systems for CubeSats using inert cold gas, hydrazine monopropellant, and green AF-M315E monopropellant thrusters.[19] A tabulated summary of these systems and their capabilities is

provided in Table 1.2. The focus placed on cold gas and monopropellant thrusters is attractive for CubeSat maneuvers due to their proven reliability on larger sized satellites. The advantages of such systems of propellant storability and simple operation are both extremely important for CubeSats. However, these systems also have significant disadvantages associated with them; most notably the use of toxic hydrazine in monopropellant thrusters and low velocity change capability for cold gas thrusters. For this reason, alternative propulsion systems that fit the standard CubeSat form factor are desirable.

Table 1.2 Aerojet Rocketdyne CubeSat Propulsion Systems[19]

Product Image	Product Number	Description	ΔV for 3U 4kg BOL	ΔV for 6U 10kg BOL
	MPS-110	• System Mass: Varies depending on selected size • Propellant: Inert gas • Propulsion: 1 to 4 cold gas thrusters	10 m/s	N/A
	MPS-120	• System Mass: <1.3kg dry, <1.6kg wet • Propellant: Hydrazine • Propulsion: Four 0.26—2.8 N (BOL) rocket engines	209 m/s	81 m/s
	MPS-130	• System Mass: <1.3kg dry, <1.6kg wet • Propellant: AF-M315E • Propulsion: Four TBD—1 N (BOL) rocket engines	340 m/s	130 m/s
	MPS-120XW	• System Mass: <2.4kg dry, <3.2kg wet • Propellant: Hydrazine • Propulsion: Four 0.26—2.8 N (BOL) rocket engines	440 m/s	166 m/s
	MPS-120XL	• System Mass: <2.4kg dry, <3.2kg wet • Propellant: Hydrazine • Propulsion: Four 0.26—2.8 N (BOL) rocket engines	539 m/s	200 m/s
Image Coming Soon	MPS-160	• System Mass: TBD • Propellant: Xenon • Propulsion: 80W Solar Electric Power/Solar Electric Propulsion System (SEP²)	N/A	>2,000 m/s

Each Aerojet Rocketdyne system, with the exception of the cold gas MPS-110, uses four rocket engines (one in each corner of the CubeSat). The cold gas system utilizes one to four thrusters and can provide up to 10 m/s of delta V for a 4 kg (3U) CubeSat. The various monopropellant systems are listed as providing anywhere between 209 m/s and 539 m/s for a 3U CubeSat, and 81 m/s to 200 m/s for a 10 kg (6U) CubeSat. The MPS-120 hydrazine monopropellant system comes in extra-wide and extra-long variants, the MPS-120XW and the

MPS-120XL, respectively, which provide the highest delta V capabilities. The extreme hazards involved with hydrazine monopropellants and the poor performance of inert cold gas thrusters leave much to be desired in the way of a safe and reliable propulsion system with high performance. However, the AF-M315E Hydroxylammonium Nitrate (HAN) based green propellant is safer than hydrazine and reduces handling concerns and cost with higher performance than traditional hydrazine monopropellant thrusters.[20] The AF-M315E green monopropellant is used in the MPS-130, a variant of the hydrazine MPS-120.

Busek systems applicable to CubeSats include electrospray, electrothermal, pulsed plasma, and green monopropellant type thrusters. The green monopropellant thruster is capable of providing up to 130 m/s velocity change to a 4 kg (3U) CubeSat and fits within 1U with a mass of less than 1.5 kg.[21,22] Clyde Aerospace is also currently developing a pulsed plasma thruster for performing drag compensation.[23] Life increases of 200% and 66% are shown for 1U and 3U CubeSats, respectively, at an altitude of 250 km. The University of Michigan is working to create a plasma thruster, termed the CubeSat Ambipolar Thruster (CAT).[24] The CAT system is designed for a 3U CubeSat and will use its plasma thruster to enable in-space maneuvers. The Massachusetts Institute of Technology's Space Propulsion Laboratory is creating an ion Electrospray Propulsion System (iEPS).[25] This system can fit 1U to 3U CubeSats and use between 4 and 32 thruster modules for attitude control and velocity change. While electric propulsion systems can fit within the CubeSat size and mass requirements, their low thrust levels mean long duration operation better suited for station keeping than orbital raising maneuvers.

The Aerospace Corporation has examined solid rocket motor propulsion systems for CubeSats, which are capable of providing velocity changes of more than 500 m/s.[26] These systems, however, are inherently dangerous due to the use of a solid propellant and production

and handling costs due to these hazards are likely to be substantial. In addition, the high thrust levels of a solid propellant could cause damage to onboard equipment, especially for CubeSats where universities and business may use inexpensive components obtained commercially that are not designed to withstand such accelerations.

The propulsion systems currently in development for CubeSats generally target station keeping and attitude control, with the exception of the solid rocket motor examined by The Aerospace Corporation. A gap exists for a propulsion system that fits between cold gas and monopropellant thrusters and a solid rocket motor. The application of a nitrous oxide hybrid rocket motor propulsion unit can address a number of these concerns while maintaining relatively high performance needed for orbital control maneuvers. The inherent safety with hybrid rocket motors makes them an appealing choice for CubeSats, where affordability and accessibility are of greatest importance. Nonhazardous, inert solid fuel grains can be used with nitrous oxide, significantly reducing handling concerns and costs associated with toxic hydrazine or a solid propellant. However, fitting a high performance hybrid rocket motor within the size and mass constraints of a CubeSat is where challenges arise.

A previously developed propulsion system using a nitrous oxide hybrid rocket motor was presented by the Experimental Propulsion Lab in Utah.[27,28] The hybrid rocket propulsion system utilized additive manufacturing to print a pressure vessel for the self-pressurizing nitrous oxide oxidizer and the fuel grain. Selective laser sintering was used by CRP Technology to print the high-strength carbon-filled polyamide material, called Windform XT 2.0.[29] The propulsion unit proof of concept is shown in Figure 1.7, and Figure 1.8 shows the unit as designed to fit within a 6U CubeSat.

The Experimental Propulsion Lab's hybrid rocket propulsion unit was a step in the right direction for using a hybrid rocket for CubeSat propulsion, however, the Windform XT 2.0 material is a low performance fuel and innovative use of the SLS print to include complex features was absent. In addition, long-term Windform XT 2.0 material exposure and other considerations were not examined in depth.

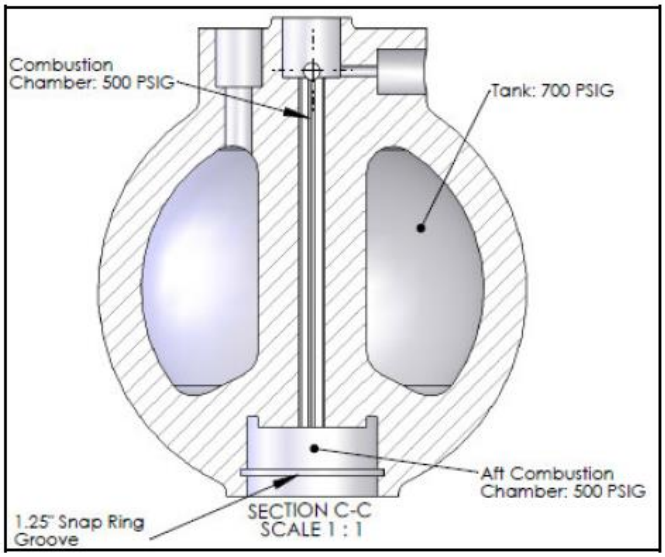

Figure 1.7 Experimental Propulsion Lab CubeSat Propulsion Unit Initial Design[27]

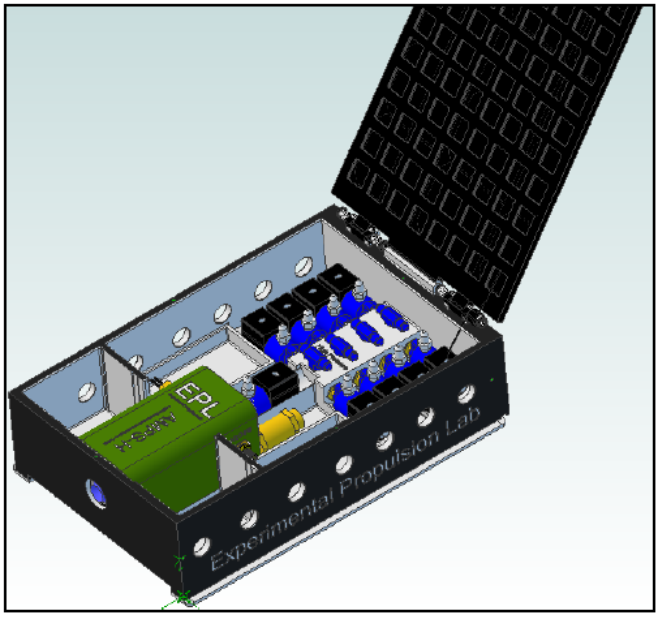

Figure 1.8 Experimental Propulsion Lab CubeSat Propulsion Unit in a 6U CubeSat[27]

1.1.3 Hybrid Rockets

Chemical rockets remain the most popular type of rocket propulsion system for launch and low Earth orbit maneuvers due to their high thrust to weight ratios. Electric propulsion technologies result in very high specific impulse, but lack the thrust of a typical chemical rocket. Hybrid rockets are, essentially, a combination of solid and liquid rockets. Instead of a solid propellant containing both fuel and oxidizer, or liquid fuel and liquid oxidizer being combined in a combustion chamber, classical hybrid rockets utilize an inert solid fuel and a liquid or gaseous oxidizer.[30] This difference is illustrated in Figure 1.9.

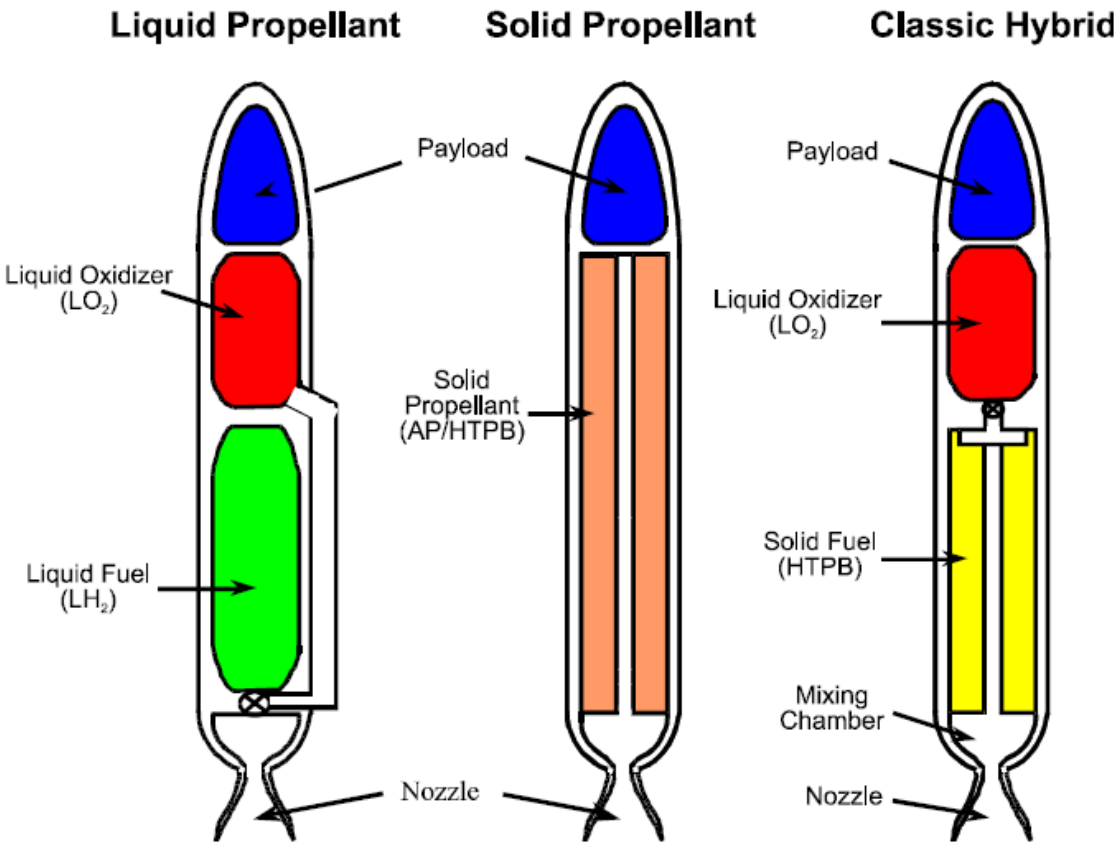

Figure 1.9 Classical Hybrid Rocket Configuration Compared to Liquid and Solid Rockets[31]

Compared to solid rockets, hybrids are significantly safer due to the separation of the fuel and oxidizer until operation. Also, unlike liquid propellant rockets, hybrid rocket feed systems only require plumbing for the oxidizer, resulting in reduced complexity. Liquid and hybrid propellant rockets share the ability to be throttled and start/stop/restart. For throttling of liquids, both the fuel and oxidizer mass flow rates must be adjusted accordingly, while for hybrids the fuel mass flow rate is a function of the oxidizer mass flux. Thus, throttling and stopping combustion is possible through control of the oxidizer mass flow rate alone. This is also a noteworthy benefit in terms of safety over solids, where combustion cannot be terminated easily.

Concerning performance, hybrid rockets are advantageous because they typically have higher specific impulse over solid rockets and higher density-specific impulse over liquid rockets.[32] However, due to limitations in regression rate of the solid fuel grain, relatively low thrust has been a problem for hybrid rocket applications. Complex port shapes have been used to increase the fuel surface area and increase overall fuel mass flow rate, however, some degree of fuel sliver must remain post-burn to ensure that large pieces do not break off and potentially plug the nozzle. The low regression rate of hybrid rockets is a result of the diffusion flame combustion process, where the flame is positioned between the solid fuel grain and the oxidizer stream. Other disadvantages of hybrids include low bulk density, low combustion efficiency, and O/F shift during firing as the fuel surface area changes with time.[30]

Hybrid rocket solid fuel grains usually consist of an inert polymer base, such as hydroxyl-terminated polybutadiene (HTPB) or paraffin wax, possibly with additives for improved performance. Additional materials such as poly-methyl methacrylate (PMMA) or acrylonitrile butadiene styrene (ABS) may also be used. Because the fuel grain is naturally inert, handling risks and the costs associated with producing and handling hazardous materials is

eliminated. Nano-particle addition may require specialized procedures, but remain significantly safer than solid rocket propellants. Small-scale hybrid fuel grains can even be shipped through ordinary mail services without the need for special classifications.

The regression rate of a gasifying hybrid rocket fuel is dependent on the heat feedback from the diffusion flame to the fuel surface. This pyrolysis behavior is present in HTPB-based hybrid rocket fuels, which have been thoroughly researched in the past.[31,33–36] Liquefying fuels, in addition to gasification, are subject to a hydrodynamic instability at the fuel surface that results in liquid droplet entrainment.[37] This process is due to the shear created by the oxidizer flow over the liquid fuel layer. This is shown in Figure 1.10. Work with paraffin wax fuel grains has closely examined this behavior and characterized its effect on regression rate.[37–40]

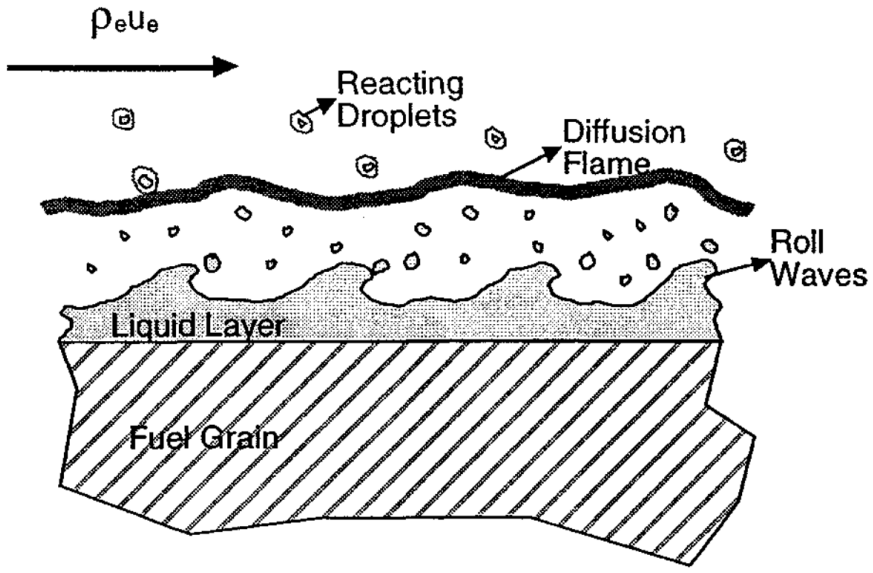

Figure 1.10 Liquid Droplet Entrainment Process for Paraffin Wax[37]

Recent works have attempted to address the low regression rate of hybrid rocket solid fuel grains using metal particle addition in HTPB and paraffin fuel grains.[34–36,41–44] Metal

particles will burn at a higher temperature and release more energy than the base polymer and help to increase heat feedback to the fuel surface. This method is beneficial as long as the particles can be burned in the residence time of the motor. Otherwise, unburned or partially burned particles will be ejected from the motor and performance will suffer. Combustion efficiency will decrease substantially if unburned mass is being ejected from the motor.

Flow disturbance features, such as swirl patterns and diaphragms, have also been used to increase regression rate. Internal features can enhance turbulent mixing and increase both regression rate and combustion efficiency.[44–53] This method does not require a long residence time to be effective and is better suited to the CubeSat-scale hybrid rocket motor than metal particle addition. To facilitate the use of complex port geometries and internal flow disturbance features, additive manufacturing can be used to print the solid fuel grains.[49] Numerous printed fuel grains have been tested with port shapes and internal geometries that would be extremely difficult or impossible to produce with casting and machining procedures.[44–46,49,53] Similar techniques will be presented in this work for the solid fuel grains tested for use in the CubeSat hybrid rocket motor propulsion unit.

Further, testing of printed, paraffin-based hybrid rocket fuel grains at elevated temperatures has examined the increase in regression rate due to the decrease in sensible heat needed to melt the liquefying fuel.[53] Without internal structures to reduce slumping and expulsion of the paraffin wax fuel, combustion efficiency is decreased at elevated temperatures. It was shown that a swirled acrylic honeycomb structure filled with paraffin wax can help alleviate the decrease combustion efficiency at elevated temperatures and maintain values near that of a typical room temperature paraffin fuel grain. This is directly applicable to a satellite exposed to direct sunlight and/or electronic waste heat. An opposite trend would be expected for

a fuel grain with an initial temperature below that of current room temperature test data, but this has not been experimentally verified. It's important to understand the effect of initial temperature of the fuel grain on performance to apply an appropriate delta V on the satellite.

For a CubeSat-scale hybrid rocket motor, regression rate and combustion efficiency need to be balanced for optimum in-space performance. Because there are strict packaging limitations for CubeSats, combustion efficiency is extremely important in achieving the highest performance possible out of the available size and mass. Expelling unburned fuel from the rocket motor will result in a decrease in performance and waste valuable fuel mass and volume. For this reason, paraffin wax may not be an ideal fuel for a CubeSat-scale hybrid rocket. Paraffin typically has lower combustion efficiency than that of HTPB because of its liquefying behavior, however, internal geometries that enhance mixing can provide improvement over straight port paraffin.

1.2 Research Goals

The goal of the present research was to develop an advanced, additively manufactured hybrid rocket motor propulsion unit for CubeSats (PUC). The hybrid rocket utilizes a 3D printed, cartridge-loaded solid fuel grain with performance enhancing composition and geometry. Nitrous oxide was selected as the oxidizer due to its high vapor pressure (580 psia at 50°F; 751 psia at 70°F; 960 psia at 90°F) and non-cryogenic storability. The vapor pressure is used to drive liquid nitrous oxide to the injector without the need for pumps usually necessary for a liquid oxidizer or large storage tanks associated with a gaseous oxidizer. The structure of the unit and the nitrous oxide tank are also additively manufactured and integrated together to optimize volume usage. The propulsion unit must fit within the standard CubeSat form factor, is limited to a 3U volume of a 6U CubeSat, and can provide the 6U satellite with the capability to perform attitude and orbital control maneuvers.

Specific goals for this project included:

- Conduct a review of commercially available flow control components to determine overall sizing of oxidizer feed system and mass flow rates expected in the actual PUC,
- Perform testing of various printed solid fuel grains with nitrous oxide in the Long-Grain Center-Perforated (LGCP) hybrid rocket motor at the Pennsylvania State University's (PSU) High Pressure Combustion Laboratory (HPCL) for regression rate and combustion efficiency,
- Complete tensile strength testing of candidate additively manufactured materials for oxidizer pressure vessel as-printed and after being exposed to nitrous oxide, and
- Use results of testing to iterate on the PUC design and draw conclusions for future work.

CHAPTER 2. CubeSat Design Considerations

2.1 Additive Manufacturing Background

A large range of additive manufacturing (AM) techniques exist to build parts from three dimensional solid computer models. These techniques are best separated into liquid polymer systems, discrete particle systems, molten material systems, solid sheet systems, metal systems, and hybrid systems.[54] Without going into too much detail regarding the individual technologies in each category, the focus in this work will be on discrete particle and molten material systems due to their application to the PUC design and fabrication.

Additive manufacturing differs from conventional subtractive machining in that the three dimensional part is created layer by layer, rather than by removing material from a piece of stock. For many AM techniques this results in very little or no wasted material. The percentage of material wasted is dependent on the printing technique used. The AM process also allows for inclusion of complex geometries, both external and internal, that would be difficult or impossible to machine. The general AM process is as follows:[54]

1. Development of computer solid model
2. Conversion of solid model file to STL file format for AM machine
3. Transfer of file to AM machine and manipulation for print
4. Machine setup
5. Build
6. Removal and cleanup
7. Post-process
8. Application

The particular AM machine and part to be printed determine many factors in the setup, build, and post-print processing. These factors include power requirements, removal of support material, and manipulation that may be needed for a particular print. The method used for supporting the part during the print process is also dependent on the particular AM technology. For nearly all AM machines, material is left surrounding and within the part to maintain structural integrity during the print process. The support material is then removed, again the method varies for each machine used, and the part is finalized. It is important that internal areas are accessible to remove support material (i.e. no closed internal sections). Individual systems may require different size access ports to remove the material based on the method used (melting, bead blasting, etc.).

These requirements should be considered during the design process, or the part may need modified prior to printing. An understanding of the machine that will be used for the print can be very helpful in designing a part that can be effectively printed. Next, the print process and machine consideration for selective laser sintering and fused deposition modeling will be discussed.

2.1.1 Selective Laser Sintering

Selective laser sintering (SLS) is a type of discrete particle system in which a bed of powder is scanned with a laser to sinter the material together. Only material that is to be included in the solid three dimensional part is scanned. After scanning the bed of powder, the machine lowers the bed and a fresh layer of powder is spread over top of the existing layer. This fresh powder layer is scanned, and the process repeats until the part is completely built from the bottom to the top. A general example selective laser sintering machine is shown in Figure 2.1.

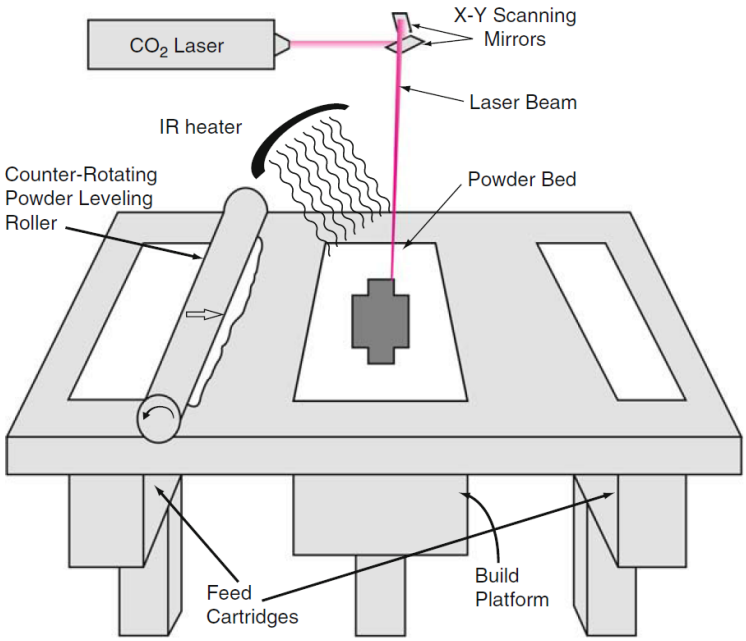

Figure 2.1 Example Selective Laser Sintering Machine[54]

This particular method is useful for high strength materials that cannot be used in other AM machines, such as polymer powders with carbon fibers or other materials for improved strength properties. The powder that is left unscanned on the outside of the part and inside internal features acts as the support material. When the print is finished, the part is removed and any unsintered powder on the outside of the part is removed. Bead blasting or other methods may be used to remove powder from internal channels. The power requirements for sintering of a particular material, powder layer thickness, and print direction are a few important considerations for SLS.

Additive manufacturing of the structure and oxidizer tank was done using the SLS AM technique because it allows the use of a large range of materials, specifically high strength composites.[55] For the PUC, a high strength material capable of withstanding the self-pressurizing nitrous oxide was needed. A thorough search of various AM techniques, and the polymer

materials that could be printed using those techniques, showed that the highest strength polymer print is achieved through using SLS. Namely, CRP Technology's Windform XT 2.0[29] and Solid Concepts' NyTek 1200 CF[56] were determined as final options for the oxidizer tank due to their high mechanical strength properties. Their material properties are provided in Appendix B. Windform XT 2.0 was chosen as the material that would be used for the structure and oxidizer tank because of its higher strength than NyTek 1200 CF, and because its capability of acting as a nitrous oxide tank was previously demonstrated by the Experimental Propulsion Lab.[27,28]

2.1.2 Fused Deposition Modeling

Fused deposition modeling (FDM) is a type of molten material system in which a polymer filament is extruded through a heated nozzle and deposited layer by layer to build a three dimensional part. This method is typically done in a machine similar to that in Figure 2.2. Almost any thermoplastic polymer with a relatively low melting point can be used in an FDM machine. These machines are easy to use and can be commercially purchased.

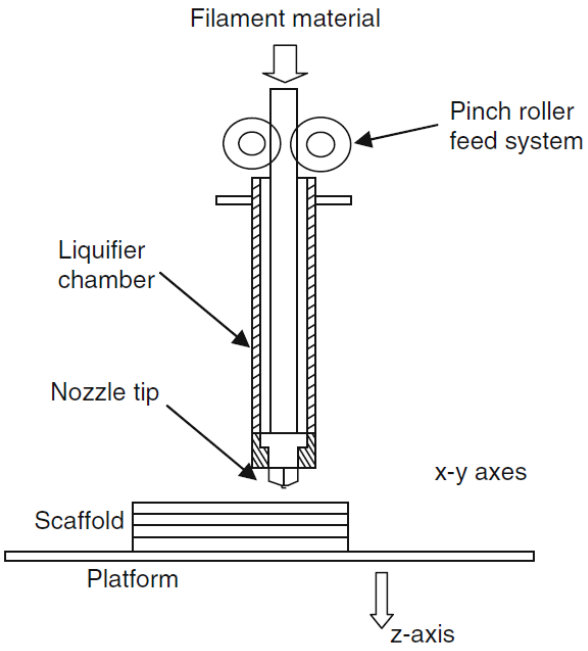

Figure 2.2 Example Fused Deposition Modeling Machine[54]

The solid fuel grain used in the PUC is created using the FDM AM technique. This method is inexpensive for printing high performance fuels such as paraffin, acrylic, and ABS. The paraffin, paraffin/acrylic, and ABS fuel grains tested in this work were provided by collaborators at The Aerospace Corporation. ABS fuel grains were printed in-house, while paraffin and paraffin/acrylic fuel grains were sent out to be printed. Previous work with printed solid fuel grains in an oxygen hybrid rocket motor proved the ability to enhance regression rate and combustion efficiency with complex geometries and composite fuel grains.[45,46,49,53] The FDM process was used in printing these fuel grains, and was now applied to the nitrous oxide PUC solid fuel grains.

2.1.3 Additive Manufacturing Disadvantages

The use of additive manufacturing for the structure and oxidizer tank allowed inclusion of internal channels that machining techniques cannot accomplish, while the use of AM for the fuel grain was useful because it enables the use of complex port shapes and internal structures to increase combustion performance. However, additive manufacturing has a number of very significant drawbacks that must be considered in the design and application of functional parts.

Print direction is extremely important during fabrication of the unit structure and oxidizer tank. Strength of the material varies significantly in all three directions. The weakest print direction for any AM technique is normal to the layer surface due to the weak interface between each individual layer. In addition, scan direction will affect the strength of the material in the layer plane.[55] These dependencies are discussed further in the tensile strength testing section and shown in the experimental results section. Additionally, quality of the print is a notable concern. Voids in a print could significantly reduce the strength by causing a stress concentration and crack initiation site. A method of nondestructive evaluation could potentially be used to examine

a printed part and reveal such flaws. One must also consider contraction of the printed material during cooling. This could lead to warping of a part and induce thermal stresses that could weaken the material and change the dimensions of the printed part.

Fuel grain fabrication using 3D printing has generally resulted in satisfactory prints. However, print density and tolerances of the print could be potential problem areas. A low density print of the fuel could waste valuable volume that could be filled with additional fuel. Tolerances on internal geometries are generally not a problem, however, outside size tolerances could result in too tight or too loose of a fit within the PUC. For the fuel grains used in this work, these particular print inconsistencies were not observed.

There are a large number of variables in any AM print process that need to be considered. Some matters may play a larger role in the functionality of a part than others depending on the specific application. Surface roughness, for example, may not be important for a single piece prototype, but for parts that need to fit together with tight tolerances this may cause interference. A particular application and its requirements need to be addressed before selecting the appropriate machine for the print.

2.2 Material Compatibility Considerations

In addition to selecting an appropriate additive manufacturing technique for achieving a high strength polymer print for the oxidizer tank, the material used had to be compatible with nitrous oxide. Polymer materials have a tendency to swell in contact with nitrous oxide and may become prone to ignition. In addition, nitrous oxide can act as a plasticizer and significantly reduce the mechanical strength of the material, which is an extremely important consideration for long-term storage of nitrous oxide within the oxidizer tank. Polyamide has been reported as acceptable for use with nitrous oxide,[57] however, it was important to conduct compatibility tests

before using the material as reported information can vary and it's important to understand the degree to which it may or may not be acceptable for use with nitrous oxide.

Oxygen cleaning procedures, outlined in Appendix C, were used on all materials in contact with the oxidizer. It was important that the cleaning solvent, EnSolv, was also compatible for use with the polyamide material and that no significant dimension or mass change was observed. The CubeSat would need to be cleaned following this procedure before being filled with nitrous oxide to ensure contaminants and unwanted fuel sources were removed. The producer of EnSolv, Enviro Tech, reports compatibility with polyamide,[58] but tests were performed to verify this information.

The oxygen cleaning procedure specifies a 30 minute soak within the EnSolv cleaning solvent. To verify no significant change in the material during this time, samples of Windform XT 2.0 and NyTek 1200 CF were exposed for 15 minutes, 30 minutes, 1 hour, and 24 hours. No significant change was observed in the mass of the samples over any duration of time tested. Therefore, it was concluded that polyamide compatibility with EnSolv was verified and cleaning of the polyamide could be performed. The results of the soak tests are given in Table 2.1.

Table 2.1 Exposure of Windform XT 2.0 and NyTek 1200 CF to EnSolv

NyTek 1200 CF - EnSolv Soak Test				
+XY Print Sections				
Section # / Exposure Time	**Initial Mass (g)**	**Final Mass (g)**	**Mass Change (g)**	**% Change**
1 / 15 min	2.6661	2.6658	-0.0003	-0.0113
2 / 30 min	1.8764	1.8758	-0.0006	-0.0320
3 / 1 hr	1.7818	1.7812	-0.0006	-0.0337
4 / 24 hr	2.6495	2.6515	0.0020	0.0755

Windform XT 2.0 - EnSolv Soak Test				
Nozzle Sections				
Section # / Exposure Time	**Initial Mass (g)**	**Final Mass (g)**	**Mass Change (g)**	**% Change**
1 / 15 min	3.8913	3.8909	-0.0004	-0.0103
2 / 30 min	3.6356	3.6349	-0.0007	-0.0193
3 / 1 hr	3.3571	3.3566	-0.0005	-0.0149
4 / 24 hr	3.6192	3.6204	0.0012	0.0332

Initial testing by collaborators at The Aerospace Corporation of Windform XT 2.0 and NyTek 1200 CF, using the setup shown in Figure 2.3, showed little swelling and mass gain after soaking in nitrous oxide. The results of a one week soak for Windform XT 2.0 and a two week soak for NyTek 1200 CF are provided in Table 2.2 and Table 2.3, respectively.

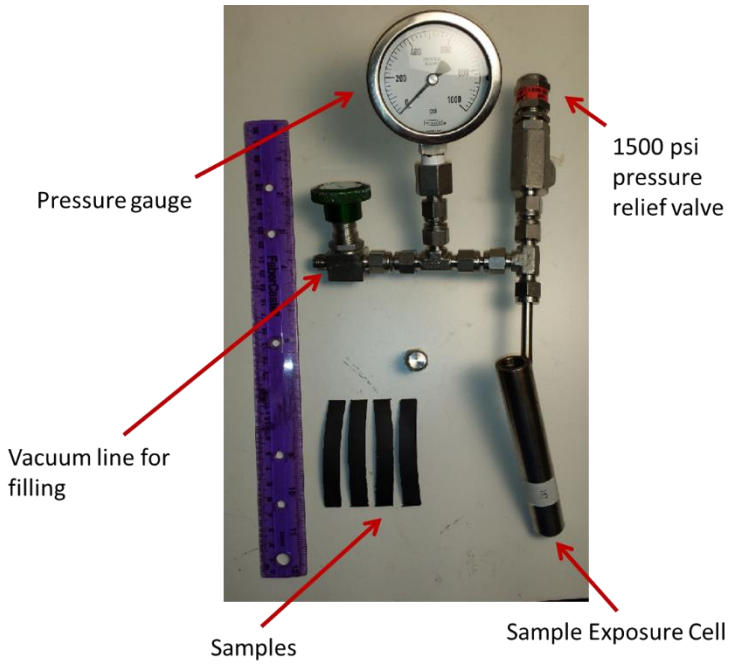

Figure 2.3 Initial Nitrous Oxide Material Compatibility Testing Setup

Table 2.2 One Week Initial Soak Test of Windform XT 2.0

Sample #	Original weight g	post g	% change %
5	1.5723	1.6058	2.13063665
4	1.7394	1.7803	2.35138554
3	1.7584	1.8002	2.37716106
1	1.7048	1.7466	2.45190052
		AVG	2.32777094

Sample #	Thickness mm	post mm	% change %
5	1.99	2.01	1.00502513
4	1.89	1.98	4.76190476
3	2.13	2.18	2.34741784
1	2.05	1.99	-2.9268293
		AVG	1.29687961

Sample #	Width mm	post mm	% change %
5	9.24	9.29	0.54112554
4	9.71	9.71	0
3	9.78	9.87	0.9202454
1	9.87	10.04	1.72239108
		AVG	0.79594051

Sample #	Height mm	post mm	% change %
5	70.17	71.19	1.45361265
4	70.11	71.14	1.46911995
3	70.17	71.17	1.42511045
1	70.33	71.15	1.16593203
		AVG	1.37844377

Table 2.3 Two Week Initial Soak Test of NyTek 1200 CF

	Weight (g)	Side 1 (mm)	Side 2 (mm)	Side 3 (mm)	Side 4 (mm)	Side 5 (mm)	Side 6 (mm)
Sample 1-Before	2.27	76.4	10.08	9.62	76.4	2.44	3.74
Sample 1- After	2.35	76.39	10.21	9.71	76.62	2.44	3.74
Percent Change	**3.5%**	**0%**	**1.3%**	**.9%**	**.3%**	**0%**	**0%**
Sample 2-Before	2.23	76.36	10.26	10.46	76.36	2.35	3.74
Sample 2-After	2.29	76.62	10.44	10.56	76.6	2.33	3.75
Percent Change	**2.7%**	**.3%**	**1.7%**	**1.0%**	**.3%**	**.9%**	**.2%**
Sample 3-Before	1.93	76.33	8.79	9.16	76.24	2.36	3.73
Sample 3-After	2.00	76.35	9.00	9.27	76.55	2.33	3.74
Percent Change	**3.6%**	**0%**	**2.4%**	**1.2%**	**.4%**	**1.2%**	**.3%**

After measuring the post-soak size and mass for comparison to the pre-soak measurements, the exposed samples were held to a lighter flame to determine whether they would be prone to ignition. A lighter held to the material for 30 seconds did not cause ignition.

These results provided the confidence needed to move forward with the Windform XT 2.0 material for the oxidizer tank. The NyTek 1200 CF material was also verified as a secondary option for building the PUC. Further analysis of nitrous oxide exposure and its effects on material strength are discussed in the tensile strength testing section. While the dimensional and mass change of the samples did not appear significant, the effect of the soak on mechanical properties is extremely important since the material is being used as a pressure vessel for potentially long duration nitrous oxide storage.

2.3 Fuel Grain Consideration

2.3.1 Chemical Equilibrium Analysis

Chemical equilibrium analysis was performed for a number of fuel compositions with nitrous oxide. NASA Chemical Equilibrium with Applications Version 2 (CEA2)[59,60] code was

used to calculate theoretical vacuum specific impulse, $I_{sp,vac}$, and characteristic velocity, c*, assuming equilibrium combustion for a rocket problem. Nitrous oxide was chosen from the NASA CEA2 thermodynamic data library[61,62], while each fuel composition was manually entered using the information in Table 2.4. Composite fuel grains were entered using the mass percentage of each component. Example input and output files for the NASA CEA2 code are provided in Appendix D for pure paraffin. The plots provided in Figure 2.4 and Figure 2.5 compare $I_{sp,vac}$ vs. O/F and c* vs. O/F for the various propellant combinations, respectively.

Table 2.4 Input Fuel Properties for NASA CEA2 Code

Fuel	**Formula**	**Molecular Weight (kg/kmol)**	**Density (kg/m^3)**	**Heat of Formation**	**Source**
Paraffin	$C_{32}H_{66}$	450.9	920	-166.5 (Kcal/mol)	[40]
PMMA	$(C_5H_8O_2)_n$	100.0	1100	-102.9 (Kcal/mol)	[40]
HTPB	$(C_{7.337}H_{10.982}O_{0.058})_n$	100.0	930	-2.97 (Kcal/mol)	[40]
ABS	$(C_{3.85}H_{4.85}N_{0.43})_n$	57.1	975	62.6 (kJ/mol)	[63]

The theoretical $I_{sp,vac}$ curve was used in determining the target operating oxidizer to fuel ratio (O/F ratio). The optimal O/F ratio determined by $I_{sp,vac}$ for each fuel occurs at the peak of the curve. From this, it is evident that pure paraffin, paraffin with 20wt% ABS, paraffin with 20wt% acrylic, and HTPB are very similar in $I_{sp,vac}$ behavior. Acrylic peaks at an $I_{sp,vac}$ value significantly lower than the other combinations and has a sharper drop at high O/F ratios. During the course of a hybrid rocket burn, the O/F ratio shifts due to changing fuel surface area. Because of this, it is desirable to have a range of O/F ratio values near the peak in which $I_{sp,vac}$ does not change appreciably. For this reason, and its slow regression rate, acrylic was used only to print

structures within paraffin fuel grains. When used with paraffin, acrylic will protrude into the gas stream as it regresses slower than the accompanying wax and can be used to alter the flow.[44,45,53]

It's also important to note that ABS peak performance occurs near an O/F ratio of 6, rather than 8 for the paraffin based fuels. This is useful for packaging concerns, because nitrous oxide is much less dense than an ABS fuel grain. Being able to have more volume taken up by the more dense ABS fuel results in better overall volume usage, which is especially convenient for a CubeSat application.

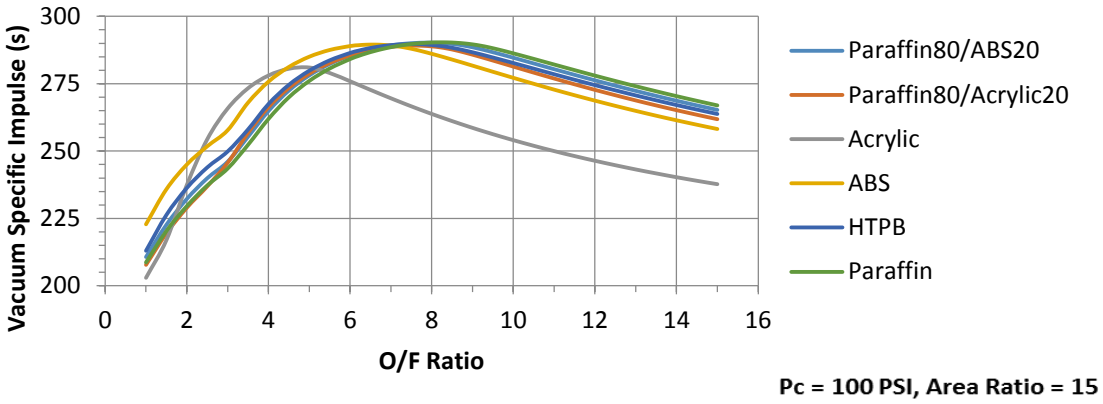

Figure 2.4 Vacuum Specific Impulse vs. O/F Ratio for Various Fuels with Nitrous Oxide

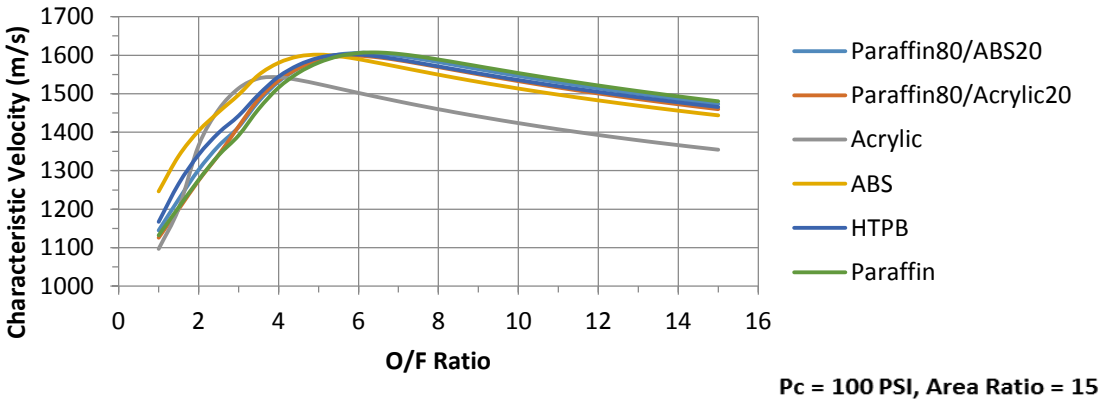

Figure 2.5 Characteristic Velocity vs. O/F Ratio for Various Fuels with Nitrous Oxide

Stoichiometric O/F ratios provided from the NASA CEA2 calculations for paraffin, paraffin with 20wt% acrylic, and ABS are 9.47, 8.63, and 7.80, respectively. The results of CEA calculations for $I_{sp,vac}$ were used to plan experimental testing at optimal O/F ratios, and c* calculations were used in determining combustion efficiency, as will be discussed in more detail in the fuel grain testing section.

2.3.2 Initial Sizing and Performance Calculations

Initial sizing of the hybrid rocket motor was based off of the optimal O/F ratio for a paraffin 80wt% / acrylic 20wt% fuel grain. These calculations represent using a honeycomb geometry paraffin/acrylic fuel grain, such as those previously tested with oxygen.[44,45,53] System analysis was performed to determine approximate delta V capabilities for a 6U (10 kg) CubeSat using a PUC with a nominal 1.25" diameter, 2.5" long fuel grain. O/F ratio was varied by adjusting the diameter of the fuel grain to add fuel mass with a constant oxidizer mass. The method and detailed results for the initial performance calculations are provided in Appendix E. A plot of the delta V results is given in Figure 2.6. The delta V that can be expected for a 6U CubeSat with a PUC at an O/F ratio of 8 is around 115.5 m/s.

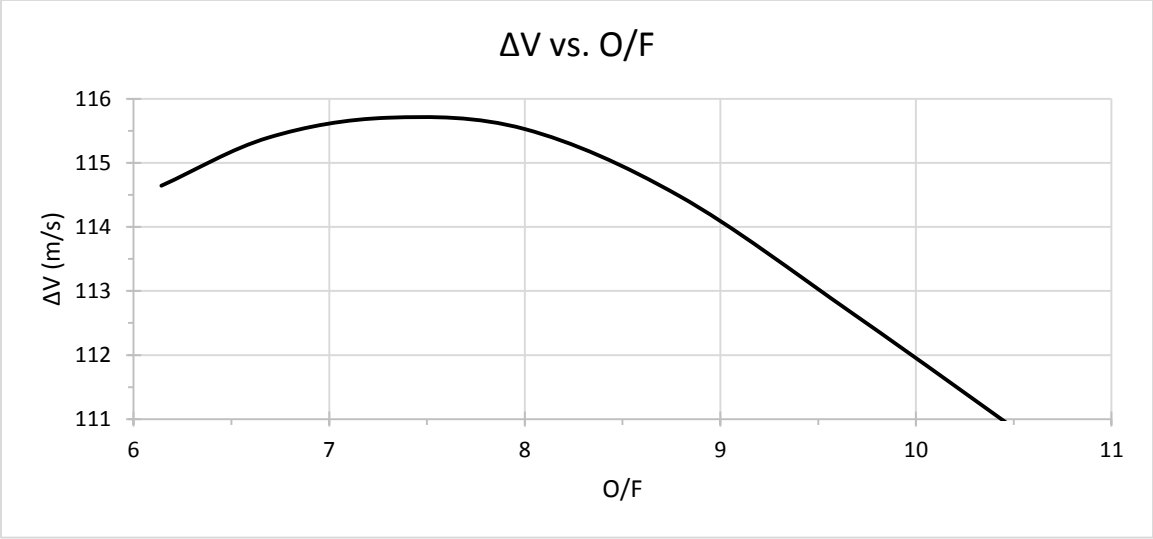

Figure 2.6 Delta V vs. O/F Ratio for Paraffin 80wt% / Acrylic 20wt% with Nitrous Oxide

This value is an approximation based on initial sizing of the fuel grain and oxidizer tank and estimating the mass of propellant fired during operation. Vacuum specific impulse from NASA CEA2 calculations was used for determining the exhaust exit velocity. This result places the PUC within the range of delta Vs expected from similarly sized Aerojet Rocketdyne monopropellant thrusters for a 6U CubeSat, without the hazards associated with hydrazine or AF-M315E.

2.4 Review of Commercially Available Flow System Components

The performance of a hybrid rocket motor is dependent on the oxidizer mass flow rate. Because of this, the primary focus of the oxidizer feed system design is the flow control components. Two options were considered for controlling the oxidizer flow:

- Draw gaseous nitrous oxide from the top of the tank, use a regulator to drop the pressure, and use a valve rated for the reduced pressure to start and stop the flow.
- Draw liquid nitrous oxide from the bottom of the tank and use a valve rated for high pressure to start and stop the flow.

A survey of small-scale regulators and valves was performed to determine the most appropriate method of oxidizer flow control without having to design and build ad-hoc flow control components. In order to make the propulsion unit as openly accessible as possible, commercial off-the-shelf (COTS) components were examined most closely. A tabulated summary of the regulator and valve search results is provided in Appendix F, Table F.1 and Table F.2, respectively. It was determined, due to the size of commercially available regulators, that a single, high-pressure valve was better suited to control the oxidizer flow of the CubeSat propulsion unit and that liquid nitrous oxide would be drawn from the bottom of the tank during operation to maintain a high mass flow rate into the combustion chamber.

A valve capable of withstanding the vapor pressure of nitrous oxide while maintaining a proper seal is extremely important to the success of the PUC design. The main valve must also be small and light to fit within the CubeSat size and mass requirements, and it must have an adequate orifice size to maintain the desired mass flow rate. These requirements led to the decision of using the Nitrous Express Incognito Solenoid valve, which contains a 0.031" orifice. A photograph of this valve is provided in Figure 2.7. This valve is designed for use with liquid nitrous oxide and has an orifice capable of flow rates useful to the PUC design and sizing.

Figure 2.7 Nitrous Express Incognito 0.031" Solenoid Valve

In addition to fitting well within the CubeSat size and mass requirements, the solenoid valve is able to operate on low power draw. This is an important consideration for CubeSats, where limited power is available onboard the nanosatellite. Voltages needed for the valve to open and hold open were examined for pressures similar to that of nitrous oxide vapor pressure at temperatures from 59 to 75°F, 650 to 800 psig, respectively (see Appendix G for nitrous oxide saturation properties). Nitrogen gas was attached to a regulator and set to 50 psi increments

within this range. A power supply was used to control the voltage being provided to the valve. The supply voltage was slowly raised until the valve opened, and then lowered until the valve closed. These values were recorded as the open and close voltages in Table 2.5. Tests up to 1000 psig (roughly the critical pressure of N_2O) showed no problems opening and closing the valve at reasonable power levels.

Table 2.5 NX Solenoid Valve Open/Close Voltages

Solenoid Characterization							
650 PSI		700 PSI		750 PSI		800 PSI	
Open (V)	Close (V)	Open (V)	Close (V)	Open (V)	Close (V)	Open (V)	Close (V)
5.25	0.545	5.20	0.545	5.24	0.528	5.31	0.520
5.28	0.520	5.25	0.528	5.25	0.540	5.40	0.420
	0.520	5.22	0.528	5.28	0.518	5.47	0.370
	0.540		0.528		0.515		0.370

Resistance of Valve
13.6 Ω

A significant result of the open and close voltage testing is that the voltage needed to hold the valve open is significantly lower than the voltage required to open the valve. Because of this, very little power is actually needed to maintain an open valve for operation of the hybrid rocket motor. The initial voltage needed to open the valve could be easily achieved through a driver circuit that releases a higher voltage pulse to open the valve followed by a much lower voltage needed to hold the valve open. This successfully addressed the power requirement concerns of operating the main control valve.

CHAPTER 3. Structural Design, Testing, and Analysis

3.1 Design and Initial Finite Element Analysis

3.1.1 Hybrid Rocket Motor PUC Design

The design of the hybrid rocket motor PUC focuses on the use of additive manufacturing to enable a high performance motor for a 6U CubeSat within 1U, with plumbing and additional components, including the primary oxidizer solenoid valve, contained within the remainder of the 3U allocated to the propulsion system. In order to accomplish this, the nitrous oxide tank and PUC structure are integrated into one piece. A 2.5" long, 1.25" diameter additively manufactured high performance fuel grain of paraffin or ABS is cartridge-loaded into the center of the unit to provide enhanced performance. This design is shown in Figure 3.1.

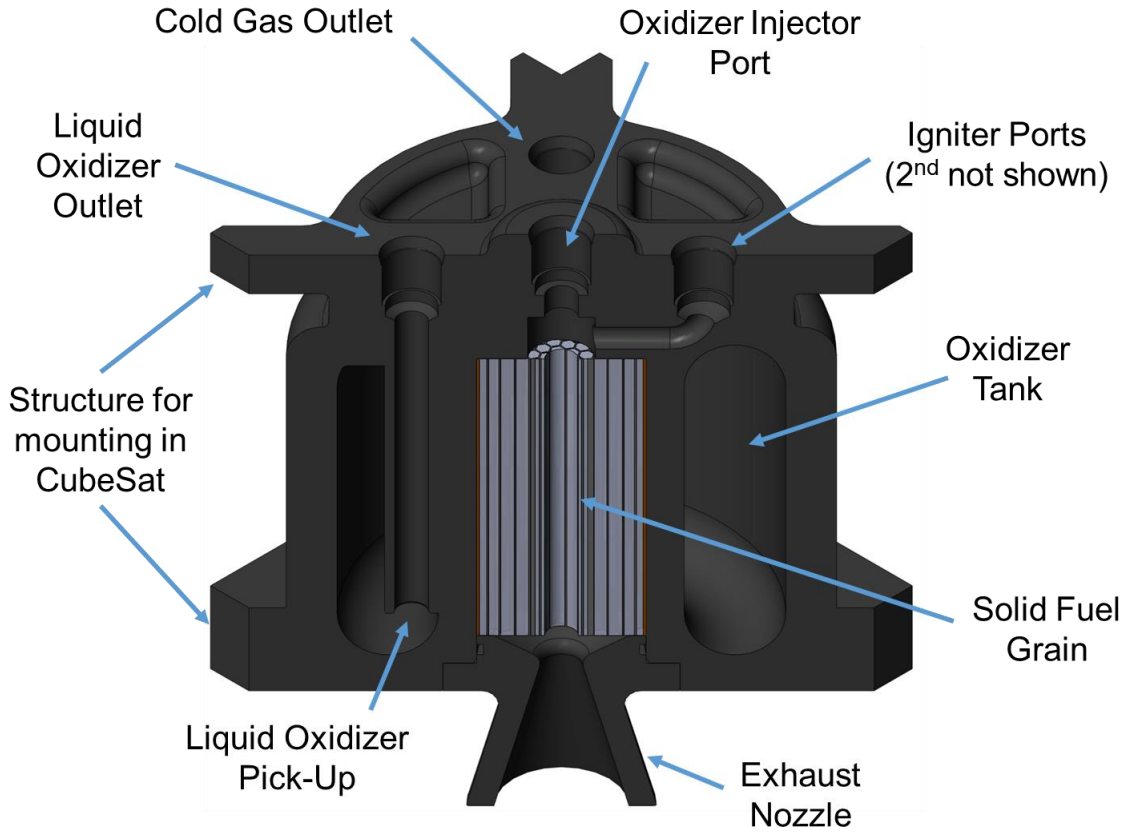

Figure 3.1 Hybrid Rocket Motor PUC 1U Design

The use of AM technology for printing the structure and oxidizer tank allows the use of a toroidal tank design with internal channels for liquid oxidizer pick-up, cold gas outlet, and igniter ports. In orbit, the liquid and gas phase nitrous oxide present in the tank will not be separated by gravity as they are on earth. The liquid pick-up is used to draw liquid nitrous oxide from the tank during operation as the acceleration of the unit keeps the liquid at the bottom of the tank. The cold gas outlet is included such that gaseous nitrous oxide can be drawn off the top of the tank for possible attitude control thrusters. Two igniter ports are purposefully redundant to ensure ignition of the unit.

The SLS printing process greatly simplified fabrication of the PUC. The PUC solid model was designed in SolidWorks and sent to CRP Technology in IGS file format for printing with Windform XT 2.0. The printed tank is shown in Figure 3.2. Bead blasting was used by CRP Technology to remove unsintered powder from the outside surfaces and within the tank through the liquid pick-up and cold gas ports.

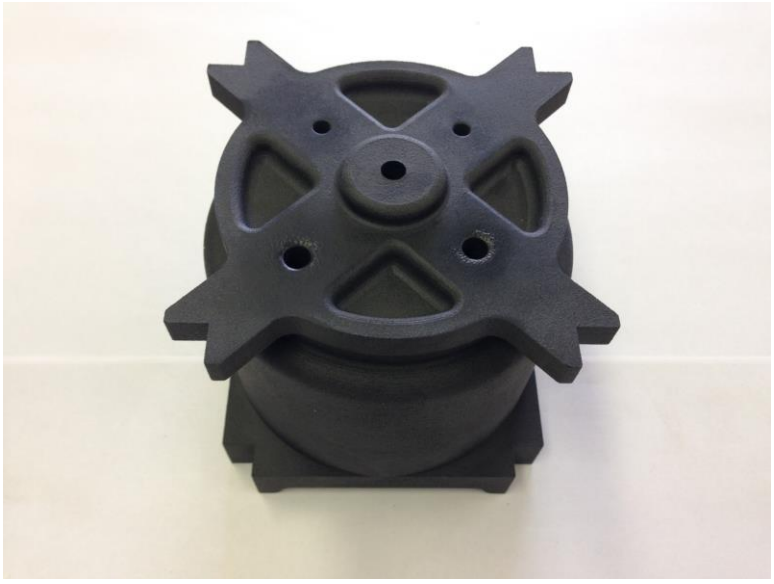

Figure 3.2 Windform XT 2.0 PUC As-Received

3.1.2 Initial Hybrid Rocket Motor PUC Finite Element Analysis

Finite element analysis (FEA) was performed on the PUC design using SolidWorks to determine the factor of safety (FOS) and the location of stress concentrations in the design. A maximum expected operating pressure (MEOP) of 1000 psig was applied to the internal surfaces of the oxidizer tank. The combustion chamber pressure (expected 100 psig) was not applied, as this would only act to reduce stresses in the internal walls. The more extreme case was used as a conservative approach.

The propulsion unit was fixed at the corner surfaces of the bottom mounting plate and roller/slider constraints were placed at the corner surfaces of the top mounting plate. These constraints fixed the PUC within the CubeSat mounting rails, but allowed for vertical expansion during pressurization of the oxidizer tank.

Material properties used for the finite element analysis were those of as-received Windform XT 2.0 based on reported data and private communication with Stewart Davis at CRP Technology.[29,64] These reported properties are provided in Appendix B. Due to the orthotropic behavior of the material, the finite element analysis was conducted using values from the weakest direction (the Z-direction).[64] This ensured conservative results on factor of safety. Little information was provided in this direction other than tensile strength and elongation at break. Due to the lack in material property information, yield strength was approximated as 90% of the tensile strength and unknown values were left blank. FOS was calculated in relation to ultimate tensile strength (UTS) of the material.

The values used for SolidWorks FEA:

- Elastic Modulus: 8,928.2 MPa
- Poisson's Ratio: 0
- Shear Modulus: ?? [MPa]
- Mass Density: 1,097 kg/m^3
- Tensile Strength: 48.83 MPa (Z-direction/weakest)
- Compressive Strength: 150 MPa
- Yield Strength: 44 MPa (~90% tensile)
- Thermal Expansion Coefficient: ?? [1/K]
- Thermal Conductivity: 0.6518 W/(m-K)
- Specific Heat: 1,741.6 J/kg-K
- Material Damping Ratio: ??

The initial FEA result is provided in Figure 3.3. The outer walls of the toroidal tank remain at a minimum factor of safety of around 1.3 based on UTS for the weakest material properties. However, a stress concentration in the upper corner (called out in Figure 3.3) drops below a FOS of 1.0. Due to known concerns with accuracy in the finite element analysis meshing, this value was taken lightly. For this reason, this particular location was left unaltered in the print. However, the resulting stress concentration does suggest that the failure point for the PUC would be expected at this particular location. As will be shown in the hydrostatic pressure test, this is consistent with the observed failure location.

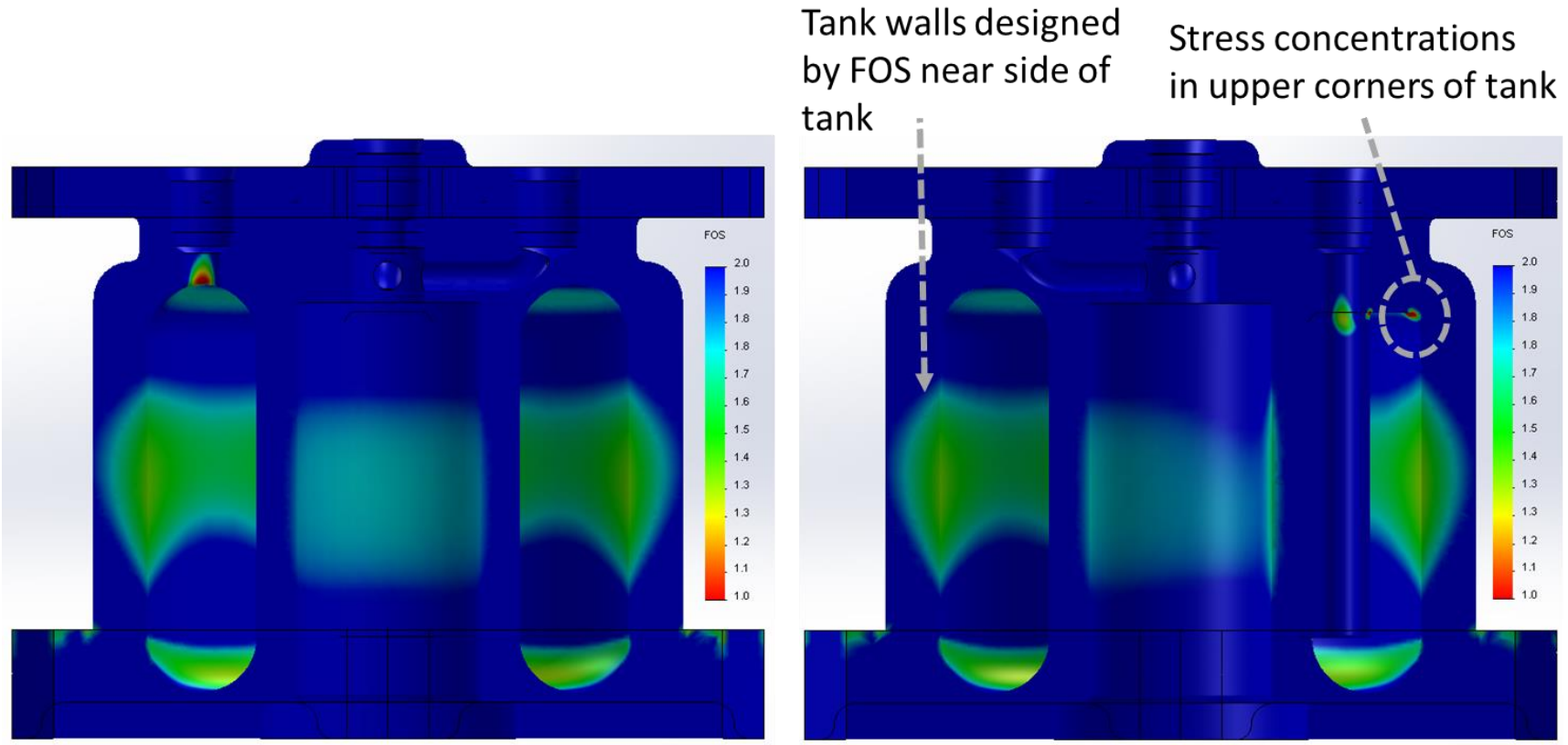

Figure 3.3 Initial Finite Element Analysis Results for Windform XT 2.0 PUC

3.2 Hydrostatic Working and Burst Pressure Test

The ports for the PUC were printed significantly under-sized so that they could be machined to the proper size and shape for an O-ring seal. It was decided that this particular method would maintain the best seal even during the vibration associated with launch and operation of the PUC. Once received, the five ports were machined to an SAE J1926-4 straight thread O-ring sealed port using a specialized port tool and tapped to add the correct threads. This was chosen over printing the threads as it was believed that machining the port would result in stronger threads and a better O-ring seal. The PUC with machined ports is shown in Figure 3.4.

Figure 3.4 Printed PUC with Machined Straight Thread O-Ring Seal Ports

One purpose of the hydrostatic pressure test was to observe the ability of the threaded Windform XT 2.0 port to withstand pressures on the order of the vapor pressure of nitrous oxide at the maximum expected temperature. The high pressure loading on the fittings could potentially rip them out of the threaded Windform XT 2.0. This was an important conclusion to be made about the best way to include threaded ports within the polyamide material.

The machined ports were fitted with the appropriate straight thread O-ring seal fitting. The torque recommendation for the fitting was first tested on an igniter port, which was not needed for the hydrostatic pressure test. Unsurprisingly, the fitting tore through the threaded Windform XT 2.0 material well below the torque specification. The torn threads is shown in Figure 3.5. From this it was decided that the torque recommendation would not be used and instead the fitting was installed using personal judgement of a "snug" fit, while ensuring the O-ring was seated properly within the shoulder groove.

Figure 3.5 Stripped Windform XT 2.0 Threads Below Recommended Torque

The PUC was mounted in a test cell at the High Pressure Combustion Lab for the hydrostatic pressure test. The goal of this test was to ensure that the oxidizer tank could withstand a maximum expected operating pressure of 1000 psig and to determine the burst pressure of the vessel. The mounted PUC was filled with water through copper tubing from outside of the test cell. A nitrogen bottle with a regulator was used as backpressure to conduct the test. A photograph of the mounted PUC is shown in Figure 3.6.

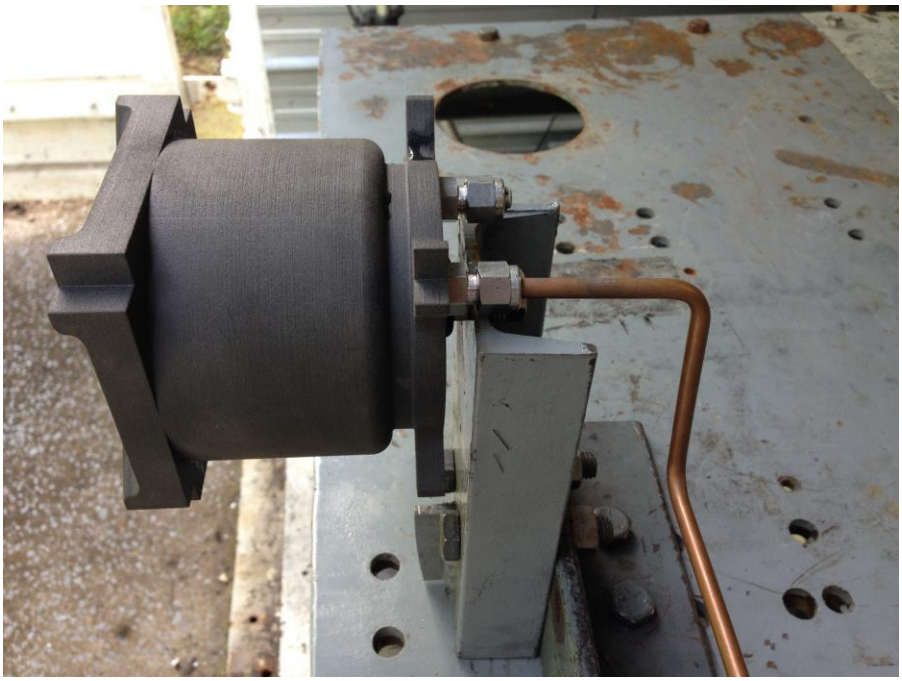

Figure 3.6 PUC Mounted Prior to Hydrostatic Pressure Test

During the test, the pressure was raised in 25 psi increments with brief holds at each pressure. The PUC successfully withstood the MEOP of 1000 psig. The pressure continued to be raised until the vessel failed. During the test, a video camera was used to monitor swelling of the tank and a high speed camera was used to capture the failure of the tank. As the pressure increased, significant swelling was observed. This can be seen in Figure 3.7. Image analysis using ImageJ[65] reveals the percentage change in tank diameter at various pressures. This is provided in Figure 3.8. The swelling observed in the side walls of tank needs to be considered when mounting within the CubeSat form factor. The walls cannot be allowed to swell during pressurization such that the PUC makes contact with the mounting structure. However, significant swelling was not observed until above the MEOP of 1000 psig.

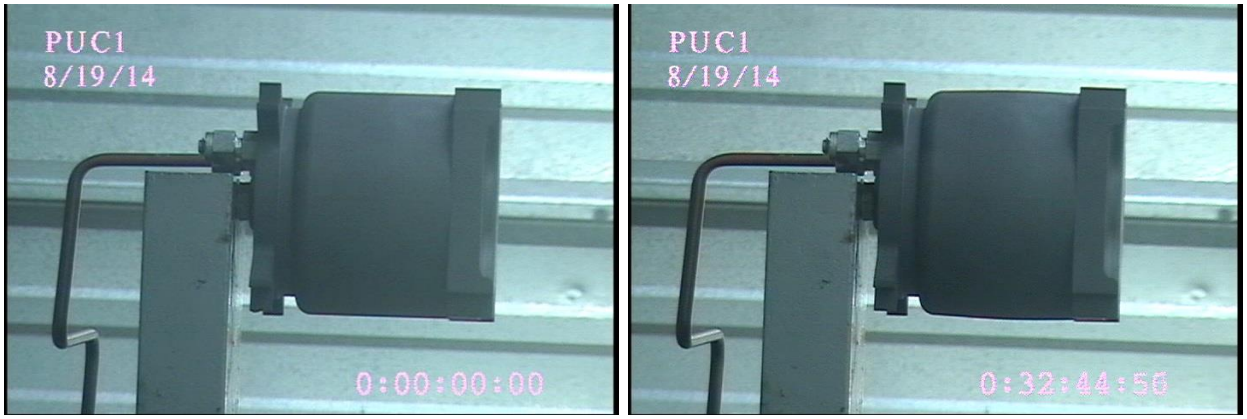

A) PUC at 0 psig

B) PUC at 2250 psig (immediately prior to failure)

Figure 3.7 PUC Hydrostatic Pressure Test Images

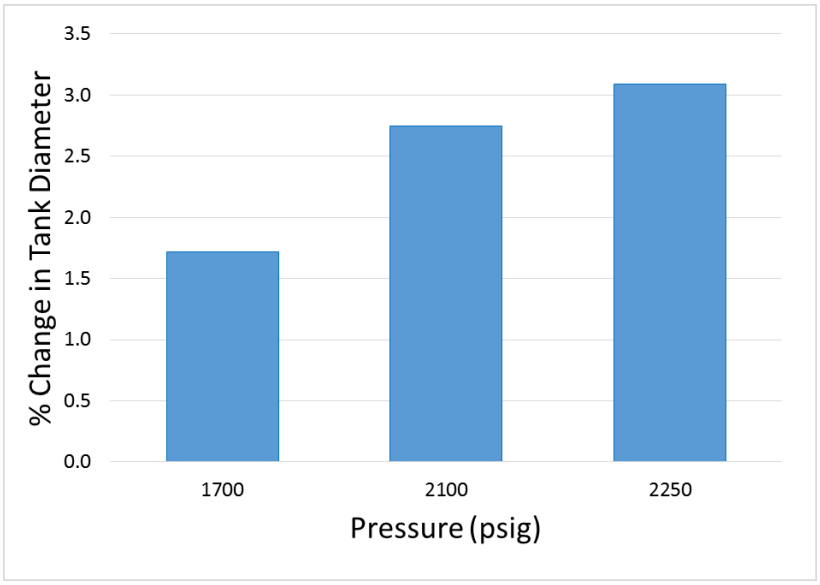

Figure 3.8 Image Analysis Results for Change in Tank Diameter with Pressure

Failure of the tank occurred at roughly 2250 psig, 2.25 times the MEOP. Analysis of the high speed camera images during failure showed the failure process. The video analysis shows a circumferential crack form at the top of the tank. The burst caused separation of the lower portion of the tank side wall. The circumferential crack initiated on the far side of the tank, as seen by the halo-like expulsion of water in Figure 3.9.

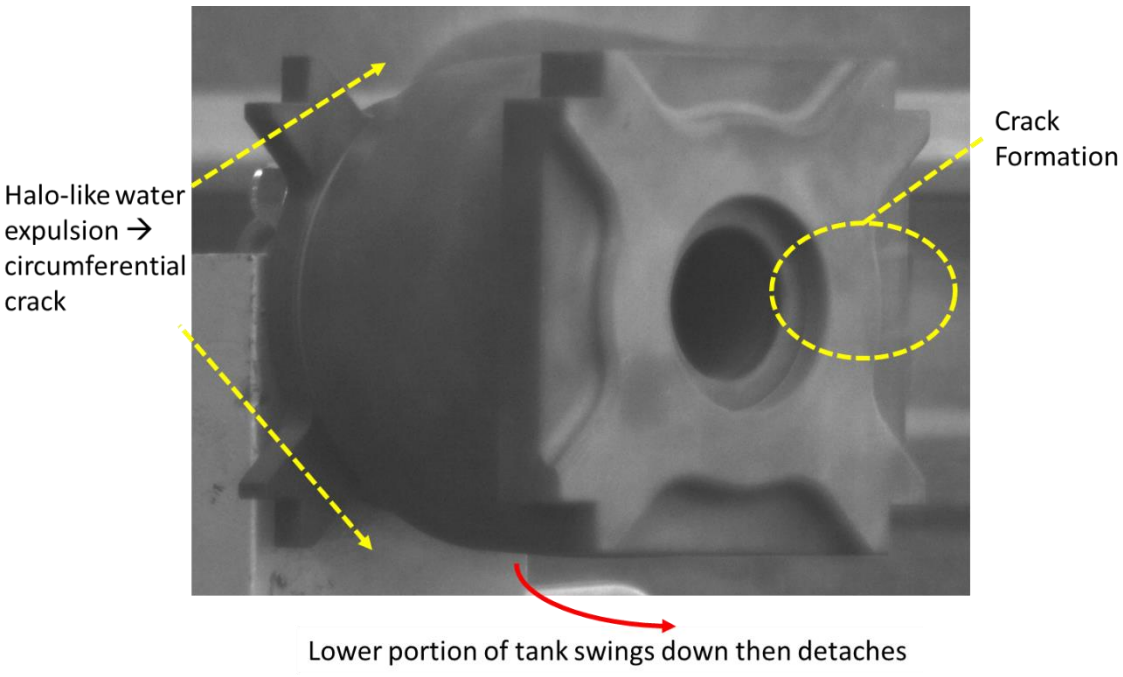

Figure 3.9 High Speed Image Captured During Failure of the PUC

Images of the post-burst PUC, given in Figure 3.10, reveal the failure point to be the top corner stress concentration identified in the FEA analysis. This result validated the location of the stress concentration and the expected failure point of the propulsion unit. Following the initial fracture, the lower portion of the tank was forced out and down causing fracture in the bottom of the PUC and separation of a piece of the wall of the tank.

An important result to note is that the O-ring shoulder seal fittings remained sealed even at the burst pressure. This concern was successfully addressed by the hydrostatic pressure test. Further testing of the shoulder seal straight thread ports should examine vibration and repeatability of the port seal. In addition, testing to failure of the threads could provide important information in determining FOS at the ports.

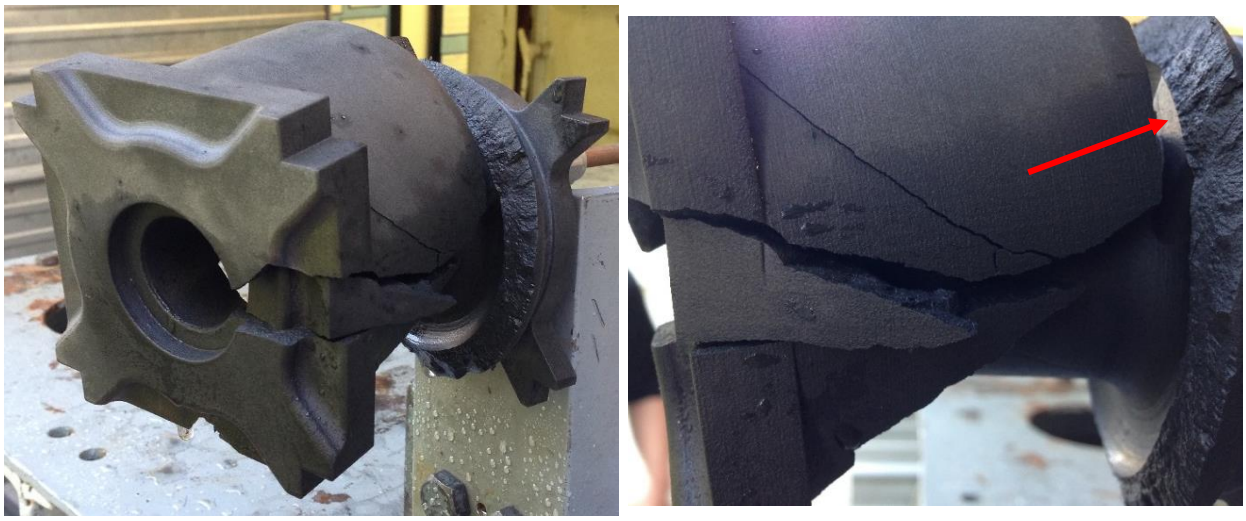

A) View of Post-Burst PUC B) Close-Up of Crack Initiation Location

Figure 3.10 Post-Burst PUC Failure Location Images

3.3 Strength Tensile Testing

Following the initial FEA and hydrostatic pressure test, it was decided that strength tensile testing would provide important information regarding unknown material properties, which could be used in future FEA. In addition, while little size and mass gain was observed for the carbon-filled polyamide material in initial compatibility testing with nitrous oxide, the effect of exposure on strength properties is extremely important. The CubeSat may be filled weeks prior to launch, and sit for additional time in orbit before being operated. This length of exposure could have detrimental effects on the strength of the tank and lead to a failure if left unaccounted. Therefore, it was determined that both as-received and post-exposure tensile samples would be strength tested using a standard tensile test method for polymers. Exposed samples were soaked in liquid nitrous oxide for two and four week durations.

Samples for tensile strength testing were designed according to Type I of ASTM D 638 – 08 Standard Test Method for Tensile Properties of Plastics and tested to this standard.[66] NyTek

1200 CF reported values reference the D 638 standard, while Windform XT 2.0 reported values reference the ISO 527-1 standard, which is technically equivalent.

The solid model of the standard tensile test sample was sent to CRP Technology to be printed from Windform XT 2.0 and to Solid Concepts to be printed from NyTek 1200 CF. Printed Windform XT 2.0 samples were provided in the X-direction, while printed samples of NyTek 1200 CF were provided in the XY+, +Z 45, and +ZX directional planes. The print bed geometry used for the NyTek 1200 CF samples was provided by Solid Concepts and is included in Figure 3.11. The test matrix for the samples is provided in Table 3.1.

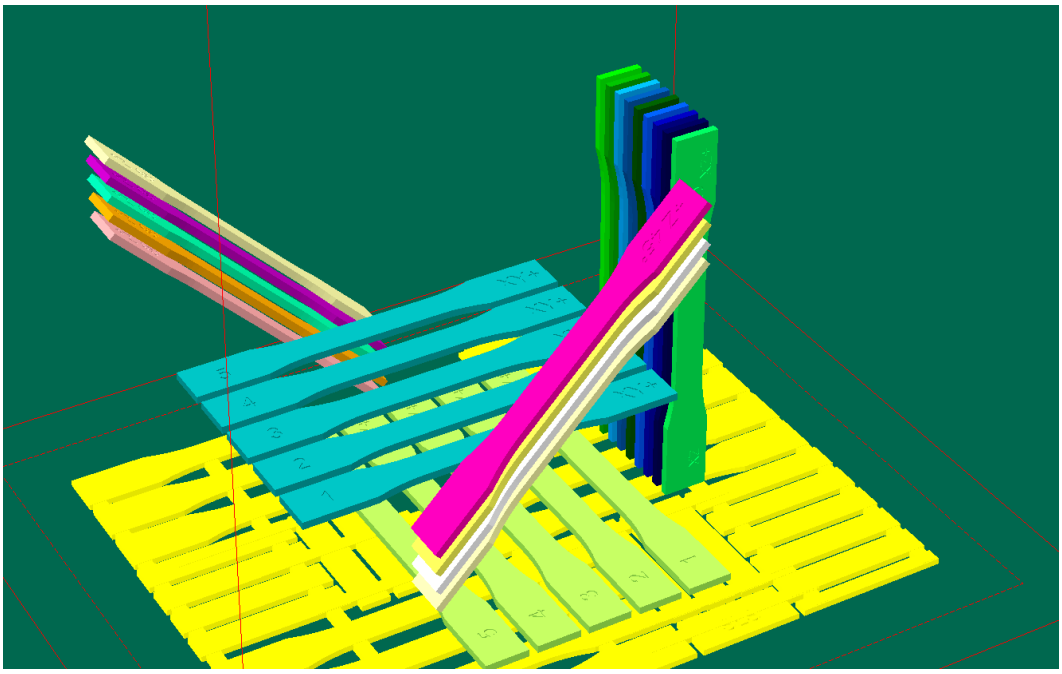

Figure 3.11 Print Bed Setup of NyTek 1200 CF Samples

Table 3.1 Samples and Test Matrix for Strength Testing

Material	# of Samples	Baseline	14 Day Exposure	28 Day Exposure	Remaining
CRP / Windform XT 2.0	8	3	3	2	0
Solid Concepts / NyTek 1200 CF [XY+]	10	3	3	3	1
Solid Concepts / NyTek 1200 CF [+Z 45]	9	3	3	3	0
Solid Concepts / NyTek 1200 CF [+ZX]	9	3	3	3	0

3.3.1 Nitrous Oxide Exposure Cell

In order to characterize the strength of the samples after exposure to nitrous oxide, an exposure cell capable of holding upwards of twelve samples was designed and fabricated. As mentioned previously, all parts were cleaned according to the oxygen cleaning procedure and compatibility of all materials with nitrous oxide was researched.

The soak cell consists of an 8” length of 2” Schedule 80 seamless stainless steel pipe with threaded ends (NPT) and two stainless steel end caps with a machined ¼”-NPT threaded port. The bottom end cap is connected to a fill line used to fill the cell with nitrous oxide from a standard K-size cylinder. This line has a 40 micron filter for incoming nitrous oxide and a hand valve to vent the line once the cell is full. The top end cap uses a siphon tube into the cell to determine the liquid level during the fill and to maintain sufficient space for the liquid nitrous oxide to expand with temperature. As shown in Figure G.2 of Appendix G, the density of saturated liquid nitrous oxide varies significantly with temperature. A pressure gauge is used to monitor the saturated state of the nitrous oxide and a safety relief valve is set to 1500 psig to allow nitrous oxide to escape in the event of over-pressurization. A diagram of the setup is provided in Figure 3.12 and a photograph of the assembled exposure cell is given in Figure 3.13.

The soak cell is filled according to the procedure in Appendix H. A spreadsheet was developed to calculate the liquid to gas volume of nitrous oxide within the soak cell. The spreadsheet, provided in Appendix I, uses the volume of the cell and nitrous oxide density properties to calculate the change in liquid level for a given temperature change. This sheet was used to ensure that a temperature rise would not cause the liquid to expand to fill the cell and cause rapid increase in pressure, possibly leading to a failure.

The exposure cell was filled within a test cell at the HPCL and left to sit for the test duration. During this time, the pressure of the cell was monitored periodically.

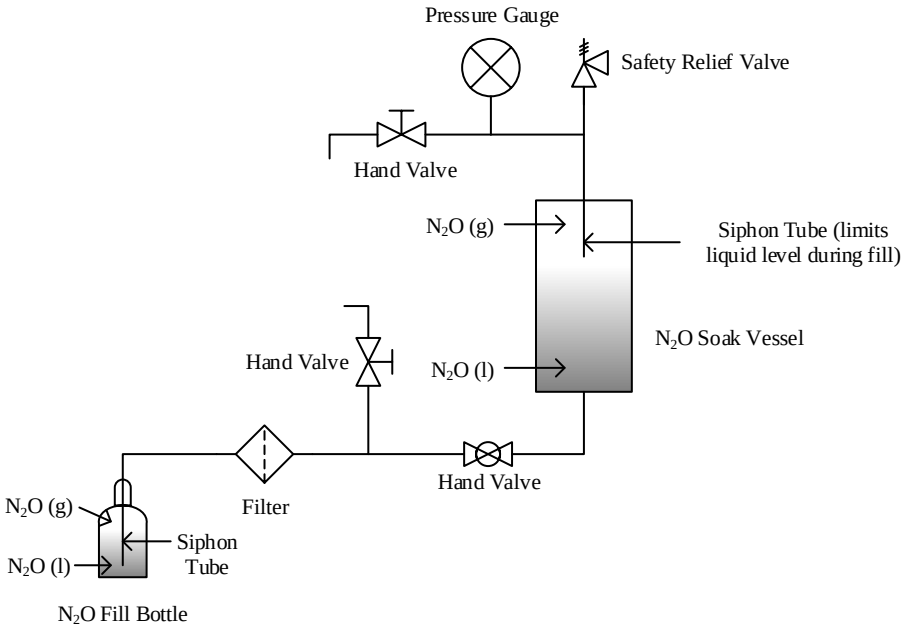

Figure 3.12 Diagram of Nitrous Oxide Exposure Cell Setup

Figure 3.13 Photograph of the Nitrous Oxide Exposure Cell

3.3.2 Tensile Testing Experimental Setup

Strength testing of the candidate PUC materials was performed at Penn State's Materials Science and Engineering Mechanical Testing Laboratory. Testing of the samples according to the ASTM D 638 – 08 standard was conducted using an Instron 5866 with a 0 – 5 kN load cell and 0 – 2 inch extensometer, as shown in Figure 3.14. The machine was operated using Bluehill software. Both the load cell and extensometer were calibrated prior to use and balanced prior to each test. The machine was set to test the samples at a constant grip separation speed of 5 mm/min. according to the ASTM standard. A test data sheet is provided in Appendix J.

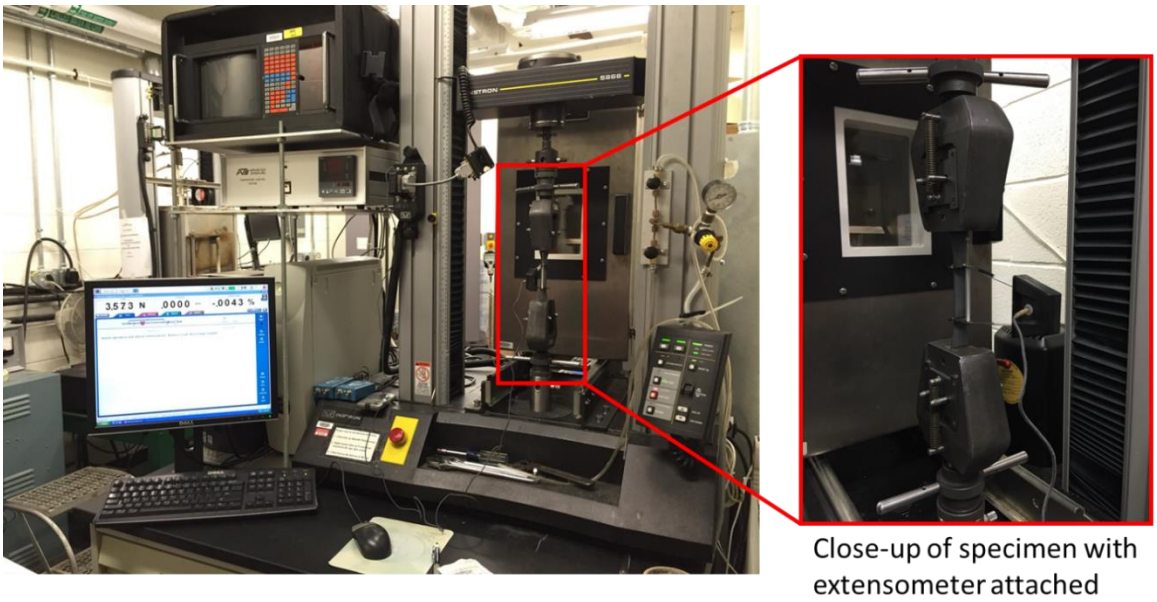

Figure 3.14 Experimental Test Setup for Strength Testing

Tests were first conducted using ABS samples to verify correct operation and data acquisition. Once these tests were complete, baseline Windform XT 2.0 and NyTek 1200 CF tests were performed as-received. During this time, the next set of samples was soaking within the nitrous oxide exposure cell. Samples from the exposure cell were removed and tested on the same day to ensure minimum outgassing of nitrous oxide from the samples prior to testing.

3.3.3 Data Analysis

Measurements of width and thickness of the gage section, as well as mass of the sample, were recorded for each sample. For samples exposed to nitrous oxide, pre- and post-soak measurements were obtained. A comparison of the change in dimensions and mass, provided in Table 3.2, shows similar swelling and mass gain to that found in initial soak testing. The two and four week exposure resulted in comparable change, however, a slight increase in mass gain was observed in the four week samples.

Table 3.2 Pre- and Post-Soak Gage Dimensions and Sample Mass

Nitrous Oxide Exposure			Width			Thickness			Mass		
Sample		Soak Duration	Pre	Post	Change	Pre	Post	Change	Pre	Post	Change
#	Material	days	mm	mm	%	mm	mm	%	g	g	%
22	NyTek 1200 CF [+Z 45]	14	12.7864	12.8659	**0.6225**	3.1665	3.1979	**0.9894**	8.2793	8.5417	**3.1694**
23		14	12.7855	12.8753	**0.7020**	3.1725	3.1852	**0.4004**	8.3130	8.5718	**3.1132**
24		14	12.7737	12.8676	**0.7358**	3.1869	3.2089	**0.6908**	8.3035	8.5646	**3.1445**
25	NyTek 1200 CF [XY+]	14	12.7728	12.8499	**0.6033**	3.4282	3.4671	**1.1361**	9.0790	9.3575	**3.0675**
26		14	12.7085	12.7627	**0.4264**	3.1615	3.2139	**1.6605**	8.4935	8.7532	**3.0576**
27		14	12.7965	12.8558	**0.4632**	3.4586	3.4908	**0.9303**	9.1292	9.4059	**3.0309**
28	NyTek 1200 CF [+ZX]	14	12.8414	12.8803	**0.3033**	3.2470	3.3215	**2.2947**	8.5758	8.8490	**3.1857**
29		14	12.7872	12.8050	**0.1391**	3.2495	3.3105	**1.8760**	8.5482	8.8215	**3.1972**
30		14	12.8524	12.8753	**0.1779**	3.3088	3.3393	**0.9212**	8.6026	8.8760	**3.1781**
31	Windform XT 2.0 [+X]	14	13.0344	13.0852	**0.3898**	3.2766	3.3232	**1.4212**	9.5856	9.8511	**2.7698**
32		14	12.9904	13.0548	**0.4954**	3.2935	3.3409	**1.4396**	9.6369	9.9014	**2.7447**
33		14	13.0243	13.0937	**0.5331**	3.2842	3.3172	**1.0055**	9.6218	9.8875	**2.7614**
34	NyTek 1200 CF [+Z 45]	28	12.7669	12.8482	**0.6366**	3.1784	3.2089	**0.9590**	8.3714	8.6421	**3.2336**
35		28	12.7813	12.8778	**0.7552**	3.1775	3.2089	**0.9859**	8.3523	8.6237	**3.2494**
36		28	12.7855	12.8609	**0.5894**	3.1691	3.2216	**1.6564**	8.3473	8.6180	**3.2430**
37	NyTek 1200 CF [XY+]	28	12.7940	12.8482	**0.4235**	3.4442	3.5010	**1.6470**	9.0956	9.3965	**3.3082**
38		28	12.7178	12.7635	**0.3595**	3.1928	3.2343	**1.2994**	8.5236	8.7949	**3.1829**
39		28	12.6983	12.7169	**0.1467**	3.1953	3.2427	**1.4838**	8.4988	8.7715	**3.2087**
40	NyTek 1200 CF [+ZX]	28	12.8397	12.8609	**0.1649**	3.3045	3.2935	**-0.3331**	8.5986	8.8947	**3.4436**
41		28	12.7838	12.8016	**0.1391**	3.3045	3.3062	**0.0512**	8.5920	8.8891	**3.4579**
42		28	12.7999	12.7974	**-0.0198**	3.2893	3.2808	**-0.2574**	8.5105	8.8041	**3.4499**
43	Windform XT 2.0 [+X]	28	13.0531	13.0768	**0.1816**	3.2978	3.3867	**2.6958**	9.6523	9.9323	**2.9009**
44		28	13.0040	13.0387	**0.2669**	3.2842	3.3951	**3.3772**	9.6239	9.9016	**2.8855**

The ASTM D 638 – 08 standard calls for calculation of tensile strength, percent elongation at yield, percent elongation at break, nominal strain at break, and modulus of elasticity. For each property, the arithmetic mean and standard deviation are to be calculated for each set of samples. Information to be reported includes full identification of the material, sample preparation, type of test specimen and dimensions, conditioning procedure, atmospheric conditions in test room, number of specimens tested, speed of testing, extensometer used, date of test, revision date of D 638 standard, and results of the above calculations.

The point of yielding was determined by the 0.002% strain offset method and break was defined as fracture. The ultimate tensile strength for the sample, σ_{UTS}, is the maximum load, F_{max}, divided by the average initial cross-sectional area of the gage section, A_0,

$$\sigma_{UTS} = \frac{F_{max}}{A_0} \tag{3.1}$$

Percent elongation is the change in gage length relative to the initial gage length, the tensile strain, ϵ, as a percent,

$$\%\ Elongation\ at\ Yield = \epsilon_{yield} \times 100\% \tag{3.2}$$

$$\%\ Elongation\ at\ Break = \epsilon_{break} \times 100\% \tag{3.3}$$

The nominal strain is the change in grip distance divided by the initial distance, as a percent,

$$Nominal\ Strain\ at\ Break = \frac{Change\ in\ Grip\ Distance\ at\ Break}{Initial\ Grip\ Distance} \times 100\% \tag{3.4}$$

The modulus of elasticity is the slope of the linear portion of the stress strain curve, the elastic region, and is calculated as,

$$Modulus\ of\ Elasticity, E = \frac{Change\ in\ Stress}{Change\ in\ Strain} \tag{3.5}$$

Full analysis of the data was performed for comparison of material strength properties using Eqs. (3.1) – (3.5). The results of the testing and analysis is presented in the following section for the as-received and post-exposure samples.

3.3.4 Results

Results of the as-received and post-exposure samples for both Windform XT 2.0 and NyTek 1200 CF show significant decrease in material strength characteristics in all print directions after exposure to nitrous oxide. A comparison of Windform XT 2.0 +X printed samples illustrates this effect in Figure 3.15. Tests 19 – 21 are for as-received samples, tests 31 – 33 are for a two week exposure, and tests 43 and 44 are for a four week exposure.

A significant plasticizing effect from the nitrous oxide is seen in the samples as ultimate tensile strength is decreased and elongation to break is increased after exposure. The ultimate tensile strength of the material post-exposure was over 20% lower than the as-received material. In addition, the modulus of elasticity and yield strength both decreased by over 40%. This result suggests significant consequences to the structural integrity of the PUC oxidizer tank.

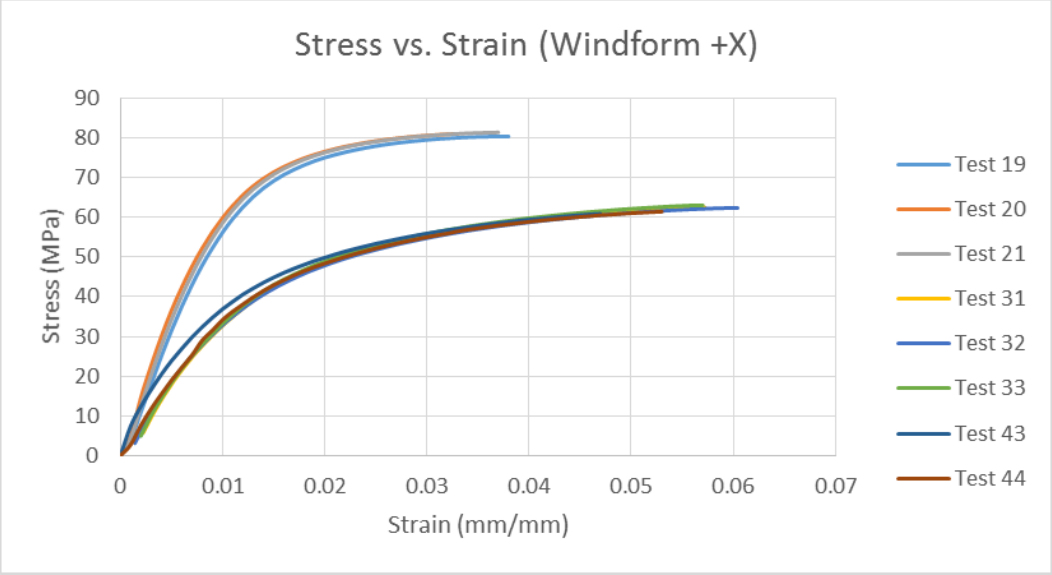

Figure 3.15 Stress vs. Strain for As-Received and Post-Exposure Windform XT 2.0 +X

The decrease in strength did not change appreciably with a four week soak compared to a two week soak. This suggests that the samples were saturated by or before the end of the two week exposure. A slight additional increase in mass gain was observed for the four week exposure, but the strength properties did not change significantly. This brings up the concern of possible loss of nitrous oxide from the pressurized vessel. The ability of nitrous oxide to penetrate the polyamide material suggests that the oxidizer could be lost through the tank walls over time.

Another outcome from the tensile testing was the two different trends for NyTek 1200 CF in the XY+ plane for both as-received and post-exposure samples, shown in Figure 3.16. Tests 13 – 15 are for the as-received material, tests 25 – 27 were for the two week soak, and tests 37 – 39 were for the four week soak. It was determined that this was the result of the two print directions in the XY+ plane, shown in Figure 3.11. Solid Concepts provided samples printed in two perpendicular directions within the XY+ plane.

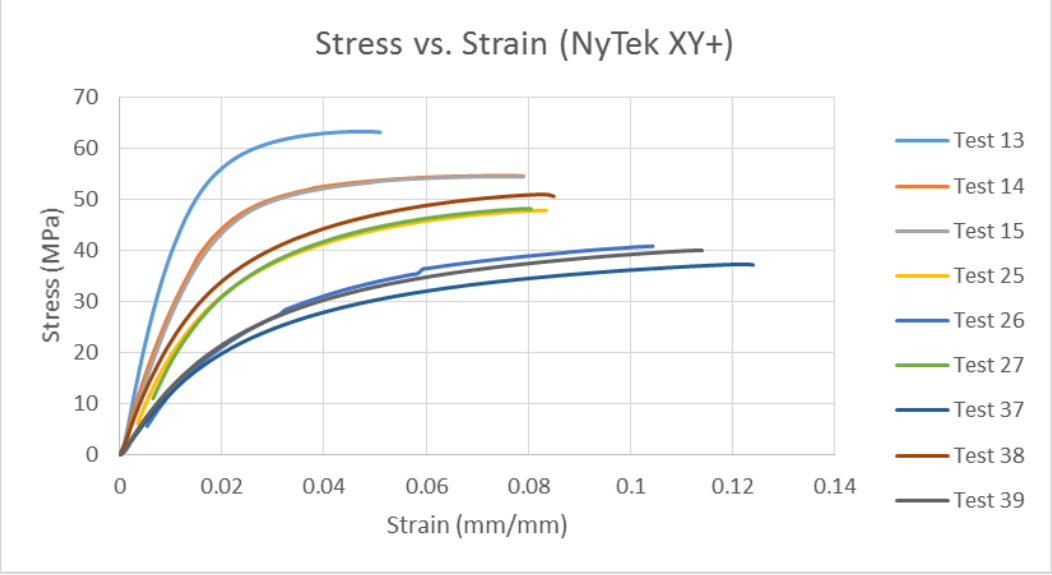

Figure 3.16 Stress vs. Strain for As-Received and Post-Exposure NyTek 1200 CF XY+

While the samples are not labeled differently, such that no conclusion can be directly made about which print direction is weaker, it is clear that the scan direction within the plane has a significant effect on the strength of the sample. This was confirmed by qualitative observation of slight differences in the shade of gray of the printed samples. The weaker samples were a slightly lighter shade of gray compared to the stronger samples. This difference is shown in Figure 3.17.

Figure 3.17 Difference in Coloration of NyTek 1200 CF XY+ Samples

The left broken sample and the left unbroken sample in Figure 3.17 are a slightly darker shade of gray than the others. This is hypothesized as being an effect due to scan direction within the plane. Sample numbers were duplicated in the XY+ plane for the different scan directions (numbered 1 – 5 for each). The duplicate 4 and 1 in the broken and unbroken samples, respectively, show that there is a difference between the two print directions in both coloration and strength.

Full data and analysis of the strength testing can be found in Appendix K for both Windform XT 2.0 and NyTek 1200 CF. It is clear from the testing that both the print plane and

the scan direction have significant effects on the strength of the sample. In order to accurately predict the behavior of anisotropic materials, a full data set of mechanical properties in each direction and an in depth understanding of the dependence on scan direction would be needed. The path followed by the laser will have an effect on the strength properties of the finalized part. Additional information on these dependencies and the way the machine prints each part is needed from the SLS companies to be confident in the numbers used for FEA.

3.4 Iteration of Initial Finite Element Analysis

With these experimental results, iterations on the initial FEA was conducted. Because of the limited reported information for Windform XT 2.0 and the lack of samples in the Y and Z directions, this analysis was performed for NyTek 1200 CF +ZX plane properties before and after exposure (the weakest properties). Figure 3.18 shows the change in FOS based on UTS, while Figure 3.19 shows the change in FOS based on yield strength.

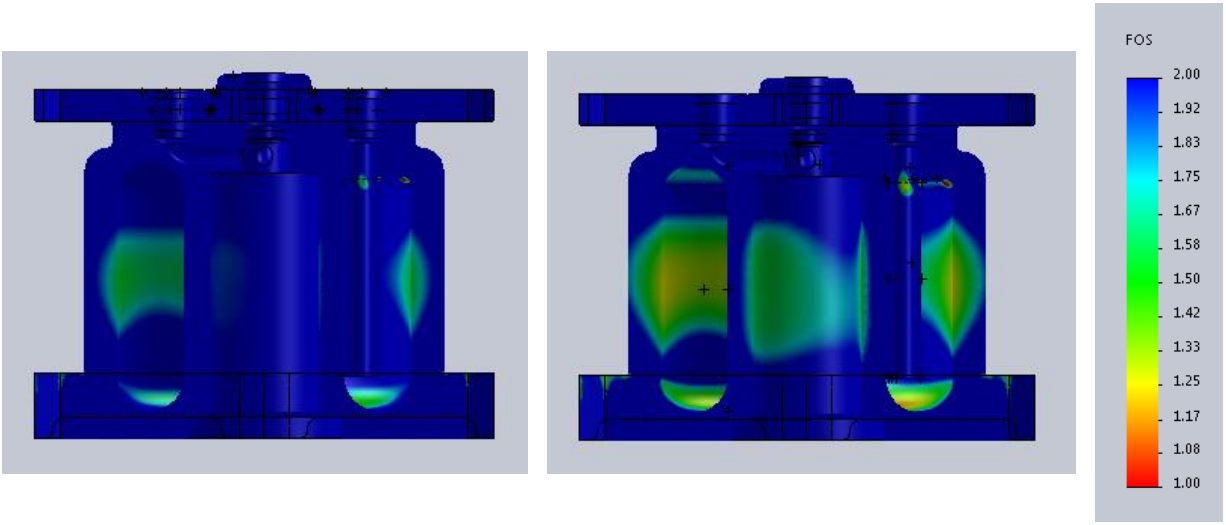

A) As-Received B) Post-Exposure

Figure 3.18 NyTek 1200 CF FEA Analysis Results for FOS Based On UTS

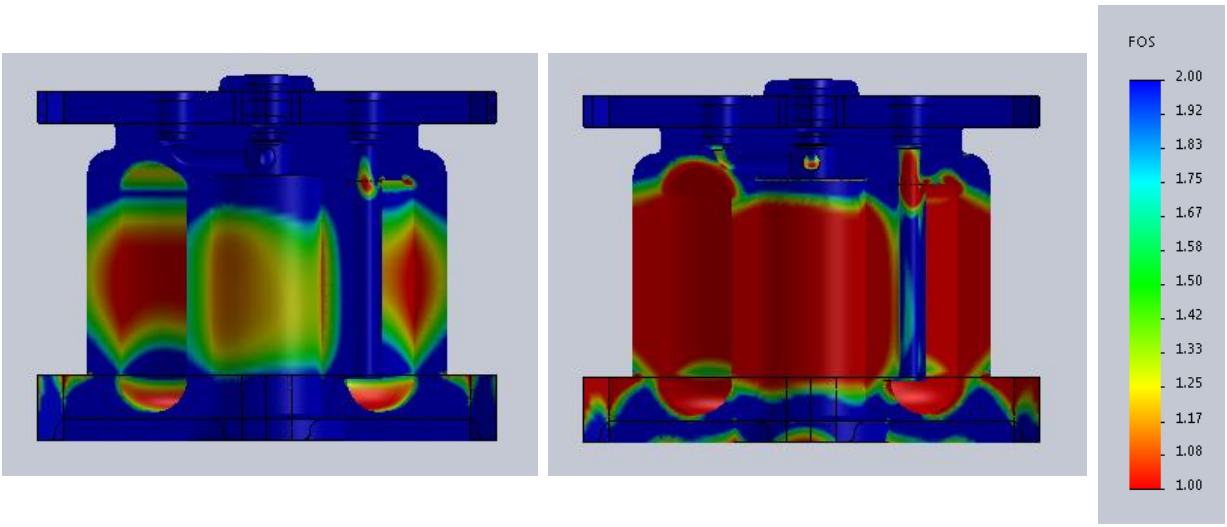

A) As-Received B) Post-Exposure

Figure 3.19 NyTek 1200 CF FEA Analysis Results for FOS Based On Yield

The FEA results for NyTek 1200 CF FOS based on UTS and yield show significant decrease in structural integrity for the post-exposure material. It is important to note that because NyTek 1200 CF is a slightly weaker material than Windform XT 2.0, the FOS for a Windform XT 2.0 printed tank would be higher. However, because of the similarity between the two carbon-filled polyamide materials, it is concluded that neither polymer material (Windform XT 2.0 or NyTek 1200 CF) is sufficient for use as the oxidizer tank. The reduction in strength due to exposure to nitrous oxide is too significant for use as the oxidizer tank, and the saturation of the material could mean mass loss of the oxidizer through the tank walls.

Possible methods for addressing N_2O penetration in the future include coating the inside of the tank, such that the nitrous oxide does not make direct contact with the polyamide, or using direct metal laser sintering (DMLS) to print the unit with a light weight metal. Direct metal laser sintering, similar in principle to SLS, is being examined as the primary method of moving forward to increase the FOS to a value high enough for safe handling of the pressurized unit.

A FOS of 4 based on yield is desired for safe handling of the pressurized unit. The SPUG lists factors of safety for pressure vessels as 1.5 times maximum design pressure (MDP) for proof and 2.0 times MDP for ultimate.[16] Because the MEOP of 1000 psig was chosen based on temperature of the saturated nitrous oxide, MEOP and MDP are technically equivalent in use for this particular unit. Other components, such as lines and fittings, require up to 2.0 times MDP for proof and 4.0 times MDP for ultimate. For this reason, a factor of safety of 4 was chosen for the entire unit to ensure safe operation and handling when pressurized.

When preparing for a launch, the unit would need to be filled with nitrous oxide and loaded into a deployment system for integration with the LV. According to the SPUG, the secondary payload could be in storage up to six months while awaiting integration.[16] During this time, the unit could see a range of environmental conditions listed in the SPUG, including temperature swings between 65 – 85 °F, and handling of the unit vertically or horizontally.[16]

A high FOS rating should be achieved for people to safely handle the unit. Reaching the target FOS with the Windform XT 2.0 material would mean extremely thick walls and reduced working volume for the remainder of the system, including the fuel and oxidizer. For the limited volume available in a CubeSat, this is undesirable. While a printed metal is much denser than a polymer, the higher strength means that material can be removed from the current design to reduce weight to within the CubeSat requirements, while maintaining a high FOS. This will be examined in the future as an iteration of the current design. Stainless steel, cobalt chrome, and titanium are potential metals that could be used to print the PUC using the DMLS technique. Of these, titanium is the lightest and will be examined first.

CHAPTER 4. Fuel Grain Design, Testing, and Analysis

4.1 Fuel Grains Selected for Testing

Screening tests of printed paraffin, paraffin with acrylic, ABS, and Windform XT 2.0 fuel grains were experimentally conducted at Penn State's HPCL using the Long-Grain Center-Perforated (LGCP) hybrid rocket motor. Windform XT 2.0 fuel grains were tested to confirm the low performance expected from the SLS printed carbon-filled polyamide material. The PUC is designed for use with a 2.5" long, 1.25" diameter fuel grain. For straight port fuel grains, the center perforation diameter is 0.25". The LGCP motor provides actual-scale testing of these fuel grains with nitrous oxide in order to determine the best fuel composition and geometry for regression rate and c* combustion efficiency.

Three primary geometries of interest for testing were straight port (SP), star-swirl port (ST-SW), and diaphragm fuel grains. Printed star-swirl port fuel grains have been tested previously at the HPCL with oxygen and showed significant improvement in regression rate for PMMA.[45] The ½ turn per inch (tpi) star-swirl geometry was selected for continued testing in this work with nitrous oxide. Example straight port and star-swirl port Windform XT 2.0 fuel grains are shown in Figure 4.1.

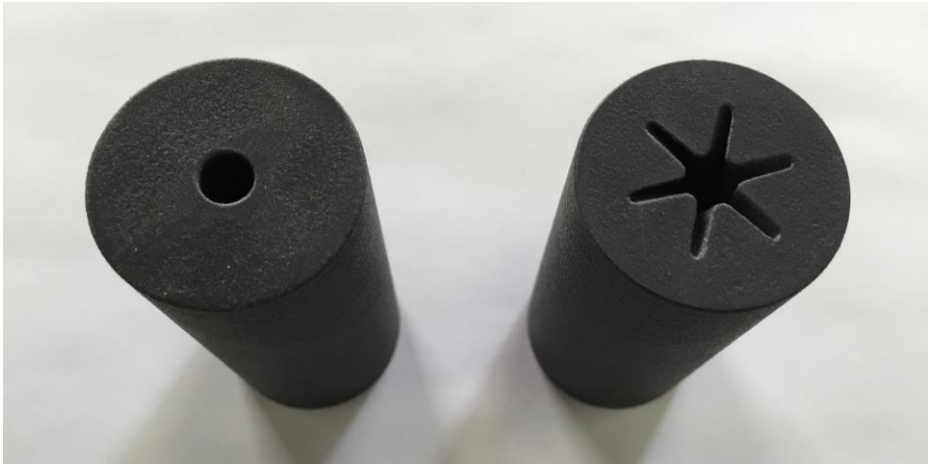

Figure 4.1 Straight Port and Star-Swirl Port Windform XT 2.0 Fuel Grains

Straight port and star-swirl port fuel grains were tested for ABS in natural, white, and black colors, as well as for Windform XT 2.0. The ABS fuel grains were tested in these colors to determine the effect of the pigment on regression rate and combustion efficiency. It was expected that the natural ABS would perform the best due to its pure composition. Due to a lack of information from the manufacturer, the pigment composition and amount used for coloring the white and black ABS is unknown.

One important consideration when using any swirl-inducing fuel grain geometry is the resulting torque on the motor. For a small CubeSat, this could be utilized as a method for spin-stabilization of the thrust vector. However, if this effect was not desired then another geometry would need to be used to avoid spinning the satellite. This is the primary reason for considering the diaphragm geometry in this work. The diaphragm fuel grains were expected to increase regression rate and combustion efficiency without creating a torque on the CubeSat.

Diaphragm fuel grains have been previously tested by researchers with nitrous oxide and simulated through computational fluid dynamics (CFD) analysis.[47,48,50,51] These previous works showed the benefits of a diaphragm with enhanced regression rate and combustion efficiency due to the formation of recirculation zones and increased turbulent mixing. Each of these tests and simulations were conducted using a metal disc insert to act as the diaphragm (little to no increase in diaphragm port size during a test).

The current work aimed to print diaphragms within a paraffin fuel grain using PMMA. The acrylic material regresses much slower than paraffin and will protrude into the flow similar to the honeycomb geometries previously tested at Penn State.[45] With this method, various diaphragm thicknesses could be examined with the hope of maintaining a sufficient height off of

the paraffin surface to disrupt the flow and increase mixing. Unlike swirl geometry fuel grains, no torque would be imparted on the CubeSat with a diaphragm fuel grain.

The initial diaphragm fuel grain design uses two diaphragms located 0.75” from each end (1” between each), and the center port diameter is 0.25”. This design was developed with consideration to previous works examining spacing and height of the diaphragms by Kumar and Kumar.[51] Both 0.050” and 0.100” thick diaphragms were tested to determine appropriate thickness to maintain sufficient height above the paraffin fuel surface for enhanced regression rate downstream of the diaphragm. These fuel grains are shown in Figure 4.2.

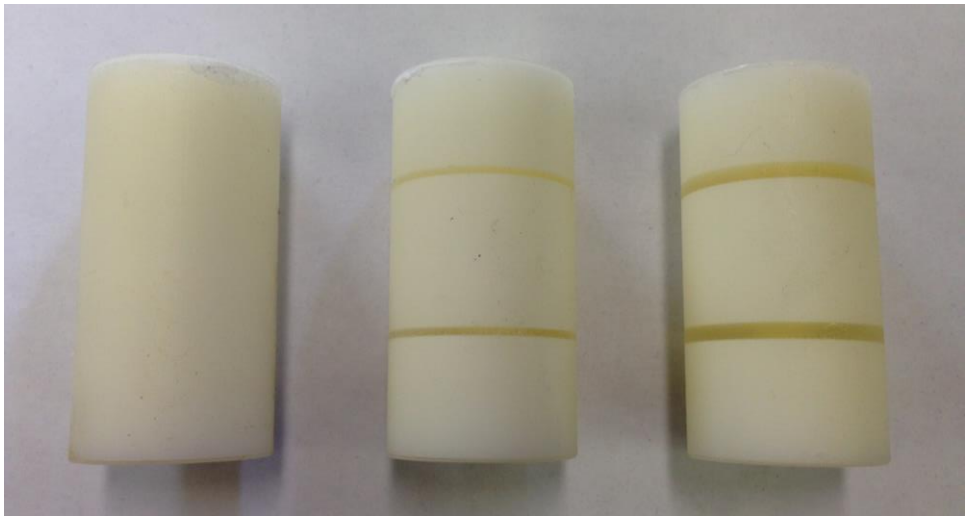

Figure 4.2 Straight Port, 0.050” Diaphragm, and 0.100” Diaphragm Paraffin/Acrylic Fuel Grains

Following initial testing of the paraffin/acrylic diaphragm geometry and examination of the data and post-firing grain internal geometries, an iteration on the design was made in attempt to increase combustion efficiency after observations of low combustion efficiency with the initial diaphragm design. Rather than using two diaphragms and three paraffin sections, the new design utilized a paraffin section followed by a 0.100” thick acrylic diaphragm and an acrylic mixing section. The acrylic diaphragm and mixing section was expected to allow more complete mixing

of the paraffin with the oxidizer to increase combustion efficiency. The advantage to this design is the use of a diaphragm to create enhanced mixing entering the acrylic mixing section, and the dual use of the acrylic as a mixing section and as additional fuel as to not waste valuable volume. The paraffin and acrylic diaphragm port diameter is initially 0.25”, while the acrylic mixing section port diameter is initially 0.60”. The mixing section port size was chosen based on predictions of regression rate with the enhancement from the diaphragm upstream. The second-generation printed design is shown in Figure 4.3.

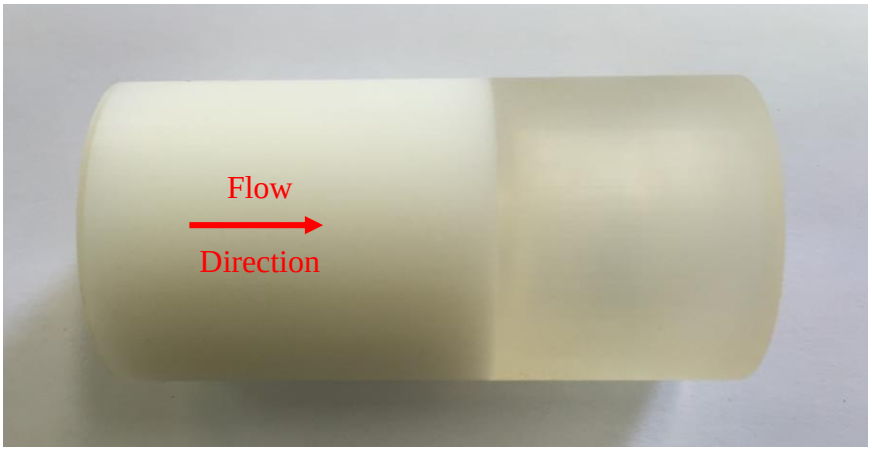

Figure 4.3 Paraffin/Acrylic 0.100” Diaphragm and Mixing Section Fuel Grain

Straight port and star-swirl port ABS fuel grains were printed in-house at The Aerospace Corporation in natural, white, and black colors, while the drawings for straight port and star-swirl port fuel grains were sent to CRP Technology to be printed from Windform XT 2.0. Straight port paraffin and paraffin/acrylic diaphragm fuel grain drawings were sent to 3D Systems, Inc. to be printed. The machine used for printing the paraffin and paraffin/acrylic fuel grains is meant for printing acrylic parts and uses the wax as the support material. Because paraffin wax is a desirable hybrid rocket fuel, it was required that the paraffin be retained within the fuel grain design.

In order to achieve printed paraffin and paraffin/acrylic fuel grains, a 0.020” shell of PMMA was designed as the outer layer of the part to be printed, with the internal diaphragms and mixing sections also included for those particular fuel grains. The printer would then print the closed acrylic shell, and the paraffin support material within the shell would not be removed. Features too small for the machine to resolve needed to be added to the drawing in order to have the machine print the enclosed geometry, since the machine would normally need an opening to remove the paraffin support material.[67]

Straight port paraffin, ABS, and Windform XT 2.0 fuel grains were first tested to determine baseline regression rate and combustion efficiency behavior. The straight port fuel grains would then be used for comparison with complex geometries. Star-swirl fuel gains with ½ tpi were tested for grains made from ABS and Windform XT 2.0 to examine performance enhancement due to the complex port shape. The paraffin/acrylic diaphragm fuel grains and the paraffin/acrylic diaphragm fuel grains with a mixing section were also tested and analyzed for regression rate and combustion efficiency. All fuel grains were printed using the FDM process, except for the SLS-manufactured Windform XT 2.0 grains.

4.2 Experimental Setup

4.2.1 Long-Grain Center-Perforated Hybrid Rocket Motor

Most small-scale hybrid rocket work at Penn State’s HPCL has used the LGCP hybrid rocket motor with gaseous oxygen.[44–46,53] This work examined the use of 3D printing techniques to fabricate solid fuel grains with complex port geometry and internal structures to enhance regression rate and combustion efficiency. The LGCP motor is cartridge-loaded and useful for conducting screening tests of fuel formulations and geometries with minimum turn-around time

and limited material requirements. Downtime between individual tests is generally around 30 minutes while a new fuel grain is loaded and other adjustments are made for the next test.

The rocket motor is a 21 in. long stainless steel pipe with a 3 in. outer diameter (O.D.) and a 1.5 in. inner diameter (I.D.). Each end of the motor has a piston O-ring-sealed stainless steel cap. The fore end cap connects to the feed system and houses an interchangeable injector plate, while the aft end cap contains a nozzle assembly that houses an interchangeable graphite nozzle. Connections for the electric match pyrotechnic igniter and pressure transducers near the injector and the nozzle are included in the wall of the motor. A schematic of the LGCP hybrid rocket motor is provided in Figure 4.4.

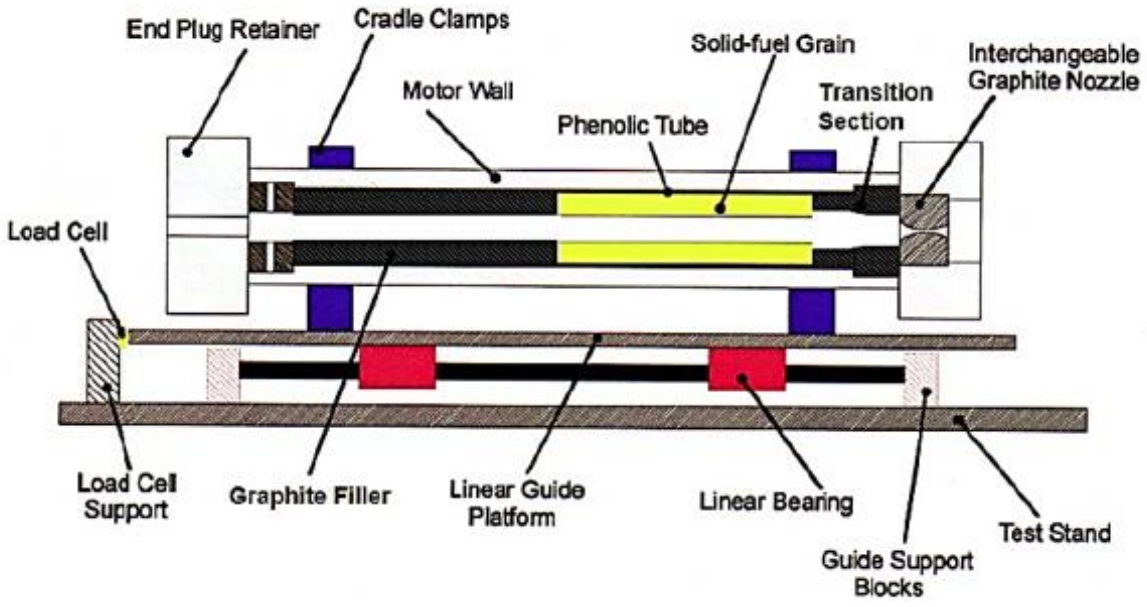

Figure 4.4 LGCP Motor Schematic and Thrust Stand Mount[36]

The stainless steel motor is designed for working pressures up to 12.1 MPa (1,750 psig), however, because hybrid rocket motor performance is not strongly dependent on chamber pressure (see Appendix L) all LGCP motor testing is planned for chamber pressures between

0.69 MPa and 2.1 MPa (100 psig to 300 psig). The interchangeable nozzle throat diameter is chosen for each test to maintain a chamber pressure of 1.4 MPa (200 psig).

Fuel grains of up to 16” in length can be tested in the LGCP motor. Individual fuel grain length is generally dependent on the target O/F ratio and is usually between 3” to 4” for pure paraffin wax. For the purpose of the PUC, all fuel grains tested were 2.5” long due to the design of the unit. However, changes in the design could be made to allow for a different size fuel grain to achieve the desired O/F ratio. The unit could then be printed for the adjusted fuel grain size.

The oxidizer mass flow rate was also adjusted such that the actual firing O/F ratio was near optimal from CEA calculations. Again, due to the constriction on fuel grain length, this was not always possible with the PUC fuel grains. Planning calculations were used to determine the O/F ratio of the test. The spreadsheet uses fuel properties to predict linear and mass regression rates for planning test duration, nozzle size, and O/F ratio. The planning calculations are then used to fill out the pre-test portion of the test data sheet, provided in Appendix M.

Fuel grains for testing in the LGCP motor are first bonded using epoxy into a paper phenolic tube with an O.D. of 1.5” and an I.D. of 1.25”. The paper phenolic protects the motor casing in the event that all of the fuel is consumed within the duration of the test. Because the LGCP motor casing can accommodate fuel grains up to 16” in length, significant empty volume can exist for short fuel grains. Filling the empty volume can account for a significant portion of the pressurization transient during ignition. To help shorten the duration of the motor pressurization, graphite filler pieces with an O.D. of 1.5” and an I.D. of 0.915” are used in the remaining length of the motor to reduce the free volume.

During each test, data are recorded from four pressure transducers, two thermocouples, and a thrust stand load cell at a rate of 1000 Hz. As previously mentioned, two of the pressure

transducers are installed for the combustion chamber, near the injector and the nozzle. In addition, the oxidizer feed system pressure and temperature upstream of the flow control orifice and upstream of the injector plate are recorded. The pressure and temperature at these locations are used to characterize the state of the nitrous oxide.

4.2.2 Nitrous Oxide Feed System

For testing of the candidate fuel grains for the PUC, a nitrous oxide feed system was designed and re-implemented based on the thesis work of Nicholas Favorito at the HPCL.[68] Changes in the feed system design were made as needed to ensure safe and reliable operation. Additional changes were made to calibrate a mass flow rate orifice by suspending the nitrous oxide run tank. A full walkthrough of the nitrous oxide LGCP motor setup is provided in Appendix N. A diagram of the nitrous oxide feed system is given in Figure 4.5.

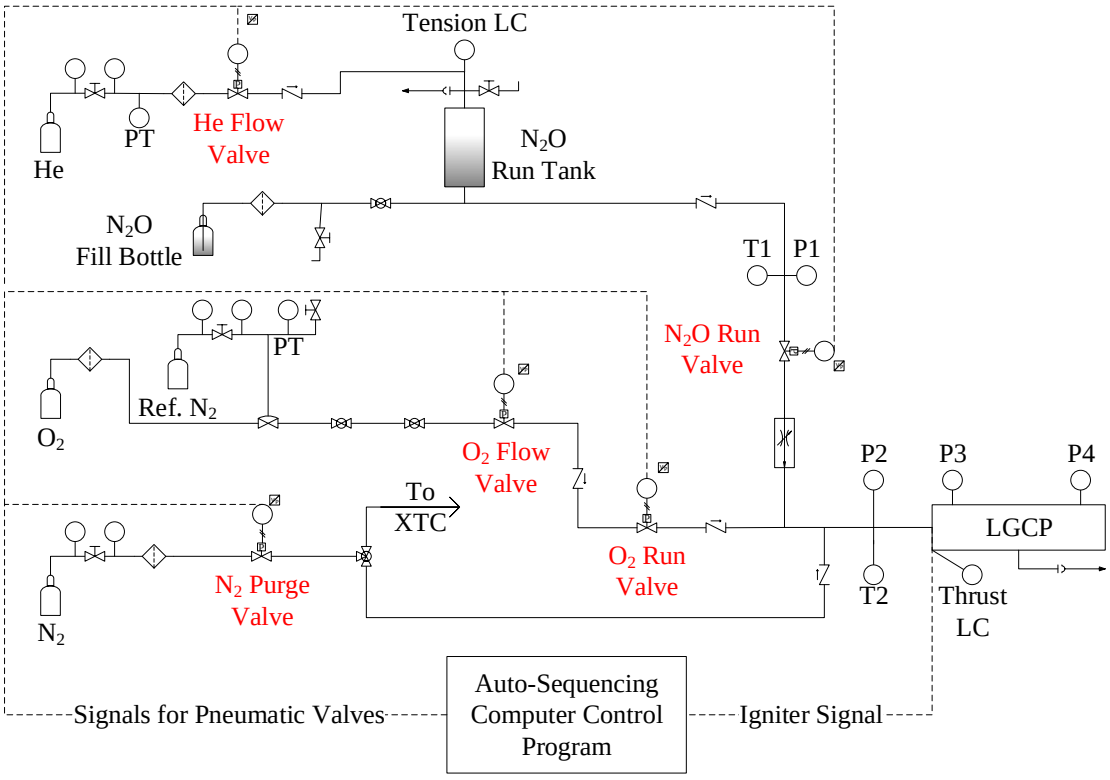

Figure 4.5 Nitrous Oxide Feed System Flow Diagram for the LGCP Motor

Safety was a primary focus during the design and setup of the nitrous oxide feed system. A full hazard analysis of the system was performed and previous papers on nitrous oxide safety were closely examined to avoid dangerous situations such as compression heating and potential ignition sources.[69–75] All flow system components in contact with the oxidizer were cleaned according to the oxygen cleaning procedure in Appendix C. Potential hazards were minimized in the design of the feed system to the extent that was possible, while all other hazards were recognized and understood prior to use of the system.

Liquid nitrous oxide is filled into the run tank at the beginning of a series of tests following the procedure in the test checklist, provided in Appendix O. During a test, a low pressure oxygen flow (50 psig regulator set pressure) is used to create a pure-oxygen environment within the chamber. The electric match igniter is then triggered and the oxygen flow provides an opportunity for rapid flame spreading to occur. Once ignition occurs, the rise in chamber pressure results in a check valve in the oxygen line closing off the supply of oxygen. This occurs within a fraction of a second at the start of the test and is closely followed by the introduction of nitrous oxide. The flow of nitrous oxide, pressurized to the desired feed pressure by helium gas, is controlled using pre-determined valve timing for the test. The use of helium as a pressurant reduces the chance for vapor phase nitrous oxide to be present in the feed system prior to the orifice and maintains a constant feed pressure for mass flow rate determination.

During blowdown of nitrous oxide without a pressurizing gas, the pressure drops as mass is extracted from the tank. The drop in pressure results in liquid nitrous oxide boiling to fill the extracted volume and the temperature in the tank to drop (also resulting in a decrease in vapor pressure of the liquid and an increase in density). This transient behavior would make determining the mass flow rate of the oxidizer extremely difficult.

Valve timing is controlled using the PowerBASIC control code provided in Appendix P. An example of the valve timing is shown in Appendix Q. All valves are pneumatically operated and fail-close except for the nitrogen purge, which is fail-open. This means that in the event of a power disruption, air supply disruption, or other failure during a test, all oxidizer related valves will shut and the nitrogen valve will open to purge the motor and extinguish the flame.

4.2.3 Nitrous Oxide Mass Flow Rate Calibration

Obtaining an accurate mass flow rate of the nitrous oxide is essential for analysis of the motor tests. The regression rate of the solid fuel grain is correlated to the oxidizer mass flux for a hybrid rocket motor, and the c* combustion efficiency is dependent on the mass flow rate of the fuel and oxidizer in the calculation of c*. Many attempts at characterizing the mass flow rate through a 0.035" diameter converging/diverging orifice resulted in inconsistent results. These attempts are discussed in detail in Appendix R and were used in arriving at the final method that will be discussed next.

The best method found for determining the nitrous oxide mass flow rate during a hot fire test was to establish a correlation with the pressure upstream of the orifice for a given test series temperature (within a few degrees Celsius) through cold flow tests. Since ambient conditions are very near the critical temperature of nitrous oxide, its properties vary significantly with temperature and thus this calibration must be done at the same temperature as the test series. Outside air temperatures were found to have a large effect on mass flow rates through the orifice due to changing the temperature of the nitrous oxide. By performing the calibration at the test condition temperature, accurate results were obtained. Thermocouple measurements ensure that the nitrous oxide during testing is within a couple degrees Celsius of the calibration flow tests. If testing is to be conducted on a day where this is not the case, the calibration must be rerun.

The nitrous oxide mass flow rates were calibrated using flow tests pressurized to 800 psig, 1,000 psig, and 1,200 psig with helium (covering the normal range of upstream operating conditions). The best setup for calibration of the orifice was to suspend the nitrous oxide run tank from a 100-lb tension quartz force sensor (zero displacement), as shown in Figure 4.6. The sensor discharge time constant was found prior to testing and the sensitivity was calibrated before and after each flow test. Each test was run using the valve timing for a 10-second test. This allowed for the calibration to be performed in almost the same way as if a test was run. A correction was performed to overcome the signal decay of the quartz sensor, and DC coupling with the signal conditioner was used to extend the discharge time constant.

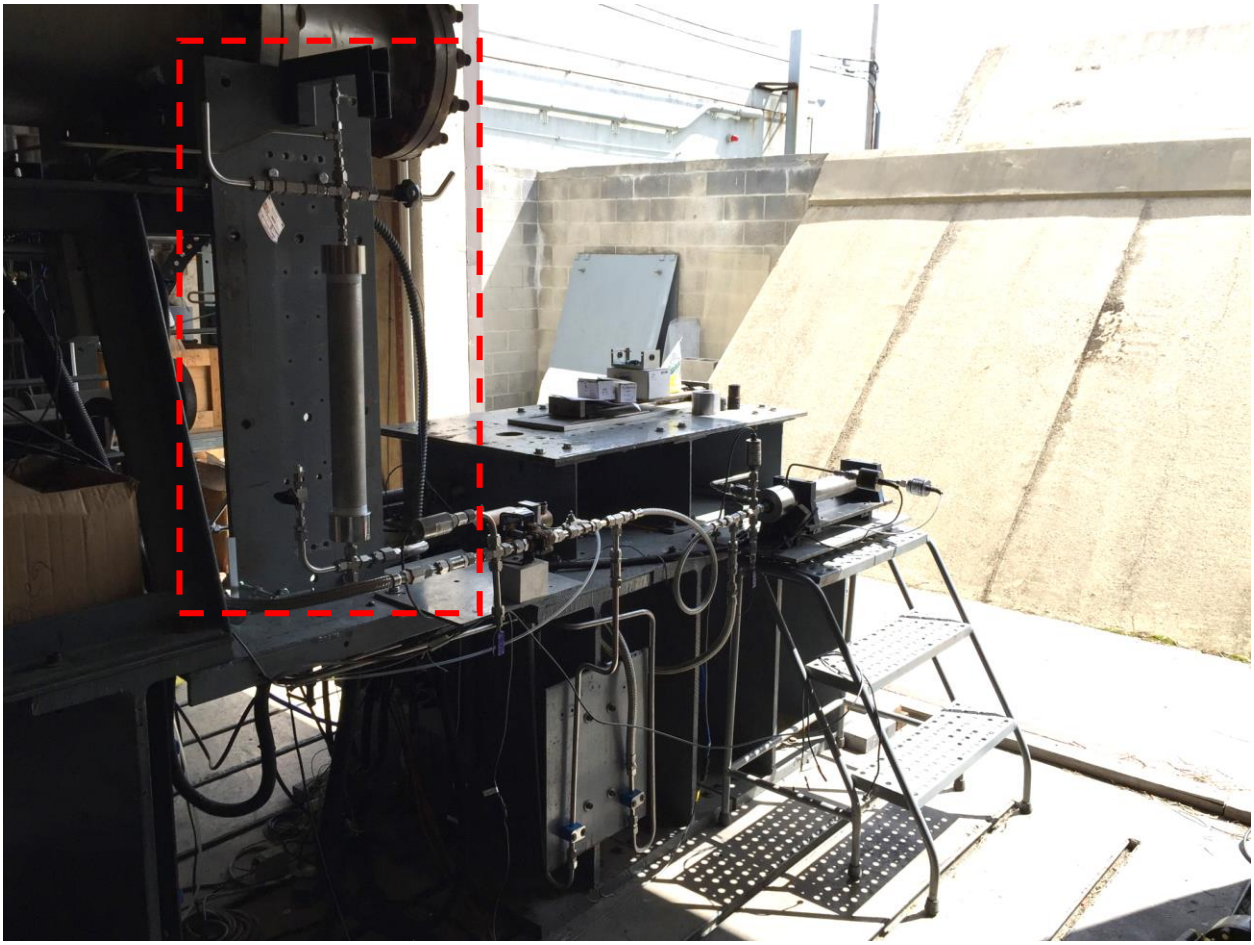

Figure 4.6 Hanging Nitrous Oxide Run Tank Setup for Mass Flow Rate Calibration

In addition, a needle valve was attached to the nozzle assembly for the calibration flow tests to maintain a chamber pressure near 200 psig (test target pressure), as shown in Figure 4.7. To reduce the pressurization transient of the empty motor chamber, aluminum fuel grain blanks with a 0.25” diameter port were machined to fill the motor volume. It is believed that in previous tests the downstream pressure indirectly affected the behavior of the nitrous oxide through the orifice. If the nitrous oxide experiences an isentropic drop from 10 °C and 800 psig to atmospheric pressure, the temperature drops to roughly -90 °C. When the motor pressure is present downstream of the orifice, the drop from 10 °C and 800 psig to 150 psig results in a temperature of roughly -40 °C. It is believed that the large temperature difference results in a significant change in the thermal condition at the orifice as a consequence of conduction through the tubing walls and orifice, and causes the liquid nitrous oxide to chill further as it enters the orifice, changing its behavior.

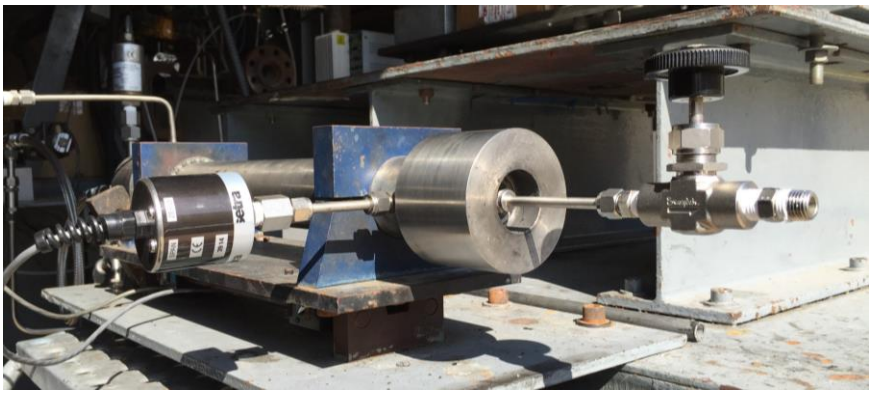

Figure 4.7 Needle Valve Attached to Interchangeable Nozzle Assembly

Previous attempts also found that the vibration due to the nitrous oxide fluid flow when the run valve opens caused too much noise in the force sensor signal to measure the mass change of the tank over the first two seconds. The control program ran the ten second test as if it was an actual motor firing, and then the slope of the force sensor signal versus time was found for the

last eight seconds. This provided a value in [V/s], which was converted to a mass flow rate in [g/s] by dividing by the sensor sensitivity calibration result in [V/g]. A plot of the corrected force sensor signal and various pressures for a 1,200 psig calibration flow test is shown in Figure 4.8.

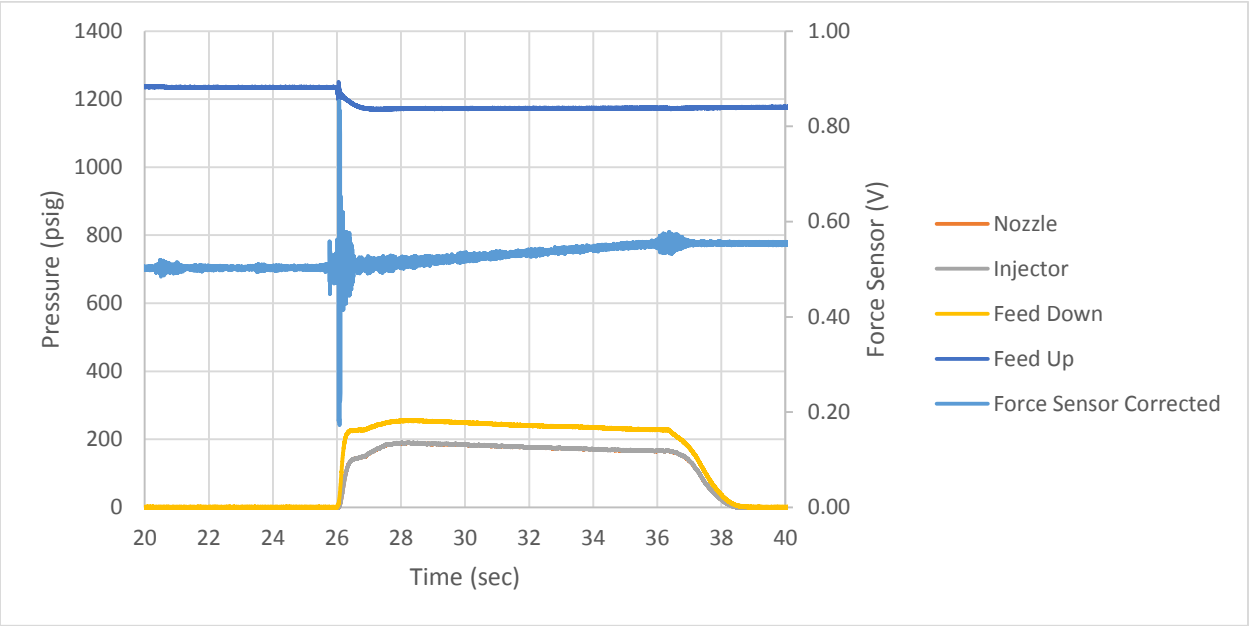

Figure 4.8 Nitrous Oxide Mass Flow Rate Calibration Flow Test for 1200 psig

The results from the calibration cold flow tests were correlated to the helium pressure upstream. The mass flow rate for each hot fire motor test was calculated using this correlation from the measured pressure upstream of the orifice.

4.3 Analysis

The use of complex fuel grain geometries makes determining linear regression rate and port area for oxidizer mass flux difficult. The typical averaging techniques commonly used for straight port fuel grains is not sufficient for complex port shapes. For this reason, this section will detail the methods used for analysis of each fuel grain type to clarify how these calculations were made. Images of post-burn straight port, star-swirl, and diaphragm fuel grains show the significant differences in geometry in Figure 4.9.

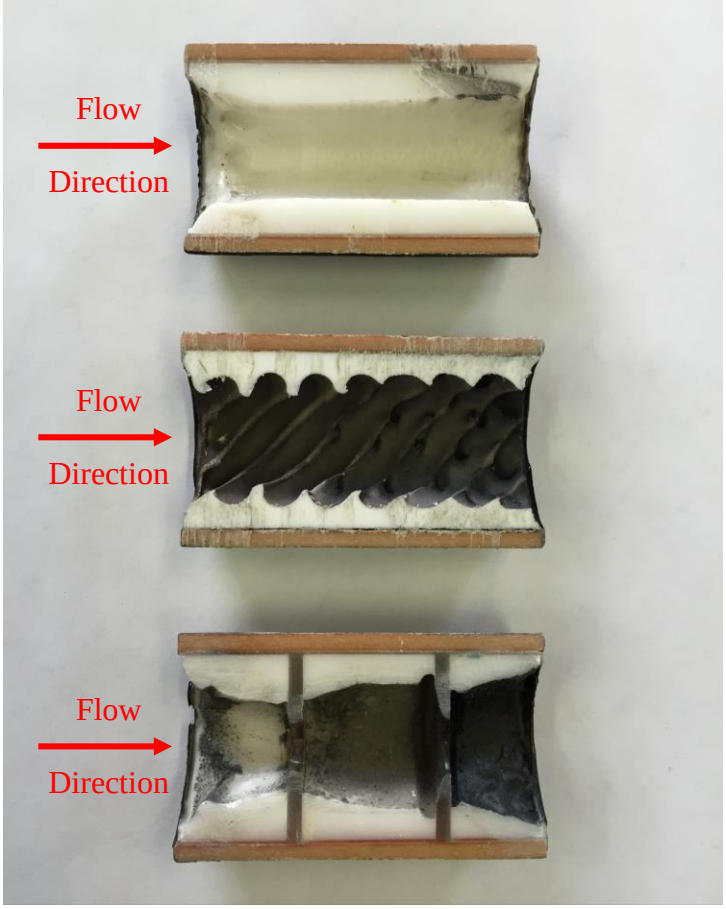

Figure 4.9 Straight Port Paraffin, Star-Swirl Port White ABS, and Paraffin/Acrylic 0.100" Diaphragm Fuel Grains Post-Burn

Prior to each test, initial fuel grain mass, length, and port diameter were recorded on the test data sheet. For star-swirl fuel grains, the solid model from SolidWorks was used for the initial dimensions. The fuel grains were printed to the dimensions from the model and confirmed prior to firing. Paraffin/acrylic fuel grains with a diaphragm and mixing section have a different initial port size for the acrylic mixing section, therefore, there are two initial dimensions. These initial measurements were used to characterize the hybrid rocket motor's performance using the techniques described in the following sections and measurements obtained after testing.

4.3.1 Straight Port Fuel Grains

Analysis for straight port fuel grains was performed using the averaging techniques typically used for determining performance of a hybrid rocket motor. Final fuel grain mass and port diameter were recorded after each test and used in calculating regression rate and combustion efficiency.

The average regression rate, $\bar{\dot{r}}$, is determined as the final port radius, r_f, subtracted by the initial port radius, r_i, divided by the burn duration, t_b. This expression is provided in Eq. (4.1). The final port radius is taken as an average of the fore and aft end radii of the fuel grain.

$$\bar{\dot{r}} = \frac{r_f - r_i}{t_b} \tag{4.1}$$

The burn duration was obtained from the pressure-time traces showing ignition and the flame being extinguished by the nitrogen purge. An example pressure-time trace is shown in Figure 4.10 and labelled to show the events during the test.

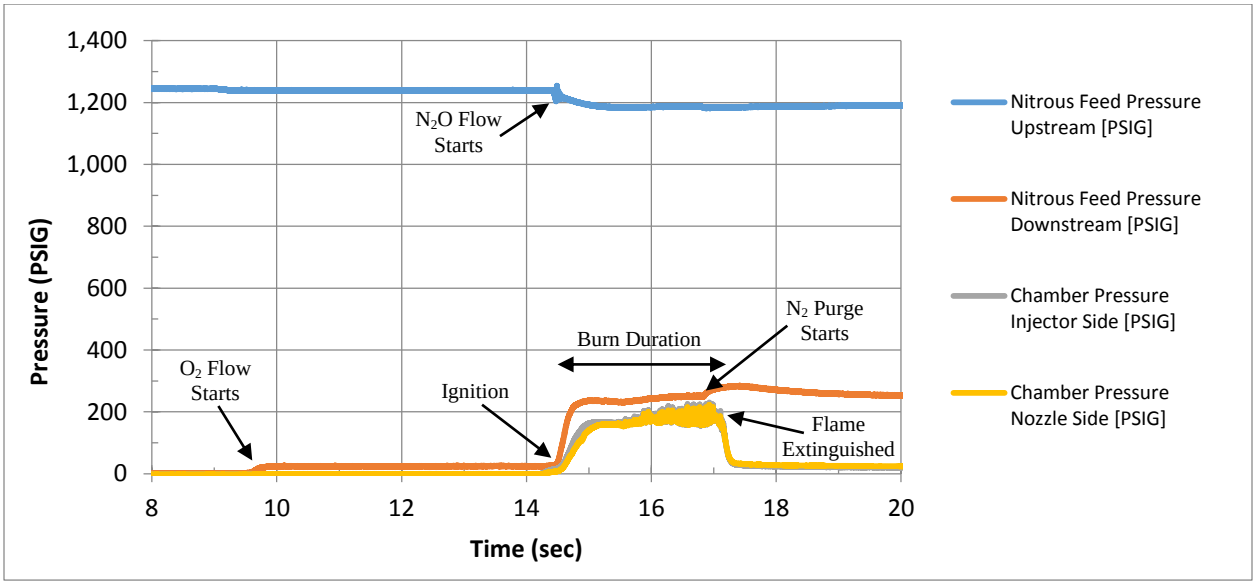

Figure 4.10 Pressure-Time Trace for a LGCP Hybrid Motor Test

The average oxidizer mass flux, $\bar{G}_{ox}$, which the regression rate is typically plotted as a function of, is simply the average oxidizer mass flow rate, $\overline{\dot{m}}_{ox}$, divided by the average port area during the burn. The oxidizer mass flow rate is calculated from the calibration correlation of mass flow rate to the average pressure upstream of the orifice (at a representative temperature).

$$\bar{G}_{ox} = \frac{2\bar{\dot{m}}_{ox}}{\pi\left(r_f + r_i\right)^2} \tag{4.2}$$

The combustion efficiency of the rocket motor is determined by comparing the experimental characteristic velocity to the theoretical value obtained from the NASA CEA2 code. The experimental c* value is calculated as in Eq. (4.4), where $\overline{P}_c$ is the average chamber pressure during the test, A^* is the nozzle throat area, and $\overline{\dot{m}}_{ox}$ and $\overline{\dot{m}}_f$ are the average oxidizer and fuel mass flow rates, respectively. The fuel mass flow rate is an average calculated using Eq. (4.3); the initial fuel mass, M_i, subtracted by the final fuel mass, M_f, divided by the burn duration. The c* combustion efficiency is then calculated using Eq. (4.5) as the ratio of the experimental c* and theoretical, or ideal, c*.

$$\bar{\dot{m}}_f = \frac{M_i - M_f}{t_b} \tag{4.3}$$

$$c^* = \frac{\overline{P}_c A^*}{\bar{\dot{m}}_{ox} + \bar{\dot{m}}_f} \tag{4.4}$$

$$\eta_{c^*} = \frac{c^*}{c^*_{ideal}} \tag{4.5}$$

This method is straight forward for calculating hybrid rocket motor performance parameters for straight port fuel grains. For complex geometry fuel grains, the c* combustion efficiency could be calculated in the same manner, however, average regression rate and oxidizer mass flux were found using the procedures in the following sections.

4.3.2 Star-Swirl Port Fuel Grains

Star-swirl port fuel grains required a special analysis technique to appropriately characterize regression rate and port area. The method used follows that developed by Armold at the HPCL.[44] The "Offset Entities" function within SolidWorks was used to model the surface regression during a burn. A "Design Study" calculated port area for incremental offsets from the original port shape to the final measured fuel grain dimensions.

Final star-swirl port fuel grain mass and port dimensions were measured and recorded. Port dimensions for "ridges" and "valleys" were individually considered, where the ridges are the peaks left behind after the burn closest to the center of the star and the valleys are the points farthest from the center of the fuel grain. Equations for determining a characteristic offset were developed by Armold to weigh the different regression rates of the ridges and valleys. Because the ridges regress faster due to the presence of the flame on both sides of the peak, the real characteristic offset was weighted towards the regression of the valley. The regressed distance for the ridges, D_r, and valleys, D_v, are calculated using Eq. (4.6) and Eq. (4.7). The resulting weighted characteristic regressed distance is given as D_c in Eq. (4.8).

$$D_r = \frac{1}{2}\left(D_{rf} - D_{ri}\right) \tag{4.6}$$

$$D_v = \frac{1}{2}\left(D_{vf} - D_{vi}\right) \tag{4.7}$$

$$D_c = D_v + \frac{1}{3}(D_r - D_v) \tag{4.8}$$

The average regression rate of the fuel surface is then calculated as the characteristic regressed distance over the duration of the burn as in Eq. (4.9).

$$\bar{\dot{r}} \cong \frac{D_c}{t_b} \tag{4.9}$$

An example of the Offset Entities Design Study analysis in SolidWorks is shown in Figure 4.11 and the resulting port area and surface area are plotted in Figure 4.12. The star-swirl geometry results in a steadily increasing port area, however, fuel surface area reaches a peak and begins to decrease due to the reduction of surface area as the ridges regress.

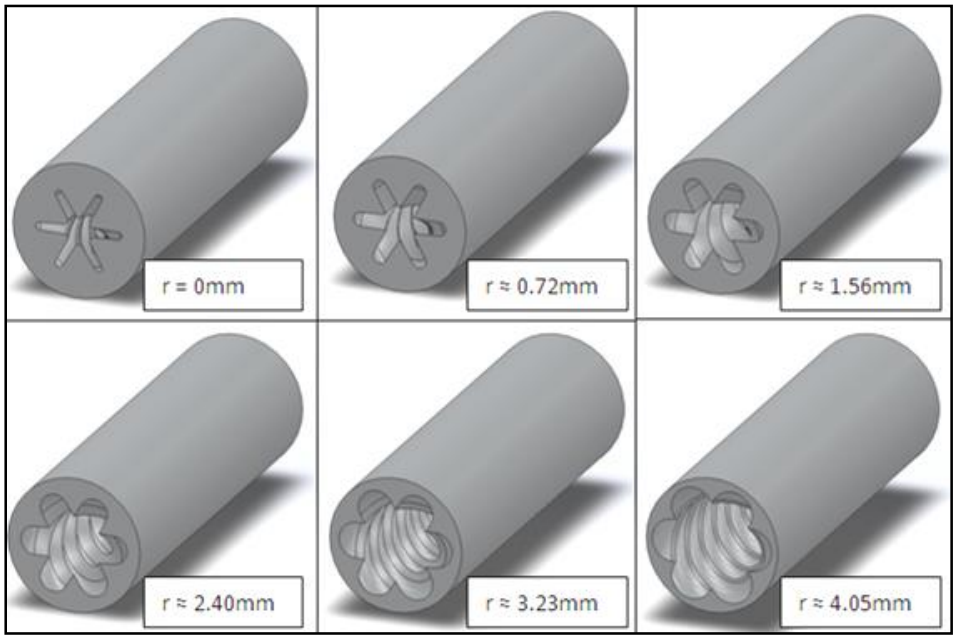

Figure 4.11 Design Study of Star-Swirl Fuel Grain Regression in SolidWorks[44]

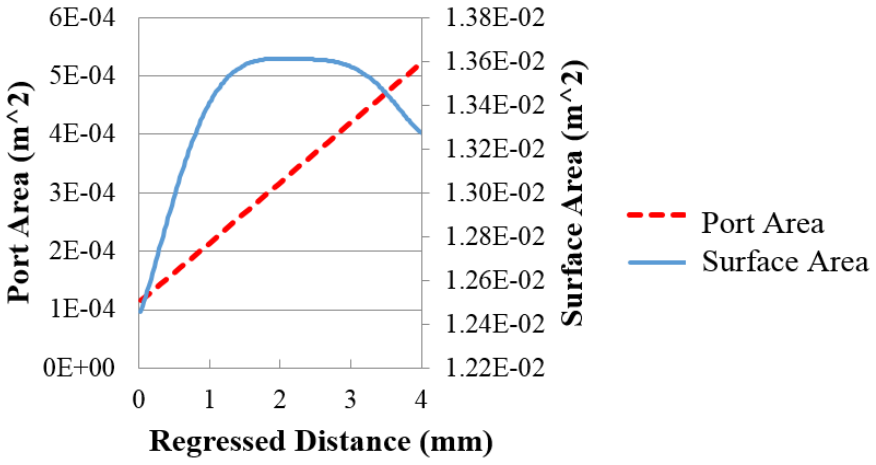

Figure 4.12 Port Area and Surface Area with Regressed Distance for Star-Swirl Fuel Grain[44]

The SolidWorks analysis technique developed by Armold at the HPCL makes use of accessible CAD software to accurately model the regression of the star-swirl fuel surface without the need for developing ad-hoc analytical methods. Armold then developed an analysis program in Microsoft Excel to use incremental time steps to calculate instantaneous regressed distance and port area. This made for accurate calculation of average oxidizer mass flux.

The regression rate is calculated using a correlation of the form given in Eq. (4.10), where a and n are empirical constants for the given fuel and oxidizer combination and f_c is a correction factor for the non-cylindrical geometry. The initial port area, A_p, is used with the oxidizer mass flow rate to calculate oxidizer mass flux in Eq. (4.11). The regressed distance from time t_n to time t_{n+1} can be calculated using Eq. (4.12). Using the new regressed distance, another iteration can be made. This is done for the duration of the burn, and the oxidizer mass flux over these times is averaged to arrive at the average oxidizer mass flux, $\bar{G}_{ox}$.

$$\dot{r} = f_c a G_{ox}^n \tag{4.10}$$

$$G_{ox} = \frac{\bar{\dot{m}}_{ox}}{A_p} \tag{4.11}$$

$$r(t) = \int_{t_n}^{t_{n+1}} \dot{r}(t)dt = \int_{t_n}^{t_{n+1}} f_c a G_{ox}^n dt = f_c a \tilde{G}_{ox}^n \Delta t \tag{4.12}$$

This method could be used for various complex port geometries, but for this work only star-swirl port fuel grains were analyzed in this manner. The diaphragm fuel grains created different challenges and the following section describes the method developed to analyze these types of fuel grains for average regression rate and oxidizer mass flux.

4.3.3 Diaphragm Fuel Grains

Diaphragm fuel grains, including the diaphragm with mixing section grains, designed and tested in this work, once fired, resulted in complex port shapes that restricted the use of typical straight port analysis techniques. In order to determine regression rate in diaphragm fuel grains, an analysis technique was developed to characterize the regression rate along the length of the fuel grain using a scanner.

4.3.3.1 Paraffin/Acrylic Diaphragm Fuel Grains

As with each method, measurements of the post-burn mass were first recorded. The diaphragm fuel grain samples were then sectioned in half along their length and both halves were placed on a flat-bed scanner and captured in a scaled image. This imaging method ensures there is no distortion in image scaling due to capture angle. The scanned image was then imported into ImageJ[65] and distance measurements could then be obtained based on the number of pixels from one location to another. The pixel scaling is built into the scanner software, however, this scaling was verified by including a ruler in the scanned image. An example of two scanned 0.050" diaphragm fuel grains is provided in Figure 4.13.

Figure 4.13 Two Scanned 0.050" Diaphragm Paraffin/Acrylic Fuel Grains

Figure 4.13 clearly shows the increased regression rate in the middle and aft ends of the fuel grain. Not unexpectedly, the behavior at the fore end of the fuel grain appears similar to that of a straight port paraffin fuel grain. Because the three individual sections have different regression rates, each was treated separately in the analysis. The averaging techniques used for straight port fuel grains are used for each section, as if each is an individual fuel grain. This method allows for accurate calculation of average regression rate and direct comparison of the fore, middle, and aft ends of each fuel grain at various oxidizer mass flux values.

The regression rate for each section is calculated following Eq. (4.1). A single average oxidizer mass flux is calculated using Eq. (4.2), however, the final port area used is the average of the individual port areas of the three sections. Combustion efficiency is calculated in the same way as for the straight port fuel grains and assumes an average O/F ratio for the fuel-oxidizer combination. In reality, the three sections experience different O/F ratios due to the increase in regression rate downstream of the diaphragms and oxidizer consumed along the length of the grain. CEA calculations were performed for the adjusted paraffin and acrylic weight ratios.

4.3.3.2 Paraffin/Acrylic 0.100” Diaphragm with Acrylic Mixing Section Fuel Grains

While similar to the initial paraffin/acrylic diaphragm fuel grain design, the diaphragm with mixing section fuel grains required a slightly different procedure for analysis. In the same manner as for the original design, the fuel grain mass was measured after the test and the fuel grains were sectioned in half. The samples were scanned and analyzed, but regression rates were calculated for two sections; upstream of the diaphragm (paraffin) and downstream of the diaphragm (acrylic). The average port area was found by averaging the average of the paraffin and acrylic mixing section port areas before and after the test. The remainder of the procedure followed that of the initial diaphragm designs.

4.4 Results

The primary focus of the experimental hybrid rocket motor test series was to determine regression rate and combustion efficiency of the various fuel compositions and geometries with nitrous oxide. The before and after measurements of the fuel grains, along with the recorded pressure and temperature data, provide the necessary information to make these calculations. The regression rate and combustion efficiency results are useful in making direct performance comparisons between fuel formulations and geometries. These comparisons are then used for selecting the fuel composition and geometry for the PUC and for refining the grain designs. Due to the limited mass and volume available, combustion efficiency is considered to be particularly important. The PUC needs to be designed such that very little mass and volume is wasted.

Plots of regression rate in the following sections, sections 4.4.1 and 4.4.2, include straight port correlations for comparison with results from other works where applicable. Nitrous oxide test data and correlations for regression rate with oxidizer mass flux are less available than those for oxygen. For the following comparisons, the correlations, provided in Eq. (4.13) and (4.14) for HTPB and PMMA, respectively, were developed by Doran et al.[76]

$$\bar{\dot{r}}_{HTPB} = 0.417\bar{G}_{ox}^{0.347} \tag{4.13}$$

$$\bar{\dot{r}}_{PMMA} = 0.284\bar{G}_{ox}^{0.335} \tag{4.14}$$

For means of comparison, the HTPB correlation is plotted with the ABS and Windform XT 2.0 data. It has been shown that ABS behaves similarly to HTPB with nitrous oxide but has a slightly lower regression rate.[63] For paraffin/acrylic fuel grains, only acrylic has been well correlated with nitrous oxide and is used for comparison with the 0.100” diaphragm with mixing section fuel grains.

4.4.1 Star-Swirl Port Fuel Grains

As mentioned previously, the ½ tpi star-swirl port geometry was tested for ABS in natural, white, and black, and for the Windform XT 2.0 carbon-filled polyamide material. This particular geometry was selected based on previous test results of PMMA fuel grains with oxygen that showed significantly increased regression rates, especially for the ½ tpi geometry as compared with ¼ and $^1/_8$ tpi geometries.[44–46]

Straight port fuel grains were tested using the LGCP motor to establish baseline data. Star-swirl port fuel grains were then tested and analyzed for comparison of regression rate and combustion efficiency to the straight port tests. A summary of the test results is provided in Table 4.1. The resulting regression rate data for straight port and star-swirl fuel grains are plotted in Figure 4.14.

Table 4.1 ABS and Windform XT 2.0 Test Results

ABS and Windform XT 2.0 Test Results Summary								
Fuel	Geometry	Length (in)	Avg. Chamber Pressure (psig)	Avg. O/F	Avg. Gox (kg/(m^2-s))	Avg. Regression Rate (mm/s)	Avg. Mass Burning Rate (kg/s)	c* Combustion Efficiency
Printed Natural ABS	Straight Port	2.5	144.3	19.31	240	0.58	0.0017	0.664
Printed Natural ABS	1/2 tpi ST-SW	2.5	132.2	4.94	169	0.73	0.0065	0.542
Printed Natural ABS	Straight Port	2.5	173.7	20.71	422	0.77	0.0022	0.709
Printed Natural ABS	1/2 tpi ST-SW	2.5	176.5	5.38	246	1.00	0.0086	0.606
Printed White ABS	Straight Port	2.5	169.3	16.89	206	0.62	0.0019	0.750
Printed White ABS	1/2 tpi ST-SW	2.5	166.5	5.80	109	0.99	0.0056	0.650
Printed Black ABS	Straight Port	2.5	144.6	17.71	232	0.61	0.0018	0.607
Printed Black ABS	1/2 tpi ST-SW	2.5	139.8	5.76	114	0.94	0.0056	0.532
Printed Windform	Straight Port	2.5	193.1	42.28	548	0.14	0.0008	0.551
Printed Windform	1/2 tpi ST-SW	2.5	276.6	12.50	156	0.26	0.0026	0.657

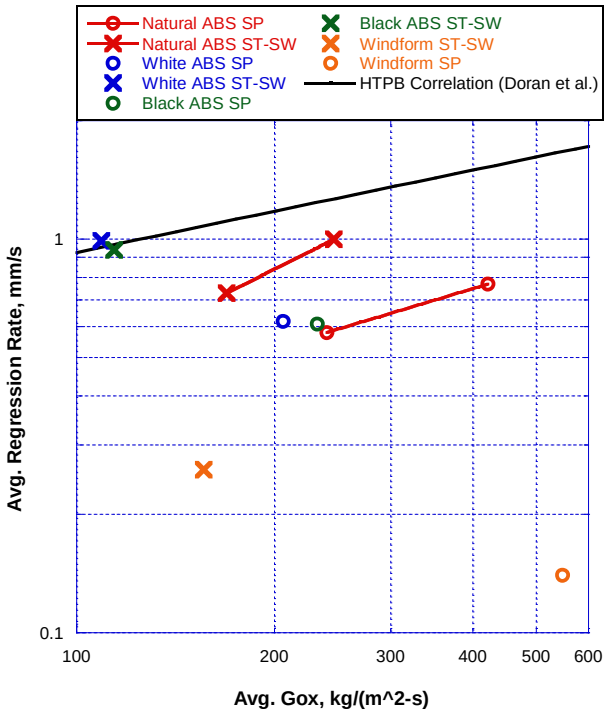

Figure 4.14 Regression Rate Data for ABS and Windform XT 2.0 Straight Port and Star-Swirl Fuel Grains

The regression rate for star-swirl port geometry fuel grains was found to be significantly higher than for straight port grains, as expected from the previous PMMA testing. Natural, white, and black ABS were tested to examine the effect of the different coloration on regression rate. It was expected that the pigment material may act to slow the regression rate compared to pure ABS. From Figure 4.14 it appears that both the white and black ABS fuel grains had higher regression rates than the pure ABS (with the white ABS slightly higher than the black). It is possible that the addition of the pigments acts to increase radiation absorption and thus heat feedback to the fuel surface, but it is difficult to make a definitive conclusion without knowing the makeup of the pigments. Additional information about the added pigments would be needed from the supplier and additional hot-fire tests would need to be run for the various colors.

From Figure 4.14 it is also evident that the Windform XT 2.0 fuel grains had extremely low regression rates, even with the star-swirl port geometry. While a low regression rate was expected for this particular fuel, it is also important to note that the O/F ratios for these tests were far from optimal and that this will also result in a decrease in regression rate. In order to reach the optimal range of O/F ratios, the fuel grain surface area would need to be dramatically increased (i.e. a very long fuel grain). This result is the primary reason for considering a cartridge-loaded fuel grain with higher performance composition, rather than including the fuel grain in the SLS print of the unit (as done previously by Dushku and Mueller[27]).

4.4.2 Diaphragm Fuel Grains

The paraffin/acrylic diaphragm fuel grains were designed to enhance regression rate without causing the satellite to spin. The 0.050" and 0.100" diaphragm designs were tested to examine the effect of diaphragm thickness on the regression rate enhancement; it was expected that the thicker diaphragms would maintain a greater height off of the paraffin fuel surface. Printed straight port paraffin fuel grains were also tested to establish a baseline for comparison. Following the test series with the original diaphragm fuel grain design, the paraffin/acrylic diaphragm with mixing section was tested and analyzed for regression rate and combustion efficiency. The focus of this design was to increase the combustion efficiency of the paraffin-based fuel grains. A summary of test results for paraffin and paraffin/acrylic fuel grains is provided in Table 4.2. The regression rate results of the 0.050" and 0.100" diaphragms are given in Figures 4.15 and 4.16, respectively. The results for the 0.100" diaphragm with mixing section fuel grains are plotted in Figure 4.19.

For these particular fuel grains, plots for regression rate are separated by section along the fuel grain. For the average oxidizer mass flux of a test, a data point is provided at each

section of the fuel grain (fore/mid/aft for diaphragms; paraffin/acrylic for diaphragm with mixing section). The fore end of the diaphragm fuel grains was fairly similar in regression rate behavior to that of a straight port fuel grain, which was expected.

Table 4.2 Paraffin and Paraffin/Acrylic Test Results

Paraffin and Paraffin/Acrylic Test Results Summary								
Fuel	**Geometry**	**Length (in)**	**Avg. Chamber Pressure (psig)**	**Avg. O/F**	**Avg. Gox (kg/(m^2-s))**	**Avg. Regression Rate (mm/s)**	**Avg. Mass Burning Rate (kg/s)**	**c* Combustion Efficiency**
Printed Paraffin/Acrylic	0.050" Diaphragm	2.5	162.0	4.24	215	2.04 2.77 3.15	0.0077	0.432
Printed Paraffin/Acrylic	0.050" Diaphragm	2.5	190.6	4.29	227	2.41 2.98 3.41	0.0091	0.553
Printed Paraffin/Acrylic	0.050" Diaphragm	2.5	187.9	4.05	316	2.76 4.07 4.79	0.0113	0.555
Printed Paraffin/Acrylic	0.100" Diaphragm	2.5	97.8	5.76	360	1.80 2.58 2.90	0.0056	0.268
Printed Paraffin/Acrylic	0.100" Diaphragm	2.5	168.6	4.16	257	2.55 3.54 4.09	0.0094	0.485
Printed Paraffin/Acrylic	0.100" Diaphragm	2.5	176.9	4.35	360	2.91 3.55 4.75	0.0106	0.334
Printed Paraffin/Acrylic	0.100" Diaphragm and Mixing Section	2.5	233.1	7.04	152	1.82 0.48 	0.0046	0.672
Printed Paraffin/Acrylic	0.100" Diaphragm and Mixing Section	2.5	230.1	7.49	205	2.08 0.53 	0.0052	0.715
Printed Paraffin/Acrylic	0.100" Diaphragm and Mixing Section	2.5	211.7	8.57	258	2.27 0.57 	0.0054	0.681
Printed Paraffin	Straight Port	2.5	132.7	5.56	208	1.92	0.0059	0.450
Printed Paraffin	Straight Port	2.5	163.5	5.54	224	2.39	0.0071	0.518
Printed Paraffin	Straight Port	2.5	174.6	6.06	275	2.61	0.0078	0.598

Note: Average regression rate for diaphragm fuel grains is separated by section. Top to bottom corresponds to fore to aft end of the fuel grain.

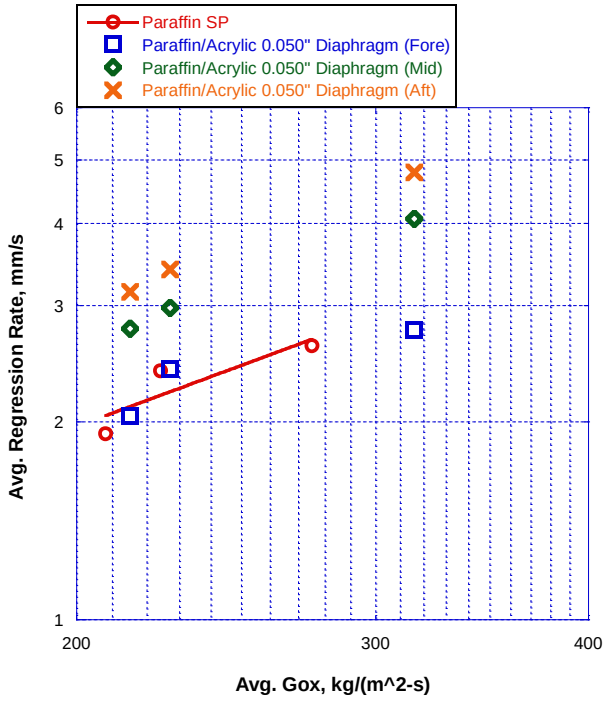

Figure 4.15 Regression Rate Data for Paraffin/Acrylic 0.050” Diaphragm Fuel Grains

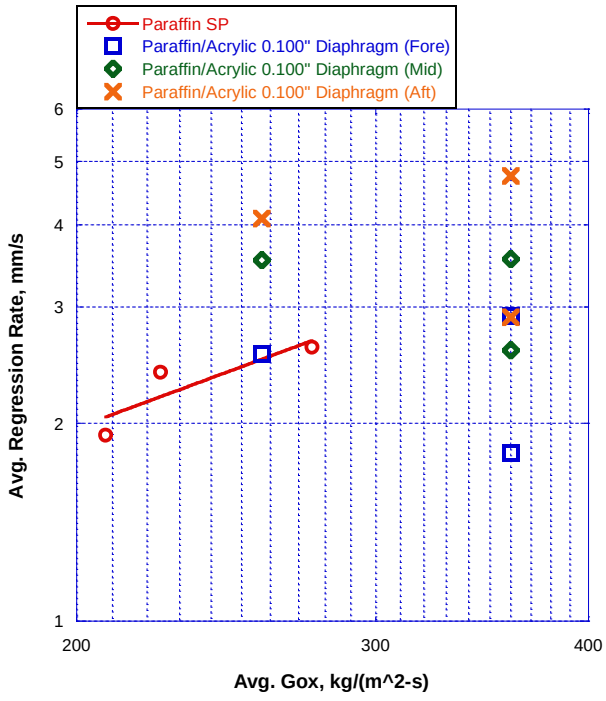

Figure 4.16 Regression Rate Data for Paraffin/Acrylic 0.100” Diaphragm Fuel Grains

In Figure 4.16, the fore/mid/aft data points overlap for two tests at an oxidizer mass flux of 360 kg/m^{2}s. The lower regression rate data points correspond to a lower oxidizer mass flow rate. However, the test duration for that test was too short and the fuel grain port did not regress significantly. This results in a high average oxidizer mass flux value and a larger error associated with that particular test. The results for 0.050” diaphragm fuel grains from Figure 4.15 are more representative of the trend that would be expected for the 0.100” diaphragm fuel grains in Figure 4.16. The other two 0.100” diaphragm data points confirm this. Figure 4.17 includes both the 0.050” and 0.100” diaphragm sets of regression rate data.

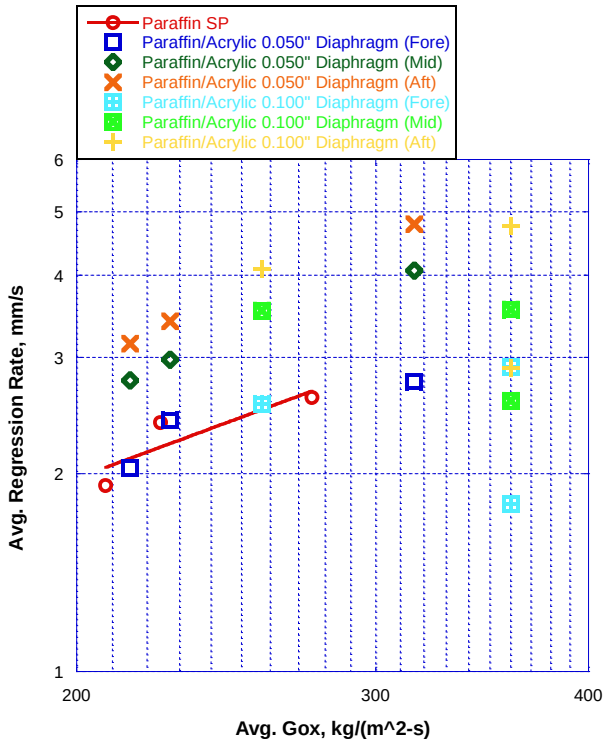

Figure 4.17 Regression Rate Comparison for 0.050” and 0.100” Diaphragm Fuel Grains

Interesting to note in comparing the 0.050” and 0.100” diaphragm fuel grains is the diaphragm height did not appear to significantly change the regression rate enhancement. However, side-by-side visual inspection revealed that the 0.050” diaphragms had a tendency to

chip away and cause uneven burning in the downstream sections, while the 0.100” diaphragms maintained a circular port much more effectively. This difference is shown in Figure 4.18. The non-uniform port can result in localized changes in regression behavior and cause burnout of the fuel on one side of the fuel grain before the other. For the PUC, this should be avoided such that all of the fuel can be consumed.

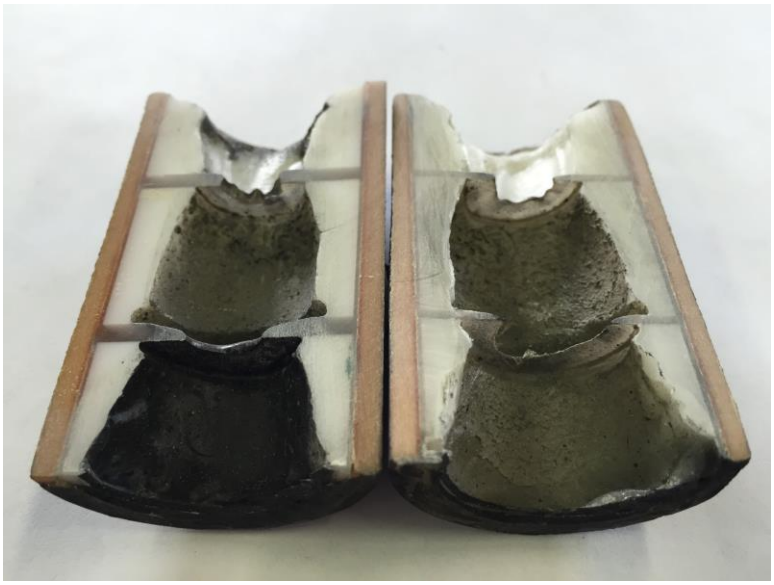

Figure 4.18 Comparison of 0.100” Diaphragm (left) and 0.050” Diaphragm (right)

For this reason, the paraffin/acrylic 0.100” diaphragm with mixing section design uses a 0.100” diaphragm. This geometry was designed to increase combustion efficiency compared to the original two diaphragm design. Combustion efficiency for the two diaphragm design was the same or lower than straight port paraffin, as seen in Table 4.2. This will be discussed in further detail in the next section.

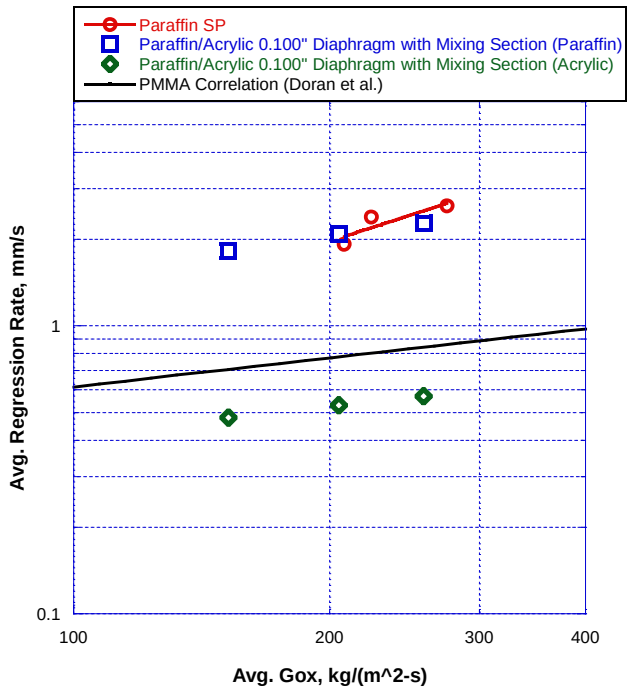

Figure 4.19 Regression Rate Data for Paraffin/Acrylic 0.100" Diaphragm with Mixing Section Fuel Grains

The regression rate results from the paraffin/acrylic diaphragm with mixing section fuel grains are provided in Figure 4.19. The data were consistent with what was expected. The front paraffin section behaved similarly to a straight port paraffin fuel grain, while the rear acrylic section acted as a mixing section and regressed more slowly. The acrylic section regressed slower than the correlation provided by Doran et al., however, the power fit of the correlation appears to be consistent with the slope of the acrylic section test data on the log-log scale.

4.4.3 Combustion Efficiency Comparisons

The combustion efficiency of the PUC motor is of particular importance due to the limited mass and volume available for the propellant. The nitrous oxide tank and the solid fuel grain must fit within these requirements, and the motor should be as efficient as possible at consuming the fuel and oxidizer fully. Any non-completely-burned fuel is a loss from the ideal performance. The combustion efficiency for motor firings of each fuel grain was calculated in the manner described previously. The experimental c* was calculated from the test data and then divided by the ideal c* from the NASA CEA2 calculation. The combustion efficiency data provided in Tables 4.1 and 4.2 are provided in a bar chart in Figure 4.20.

Combustion efficiency of the ABS fuel grains was calculated using pure ABS in the NASA CEA2 code because no information was available regarding the added pigment. The natural and white ABS seem to have similar combustion efficiencies. The white ABS has a slightly higher combustion efficiency for both the straight port and star-swirl port geometries, but with one data point this conclusion is difficult to justify. Similarly, the black ABS appears to have a lower combustion efficiency. Depending on what is used for pigment, this could be explained by the addition of carbon black or similar.

For all the ABS fuel grains combustion efficiency was higher for the straight port geometry than the star-swirl port. This is likely due to the flow condition within the fuel grain using the star-swirl geometry. Unlike for ABS, the star-swirl port provided a higher combustion efficiency than the straight port for the Windform XT 2.0 fuel grains. The combustion efficiency of the carbon-filled polyamide is closest to that of the black ABS.

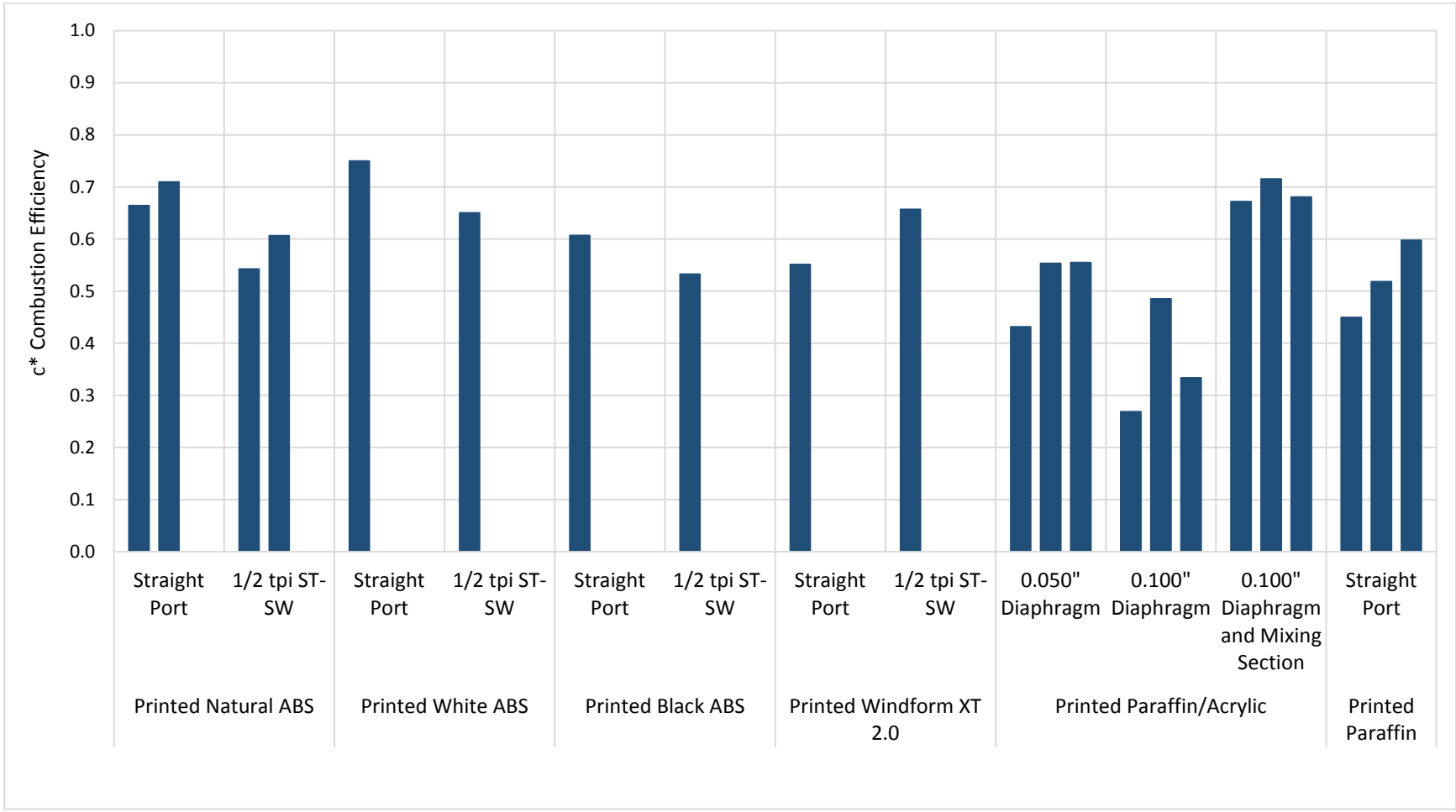

Figure 4.20 Combustion Efficiency Data by Fuel Composition and Geometry

The combustion efficiency calculations of the paraffin and paraffin/acrylic fuel grains also provided meaningful results. The straight port paraffin fuel grains maintained combustion efficiencies between 45% and 60%. This is much lower than the straight port ABS fuel grains. This is expected as the melt layer leads to slumping and liquid droplet entrainment that can expel unburned wax out of the nozzle due to the short residence time within the motor. The original diaphragms were designed in an attempt to increase regression rate and combustion efficiency of the paraffin fuel grains by creating recirculation zones and enhanced mixing.

The 0.050" diaphragm led to similar combustion efficiencies to that of the straight port tests, while the 0.100" diaphragm fuel grains resulted in a substantial decrease in combustion efficiency. This is thought to be due to the 0.050" diaphragms chipping away and weakening the diaphragm effect. The 0.100" diaphragms maintained a larger height off of the paraffin surface and maintained a circular port during the burn. The recirculation zones and enhanced mixing were much stronger due to this and resulted in a much lower combustion efficiency. Large amounts of paraffin were entrained into the flow, however, the short residence time led to a large amount of this being expelled without being completely burned. In addition, large amounts unburned wax collected on the post combustion chamber and nozzle.

The refined diaphragm design utilizes a 0.100" diaphragm and acrylic mixing section to allow for more complete mixing before entering the nozzle. The new design resulted in combustion efficiencies of around 70%. This is greater than the straight port tests and near that of the natural and white ABS straight port fuel grains. A post-burn sectioned paraffin/acrylic 0.100" diaphragm with mixing section fuel grain is shown in Figure 4.21. Unlike a typical paraffin fuel grain, very little unburned paraffin was observed inside of the motor near the post combustion chamber and nozzle.

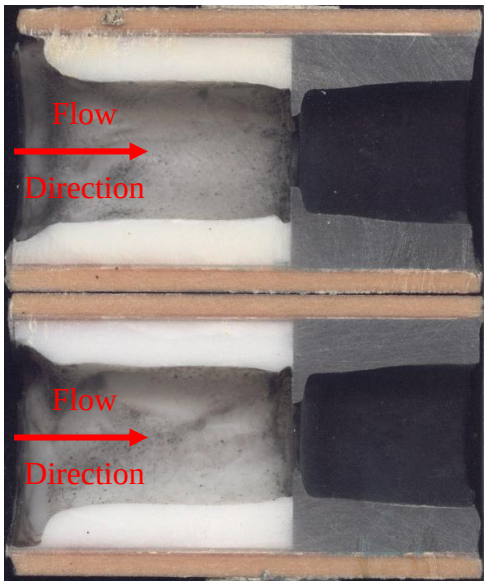

Figure 4.21 Post-Burn Paraffin/Acrylic 0.100” Diaphragm with Mixing Section

Because the regression rate of the acrylic is substantially slower than that of the paraffin wax, the paraffin wax will be consumed prior to the acrylic if allowed to burn to the phenolic cartridge wall with the current design. This design can be further adjusted to match the consumption time of both materials such that the motor burns out to the cartridge wall at nearly the same time for both sections. This would be done by enlarging the acrylic mixing chamber initial port size from the current diameter of 0.60”, or enlarging the paraffin section diameter in the motor grain fore end section of the integrated PUC design. The overall effect of increased combustion efficiency with the diaphragm and mixing chamber design would expect to hold with the adjusted mixing chamber port size or increased paraffin section outer diameter.

4.5 Additional Testing

Additional testing at the HPCL examined the use of the printed Windform XT 2.0 material as a nozzle. The ability to print a nozzle greatly simplifies the fabrication and machining

needed to achieve an optimal shape and could be used to greatly reduce production cost. The following two sections describe two attempts at using the printed polyamide as a nozzle material.

4.5.1 Printed LGCP Motor Nozzle

After confirming the low regression rate of the Windform XT 2.0 carbon-fiber filled polyamide material, nozzles for the LGCP motor were printed out of the material to examine the possibility of using it as a nozzle material. The nozzle was printed such that it could be inserted into the LGCP motor interchangeable nozzle assembly. Due to the extreme conditions expected at the nozzle, particularly at the throat, it was expected that the nozzle would erode very quickly. A photograph of a printed Windform XT 2.0 LGCP motor nozzle is provided in Figure 4.22.

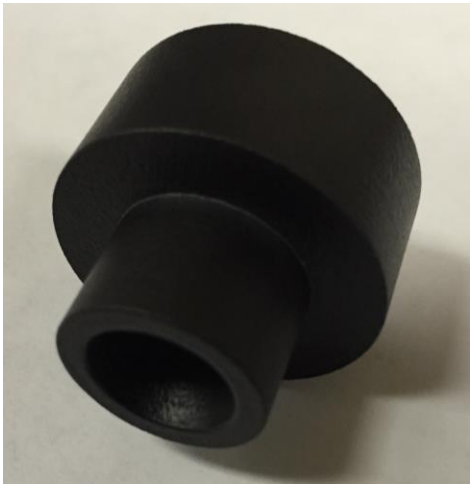

Figure 4.22 Printed Windform XT 2.0 LGCP Nozzle

Testing of the printed nozzle was performed with a printed straight port paraffin fuel grain. The paraffin fuel grain was expected to give a best case scenario for the nozzle, because the paraffin tests result in relatively low O/F ratios. A large amount of oxidizer in the gas entering the nozzle would only lead to increased erosion. The test lasted for roughly 2.5 seconds. If the nozzle was able to withstand this test, a longer duration ABS test would be attempted.

Following the test the nozzle was removed and it was obvious that the nozzle throat had opened up significantly, almost to the diameter of the nozzle assembly. The pressure-time traces and video also indicated the throat area increased significantly over the course of the test. A photograph of the nozzle after the test is provided in Figure 4.23.

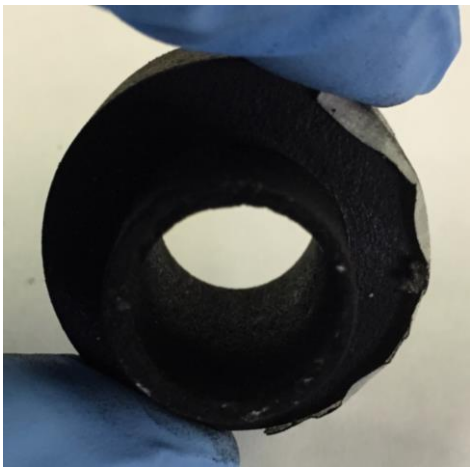

Figure 4.23 Printed Windform XT 2.0 LGCP Nozzle Post-Test

The printed carbon-filled polyamide was obviously not capable of withstanding the environment at the nozzle throat. The next attempt was to create a printed design that could act as the entrance and diverging section of the nozzle, but utilized a graphite or silica phenolic insert to maintain a throat.

4.5.2 Printed LGCP Motor Nozzle with Insert

The design for the LGCP motor nozzle and insert was such that the graphite or silica phenolic throat insert could be bonded with epoxy. This design, due to the insert, was created such that the LGCP motor aft end cap would directly hold the larger nozzle section in place, rather than using the interchangeable nozzle assembly. The nozzle was piston sealed with an O-ring. Photographs of the printed nozzle and the graphite and silica phenolic inserts are provided in Figure 4.24 and Figure 4.25.

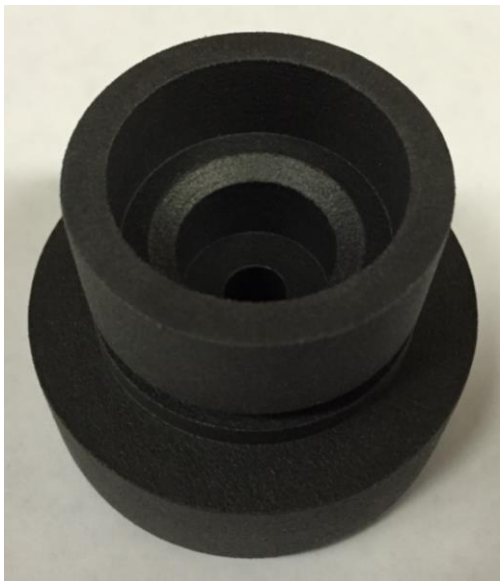

A) Printed Nozzle Fore End for Insert

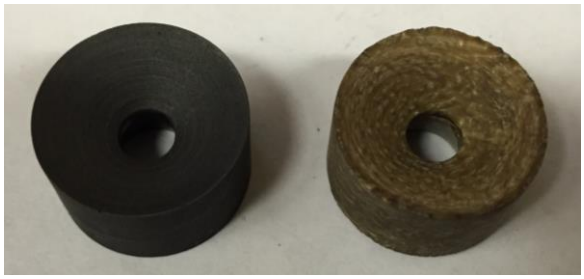

B) Graphite (left) and silica phenolic (right) inserts for nozzle

Figure 4.24 Printed Windform XT 2.0 LGCP Nozzle for Insert and Inserts

A) Printed Nozzle Fore End with Graphite Insert

B) Printed Nozzle Fore End with Silica Phenolic Insert

Figure 4.25 Printed Windform XT 2.0 LGCP Nozzle with Insert

The graphite and silica phenolic inserts were tested similarly to the non-insert printed nozzle. The tests were each conducted with a straight port paraffin fuel grain for just over 4 seconds. The nozzle with the graphite insert did not last the duration of the test. During the firing it was clear from the video that the nozzle did not stay in place, and after the test during the nitrogen purge the graphite insert melted its way through the back of the nozzle and was ejected. The post-test nozzle and insert are shown in Figure 4.26.

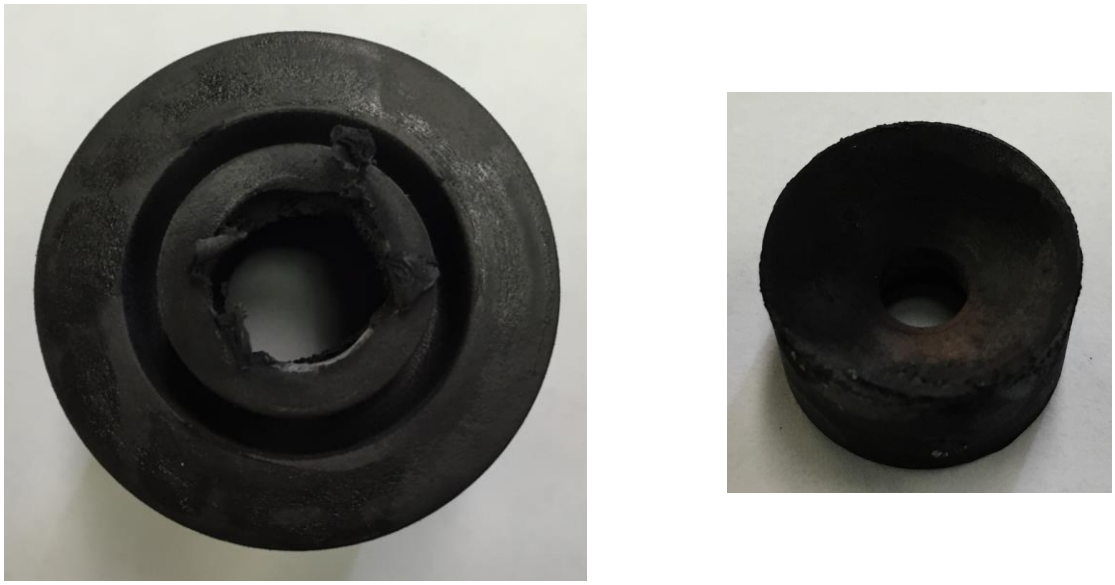

A) Printed Nozzle Aft End B) Graphite Insert

Figure 4.26 Printed Windform XT 2.0 LGCP Nozzle with Graphite Insert Post-Test

The graphite insert became extremely hot and due to its high back-side temperature and high thermal conductivity melted through the back of the printed nozzle. The next test utilized a silica phenolic insert to see whether the ablative throat and insulating properties would better handle the nozzle conditions. The post-test nozzle and insert are shown in Figure 4.27.

A) Printed Nozzle Fore End

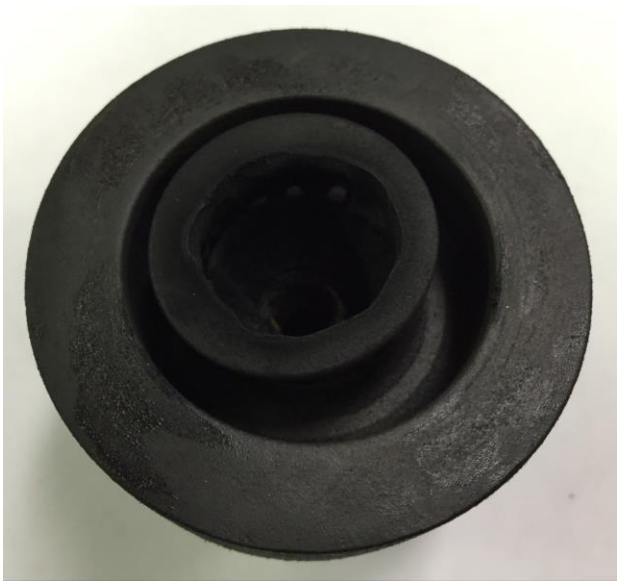

B) Printed Nozzle Aft End

Figure 4.27 Printed Windform XT 2.0 LGCP Nozzle with Silica Phenolic Insert Post-Test

The silica phenolic insert stayed in place and was effective at acting as a nozzle throat. The Windform XT 2.0 upstream of the throat began to thermally degrade, but it was very slow and withstood the duration of the test. However, the diverging section of the nozzle, printed from Windform XT 2.0, did not stand up to the downstream expansion condition. The heat from the exhaust gases began to erode the material and the diverging section began to collapse on itself as holes formed near the middle of the diverging section.

The result of these tests show that even with a throat insert, the printed Windform XT 2.0 material is not suitable as a nozzle throat or converging/diverging section. The material is not able to withstand the extreme temperatures of the exhaust gases. Further investigation into a low-cost easily produced nozzle for the PUC is needed and beyond the scope of this research program. This could include non-printed nozzles or discs, or a printed metal or other high temperature material.

CHAPTER 5. Integration Summary and Conclusions

5.1 Strength Testing and PUC Design

1. The use of additive manufacturing for a hybrid rocket motor propulsion unit has been demonstrated to allow for complex internal structures and channels that would not be possible with conventional subtractive machining.
2. The use of the selective laser sintering manufactured integrated oxidizer tank (using Windform XT 2.0) has been shown to be capable of withstanding the MEOP of the hybrid rocket motor through a hydrostatic pressure test to failure.
3. The use of straight thread O-ring seal fittings within the polyamide material was shown to withstand the MEOP after disregarding the torque specification of the fitting and using a "snug" fit.
4. Tensile testing of Windform XT 2.0 and NyTek 1200 CF samples was conducted using an Instron 5866 test machine. Tests were conducted in various print directions and for pre- and post-exposure to nitrous oxide. Print direction was shown to have a significant effect on the strength of the polymer materials and soaking of the materials in nitrous oxide significantly weakened their strength properties. For both the two and four week duration soak, UTS decreased by over 20% and modulus of elasticity decreased by over 40%. This is a significant concern for the structural integrity and rigidity of the PUC and suggests that the material was saturated by the end of the two week exposure.
5. The plasticizing effect of the nitrous oxide on the polyamide material is unacceptable. Further work will begin to examine the use of DMLS to print a titanium (or another metal) PUC.

5.2 Fuel Grain Testing

1. A nitrous oxide feed system was designed and implemented based on the work of Nicholas Favorito.[68] Minor changes were made to enhance the safety of operation. More significant changes were made in developing a new method for calibration of the mass flow rate through a converging/diverging orifice.
2. Testing of printed ABS, Windform XT 2.0, paraffin, and paraffin/acrylic fuel grains was performed with nitrous oxide in the LGCP motor to determine regression rate and combustion efficiency of various compositions and geometries.
3. Star-swirl port fuel grains were shown to increase regression rate for ABS and Windform XT 2.0 fuel grains. Windform XT 2.0 was an extremely low regression rate hybrid rocket fuel. White and black ABS appear to have regression rates higher than natural ABS. Star-swirl fuel grains resulted in decreased combustion efficiency for ABS and increased combustion efficiency for Windform XT 2.0.
4. Paraffin/acrylic diaphragm fuel grains were shown to significantly increase regression rate downstream of the diaphragms for both 0.050” and 0.100” diaphragms. In some cases, the 0.050” diaphragms chipped away and resulted in uneven regression. Combustion efficiency for 0.050” diaphragms was the same or lower than straight port tests, whereas combustion efficiency for 0.100” diaphragms was significantly lower.
5. An iteration on the paraffin/acrylic diaphragm design used an acrylic diaphragm with an acrylic mixing section. The regression rate for the paraffin section was nearly the same as for straight port tests, and the regression rate for the acrylic section was lower than the correlation provided by Doran et al.[76] However, combustion efficiency was shown to be around 70% for the updated design; a significant improvement.

6. Two printed polyamide/carbon fiber nozzle design attempts were tested in the LGCP motor and showed that the Windform XT 2.0 material is not capable of serving as a nozzle material.

5.3 Future Work Recommendations

1. Further investigation into the PUC structure and oxidizer tank material will be needed. A DMLS-printed unit appears to be the best method for moving forward at this point. While costly, a printed metal tank will address the strength concerns of a polymer exposed to nitrous oxide and can use less material to make up for the increase in density.
2. Examine the use of a titanium tank. Have tensile test samples printed in various print directions and perform strength testing to determine material properties and the effect of print direction. Perform FEA on a design optimal for the light weight metal and print a tank for hydrostatic pressure testing.
3. The fuel grain for the PUC needs to be selected based on a number of criteria for a particular mission. If spin stabilization of the thrust vector is desired, a star-swirl white ABS fuel grain may prove to be the most effective for the unit based on the current data set. However, if combustion efficiency is weighted more heavily than regression rate a straight port white ABS fuel grain may be required. A paraffin/acrylic diaphragm with mixing section may be optimal given its fast paraffin regression rate and good combustion efficiency due to the acrylic mixing section. For the CubeSat application, it is important that combustion efficiency is relatively high. The unit has limited mass and volume available for the propellant and thus extracting as much energy as possible is extremely important.

4. The nozzle of the PUC will also need further investigation. It was shown that Windform XT 2.0 is not capable of being used for a nozzle material. Investigation into the use of a disc or printed metal nozzle should be completed.
5. The current PUC is designed with two igniter ports. These are notionally for two pyrotechnic igniters, such as the electric matches used in LGCP motor test firings. The two ports provide redundancy in the event of a failure of one igniter. Special consideration would need to be given to a pyrotechnic in the CubeSat as a secondary payload. Additional investigation into the use of a catalyst bed igniter and other non-pyrotechnic methods should be completed. These methods should be tested with pure nitrous oxide to confirm proper ignition. Nitrous oxide can be difficult to ignite, which is why the test firings in this work used a low pressure flow of oxygen to establish flame spreading prior to the introduction of nitrous oxide.

REFERENCES

[1] "CubeSat Design Specification Rev. 13," *The CubeSat Program, California Polytechnic State University, San Luis Obispo*, 2014.

[2] Heidt, H., Puig-suari, J., Moore, A. S., Nakasuka, S., and Twiggs, R. J., "CubeSat: A New Generation of Picosatellite for Education and Industry Low-Cost Space Experimentaion," *14th Annual AIAA/USU Conference on Small Satellites*, 2000.

[3] Konecny, G., "Small Satellites - A Tool for Earth Observation?," *ISPRS XXXV Congress Proceedings, Commission IV*, 2004.

[4] "Small Spacecraft Technology State of the Art, NASA/TP–2014–216648/REV1," *Mission Design Division Staff. Ames Research Center*, 2014.

[5] Mahoney, E., and Dunbar, B., "CubeSat Launch Initiative (CSLI)," *NASA Human Exploration and Operations* , URL: http://www.nasa.gov/directorates/heo/home/CubeSats_initiative.html [cited February 19, 2015].

[6] ISIS Innovative Solutions In Space, "ISIPOD CubeSat Deployer" , URL: http://www.isispace.nl/brochures/ISIS_ISIPOD_Brochure_v.7.11.pdf [cited February 20, 2015].

[7] "EZPOD," *Andrews Space* , URL: http://andrews-space.com/ezpod/ [cited March 8, 2015].

[8] Puig-Suari, J., Turner, C., and Ahlgren, W., "Development of the Standard CubeSat Deployer and a CubeSat Class PicoSatellite," *IEEE Aerospace Conference Proceedings*, vol. 1, 2001.

[9] Nason, I., Puig-Suari, J., and Twiggs, R., "Development of a Family of Picosatellite Deployers Based on the CubeSat Standard," *IEEE Aerospace Conference Proceedings*, vol. 1, 2002.

[10] Yost, B. B., Hines, J. W., Agasid, E. F., and Buckley, S. J., "Nanosatellite Launch Adapter System (NLAS)," *AIAA/8th Responsive Space Conference*, 2010.

[11] "Canisterized Satellite Dispenser," *Planetary Systems Corporation* , URL: http://www.planetarysystemscorp.com/?post_type=product&p=448 [cited March 8, 2015].

[12] NASA, "Nano-Satellite Launch Adapter System (NLAS) - Overview," *11th Annual CubeSat Developers' Workshop*, 2014.

[13] "NanoRacks CubeSat Deployer (NRCSD) Interface Control Document," *NanoRacks, LLC*, 2013.

[14] JAXA, "JEM Small Satellite Orbital Deployer (J-SSOD)" , URL: http://iss.jaxa.jp/en/kiboexp/jssod/ [cited February 20, 2015].

[15] Wright, J., and Dunbar, B., "CubeSats and Robotics on Station Thursday," *NASA Space Station Research and Technology,* 2014.

[16] NASA, "Space Launch System (SLS) Secondary Payload User's Guide (SPUG), SLS-SPIE-HDBK-005," 2015.

[17] Cheney, L. J., "Development of Safety Standards for CubeSat Propulsion Systems," California Polytechnic State University, San Luis Obispo, 2014.

[18] Mueller, J., Hofer, R., Parker, M., and Ziemer, J., "Survey of Propulsion Options for CubeSats," *57th JANNAF Propulsion Meeting,* 2010.

[19] Carpenter, C. B., Schmuland, D., Overly, J., and Masse, R., "CubeSat Modular Propulsion Systems Product Line Development Status and Mission Applications," *49th AIAA/ASME/SAE/ASEE Joint Propulsion Conference & Exhibit*, 2013.

[20] Spores, R. A., Masse, R., Kimbrel, S., and McLean, C., "GPIM AF-M315E Propulsion System," *49th AIAA/ASME/SAE/ASEE Joint Propulsion Conference & Exhibit*, 2013.

[21] "Green Monoprop Thrusters," *Busek Space Propulsion and Systems* , URL: http://www.busek.com/index_htm_files/70008517C.pdf [cited February 19, 2015].

[22] Tsay, M., Frongillo, J., Lafko, D., and Zwahlen, J., "Development Status and 1U CubeSat Application of Busek's 0.5N Green Monopropellant Thruster," *28th Annual AIAA/USU Conference on Small Satellites*.

[23] "Pulsed Plasma Thrusters," *Clyde Space* , URL: http://www.clyde-space.com/cubesat_shop/propulsion [cited February 19, 2015].

[24] "PEPL Thrusters: CubeSat Ambipolar Thruster," *The University of Michigan* , URL: http://pepl.engin.umich.edu/thrusters/CAT.html [cited February 19, 2015].

[25] "ion Electrospray Propulsion System for CubeSats (iEPS)," *The Massachusetts Institute of Technology Space Propulsion Laboratory* , URL: http://web.mit.edu/aeroastro/labs/spl/research_ieps.htm [cited February 19, 2015].

[26] Fuller, J., Rowen, D., Hardy, B., Kobel, C., Chen, S.-H., Morrison, P., Smith, T., and Kremer, A., "CubeSat Solid Rocket Motor Propulsion Systems providing ΔVs greater than 500 m/s," *28th Annual AIAA/USU Conference on Small Satellites*.

[27] Dushku, M., and Mueller, P., "Additively Manufactured Propulsion System," *26th Annual AIAA/USU Conference on Small Satellites*.

[28] Dushku, M., and Holemans, W., "Additive Manufactured Propulsion System," US 2012/0060468 A1, 2012.

[29] "Windform XT 2.0," *CRP Technology* , URL: http://www.windform.com/PDF/SCHEDA_WF_XT_2_0_ENG.pdf [cited February 24, 2015].

[30] Chiaverini, M. J., and Kuo, K. K., *Fundamentals of Hybrid Rocket Combustion and Propulsion*, Reston, VA: American Institute of Aeronautics and Astronautics, 2007.

[31] Chiaverini, M. J., "Regression Rate and Pyrolysis Behavior of HTPB-Based Solid Fuels in a Hybrid Rocket Motor," The Pennsylvania State University, 1997.

[32] Sutton, G. P., and Biblarz, O., "Hybrid Propellant Rockets," *Rocket Propulsion Elements*, New York: John Wiley & Sons, 2001.

[33] Chiaverini, M. J., Harting, G. C., Lu, Y.-C., Kuo, K. K., Peretz, A., Jones, H. S., Wygle, B. S., and Arves, J. P., "Pyrolysis Behavior of Hybrid-Rocket Solid Fuels Under Rapid Heating Conditions," *Journal of Propulsion and Power*, vol. 15, 1999, pp. 888–895.

[34] Risha, G. A., Boyer, E., Wehrman, R. B., and Kuo, K. K., "Performance Comparison of HTPB-Based Solid Fuels Containing Nano-Sized Energetic Powder in a Cylindrical Hybrid Rocket Motor," *38th AIAA/ASME/SAE/ASEE Joint Propulsion Conference & Exhibit*, 2002.

[35] Risha, G. A., Ulas, A., Boyer, E., Kumar, S., and Kuo, K. K., "Combustion of HTPB-Based Solid Fuels Containing Nano-Sized Energetic Powder in a Hybrid Rocket Motor," *37th AIAA/ASME/SAE/ASEE Joint Propulsion Conference & Exhibit*, 2001.

[36] Risha, G. A., "Enhancement of Hybrid Rocket Combustion Performance Using Nano-Sized Energetic Particles," The Pennsylvania State University, 2003.

[37] Karabeyoglu, M. A., Cantwell, B. J., and Altman, D., "Development and Testing of Paraffin Based Hybrid Rocket Fuels," *37th AIAA/ASME/SAE/ASEE Joint Propulsion Conference & Exhibit*, 2001.

[38] Karabeyoglu, A., Zilliac, G., Cantwell, B. J., DeZilwa, S., and Castellucci, P., "Scale-Up Tests of High Regression Rate Paraffin-Based Hybrid Rocket Fuels," *Journal of Propulsion and Power*, vol. 20, 2004, pp. 1037–1045.

[39] Karabeyoglu, M. A., Cantwell, B. J., and Zilliac, G., "Development of Scalable Space-Time Averaged Regression Rate Expressions for Hybrid Rockets," *41st AIAA/ASME/SAE/ASEE Joint Propulsion Conference & Exhibit*, 2005.

[40] Zilliac, G., and Karabeyoglu, M. A., "Hybrid Rocket Fuel Regression Rate Data and Modeling," *42nd AIAA/ASME/SAE/ASEE Joint Propulsion Conference & Exhibit*, 2006.

[41] Evans, B., Favorito, N. A., Boyer, E., Risha, G. A., Wehrman, R. B., and Kuo, K. K., "Characterization of Nano-Sized Energetic Particle Enhancement of Solid-Fuel Burning Rates in an X-Ray Transparent Hybrid Rocket Engine," *40th AIAA/ASME/SAE/ASEE Joint Propulsion Conference & Exhibit*, 2004.

[42] Larson, D. B., Boyer, E., Wachs, T., Kuo, K. K., DeSain, J. D., Curtiss, T. J., and Brady, B. B., "Characterization of the Performance of Paraffin / LiAlH4 Solid Fuels in a Hybrid Rocket System," *47th AIAA/ASME/SAE/ASEE Joint Propulsion Conference & Exhibit*, 2011.

[43] Evans, B., Favorito, N. A., and Kuo, K. K., "Oxidizer-Type and Aluminum-Particle Addition Effects on Solid-Fuel Burning Behavior," *42nd AIAA/ASME/SAE/ASEE Joint Propulsion Conference & Exhibit*, 2006.

[44] Armold, D. M., "Formulation and Characterization of Paraffin-Based Solid Fuels Containing Swirl Inducing Grain Geometry and/or Energetic Additives," The Pennsylvania State University, 2014.

[45] Armold, D., Boyer, E., McKnight, B., Kuo, K., DeSain, J., Fuller, J., Brady, B., and Curtiss, T., "Performance Characterization of Hybrid Rocket Fuel Grains with Complex Port Geometries Fabricated Using Rapid Prototyping Technology," *International Journal of Energetic Materials and Chemical Propulsion*, vol. 13, 2014, pp. 287–307.

[46] Armold, D., Boyer, J. E., Kuo, K. K., DeSain, J. D., Curtiss, T. J., and Fuller, J. K., "Test of Hybrid Rocket Fuel Grains with Swirl Patterns Fabricated Using Rapid Prototyping Technology," *49th AIAA/ASME/SAE/ASEE Joint Propulsion Conference & Exhibit*, 2013.

[47] Bellomo, N., Lazzarin, M., Barato, F., and Grosse, M., "Numerical Investigation of the Effect of a Diaphragm on the Performance of a Hybrid Rocket Motor," *46th AIAA/ASME/SAE/ASEE Joint Propulsion Conference & Exhibit*, 2010.

[48] Bettella, A., Lazzarin, M., Bellomo, N., Barato, F., Pavarin, D., and Grosse, M., "Testing and CFD Simulation of Diaphragm Hybrid Rocket Motors," *47th AIAA/ASME/SAE/ASEE Joint Propulsion Conference & Exhibit*, 2011.

[49] Fuller, J. K., Ehrlich, D. A., Lu, P. C., Jansen, R. P., and Hoffman, J. D., "Advantages of Rapid Prototyping for Hybrid Rocket Motor Fuel Grain Fabrication," *47th AIAA/ASME/SAE/ASEE Joint Propulsion Conference & Exhibit*, 2011.

[50] Grosse, M., "Effect of a Diaphragm on Performance and Fuel Regression of a Laboratory Scale Hybrid Rocket Motor Using Nitrous Oxide and Paraffin," *45th AIAA/ASME/SAE/ASEE Joint Propulsion Conference & Exhibit*, 2009.

[51] Kumar, C. P., and Kumar, A., "Effect of Diaphragms on Regression Rate in Hybrid Rocket Motors," *Journal of Propulsion and Power*, vol. 29, 2013, pp. 559–572.

[52] Mon, K. O., and Lee, C., "Interaction of Vortices due to Diaphragm on the Wall Blowing Surface," *49th AIAA/ASME/SAE/ASEE Joint Propulsion Conference & Exhibit*, 2013.

[53] McKnight, B. R., Armold, D., Boyer, J. E., Kuo, K. K., DeSain, J. D., Fuller, J. K., Brady, B. B., and Curtiss, T. J., "Testing of Hybrid Rocket Fuel Grains at Elevated Temperatures with Swirl Patterns Fabricated Using Rapid Prototyping Technology," *50th AIAA/ASME/SAE/ASEE Joint Propulsion Conference & Exhibit*, 2014.

[54] Gibson, I., Rosen, D. W., and Stucker, B., *Additive Manufacturing Technologies: Rapid Prototyping to Direct Digital Manufacturing*, New York: Springer, 2010.

[55] Gibson, I., and Shi, D., "Material properties and fabrication parameters in selective laser sintering process," *Rapid Prototyping Journal*, vol. 3, 1997, pp. 129–136.

[56] "NyTek 1200 CF," *Solid Concepts* , URL: https://www.solidconcepts.com/content/pdfs/material-specifications/sls-nytek-1200-cf.pdf [cited February 24, 2015].

[57] "Chemical Resistance Chart," *Burkert Fluid Control Systems* , URL: https://www.burkert.fr/fr/content/download/9318/334992/file/COM_Chemical_Resistance_Chart.pdf [cited March 8, 2015].

[58] "Technical Information - Compatibility Recommendations," *EnSolv* , URL: http://www.ensolv-europe.com/compatibility_recommendations.php#.VPzKluFL1pg [cited March 8, 2015].

[59] Gordon, S., and McBride, B. J., "Computer Program for Calculation of Complex Chemical Equilibrium Compositions and Applications I. Analysis," *NASA RP-1311*, 1994.

[60] McBride, B. J., and Gordon, S., "Computer Program for Calculation of Complex Chemical Equilibrium Compositions and Applications II. User's Manual and Program Description," *NASA RP-1311-P2*, 1996.

[61] McBride, B. J., Zehe, M. J., and Gordon, S., "NASA Glenn Coefficients for Calculating Thermodynamic Properties of Individual Species," *NASA TP-2002-211556*, 2002.

[62] Svehla, R. A., "Transport Coefficients for the NASA Lewis Chemical Equilibrium Program," *NASA TM-4647*, 1995.

[63] Whitmore, S. A., Peterson, Z. W., and Eilers, S. D., "Analytical and Experimental Comparisons of HTPB and ABS as Hybrid Rocket Fuels," *47th AIAA/ASME/SAE/ASEE Joint Propulsion Conference & Exhibit*, 2011.

[64] "Windform XT 2.0 Properties," *Stewart Davis, Personal Communication, CRP Technology.*

[65] Rasband, W. S., "ImageJ," *U.S. National Institutes of Health* , URL: http://imagej.nih.gov/ij/, 1997-2014.

[66] "D 638 - 08 Standard Test Method for Tensile Properties of Plastics," *ASTM International*, 2008.

[67] "Method for Printing an Enclosed Geometry Using an Acrylic/Paraffin FDM Machine," *Jerry Fuller, Personal Communication, The Aerospace Corporation.*

[68] Favorito, N. A., "Development and Testing of a Nitrous Oxide Feed System for an Experimental Hybrid Rocket Motor," The Pennsylvania State University, 2005.

[69] Thicksten, Z., Macklin, F., and Campbell, J., "Handling Considerations of Nitrous Oxide in Hybrid Rocket Motor Testing," *44th AIAA/ASME/SAE/ASEE Joint Propulsion Conference & Exhibit*, 2008.

[70] Karabeyoglu, A., Dyer, J., Stevens, J., and Cantwell, B., "Modeling of N2O Decomposition Events," *44th AIAA/ASME/SAE/ASEE Joint Propulsion Conference & Exhibit*, 2008.

[71] "Scaled Composites Safety Guidelines for N2O," *Scaled Composites, LLC*, 2009.

[72] Merrill, C., *Nitrous Oxide Explosive Hazards (Preprint)*, 2008.

[73] Cawthra, J. K., and Eisenstadt, M., *Summary of Nitrous Oxide Investigations*, 1976.

[74] Rhodes, G. W., *Investigation of Decomposition Characteristics of Gaseous and Liquid Nitrous Oxide*, 1974.

[75] AIGA, *Safe Practices for Storage and Handling of Nitrous Oxide 081/13*, 2013.

[76] Doran, E., Dyer, J., Lohner, K., Dunn, Z., and Zilliac, G., "Nitrous Oxide Hybrid Rocket Motor Fuel Regression Rate Characterization," *43rd AIAA/ASME/SAE/ASEE Joint Propulsion Conference & Exhibit*, 2007.

APPENDIX A CubeSat Design Specification Drawings

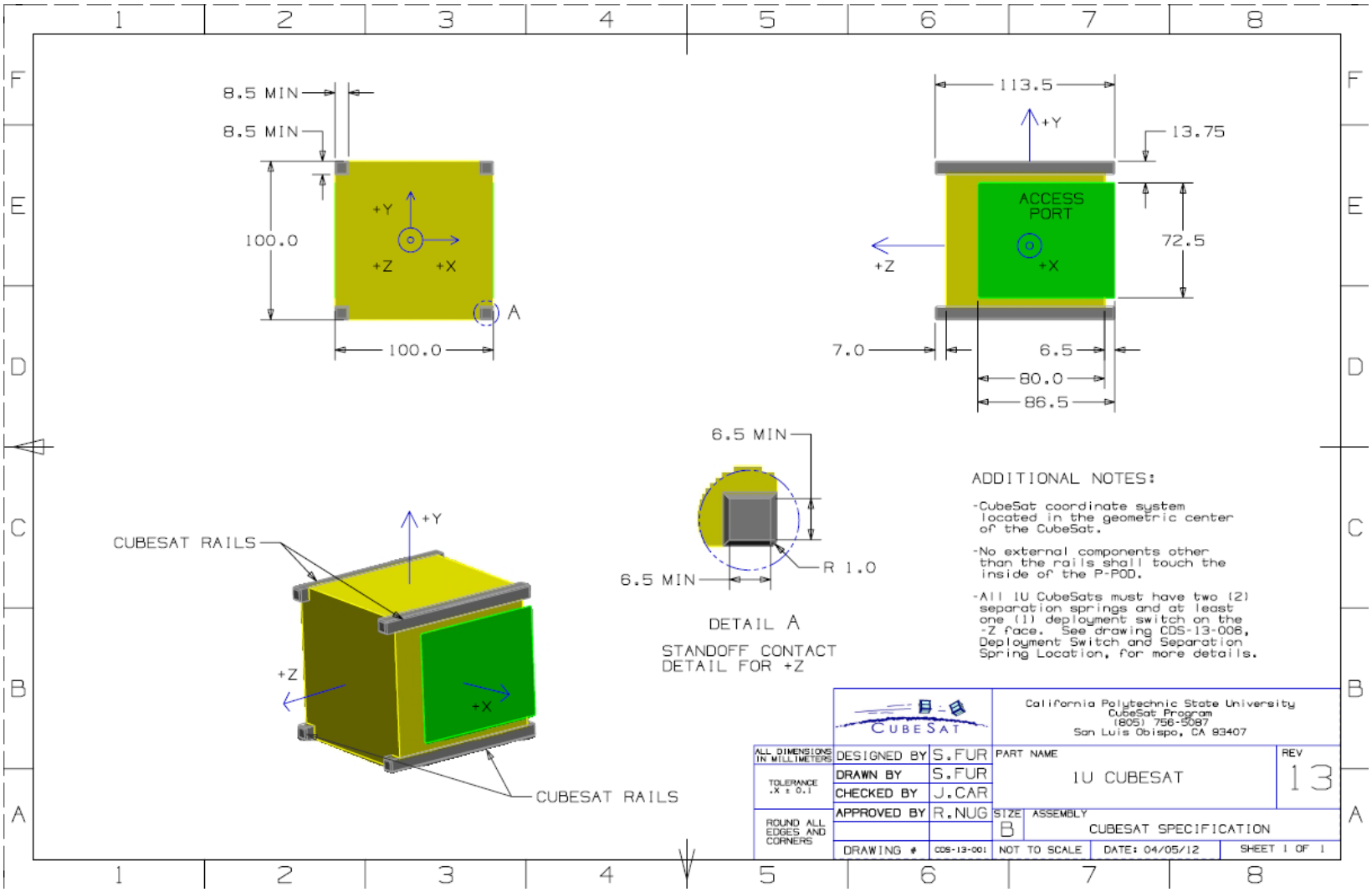

Figure A.1 Drawing for 1U CubeSat[1]

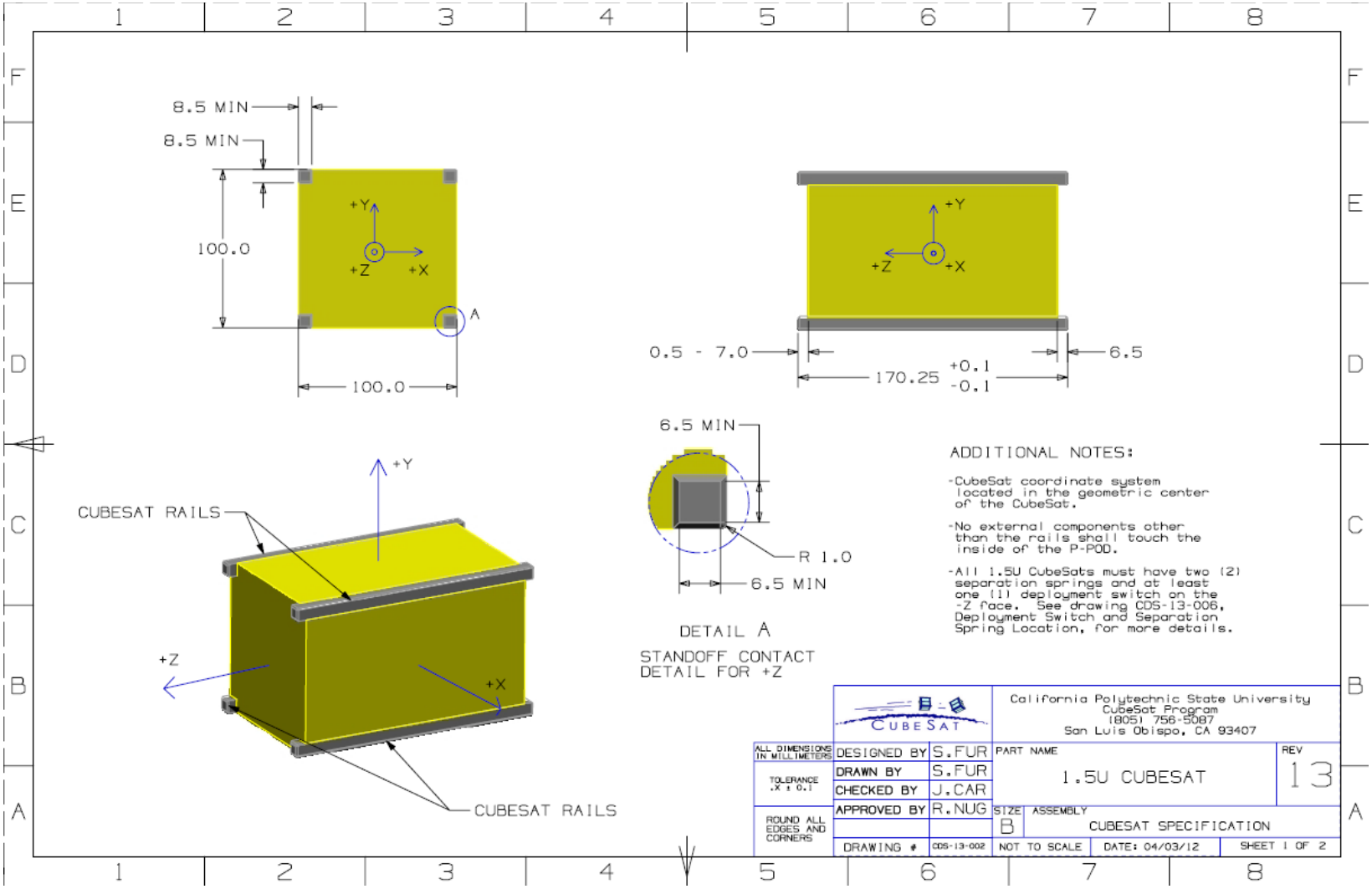

Figure A.2 Drawing for 1.5U CubeSat[1]

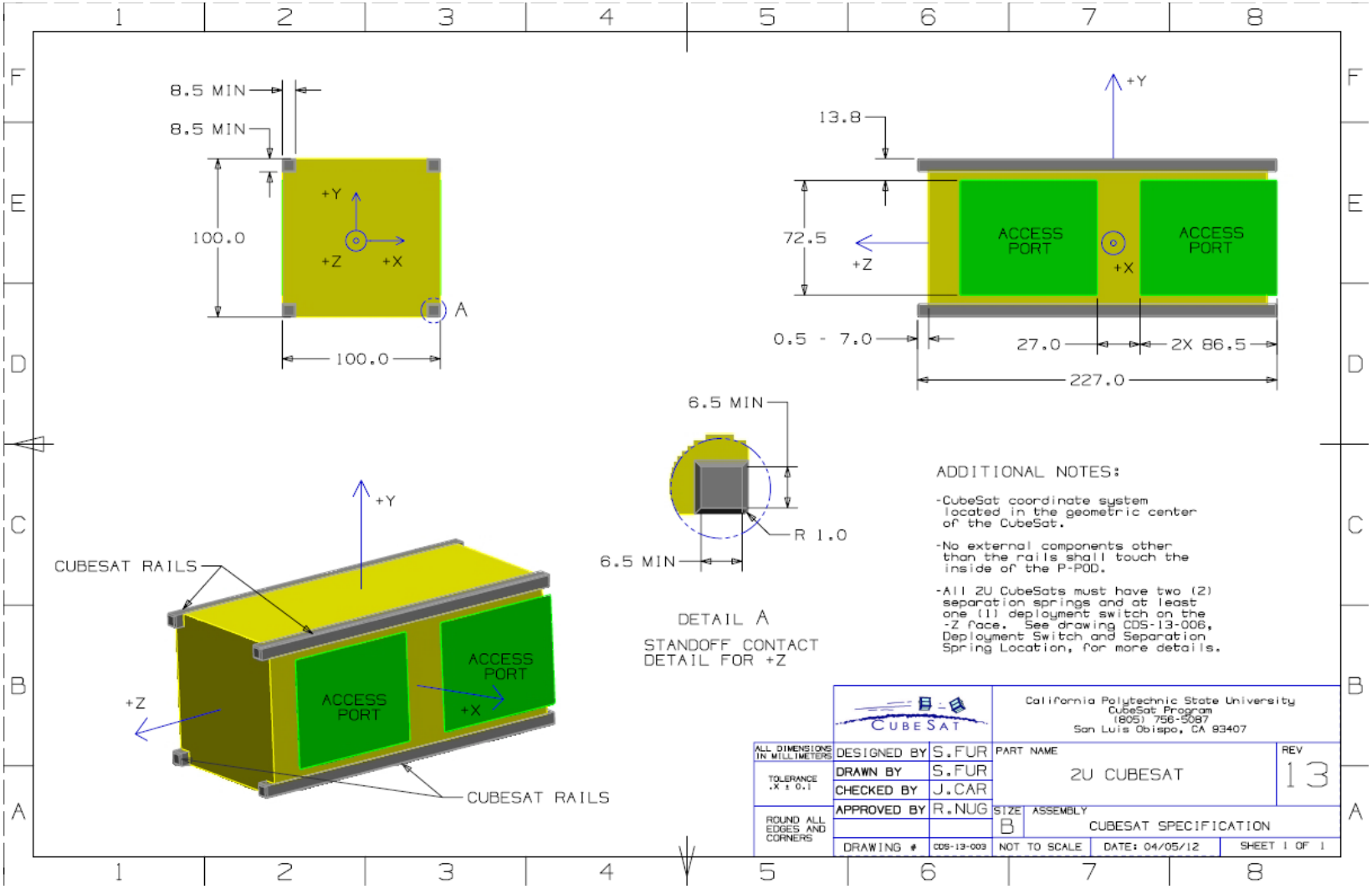

Figure A.3 Drawing for 2U CubeSat[1]

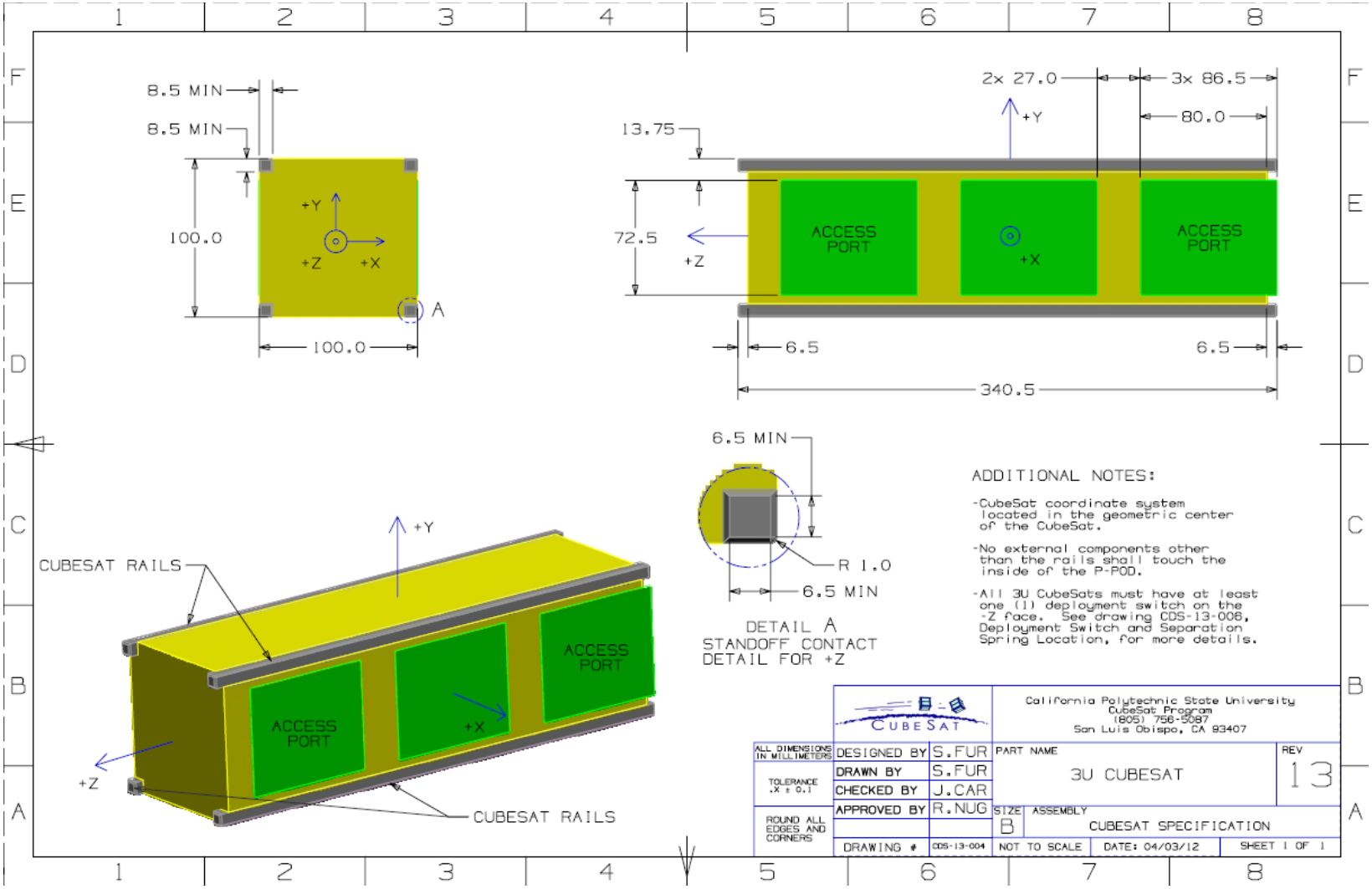

Figure A.4 Drawing for 3U CubeSat[1]

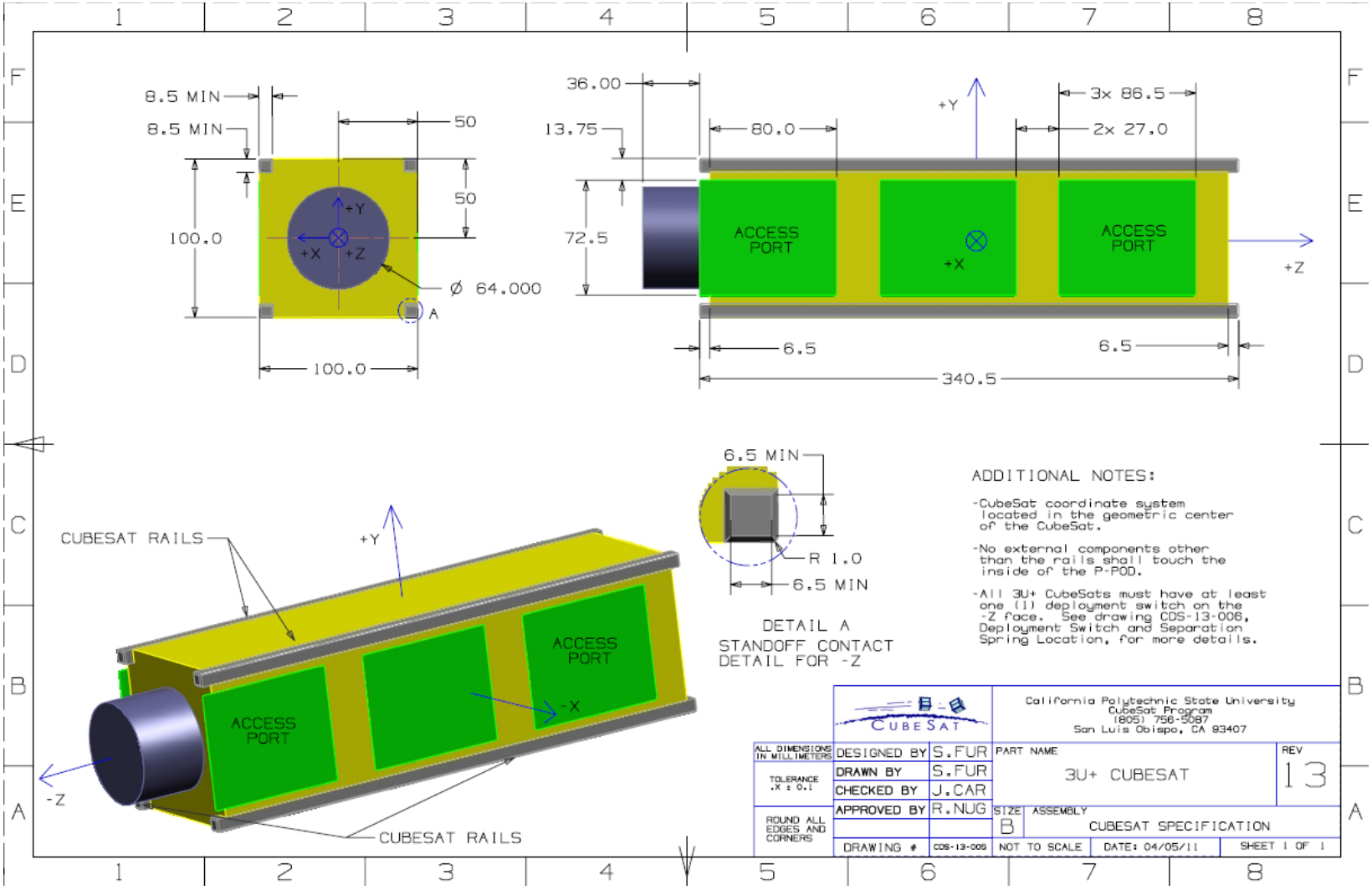

Figure A.5 Drawing for 3U+ CubeSat[1]

APPENDIX B SLS High Strength Polymer Material Properties

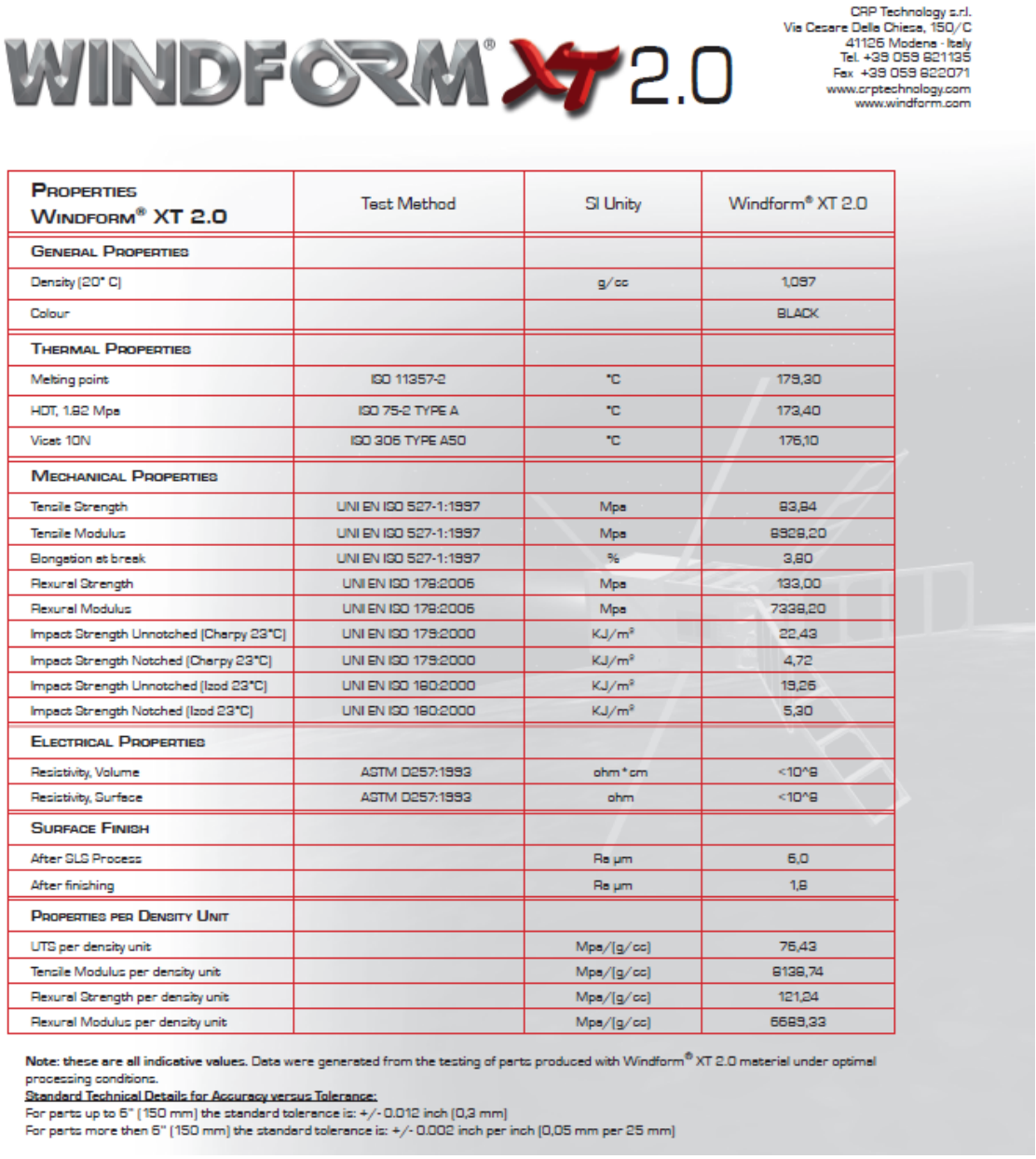

WINDFORM® XT 2.0

CRP Technology s.r.l.
Via Cesare Della Chiesa, 150/C
41126 Modena - Italy
Tel. +39 059 821135
Fax +39 059 822071
www.crptechnology.com
www.windform.com

PROPERTIES WINDFORM® XT 2.0	Test Method	SI Unity	Windform® XT 2.0
GENERAL PROPERTIES			
Density (20° C)		g/cc	1,097
Colour			BLACK
THERMAL PROPERTIES			
Melting point	ISO 11357-2	°C	179,30
HDT, 1.82 Mpa	ISO 75-2 TYPE A	°C	173,40
Vicat 10N	ISO 306 TYPE A50	°C	176,10
MECHANICAL PROPERTIES			
Tensile Strength	UNI EN ISO 527-1:1997	Mpa	83,84
Tensile Modulus	UNI EN ISO 527-1:1997	Mpa	6928,20
Elongation at break	UNI EN ISO 527-1:1997	%	3,80
Flexural Strength	UNI EN ISO 179:2006	Mpa	133,00
Flexural Modulus	UNI EN ISO 179:2006	Mpa	7338,20
Impact Strength Unnotched (Charpy 23°C)	UNI EN ISO 179:2000	KJ/m²	22,43
Impact Strength Notched (Charpy 23°C)	UNI EN ISO 179:2000	KJ/m²	4,72
Impact Strength Unnotched (Izod 23°C)	UNI EN ISO 180:2000	KJ/m²	19,26
Impact Strength Notched (Izod 23°C)	UNI EN ISO 180:2000	KJ/m²	5,30
ELECTRICAL PROPERTIES			
Resistivity, Volume	ASTM D257:1993	ohm*cm	<10^8
Resistivity, Surface	ASTM D257:1993	ohm	<10^8
SURFACE FINISH			
After SLS Process		Ra µm	6,0
After finishing		Ra µm	1,8
PROPERTIES PER DENSITY UNIT			
UTS per density unit		Mpa/[g/cc]	76,43
Tensile Modulus per density unit		Mpa/[g/cc]	6138,74
Flexural Strength per density unit		Mpa/[g/cc]	121,24
Flexural Modulus per density unit		Mpa/[g/cc]	6689,33

Note: these are all indicative values. Data were generated from the testing of parts produced with Windform® XT 2.0 material under optimal processing conditions.

Standard Technical Details for Accuracy versus Tolerance:
For parts up to 6" (150 mm) the standard tolerance is: +/- 0.012 inch (0,3 mm)
For parts more then 6" (150 mm) the standard tolerance is: +/- 0.002 inch per inch (0,05 mm per 25 mm)

Figure B.1 Reported Windform XT 2.0 Material Properties[29]

Private Communication with CRP Technology Regarding Windform XT 2.0:[64]

X (left to right facing the front of the machine):

- Tensile Strength: 82.37 Mpa (Average of 5 tests)

- Elongation at break: 2.75 % (Average of 5 tests)

Y (front to back):

- Tensile Strength: 64.23 Mpa (Average of 5 tests)

- Elongation at break: 4.02 % (Average of 5 tests)

Z (up and down):

- Tensile Strength: 48.83 Mpa (Average of 5 tests)

- Elongation at break: 2.76 % (Average of 5 tests)

Strongest direction is the X–direction; weakest direction is the Z-direction.

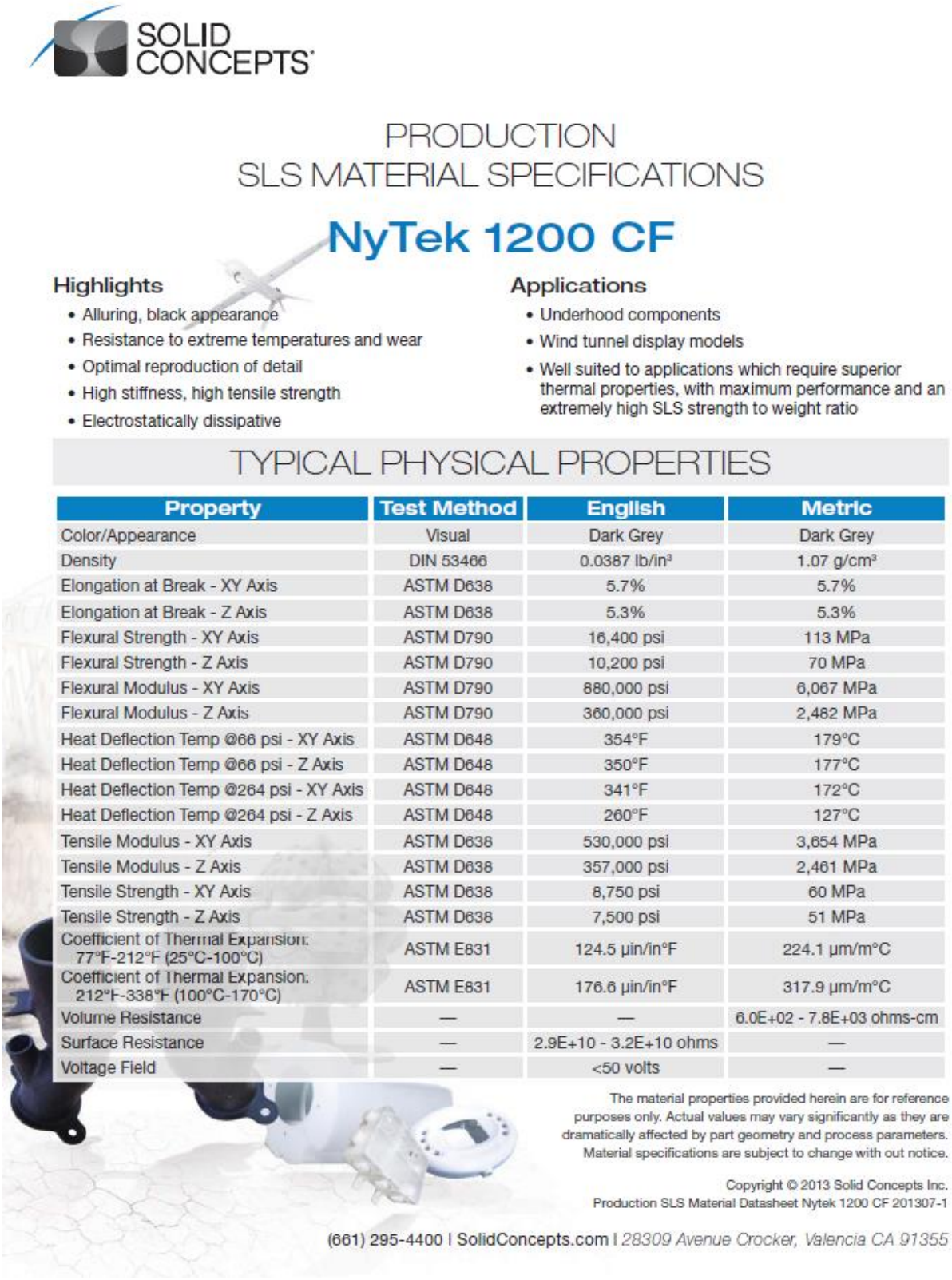

Figure B.2 Reported NyTek 1200 CF Material Properties[56]

APPENDIX C Oxygen Cleaning Procedure

1. Remove all tube sections and fittings used in the oxidizer flow line.
2. For sections that do not need cleaned, cover open ends with aluminum foil or seal with a clean Swagelok plug. This keeps dust and contaminants from entering clean sections of the oxidizer line.
3. Separate removed sections into individual tube pieces and fittings for cleaning.
4. Go to the Flammable Liquids cabinet and remove the EnSolv container. Bring it into the chemical room.
5. Fill a container with enough EnSolv to submerge a number of fittings or short tube pieces at a time.
6. Clean any visible oil, lubricant, grease etc.
7. Submerge small fittings and tube sections in the EnSolv cleaning solvent.
8. If there are long tube sections, which are difficult to submerge in containers, plug one end of the tube using a Swagelok plug. Then, fill the tube with EnSolv using a funnel or pipet and close the open end using another Swagelok plug.
9. Keep the fittings and tubing in the EnSolv for a minimum of 30 minutes.
10. After this time, remove submerged fittings and drain tube sections. Wear gloves to avoid getting oils on parts that may be contacted by the oxidizer.
11. Thoroughly rinse clean fittings and tubing with distilled water.
12. Dry tubing and fittings with nitrogen gas, if possible.
13. Reassemble oxidizer flow line and use nitrogen to check for leaks and dry with a steady flow, if possible. For pieces not being installed immediately, cover ends with aluminum foil or place in a sealed plastic bag.

APPENDIX D Sample NASA CEA2 Code Input and Output Files

Input File:

```
problem   case=N2OParaffin o/f=8,
   rocket  equilibrium  tcest,k=3000
  p,psia=100,
  sup,ae/at=10,
react
  oxid=N2O wt=1  t,k=298
  fuel=Paraffin  wt=1  t,k=298
    h,kcal/mol=-166.5  C 32 H 66
output
     siunits short
end
```

Output File:

COMPOSITION DURING EXPANSION FROM INFINITE AREA COMBUSTOR

Pin = 100.0 PSIA
CASE = N2OParaffin

REACTANT		WT FRACTION (SEE NOTE)	ENERGY KJ/KG-MOL	TEMP K
OXIDANT	N2O	1.0000000	81594.206	298.000
FUEL	Paraffin	1.0000000	-696636.000	298.000

O/F= 8.00000 %FUEL= 11.111111 R,EQ.RATIO= 1.183621 PHI,EQ.RATIO= 1.183621

	CHAMBER	THROAT	EXIT
Pinf/P	1.0000	1.7321	73.446
P, BAR	6.8947	3.9805	0.09388
T, K	3181.82	3017.31	1871.27
RHO, KG/CU M	6.7517-1	4.1647-1	1.6656-2
H, KJ/KG	1476.21	933.44	-1917.21
U, KJ/KG	455.02	-22.327	-2480.83
G, KJ/KG	-31779.2	-30602.5	-21475.2
S, KJ/(KG)(K)	10.4517	10.4517	10.4517
M, (1/n)	25.906	26.248	27.605
(dLV/dLP)t	-1.02606	-1.02214	-1.00015
(dLV/dLT)p	1.5211	1.4702	1.0051

Cp, KJ/(KG)(K)	5.0265	4.8324	1.5915
GAMMAs	1.1385	1.1358	1.2361
SON VEL,M/SEC	1078.3	1041.9	834.7
MACH NUMBER	0.000	1.000	3.121

PERFORMANCE PARAMETERS

Ae/At	1.0000	10.000
CSTAR, M/SEC	1588.9	1588.9
CF	0.6557	1.6395
Ivac, M/SEC	1959.2	2821.5
Isp, M/SEC	1041.9	2605.2

MOLE FRACTIONS

*CO	0.13010	0.12177	0.07627
*CO2	0.07420	0.08522	0.14142
*H	0.01881	0.01471	0.00034
HO2	0.00002	0.00001	0.00000
*H2	0.03399	0.03097	0.02608
H2O	0.15029	0.16119	0.19813
*N	0.00001	0.00001	0.00000
*NO	0.01394	0.01074	0.00002
NO2	0.00001	0.00000	0.00000
*N2	0.51623	0.52474	0.55750
*O	0.01042	0.00744	0.00000
*OH	0.03398	0.02789	0.00023
*O2	0.01802	0.01530	0.00001

* THERMODYNAMIC PROPERTIES FITTED TO 20000.K

NOTE. WEIGHT FRACTION OF FUEL IN TOTAL FUELS AND OF OXIDANT IN TOTAL OXIDANTS

APPENDIX E Initial Sizing and Performance Calculations

- Enter fuel grain Diameter [in.], Port Diameter [in.], and Length [in.]
    - Fuel Grain Volume [m^3] is calculated,
        - $Fuel\ Grain\ Volume[m^3] = \frac{\pi}{4}\left(\left(Diameter[in.] * 0.0254\frac{m}{in.}\right)^2 - \left(Port\ Diameter[in.] * 0.0254\frac{m}{in.}\right)^2\right)\left(Length[in.] * 0.0254\frac{m}{in.}\right)$
- Enter Fuel Density [kg/m^3]
    - Fuel Mass [kg] is calculated,
        - $Fuel\ Mass[kg] = Fuel\ Grain\ Volume[m^3] * Fuel\ Density\left[\frac{kg}{m^3}\right]$
- Enter Firing Volume [m^3] total of fuel and nitrous oxide
    - Firing N_2O Volume [m^3] is calculated,
        - $Firing\ N2O\ Volume[m^3] = Firing\ Volume[m^3] - Fuel\ Grain\ Volume[m^3]$
- Enter Initial Mass [kg] of the CubeSat
- Enter N_2O Density [kg/m^3] for saturation conditions
    - Firing N_2O Mass [kg] is calculated,
        - $Firing\ N2O\ Mass[kg] = Firing\ N2O\ Volume[m^3] * N2O\ Density\left[\frac{kg}{m^3}\right]$
    - Firing Mass [kg] is calculated,
        - $Firing\ Mass[kg] = Fuel\ Mass[kg] + Firing\ N2O\ Mass[kg]$

- Final Mass [kg] is calculated,
  - $Final\ Mass[kg] = Initial\ Mass[kg] - Firing\ Mass[kg]$
- Firing O/F is calculated,
  - $Firing\ \frac{O}{F} = \frac{Firing\ N2O\ Mass[kg]}{Fuel\ Mass[kg]}$
- Total O/F is calculated,
  - $Total\ \frac{O}{F} = Firing\ \frac{O}{F} + 1.5$
- Total N_2O Mass [kg] is calculated,
  - $Total\ N2O\ Mass[kg] = Total\ \frac{O}{F} * Fuel\ Mass[kg]$
- Total N_2O Volume [m^3] is calculated,
  - $Total\ N2O\ Volume[m^3] = \frac{Total\ N2O\ Mass[kg]}{N2O\ Density\left[\frac{kg}{m^3}\right]}$

- Enter $I_{sp,vac}$ [s] from NASA CEA2 for the Firing O/F ratio
- Enter the gravitational acceleration g [m/s^2]
  - Exhaust exit velocity V_e [m/s] is calculated,
    - $Ve\left[\frac{m}{s}\right] = I_{sp,vac}[s] * g\left[\frac{m}{s^2}\right]$
- Delta V [m/s] is calculated,
  - $Delta\ V\left[\frac{m}{s}\right] = Ve\left[\frac{m}{s}\right] * \ln\left(\frac{Initial\ Mass[kg]}{Final\ Mass[kg]}\right)$

Table E.1 Table of Initial Sizing and Performance Calculations

Diameter (in)	Port Diameter (in)	Length (in)	Fuel Grain Volume (m^3)	Fuel Density (kg/m^3)	Fuel Mass (kg)	Firing O/F	Total O/F
1.25	0.250	2.50	4.83E-05	920	0.0444	8.00	9.50
1.10	0.250	2.50	3.69E-05	920	0.0340	10.7	12.2
1.15	0.250	2.50	4.05E-05	920	0.0373	9.69	11.2
1.20	0.250	2.50	4.43E-05	920	0.0408	8.79	10.3
1.30	0.250	2.50	5.24E-05	920	0.0482	7.31	8.81
1.35	0.250	2.50	5.66E-05	920	0.0521	6.69	8.19
1.40	0.250	2.50	6.11E-05	920	0.0562	6.14	7.64

Firing N2O Mass (kg)	Total N2O Mass (kg)	N2O Density (kg/m^3)	Firing N2O Volume (m^3)	Total N2O Volume (m^3)
0.355	0.422	800	0.000444	0.000527
0.364	0.415		0.000455	0.000519
0.361	0.417		0.000452	0.000522
0.358	0.420		0.000448	0.000524
0.352	0.424		0.000440	0.000530
0.349	0.427		0.000436	0.000533
0.345	0.429		0.000431	0.000537

Isp,vac from NASA CEA2 (s)	g (m/s^2)	Ve (m/s)	Initial Mass (kg)	Firing Volume (m^3)	Firing Mass (kg)	Final Mass (kg)	Delta V (m/s)
289	9.81	2833	10.0	0.000492	0.400	9.60	115.5
277		2716	10.0	0.000492	0.398	9.60	110.4
282		2768	10.0	0.000492	0.399	9.60	112.6
287		2811	10.0	0.000492	0.399	9.60	114.5
289		2834	10.0	0.000492	0.400	9.60	115.7
288		2822	10.0	0.000492	0.401	9.60	115.4
286		2800	10.0	0.000492	0.401	9.60	114.6

APPENDIX F Review of Commercially Available Flow System Components

Table F.1 Review of Commercially Available Small-Scale Regulators

Make	Model / Material and Seals	Max. Pressure	Cv (orifice)	Size / Weight	Cost	Picture
Aerocon Systems [1]	Model 1247 Inline Reducing Regulator Brass for O2 use with Kel-F seat and Viton O-rings	6000 PSI	0.03 (0.045” orifice)	1” hex x 3.5” long 0.38 lb	$119.00	
TESCOM [2]	04 Series Regulator Stainless steel, brass, or aluminum with CTFE, Teflon, or Vespel	3500 PSI	0.06	3” long 0.5 lb aluminum 1 lb stainless steel or brass		
Aqua Environment Inc. [3]	969 Regulator Stainless steel and brass with Viton and Kel-F	6000 PSI	0.05 (0.08” orifice)	1.37” hex x 3.7” long		

Vonberg [4]	24000 Series Flow Regulator Steel body and internals, no internal packings	5000 PSI	Flow range of 0.25 to 8.0 GPM	0.75” hex x 3” long		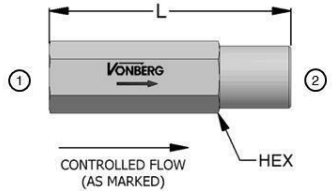
Nuvair [5]	1120 Regulator Aluminum	6000 PSI			$205.00	
Palmer Paintball [6]	Boulder, Pebble, or Micro Rock Regulator	1500 PSI		0.875” diameter x 3” long 3 oz. (Micro Rock)	$55.00	
Ninja Paintball [7]	Nitrogen Tank Regulator Plated aluminum	Use with 4500 PSI tank			$35.95	

Table F.2 Review of Commercially Available Small-Scale Solenoid Valves

Make	Model / Material and Seals	Max. Pressure	Power	C_v	Size / Weight	Cost	Picture
The Lee Company [8]	IEP Series Solenoid Valves Stainless steel with FFKM, FKM, or EPDM	300 PSI or 800 PSI	0.25 W	0.005	0.25" diameter x 1.11" long + port lengths 4.7 grams		
ValveTech Inc. [9]	Solenoid, Miniature High Pressure and Propellant Stainless steel						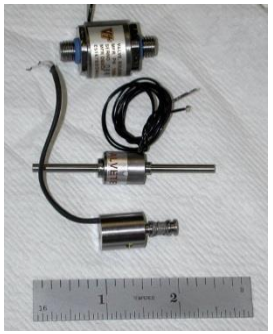
Gems Sensors and Controls [10]	E and EH Series Subminiature Gas Solenoid Valve Nickel-plated brass body with Viton plunger seal and O-ring (others available)	175 PSI	0.65 or 2 W	0.018 – 0.070	0.73" diameter x 1.61" long	~ $50	

Gems Sensors and Controls [11]	M Series Subminiature Solenoid Valve Brass body with EPDM plunger seal and O-ring (others available)	100 PSI	0.5 W	0.018 – 0.070	0.610” diameter (0.675” max) x 2.02” long	~ $32	
Asco Valves [12]	RB Series 15mm Solenoid Valve Stainless steel, PBT, and Brass with FKM, NBR, PBT seals	100 PSI	0.5 W – 2 W	0.025 – 0.080 (0.030” – 0.080” orifice)	0.76” diameter x 1.62” long 1.5 oz.		
Asco Valves [13]	411 Series 19mm Solenoid Valve Plastic or stainless steel body	100 PSI	0.65 W – 2 W	0.01 – 0.07 (0.025” – 0.080” orifice)	0.05 lb	~ $42	
Asco Valves [14]	MU8262 Series Magnetic Latching Solenoid Valve Brass or stainless steel with NBR / UR	1500 PSI – 2025 PSI	33.2 W	0.06 (3/64” orifice)	2.8” long x 1.19” diameter		

Busek [15]	Miniature Valve	> 500 PSI	< 40 mW		< 10 cc 35g		
Nitrous Oxide Systems [16]	Car Nitrous Valve 18045NOS	> 600 PSI, leaks below	8.60 amps	400 HP		$153.95	
Nitrous Oxide Systems [17]	Car Nitrous Valve 18020NOS	> 600 PSI, leaks below	8.60 amps	150 HP		$109.95	
Nitrous Express [18]	R/C Nitrous Solenoid (0.031 orifice)	1100 PSI	Two 9V batteries	0.031” orifice	1.053” diameter with maximum width of 1.23”, 2.4” tall, 0.22 kg	$106.43	

Gems Sensors & Controls [19]	A Series Solenoid Valve Stainless steel, brass, or plastic body with many seal and O-ring options	1000 PSI MOPD	6 Watts	0.020 Cv (1/32" orifice) at 1000 PSI	1.97" tall x 1.03" diameter	~ $45	
Parker [20]	Series 9 – Miniature Calibrant Gas Valve Stainless steel with PTFE and FKM or FKM and Vespel	1250 PSI	12 W	0.030" orifice at 1250 PSI	1.64" tall, 1.63" long, 0.75" width		
Omega [21]	2-Way General Purpose Solenoid Valves SV120 Series Stainless steel, copper, and KEL-F, FKM, or PTFE seal	1000 PSI	10 W	0.06 (3/64" orifice)	2.84" tall, 2.76" wide with 1.62" diameter 500 g	$99.00	
Valcor Engineering [22]	SV350 Normally Closed High Pressure Piloted Piston Solenoid Valves Stainless steel with Viton and PTFE	2200 PSI	10 W	1.1 (3/8" orifice)	3.61" tall, 1.87" diameter 1.8 lb		

Valcor Engineering [23]	Solenoid Valve Series V3400-52	1000-1200 PSIG	1 A, 18 VDC Max 30 VDC	0.073 Cv (0.062" orifice)	0.9" square, 2.85" + 0.9" tall 0.38 lb		
Valcor Engineering [24]	Solenoid Valve Series V27200M	1000 PSIG 2250 PSIG proof	0.65 A at 30 VDC Min. 18 VDC	0.02 (0.033" orifice)	0.938" diameter, 1.969" tall 0.22 lb		
Marotta Controls [25]	Latching Miniature Solenoid Valve Stainless steel with plastic seat	2000 PSI	10 W peak Pulse open				
Marotta Controls [26]	Non-Latching Miniature Solenoid Valve	MEOP = 10 bar Proof = 15 bar Burst = 40 bar	4 W, 6.2 W maximum		< 30 g		

Regulator Source Links:

[1] http://aeroconsystems.com/cart/reducing-regulators/model-1247-inline-reducing-regulator/

[2] http://www2.emersonprocess.com/en-US/brands/tescom/PressureReducing/Multi-Purpose/Cvlessthan03/04/Pages/04.aspx

[3] http://www.aquaenvironmentinc.com/om-sheets.html

[4] http://vonberg.com/catalog_detail.html?partID=85

[5] http://www.nuvair.com/store/valve-ss2.shtml

[6] http://palmer-pursuit.com/cart/index.php?main_page=index&cPath=25_27

[7] http://www.punisherspb.com/Product/Ninja-Nitrogen-Tank-Regulator-4500psi__NINJA-NITROGEN-REGULATOR-4500PSI.aspx?gclid=CO_x1v39lLwCFRSFfgod2DEAVA#.UuFnIBDTmHs

Solenoid Valve Source Links:

[8] http://www.theleeco.com/electro-fluidic-systems/special-products/iep/iep-series-solenoid-valves.cfm

[9] http://www.valvetech.net

[10] http://www.gemssensors.com/en/Products/Solenoid-Valves/General-Purpose/E-EH-Series-Solenoid-Valve

[11] http://www.gemssensors.com/en/Products/Solenoid-Valves/General-Purpose/M-Series-Valves

[12] http://www.ascovalve.com/Common/PDFFiles/Product/RBSERIES_PG65.pdf

[13] http://www.ascovalve.com/Applications/Products/MiniatureGeneralServiceValves.aspx

[14] http://www.ascovalve.com/Common/PDFFiles/Product/Mag_Latch_R2.pdf

[15] http://www.busek.com/index_htm_files/70008501E.pdf

[16] http://www.summitracing.com/parts/nos-18045nos/overview/

[17] http://www.summitracing.com/parts/nos-18020nos/overview/

[18] http://www.nitrousexpress.com/15098-rc-nitrous-solenoid-031-orifice.html

[19] http://www.gemssensors.com/en/Products/Solenoid-Valves/General-Purpose/A-Series-Solenoid-Valve

[20] http://ph.parker.com/us/12051/en/series-9-miniature-calibrant-gas-valve

[21] http://www.omega.com/pptst/SV120_Series.html

[22] http://www.valcor.com/valcor-technical-datasheets/2-way-high-pressure-pilot-operated-solenoid-valve-SV350-450.pdf

[23] http://www.valcor.com/valcor-technical-datasheets/2-way-fuel-control-solenoid-shutoff-valve-SV3400.pdf

[24] http://www.valcor.com/valcor-technical-datasheets/2-way-miniaturized-direct-acting-solenoid-shutoff-valve-SV27200%20-%20MINIATURIZED.pdf

[25] http://www.marotta.com/fluid-control-building-blocks/miniature-latch-systems.html

APPENDIX G Nitrous Oxide Saturation Properties

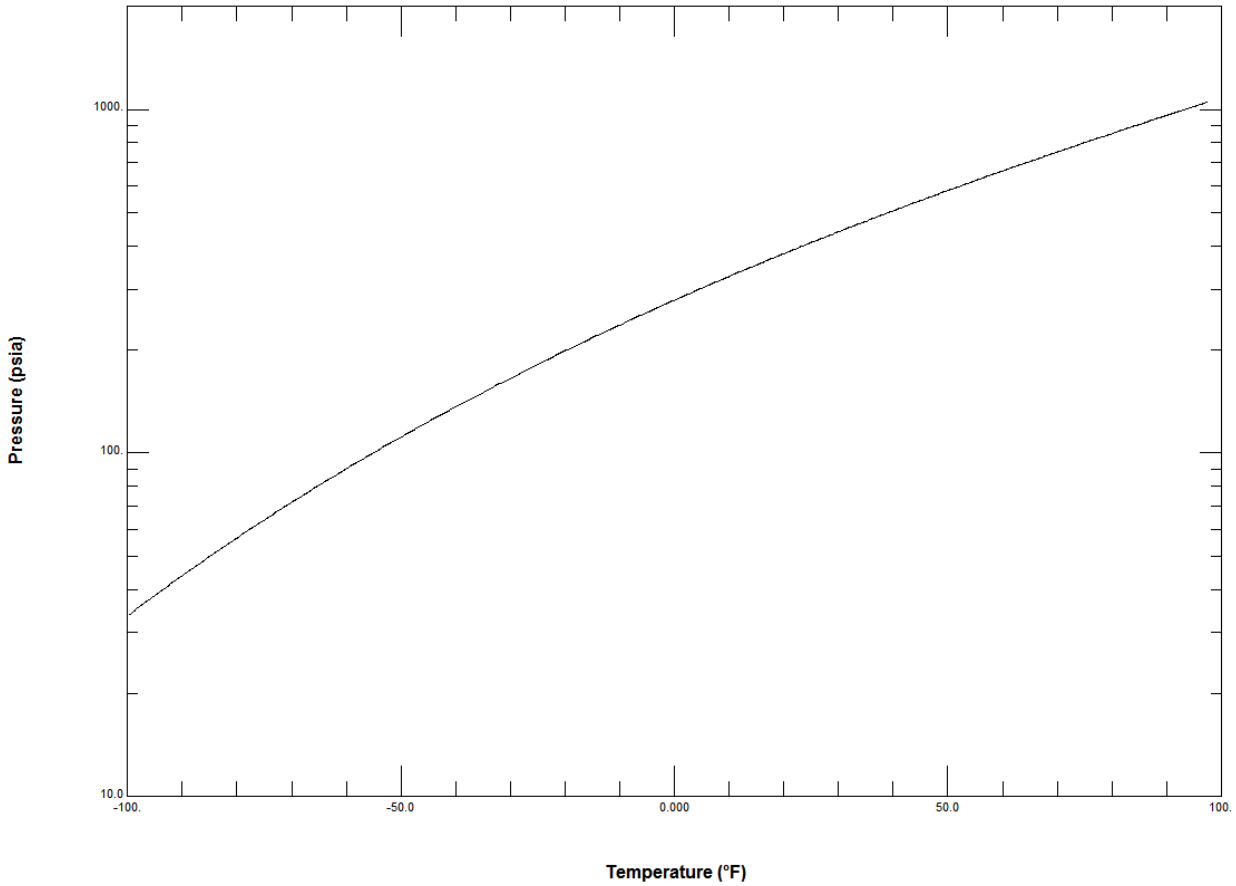

Figure G.1 Nitrous Oxide Vapor Pressure vs. Temperature

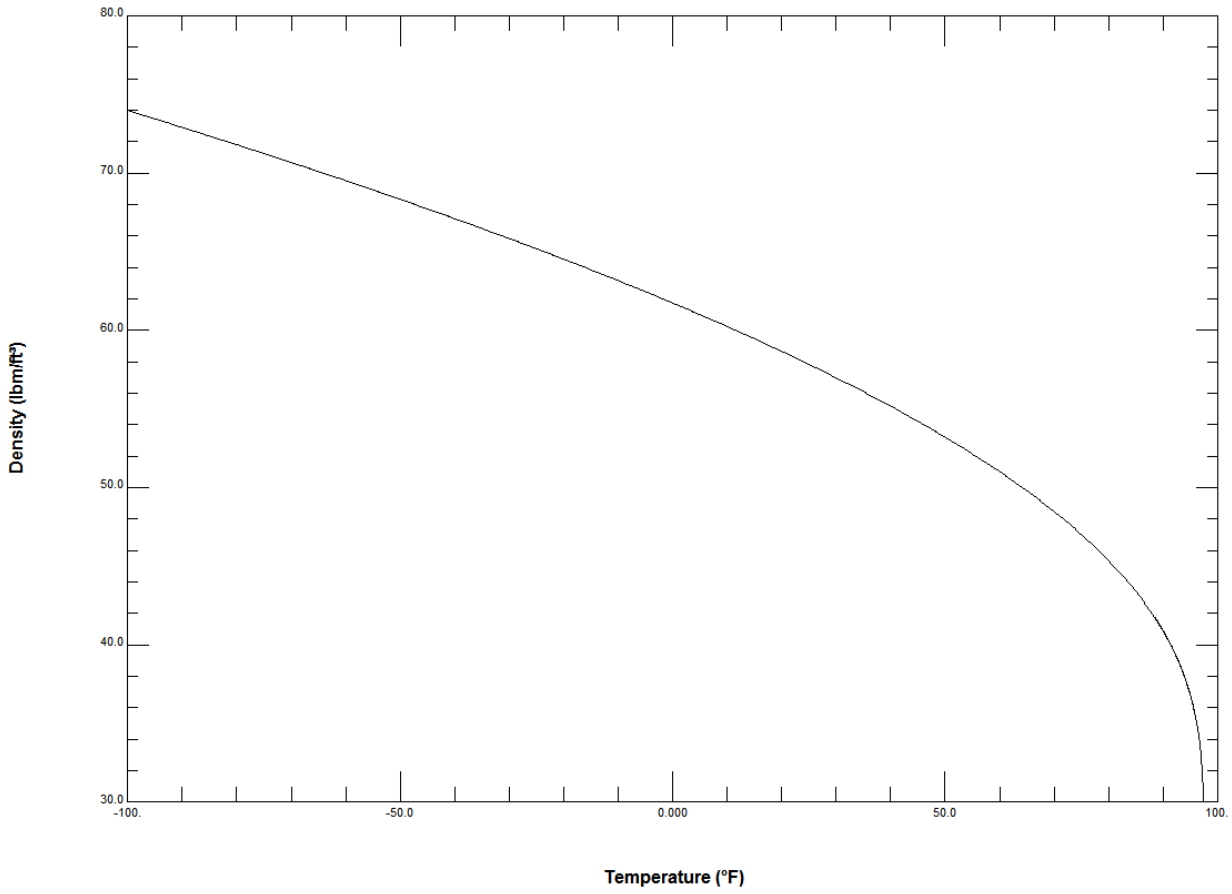

Figure G.2 Nitrous Oxide Density vs. Temperature

APPENDIX H N2O Soak Cell Fill Checklist

Nitrous Oxide Soak Cell Filling Procedure:

- ❑ Open the test cell bay door.
- ❑ Place a box fan to help force venting nitrous oxide out of the test cell.
- ❑ Bring the nitrous oxide fill bottle into the test cell using the bottle cart and chain it to the wall.
- ❑ Ensure that all valves to and from the soak cell are closed.
- ❑ Connect the flex hose from the fill line to the fill bottle.
- ❑ Slowly open the fill bottle. Once fully pressurized, open completely and move to the next step.
- ❑ Slowly open the vent valve in the fill line. When liquid nitrous oxide is seen escaping, close the valve. The fill line should now be full of liquid nitrous oxide. Do not place any body parts near or on the gas, liquid, or frost. Nitrous oxide gas, liquid, and frost is extremely cold.
- ❑ Slowly open the hand valve at the bottom of the soak cell. The soak cell should begin to fill.
- ❑ After several seconds, open the vent valve at the top of the soak cell to allow nitrous oxide gas to vent from the top of the tank. This causes the tank pressure to drop and liquid nitrous oxide from the fill bottle to transfer into the soak cell. Do not place any body parts in front of the exhaust gas. Gas is extremely cold.
- ❑ Fill the nitrous oxide soak cell until liquid is seen exhausting from the vent valve. This transition from gas to liquid can be both audibly and visually observed. At this point, liquid has reached the siphon tube in the soak cell. This ensures sufficient head space remains above the liquid level to allow for changes in density with temperature.
- ❑ Once filled, close the vent valve at the top of the soak cell and the hand valve at the bottom of the soak cell.

❑ Close the fill bottle.

❑ Slowly open the vent valve in the fill line to clear the line of nitrous oxide. Do not place any body parts near or on the gas, liquid, or frost. Nitrous oxide gas, liquid, and frost is extremely cold.

❑ Once the nitrous oxide is completely vented, close the vent valve.

❑ Disconnect the flex line from the nitrous oxide fill tank and remove the nitrous oxide fill bottle from the test cell.

Test Procedure:

❑ Monitor the soak cell pressure each day.

❑ Wait the soak duration and continue to the new test or test concluded section.

New Test:

❑ Using the vent valve at the top of the soak cell, vent all nitrous oxide. Once completely empty, leave vent valve open.

❑ Disassemble the soak cell setup, place foil over any exposed connections or tubing to preserve oxygen cleaning.

❑ Remove the test samples for analysis.

❑ Insert new test samples and close the soak cell. Reconnect all connections that were disconnected for removing the soak cell.

❑ Leak check the soak cell up to 1000 psi using nitrogen gas.

❑ Remove the nitrogen gas bottle and proceed to the soak cell filling procedure.

Test Concluded:

❑ Using the vent valve at the top of the soak cell, vent all nitrous oxide. Once completely empty, leave vent valve open.

- ❑ Disassemble the soak cell setup, place foil over any exposed connections or tubing to preserve oxygen cleaning.
- ❑ Remove the test samples for analysis.
- ❑ Close the soak cell and reconnect all connections to preserve oxygen clean state.

APPENDIX I Soak Cell Liquid Level Spreadsheet

Calculations for initial fill and mass removal:	
Initial Temperature (°F)	35
Total Volume of Soak Cell (in^3)	29.99
Gaseous Density at Ti (lbm/in^3)	3.23E-03
Liquid Density at Ti (lbm/in^3)	3.25E-02
Full Mass of Nitrous Oxide (lbm)	0.97
Removed Nitrous Oxide Mass (lbm)	0.27
Mass of Nitrous Oxide (lbm)	0.70
mtot = ml + mg = rhol*Vl + rhog*Vg	
Vtot = Vl + Vg	
Volume of Gaseous Nitrous Oxide (in^3)	9.24
Volume of Liquid Nitrous Oxide (in^3)	20.75
	Okay
If the temperature changes after the initial fill and mass removal:	
Temperature Final (°F)	85
Gaseous Density at Tf (lbm/in^3)	8.19E-03
Liquid Density at Tf (lbm/in^3)	2.51E-02
Volume of Gaseous Nitrous Oxide (in^3)	2.94
Volume of Liquid Nitrous Oxide (in^3)	27.04
	Okay

Liquid volume for a dip tube 2 inches into 8 inch pipe section (in^3)	20.90

select multiple of 5 between 35 and 95

insert positive value

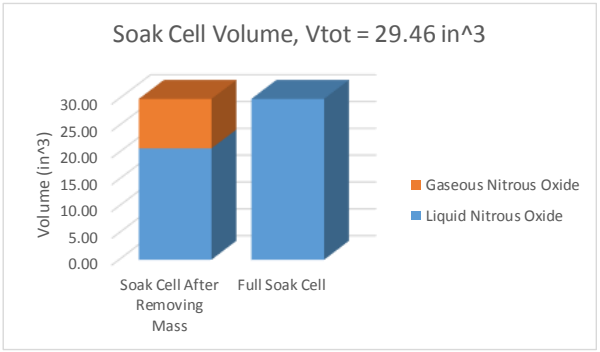

select multiple of 5 between 35 and 95

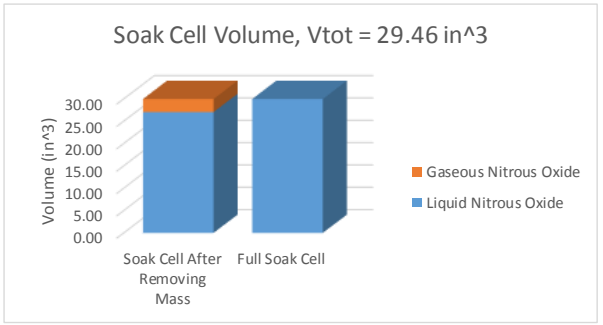

APPENDIX J Tensile Test Data Sheet

PSU-Aero Tensile Test _____		Date _____
ASTM D 638 - 08 Standard Test Method for Tensile Properties of Plastics Type I Specimen		
Testing Apparatus	Instron 5866 with 5 kN load cell and 2 inch extensometer	
Specimen Material		
Specimen Preparation		
Specimen Gage Dimensions	Model	Printed
Length (mm)	50	50
Width (mm)	13	
Thickness (mm)	3.2	
Test Conditions		
Temperature (°C)		
Relative Humidity (%)		
Speed of Testing (mm/min)		
Comments		

APPENDIX K Strength Tensile Testing Results

Table K.1 Specimen Information and Test Conditions

Summary of PSU-Aero Tensile Testing										
Test #	Material	Soak Duration (days)	Orientation	Specimen Type	Specimen Preparation	Gage Width (mm)	Gage Thickness (mm)	Temperature (°C)	Relative Humidity (%)	Test Speed (mm/min)
1	Aero Blue ABS	0	XY+	Check out tests						
2	Aero Blue ABS	0	XY+							
3	Aero Blue ABS	0	XY+							
4	Aero Blue ABS	0	XY+	I	filed edges	13.1868	3.4121	23.0	22	5
5	Aero Blue ABS	0	XY+	I	filed edges	13.1953	3.5069	23.1	22	5
6	Aero Blue ABS	0	XY+	I						
7	Aero Blue ABS	0	XY+	I						
8	Aero Blue ABS	0	XY+	I						
9	Aero Blue ABS	0	XY+	I						
10	NyTek 1200 CF	0	+ZX	I		12.8583	3.3139	23.3	22	5
11	NyTek 1200 CF	0	+ZX	I		12.8634	3.3130	23.3	22	5
12	NyTek 1200 CF	0	+ZX	I		12.7745	3.2986	23.3	22	5
13	NyTek 1200 CF	0	XY+	I		12.7813	3.4671	23.3	22	5
14	NyTek 1200 CF	0	XY+	I		12.7830	3.2063	23.3	22	5
15	NyTek 1200 CF	0	XY+	I		12.7906	3.2283	23.3	22	5
16	NyTek 1200 CF	0	+Z 45	I		12.8058	3.1919	23.4	22	5
17	NyTek 1200 CF	0	+Z 45	I		12.7906	3.2266	23.4	22	5
18	NyTek 1200 CF	0	+Z 45	I		12.8058	3.1462	23.4	22	5
19	Windform XT 2.0	0	+X	I		12.9709	3.2876	23.4	22	5
20	Windform XT 2.0	0	+X	I		13.0310	3.3155	23.4	22	5
21	Windform XT 2.0	0	+X	I		13.0497	3.3130	23.4	22	5
22	NyTek 1200 CF	14	+Z 45	I	14 day soak	12.8659	3.1979	22.9	22	5
23	NyTek 1200 CF	14	+Z 45	I	14 day soak	12.8753	3.1852	23.3	22	5
24	NyTek 1200 CF	14	+Z 45	I	14 day soak	12.8676	3.2089	23.3	22	5
25	NyTek 1200 CF	14	XY+	I	14 day soak	12.8499	3.4671	23.4	22	5
26	NyTek 1200 CF	14	XY+	I	14 day soak	12.7627	3.2139	23.4	22	5
27	NyTek 1200 CF	14	XY+	I	14 day soak	12.8803	3.4908	23.4	22	5
28	NyTek 1200 CF	14	+ZX	I	14 day soak	12.8803	3.3215	23.4	22	5
29	NyTek 1200 CF	14	+ZX	I	14 day soak	12.8050	3.3105	23.5	22	5
30	NyTek 1200 CF	14	+ZX	I	14 day soak	12.8753	3.3393	23.5	22	5
31	Windform XT 2.0	14	+X	I	14 day soak	13.0852	3.3232	23.5	22	5
32	Windform XT 2.0	14	+X	I	14 day soak	13.0548	3.3409	23.6	22	5
33	Windform XT 2.0	14	+X	I	14 day soak	13.0937	3.3172	23.6	22	5
34	NyTek 1200 CF	28	+Z 45	I	28 day soak	12.8482	3.2089	22.9	22	5
35	NyTek 1200 CF	28	+Z 45	I	28 day soak	12.8778	3.2089	23.3	22	5
36	NyTek 1200 CF	28	+Z 45	I	28 day soak	12.8609	3.2216	23.3	22	5
37	NyTek 1200 CF	28	XY+	I	28 day soak	12.8482	3.5010	23.4	22	5
38	NyTek 1200 CF	28	XY+	I	28 day soak	12.7635	3.2343	23.4	22	5
39	NyTek 1200 CF	28	XY+	I	28 day soak	12.7169	3.2427	23.4	22	5
40	NyTek 1200 CF	28	+ZX	I	28 day soak	12.8609	3.2935	23.4	22	5
41	NyTek 1200 CF	28	+ZX	I	28 day soak	12.8016	3.3062	23.5	22	5
42	NyTek 1200 CF	28	+ZX	I	28 day soak	12.7974	3.2808	23.5	22	5
43	Windform XT 2.0	28	+X	I	28 day soak	13.0768	3.3867	23.5	22	5
44	Windform XT 2.0	28	+X	I	28 day soak	13.0429	3.3951	23.6	22	5

Table K.2 Strength Tensile Testing Results

Summary of PSU-Aero Tensile Testing										
Test #	Material	Soak Duration (days)	Orientation	Tensile Strength (MPa)	Yield Strength (MPa)	Fracture Strength (MPa)	Percent Elongation at Yield (%)	Percent Elongation at Break (%)	Nominal Strain at Break (mm/mm)	Modulus of Elasticity (MPa)
1	Aero Blue ABS	0	XY+	Check out tests						
2	Aero Blue ABS	0	XY+							
3	Aero Blue ABS	0	XY+							
4	Aero Blue ABS	0	XY+	32.4	30.1	29.7	1.88	4.58	0.0497	1799
5	Aero Blue ABS	0	XY+	31.4	29.4	29.2	1.85	4.35	0.0514	1768
6	Aero Blue ABS	0	XY+							
7	Aero Blue ABS	0	XY+							
8	Aero Blue ABS	0	XY+							
9	Aero Blue ABS	0	XY+							
10	NyTek 1200 CF	0	+ZX	43.6	32.4	43.5	1.71	5.01	0.0577	2181
11	NyTek 1200 CF	0	+ZX	44.0	32.2	43.9	1.64	5.24	0.0587	2232
12	NyTek 1200 CF	0	+ZX	42.8	33.8	42.7	1.70	3.70	0.0444	2259
13	NyTek 1200 CF	0	XY+	62.8	48.1	63.0	1.33	5.10	0.0634	4268
14	NyTek 1200 CF	0	XY+	52.5	40.0	54.6	1.60	7.90	0.0831	2867
15	NyTek 1200 CF	0	XY+	53.2	37.5	54.4	1.49	7.90	0.0781	2899
16	NyTek 1200 CF	0	+Z 45	47.8	34.8	48.8	1.60	5.70	0.0643	2480
17	NyTek 1200 CF	0	+Z 45	48.9	34.6	49.0	1.58	7.10	0.0768	2504
18	NyTek 1200 CF	0	+Z 45	48.2	35.8	49.4	1.60	6.10	0.0660	2547
19	Windform XT 2.0	0	+X	80.3	63.7	80.2	1.19	3.80	0.0514	6436
20	Windform XT 2.0	0	+X	81.0	63.6	81.0	1.08	3.30	0.0491	7261
21	Windform XT 2.0	0	+X	81.3	63.4	81.3	1.11	3.70	0.0490	6995
22	NyTek 1200 CF	14	+Z 45	35.8	18.4	35.7	2.15	11.1	0.108	945
23	NyTek 1200 CF	14	+Z 45	36.2	20.8	36.1	2.31	10.6	0.103	985
24	NyTek 1200 CF	14	+Z 45	35.9	18.1	35.5	2.21	11.5	0.112	902
25	NyTek 1200 CF	14	XY+	47.9	25.1	47.3	1.35	8.35	0.0849	2176
26	NyTek 1200 CF	14	XY+	40.9	20.1	40.6	1.80	10.4	0.111	1255
27	NyTek 1200 CF	14	XY+	48.3	28.6	48.1	1.71	8.05	0.0837	1897
28	NyTek 1200 CF	14	+ZX	29.0	15.3	28.2	1.49	6.80	0.0714	1190
29	NyTek 1200 CF	14	+ZX	30.0	15.3	29.8	1.49	7.70	0.0578	1189
30	NyTek 1200 CF	14	+ZX	30.6	15.0	30.4	1.50	8.73	0.0851	1152
31	Windform XT 2.0	14	+X	62.5	37.0	61.2	1.15	5.72	0.0644	3909
32	Windform XT 2.0	14	+X	62.3	34.5	62.1	1.02	6.04	0.0656	4197
33	Windform XT 2.0	14	+X	63.0	37.4	62.9	1.13	5.70	0.0626	4000
34	NyTek 1200 CF	28	+Z 45	35.6	19.9	35.4	2.039	9.700	0.10470	1082
35	NyTek 1200 CF	28	+Z 45	35.3	19.5	35.3	2.073	10.300	0.10176	1044
36	NyTek 1200 CF	28	+Z 45	35.6	20.2	35.4	2.232	10.800	0.10636	994
37	NyTek 1200 CF	28	XY+	37.4	22.9	36.9	2.508	12.400	0.11915	991
38	NyTek 1200 CF	28	XY+	51.0	29.4	50.6	1.485	8.500	0.08607	2292
39	NyTek 1200 CF	28	XY+	40.1	23.7	40.0	2.297	11.400	0.11136	1129
40	NyTek 1200 CF	28	+ZX	30.0	19.2	29.8	2.034	7.700	0.08249	1046
41	NyTek 1200 CF	28	+ZX	30.0	19.2	29.8	1.940	7.000	0.07201	1102
42	NyTek 1200 CF	28	+ZX	Extensometer Slipped						
43	Windform XT 2.0	28	+X	60.9	42.5	60.6	1.281	4.700	0.05937	3928
44	Windform XT 2.0	28	+X	61.4	42.0	61.3	1.385	5.300	0.06227	3544

Table K.3 Comparison of Pre- and Post-Soak NyTek 1200 CF +ZX

Test #	Material	Soak Duration (days)	Orientation	Tensile Strength (MPa)	Yield Strength (MPa)	Fracture Strength (MPa)	Percent Elongation at Yield (%)	Percent Elongation at Break (%)	Nominal Strain at Break (mm/mm)	Modulus of Elasticity (MPa)
10	NyTek 1200 CF	0	+ZX	43.6	32.4	43.5	1.71	5.01	0.0577	2181
11	NyTek 1200 CF	0	+ZX	44.0	32.2	43.9	1.64	5.24	0.0587	2232
12	NyTek 1200 CF	0	+ZX	42.8	33.8	42.7	1.70	3.70	0.0444	2259
		Average		43.4	32.8	43.4	1.68	4.65	0.0536	2224
		Standard Deviation		0.499	0.733	0.469	0.0306	0.678	0.00651	32.5
28	NyTek 1200 CF	14	+ZX	29.0	15.3	28.2	1.49	6.80	0.0714	1190
29	NyTek 1200 CF	14	+ZX	30.0	15.3	29.8	1.49	7.70	0.0578	1189
30	NyTek 1200 CF	14	+ZX	30.6	15.0	30.4	1.50	8.73	0.0851	1152
		Average		29.9	15.2	29.5	1.49	7.74	0.0715	1177
		Standard Deviation		0.682	0.155	0.946	0.00628	0.788	0.0111	17.5
40	NyTek 1200 CF	28	+ZX	30.0	19.2	29.8	2.034	7.700	0.08249	1046
41	NyTek 1200 CF	28	+ZX	30.0	19.2	29.8	1.940	7.000	0.07201	1102
42	NyTek 1200 CF	28	+ZX	Extensometer Slipped						
		Average		30.0	19.2	29.8	1.99	7.35	0.0772	1074
		Standard Deviation		0.0365	0.00890	0.00300	0.0470	0.350	0.00524	27.7

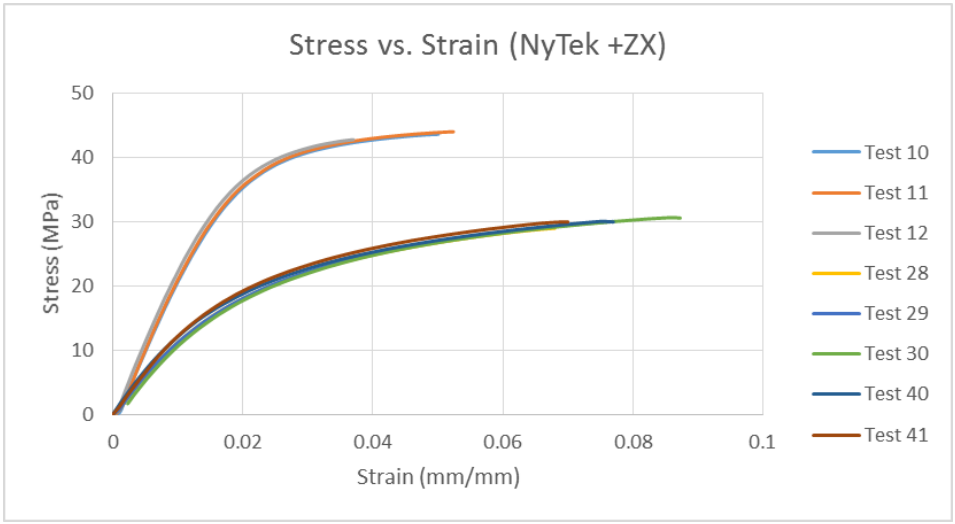

Figure K.1 Stress versus Strain for NyTek 1200 CF +ZX

Table K.4 Comparison of Pre- and Post-Soak NyTek 1200 CF XY+

Test #	Material	Soak Duration (days)	Orientation	Tensile Strength (MPa)	Yield Strength (MPa)	Fracture Strength (MPa)	Percent Elongation at Yield (%)	Percent Elongation at Break (%)	Nominal Strain at Break (mm/mm)	Modulus of Elasticity (MPa)
13	NyTek 1200 CF	0	XY+	62.8	48.1	63.0	1.33	5.10	0.0634	4268
14	NyTek 1200 CF	0	XY+	52.5	40.0	54.6	1.60	7.90	0.0831	2867
15	NyTek 1200 CF	0	XY+	53.2	37.5	54.4	1.49	7.90	0.0781	2899
		Average		56.2	41.9	57.3	1.47	6.97	0.0749	3345
		Standard Deviation		4.71	4.53	4.01	0.112	1.32	0.00836	653
25	NyTek 1200 CF	14	XY+	47.9	25.1	47.3	1.35	8.35	0.0849	2176
26	NyTek 1200 CF	14	XY+	40.9	20.1	40.6	1.80	10.4	0.111	1255
27	NyTek 1200 CF	14	XY+	48.3	28.6	48.1	1.71	8.05	0.0837	1897
		Average		45.7	24.6	45.4	1.62	8.95	0.0932	1776
		Standard Deviation		3.38	3.49	3.35	0.194	1.06	0.0126	386
37	NyTek 1200 CF	28	XY+	37.4	22.9	36.9	2.508	12.400	0.11915	991
38	NyTek 1200 CF	28	XY+	51.0	29.4	50.6	1.485	8.500	0.08607	2292
39	NyTek 1200 CF	28	XY+	40.1	23.7	40.0	2.297	11.400	0.11136	1129
		Average		42.8	25.3	42.5	2.10	10.8	0.106	1471
		Standard Deviation		5.91	2.93	5.83	0.441	1.65	0.0141	583

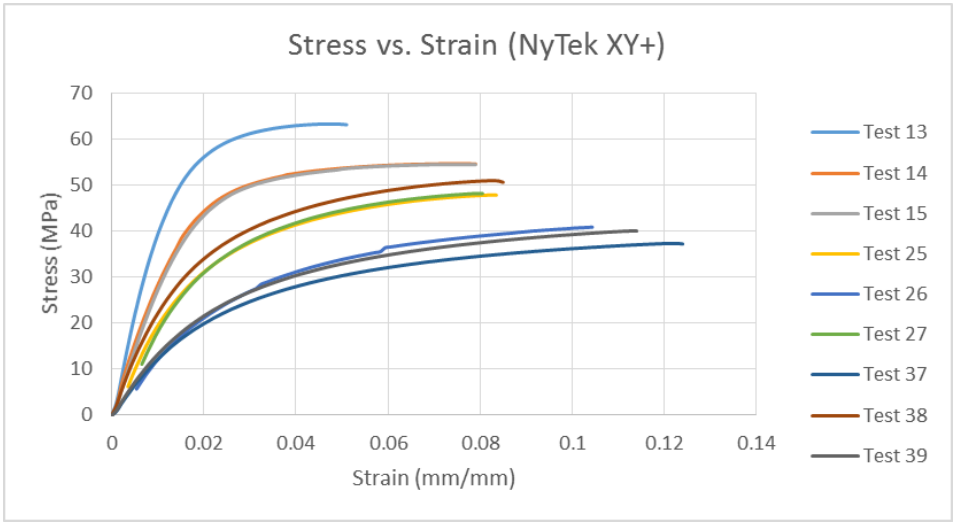

Figure K.2 Stress versus Strain for NyTek 1200 CF XY+

Table K.5 Comparison of Pre- and Post-Soak NyTek 1200 CF +Z 45

Test #	Material	Soak Duration (days)	Orientation	Tensile Strength (MPa)	Yield Strength (MPa)	Fracture Strength (MPa)	Percent Elongation at Yield (%)	Percent Elongation at Break (%)	Nominal Strain at Break (mm/mm)	Modulus of Elasticity (MPa)
16	NyTek 1200 CF	0	+Z 45	47.8	34.8	48.8	1.60	5.70	0.0643	2480
17	NyTek 1200 CF	0	+Z 45	48.9	34.6	49.0	1.58	7.10	0.0768	2504
18	NyTek 1200 CF	0	+Z 45	48.2	35.8	49.4	1.60	6.10	0.0660	2547
		Average		48.3	35.0	49.1	1.60	6.30	0.0690	2510
		Standard Deviation		0.449	0.518	0.245	0.0118	0.589	0.00553	27.7
22	NyTek 1200 CF	14	+Z 45	35.8	18.4	35.7	2.15	11.1	0.108	945
23	NyTek 1200 CF	14	+Z 45	36.2	20.8	36.1	2.31	10.6	0.103	985
24	NyTek 1200 CF	14	+Z 45	35.9	18.1	35.5	2.21	11.5	0.112	902
		Average		36.0	19.1	35.8	2.22	11.1	0.108	944
		Standard Deviation		0.183	1.19	0.257	0.0664	0.355	0.00348	34.0
34	NyTek 1200 CF	28	+Z 45	35.6	19.9	35.4	2.039	9.700	0.10470	1082
35	NyTek 1200 CF	28	+Z 45	35.3	19.5	35.3	2.073	10.300	0.10176	1044
36	NyTek 1200 CF	28	+Z 45	35.6	20.2	35.4	2.232	10.800	0.10636	994
		Average		35.5	19.9	35.4	2.11	10.3	0.104	1040
		Standard Deviation		0.165	0.267	0.0605	0.0842	0.450	0.00190	36.0

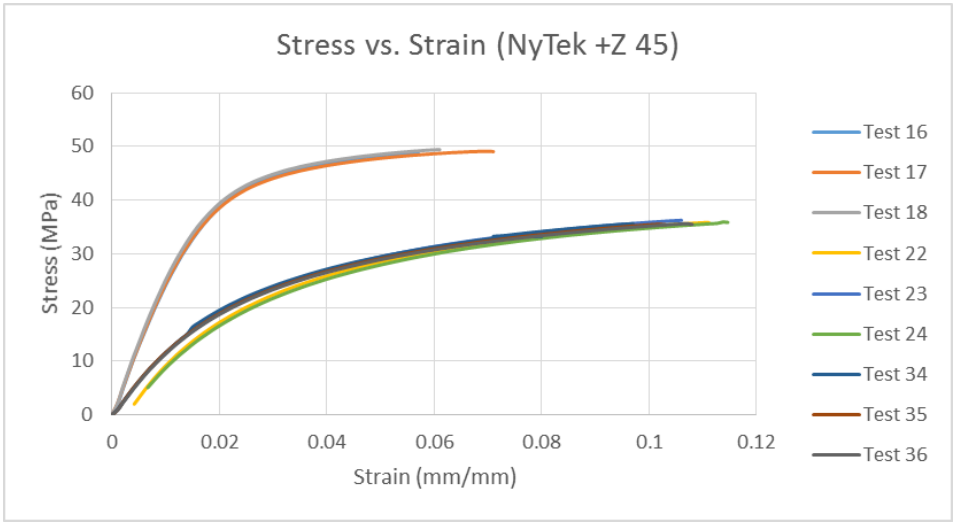

Figure K.3 Stress versus Strain for NyTek 1200 CF +Z 45

Table K.6 Comparison of Pre- and Post-Soak Windform XT 2.0 +X

Test #	Material	Soak Duration (days)	Orientation	Tensile Strength (MPa)	Yield Strength (MPa)	Fracture Strength (MPa)	Percent Elongation at Yield (%)	Percent Elongation at Break (%)	Nominal Strain at Break (mm/mm)	Modulus of Elasticity (MPa)
19	Windform XT 2.0	0	+X	80.3	63.7	80.2	1.19	3.80	0.0514	6436
20	Windform XT 2.0	0	+X	81.0	63.6	81.0	1.08	3.30	0.0491	7261
21	Windform XT 2.0	0	+X	81.3	63.4	81.3	1.11	3.70	0.0490	6995
		Average		80.9	63.6	80.8	1.12	3.60	0.0499	6897
		Standard Deviation		0.414	0.107	0.429	0.0480	0.216	0.00111	344
31	Windform XT 2.0	14	+X	62.5	37.0	61.2	1.15	5.72	0.0644	3909
32	Windform XT 2.0	14	+X	62.3	34.5	62.1	1.02	6.04	0.0656	4197
33	Windform XT 2.0	14	+X	63.0	37.4	62.9	1.13	5.70	0.0626	4000
		Average		62.6	36.3	62.1	1.10	5.82	0.0642	4035
		Standard Deviation		0.291	1.29	0.695	0.0565	0.156	0.00122	120
43	Windform XT 2.0	28	+X	60.9	42.5	60.6	1.281	4.700	0.05937	3928
44	Windform XT 2.0	28	+X	61.4	42.0	61.3	1.385	5.300	0.06227	3544
		Average		61.2	42.2	61.0	1.33	5.00	0.0608	3736
		Standard Deviation		0.267	0.222	0.348	0.0523	0.300	0.00145	192

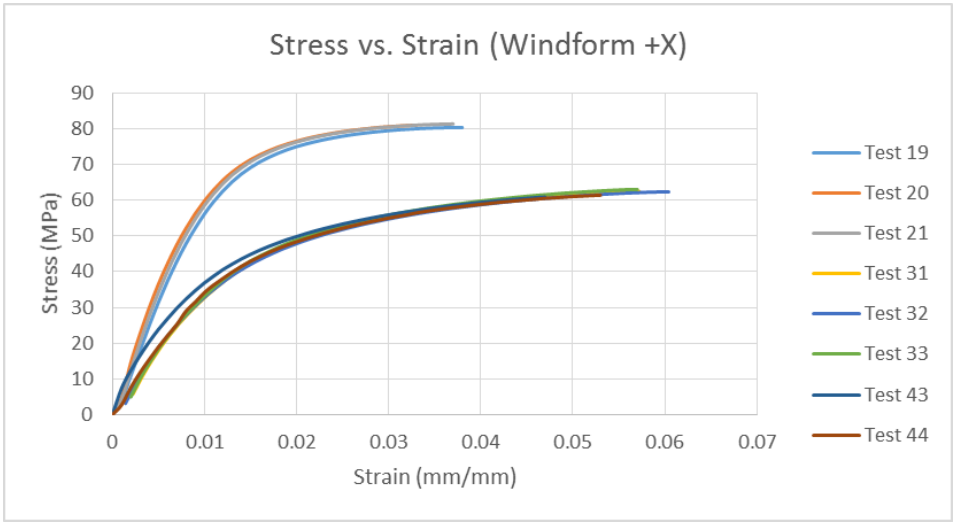

Figure K.4 Stress versus Strain for Windform XT 2.0 +X

APPENDIX L Hybrid Rocket Performance Pressure Dependence

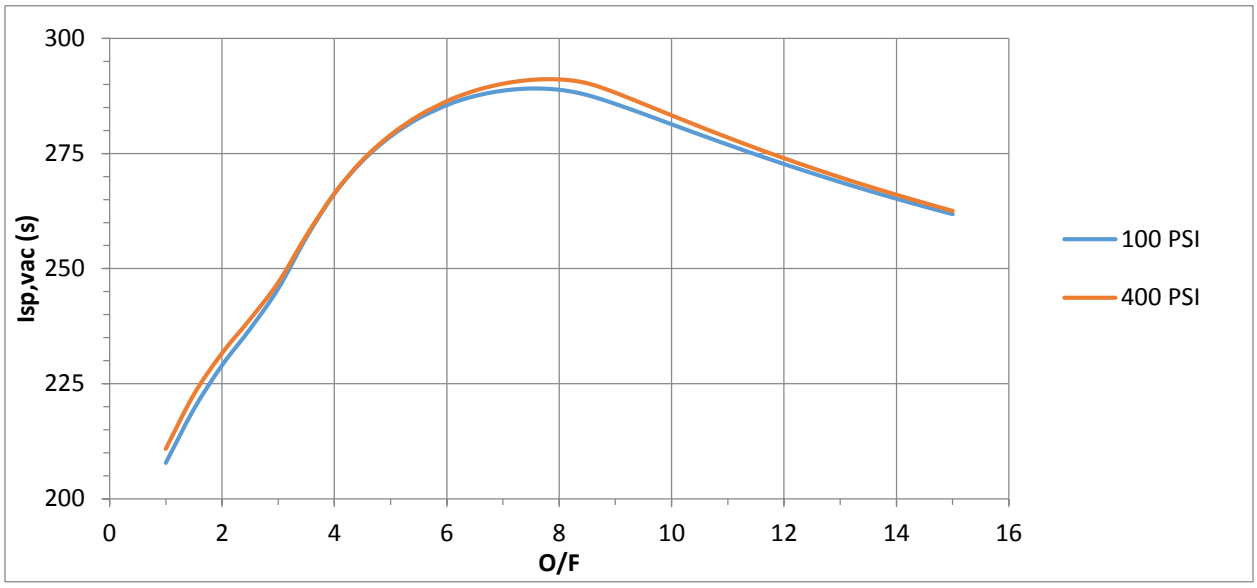

Figure L.1 Vacuum Specific Impulse vs. O/F Ratio for Paraffin 80wt% / Acrylic 20wt% with Nitrous Oxide at 100 psig and 400 psig Chamber Pressure

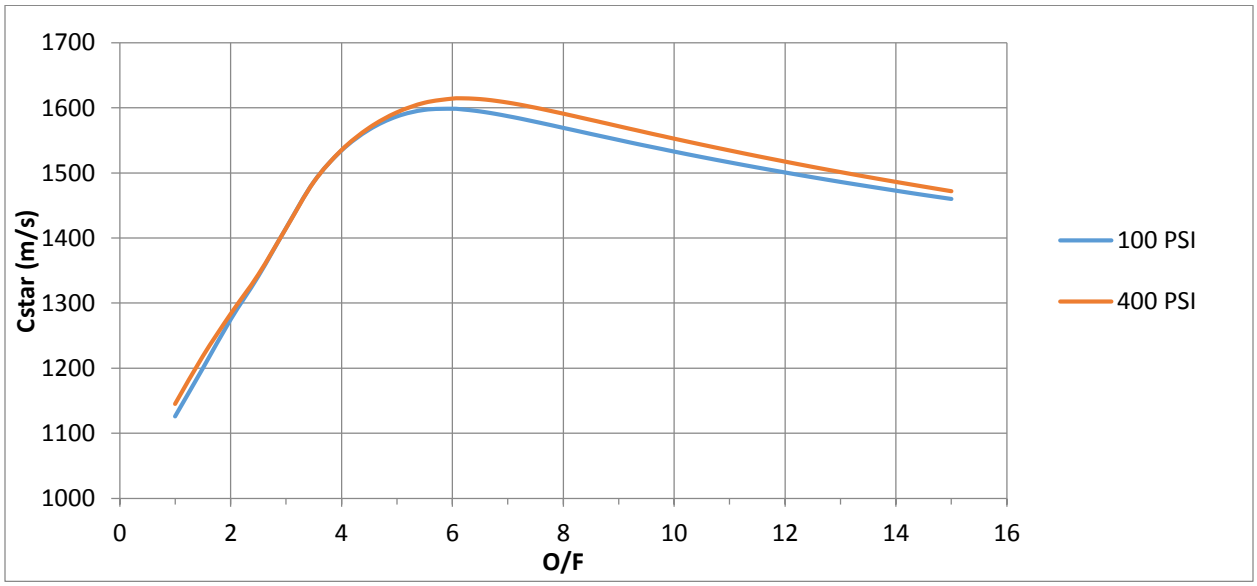

Figure L.2 c* vs. O/F Ratio for Paraffin 80wt% / Acrylic 20wt% with Nitrous Oxide at 100 psig and 400 psig Chamber Pressure

APPENDIX M N_2O LGCP Motor Test Data Sheet

PSU-Aero Test #_____ Date_____

Test Parameters

_____	%		He Reg. Press.	_____	psi
_____	%		N2O Mass Flow	_____	g/s
_____	%		act.	_____	g/s
_____	%		N2O Mass Flux	_____	kg/(m^2*s)
			Orifice Size	_____	in
Fuel Grain Mass			O2 Reg. Press.	_____	psi
Preburn	_____	g	O2 Pintle Pos.	_____	in
Postburn	_____	g	Test duration est.	_____	s
			act.	_____	s
Fuel Length	_____	in	Nozzle size	_____	in (dia)
Bore Preburn	_____	in (dia)	N2 Purge Press.	_____	psi
Bore Postburn	_____	in (dia)	He Bottle	_____	psi
			O2 Manifold	_____	psi
			N2 Purge Bottle	_____	psi

Data Acquisition

File Name _____ Sampling Rate _____ sec^-1

Pressure #1	_____	Channel	_____	Pressure #3	_____	Channel	_____
		Red				Green	
Pressure #2	_____	Channel	_____	Pressure #4	_____	Channel	_____
		Blue				Yellow	
TC #1	_____	Channel	_____	Load Cell	_____	Channel	_____
TC #2	_____	Channel	_____	LC Ref	_____	Channel	_____
Igniter Signal	_____	Channel	_____				

Comments

Test Personnel

Timing Sequence		
Open N2O Flow Valve	_____	sec
Open He Flow Valve	_____	sec
Open O2 Solenoid Valve	_____	sec
Open O2 Run Valve	_____	sec
Open O2 Flow Valve	_____	sec
Energize Igniter 1 Leads	_____	sec
De-energize Igniter 1 Leads	_____	sec
Open N2O Run Valve	_____	sec
Close O2 Solenoid Valve	_____	sec
Close O2 Run Valve	_____	sec
Close O2 Flow Valve	_____	sec
Close N2O Run Valve	_____	sec
Close He Flow Valve	_____	sec
Close N2O Flow Valve	_____	sec
Open N2 Purge Valve	_____	sec
Close N2 Purge Valve	_____	sec

APPENDIX N N_2O LGCP Motor Setup Walkthrough

Oxygen Tubing (in order):

Oxygen Manifold (RM 128)

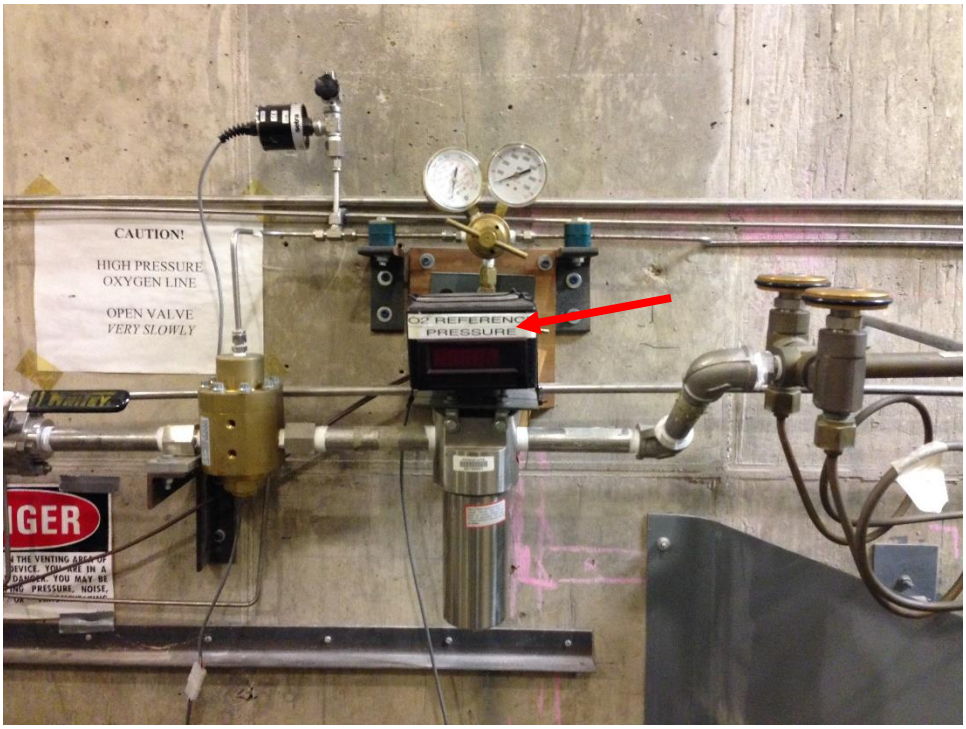

Oxygen Pressure Regulator and Filter (RM 128)

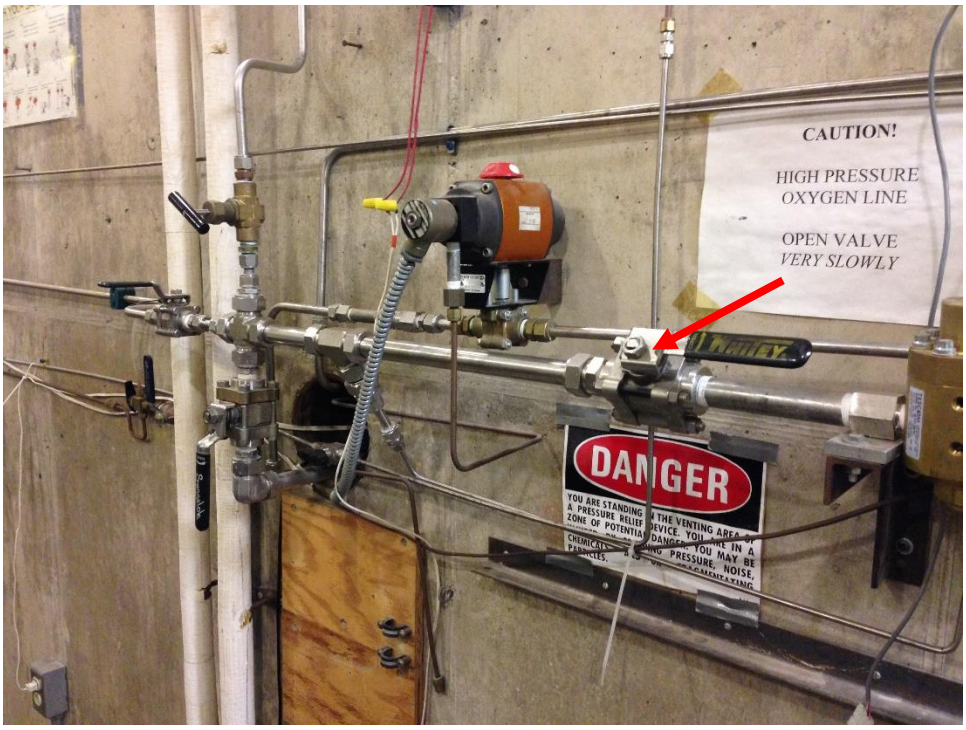

Oxygen Hand Valve (RM 128)

Nitrogen Reference for Oxygen Pressure Regulator (RM 128)

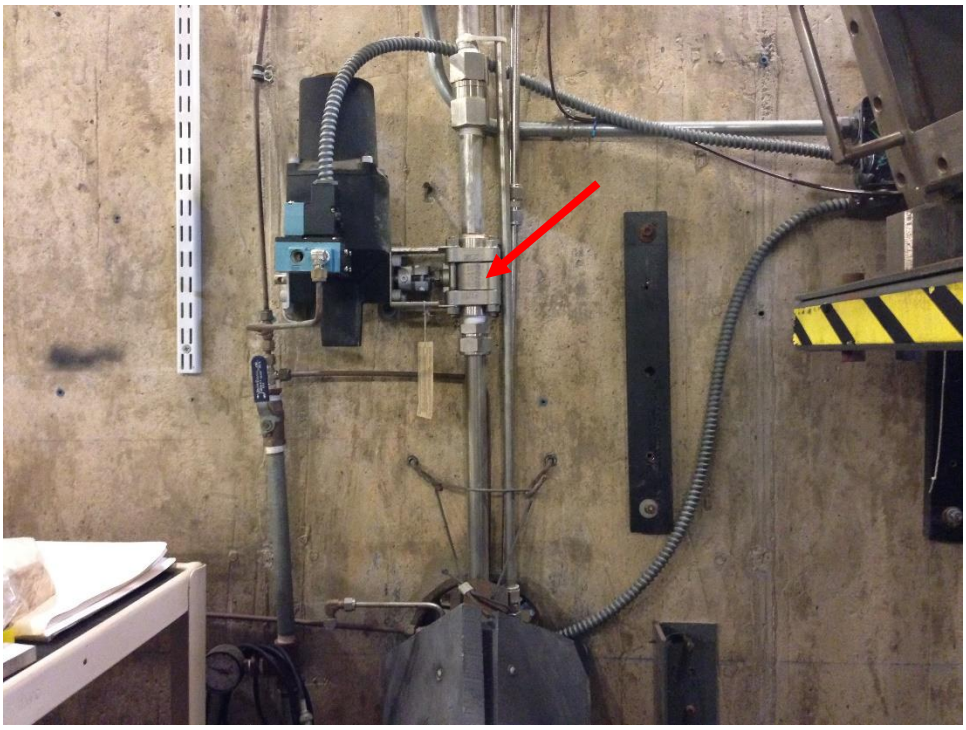

Oxygen Manifold Valve (RM 127)

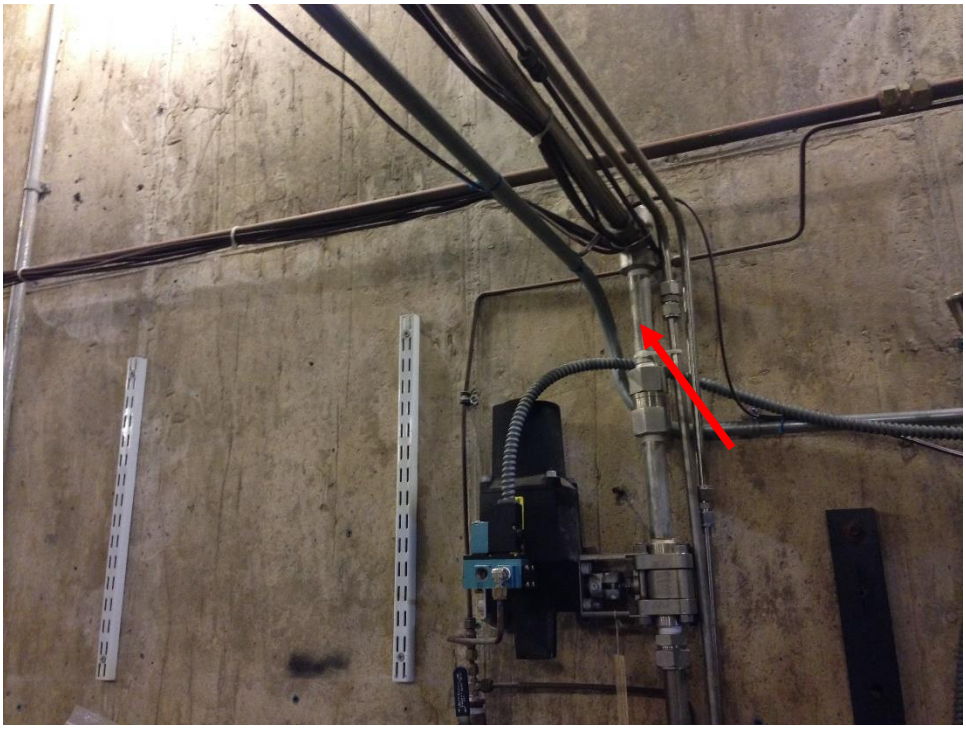

Oxygen Line (RM 127)

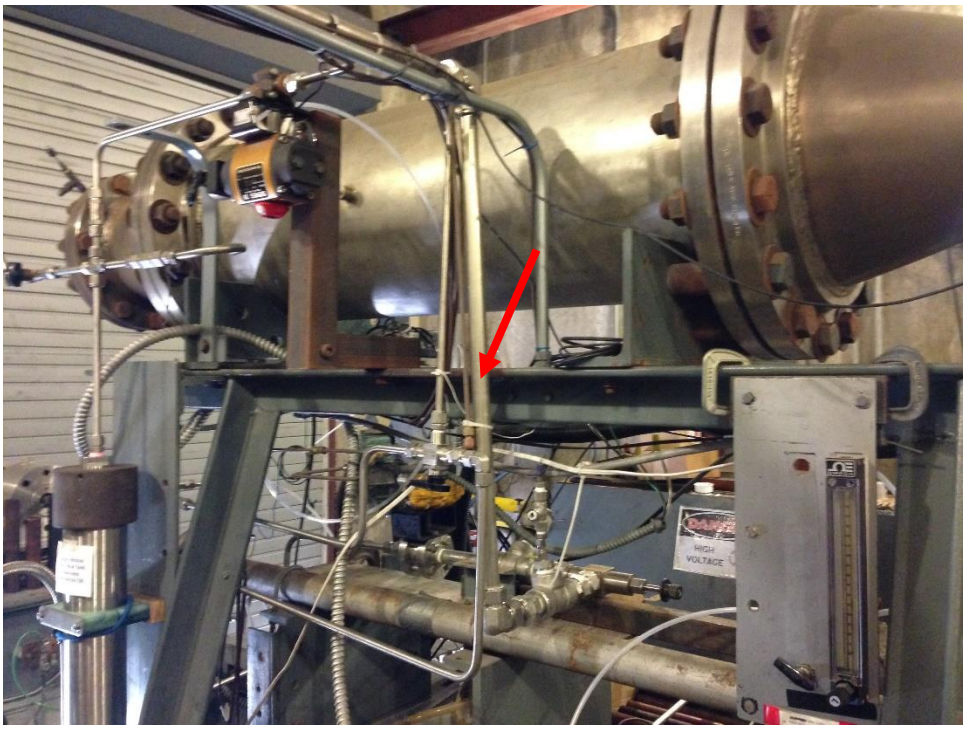

Oxygen Line (RM 127)

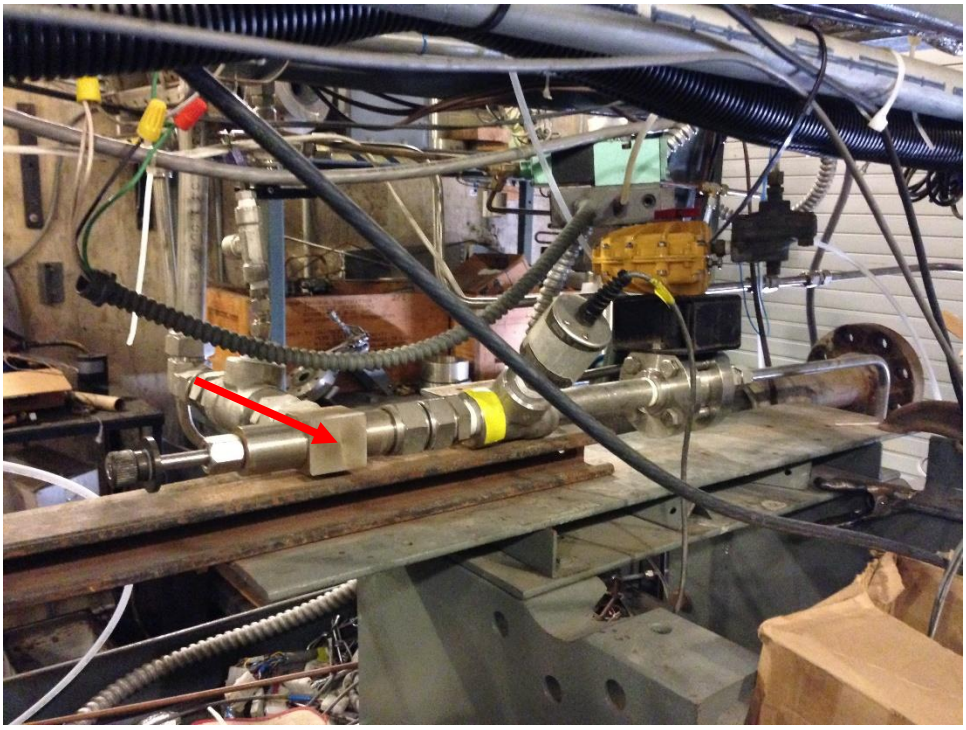
Oxygen Venturi Pintle and Run Valve (RM 127)

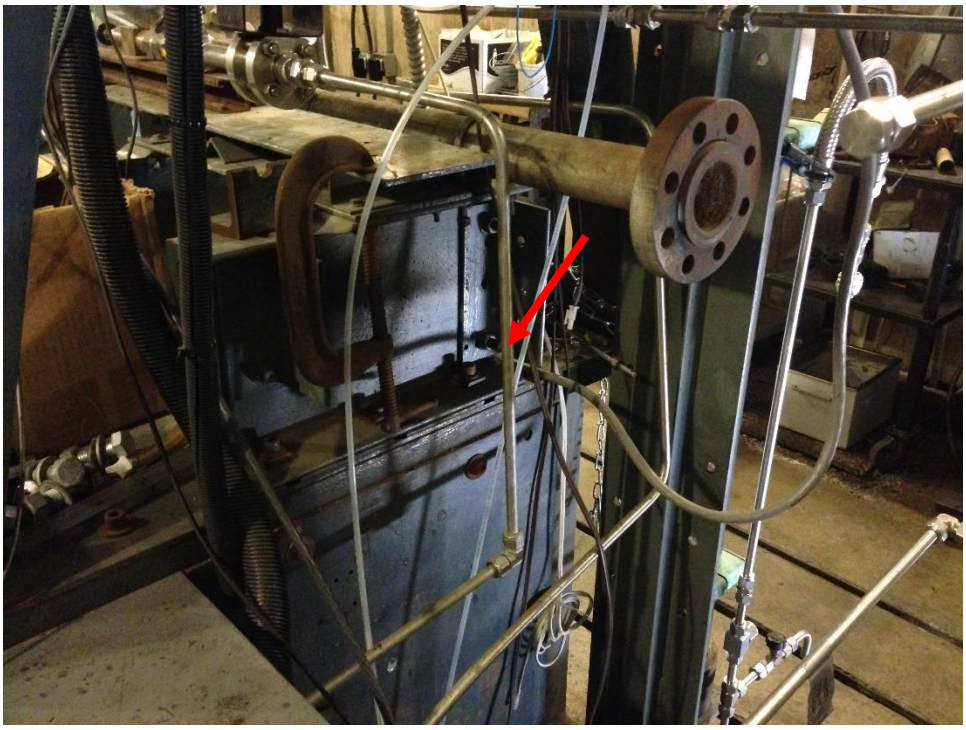

Oxygen Line (RM 127)

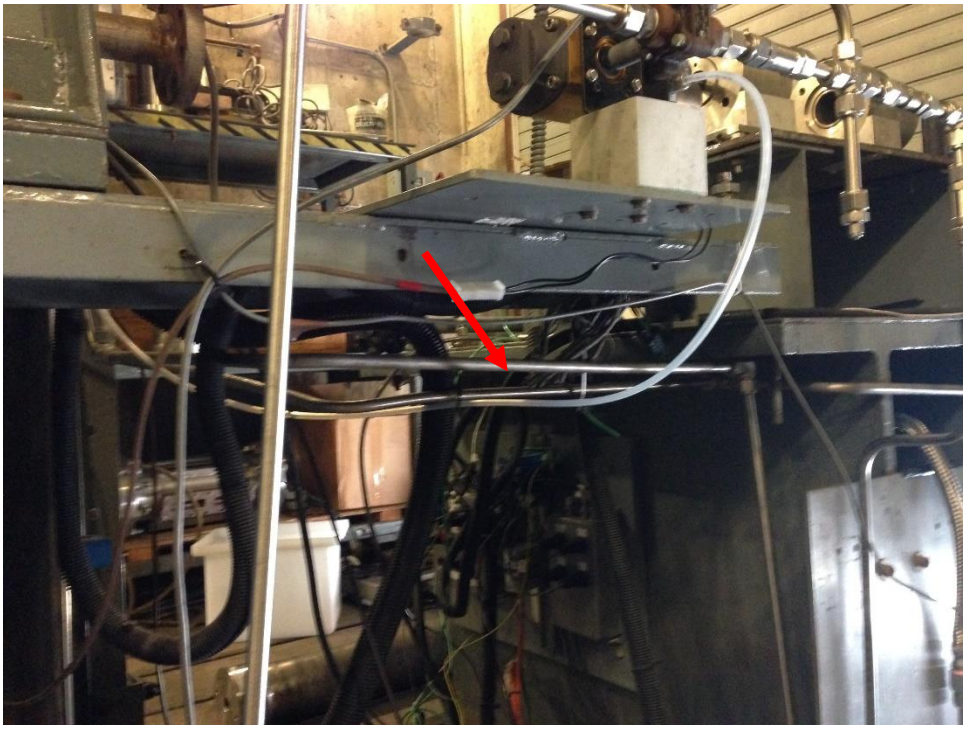

Oxygen Line (RM 127)

Oxygen Line (RM 127)

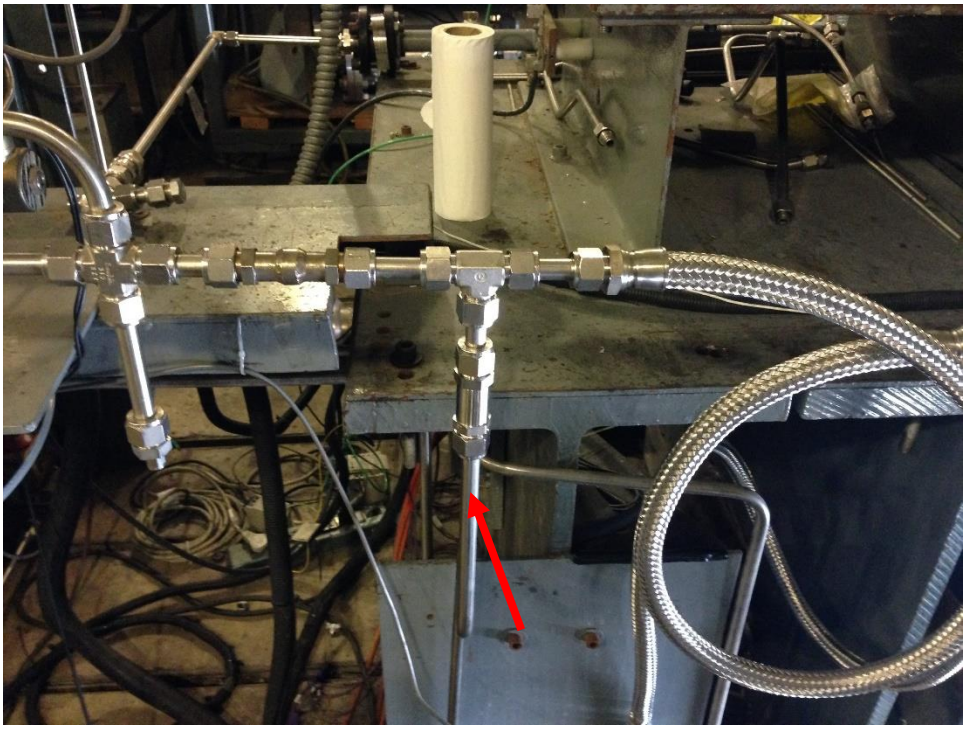

Oxygen Line (RM 127)

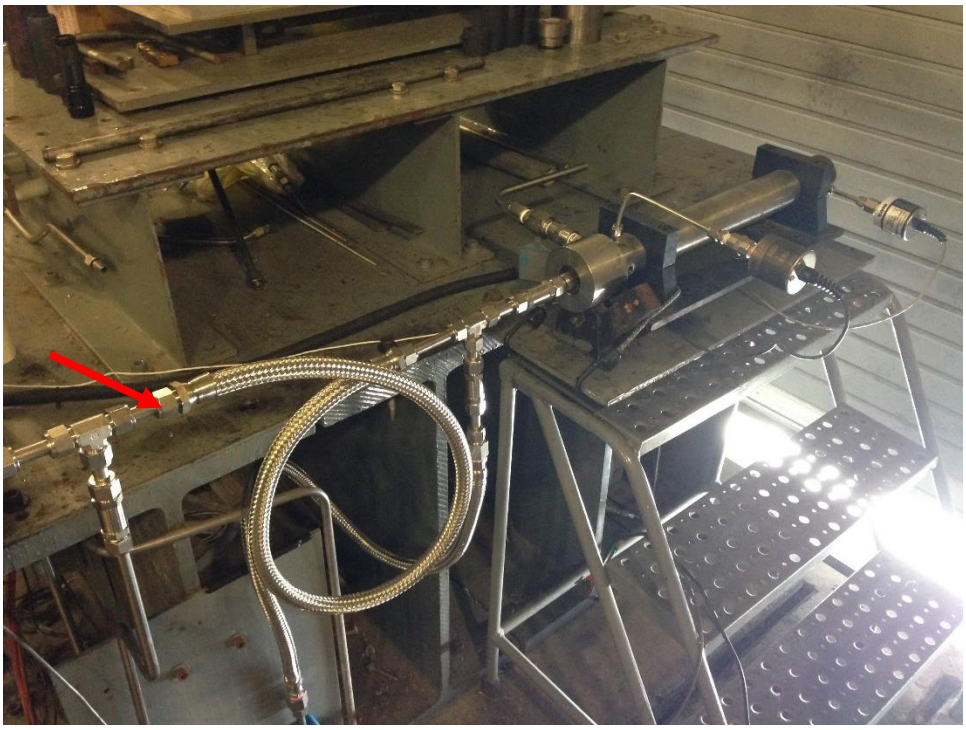

Oxygen into Motor (RM 127)

Nitrogen Tubing (in order):

Nitrogen Purge Bottle and Regulator (RM 128)

Nitrogen Purge Bottle and Regulator into Filter (RM 128)

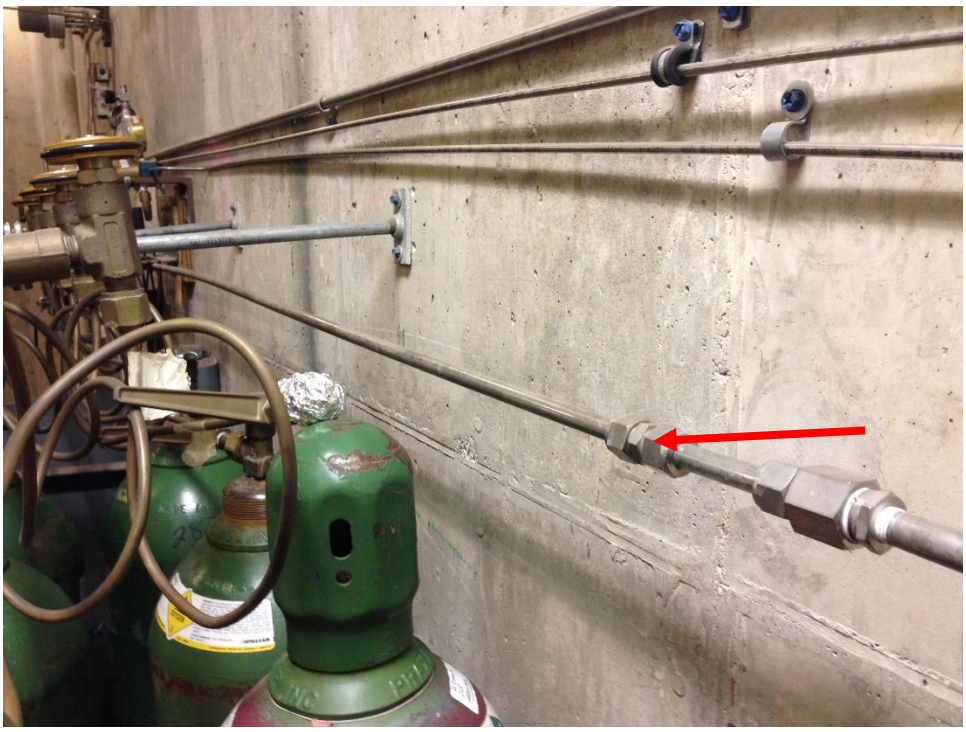
Nitrogen Purge Line (RM 128)

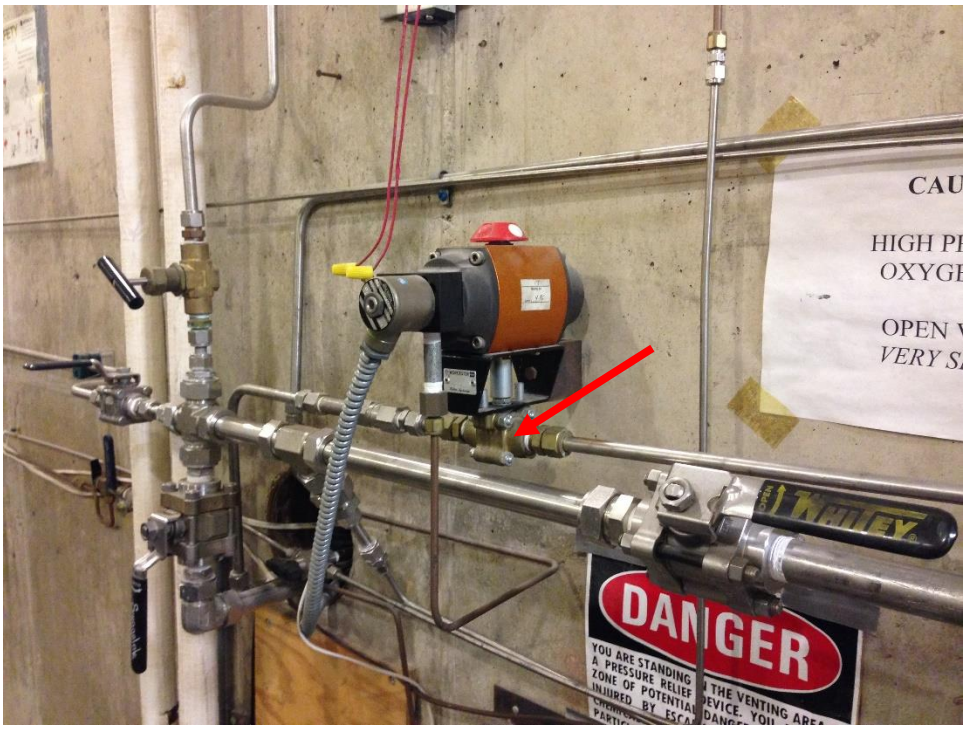

Nitrogen Purge Valve (RM 128)

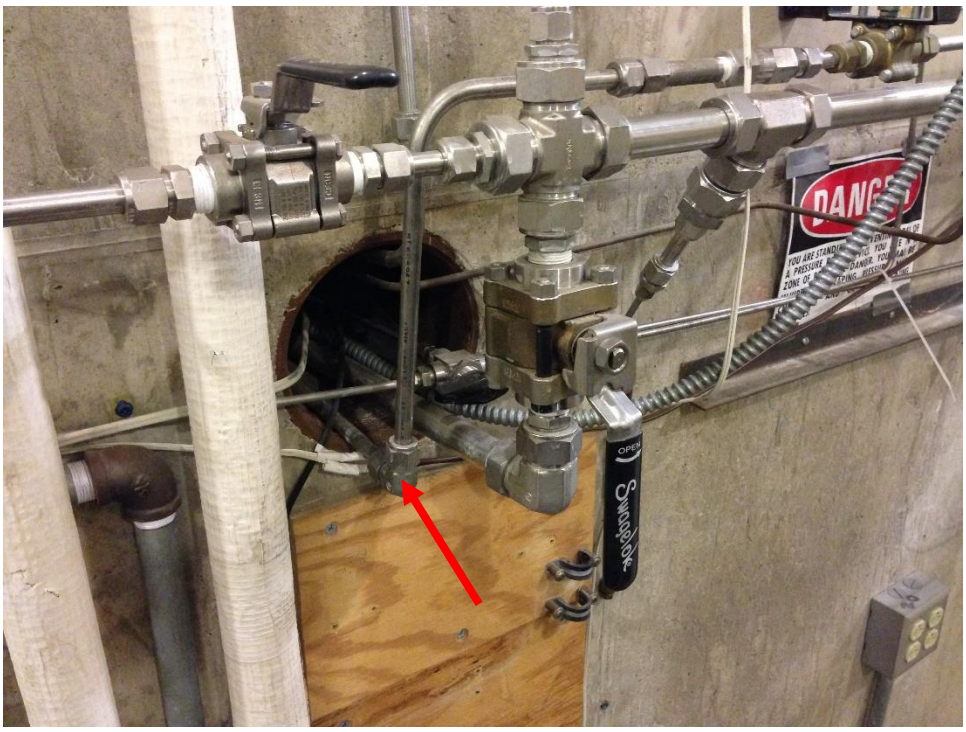
Nitrogen Purge Line (RM 128)

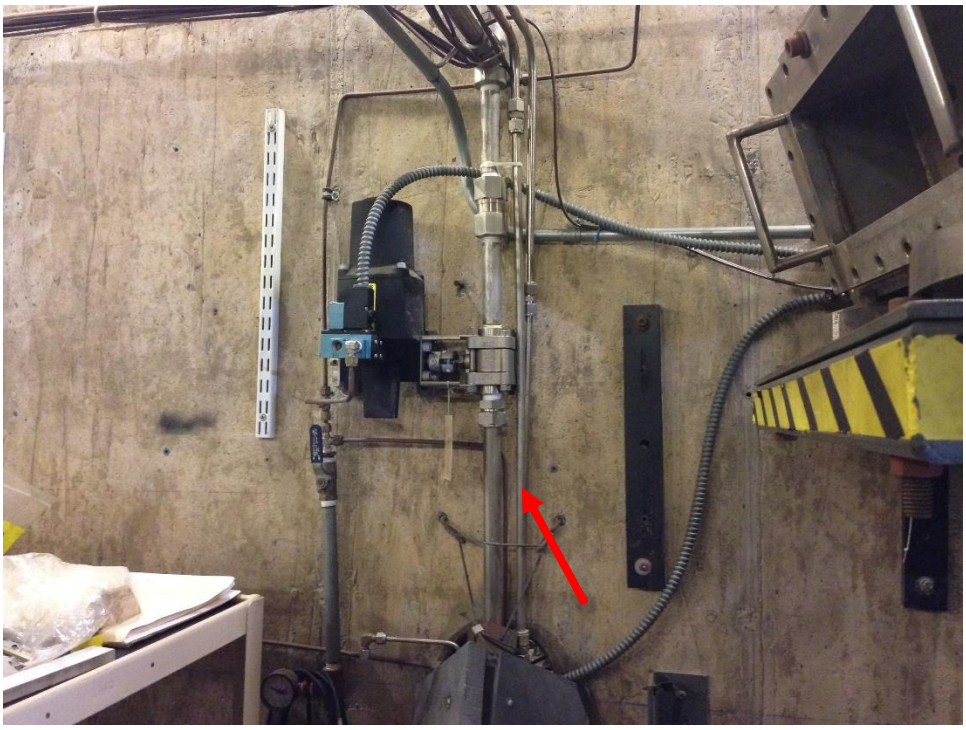

Nitrogen Purge Line (RM 127)

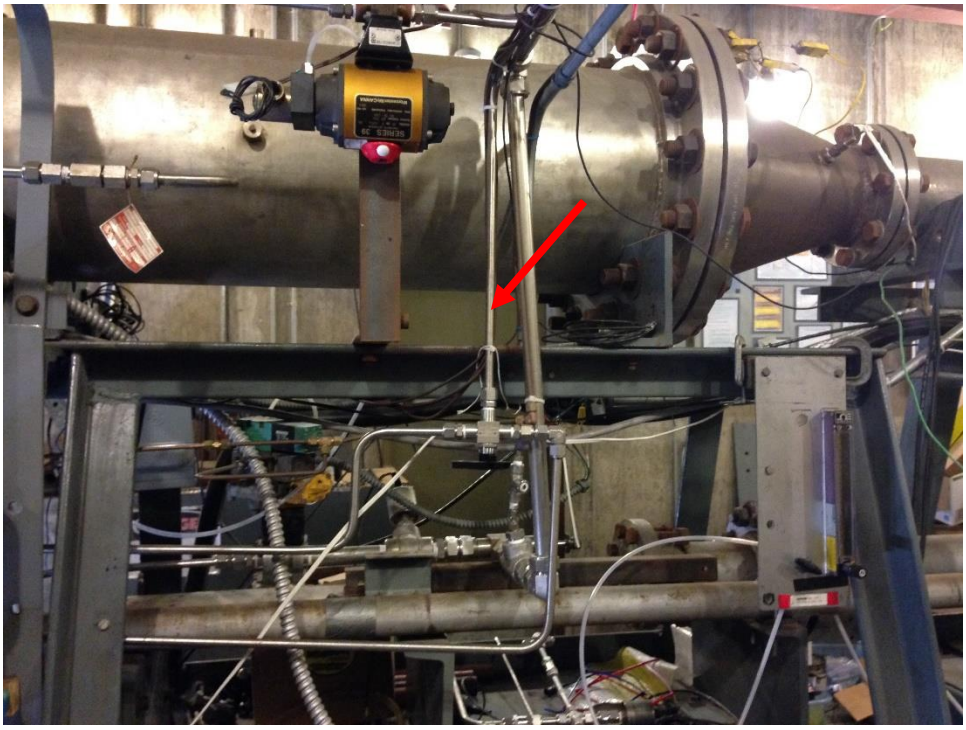

Nitrogen Purge Line (RM 127)

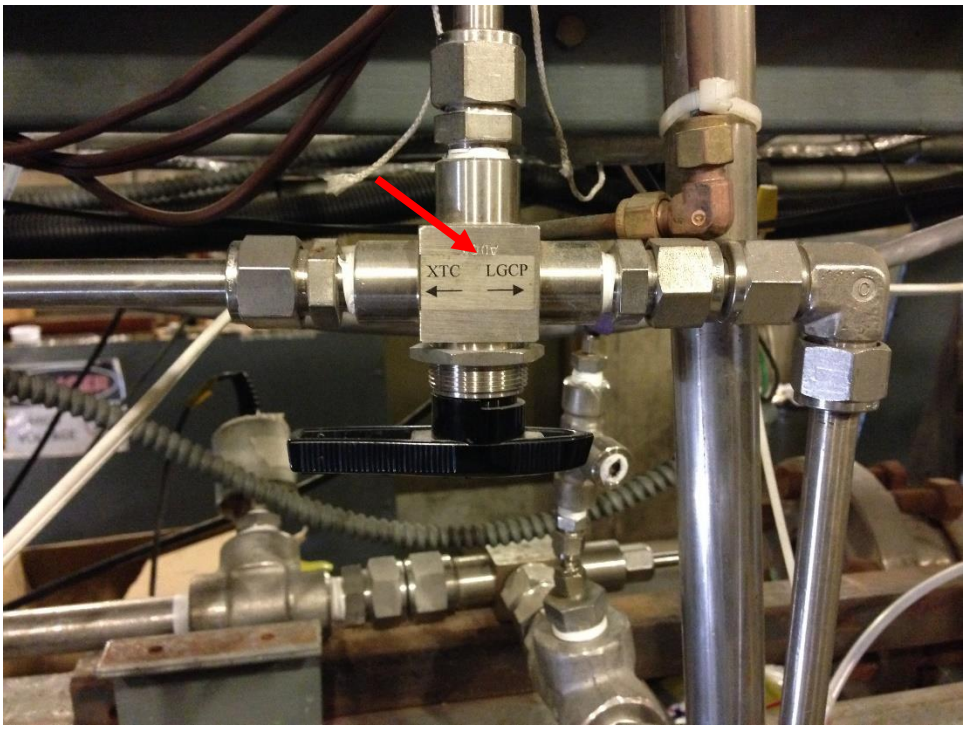

Nitrogen Ball Valve (RM 127)

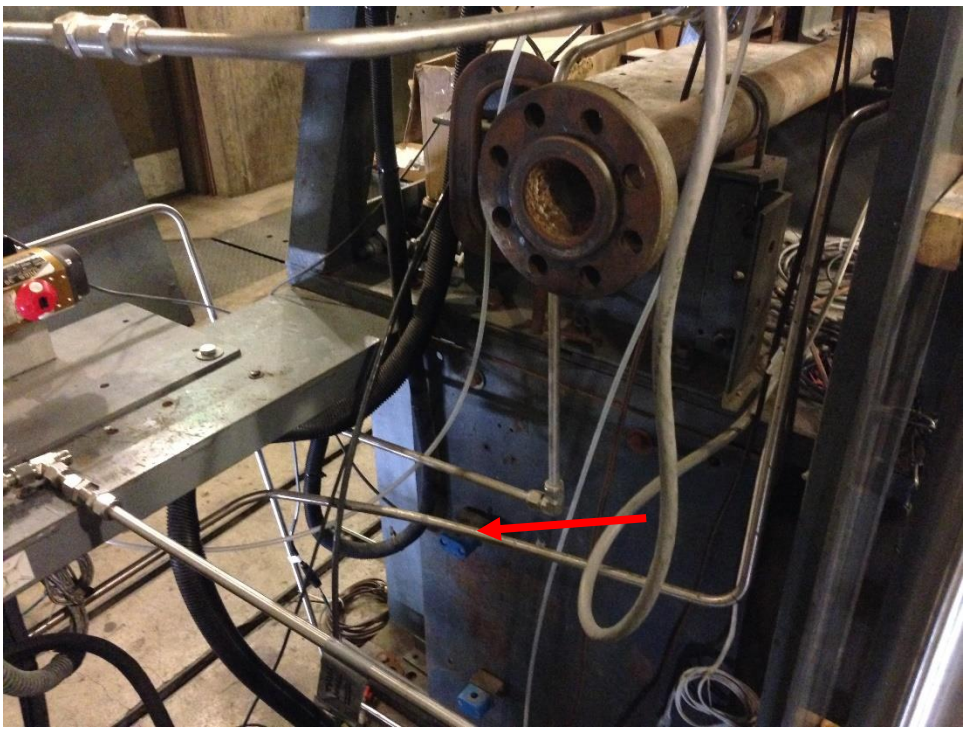
Nitrogen Purge Line (RM 127)

Nitrogen Purge Line (RM 127)

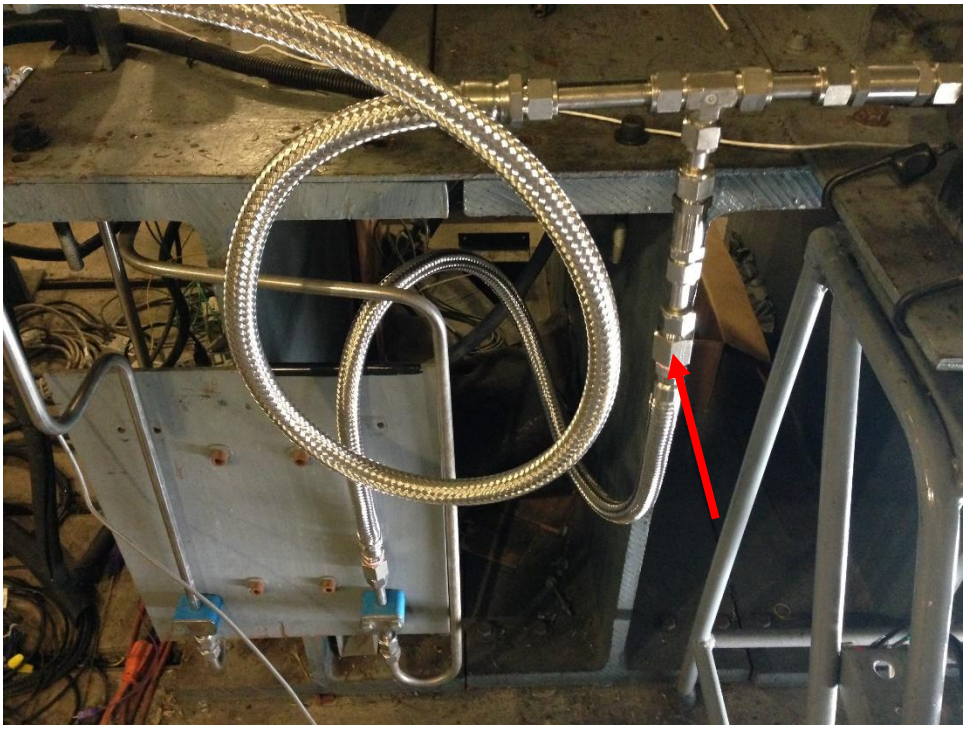

Nitrogen Purge Line (RM 127)

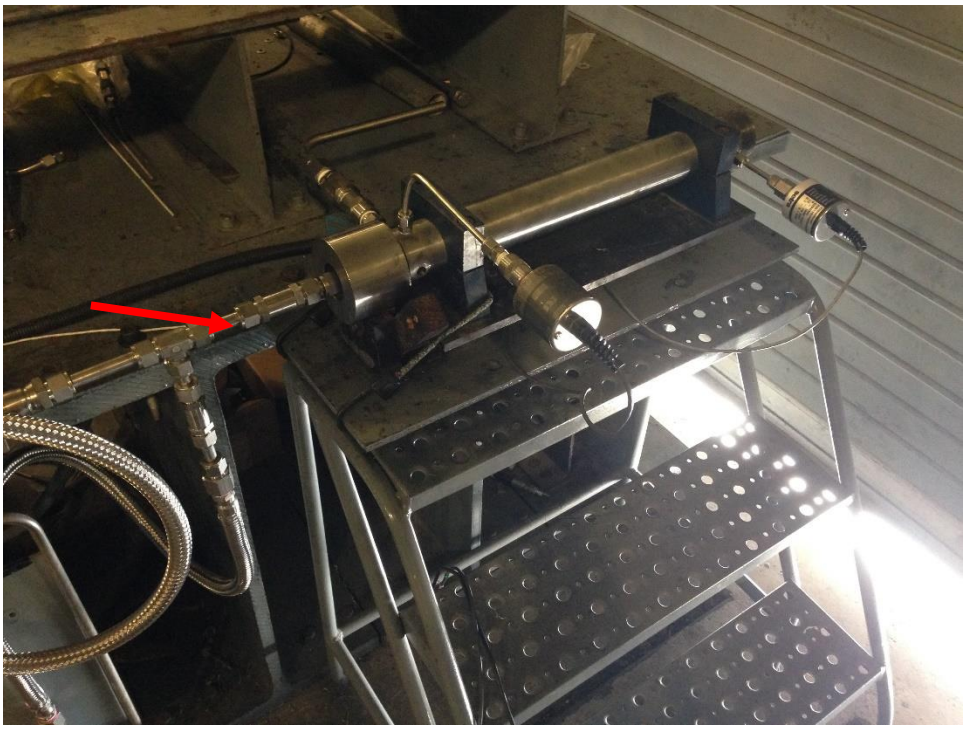

Nitrogen Purge Line into Motor (RM 127)

Helium/Nitrous Oxide Tubing (in order):

Helium Bottle and Regulator into Filter (RM 128)

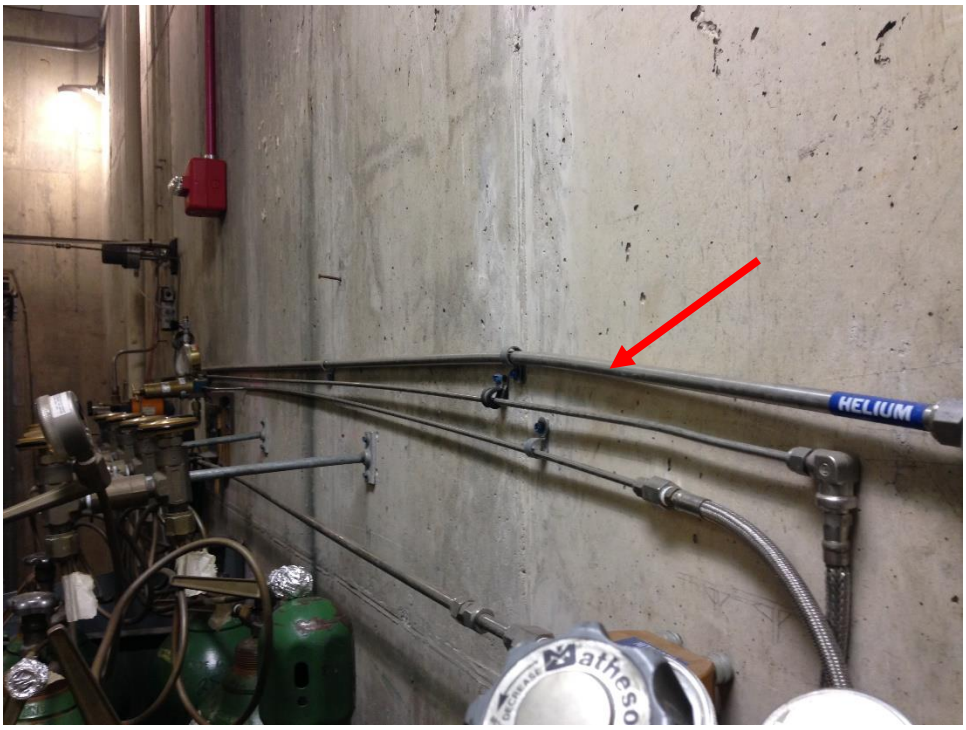

Helium Line (RM 128)

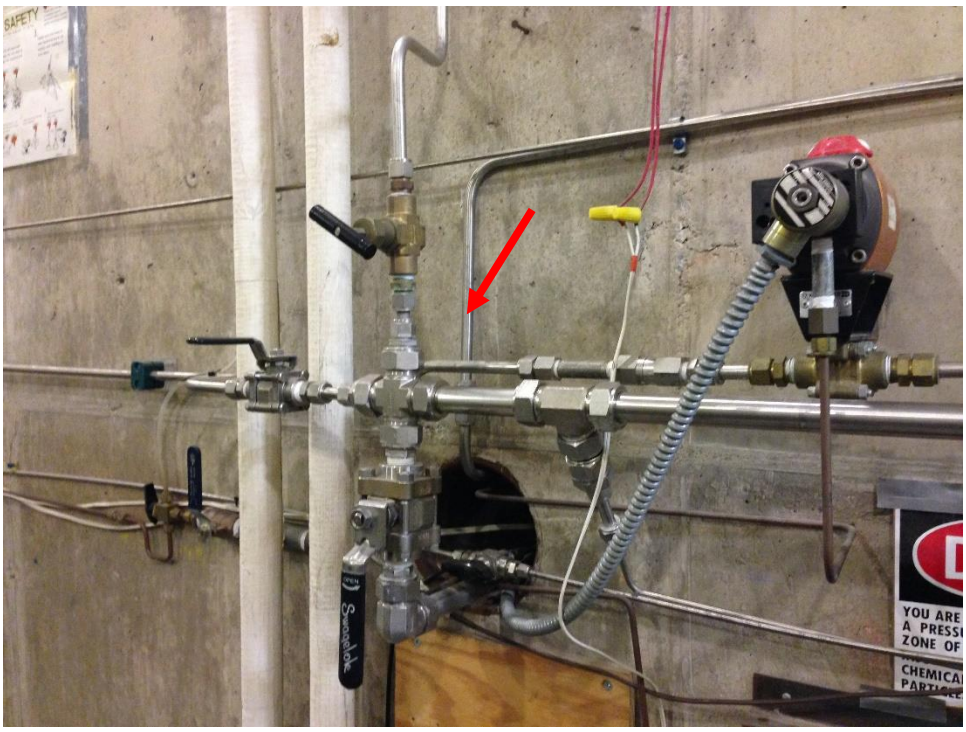
Helium Line (RM 128)

Helium Line (RM 127)

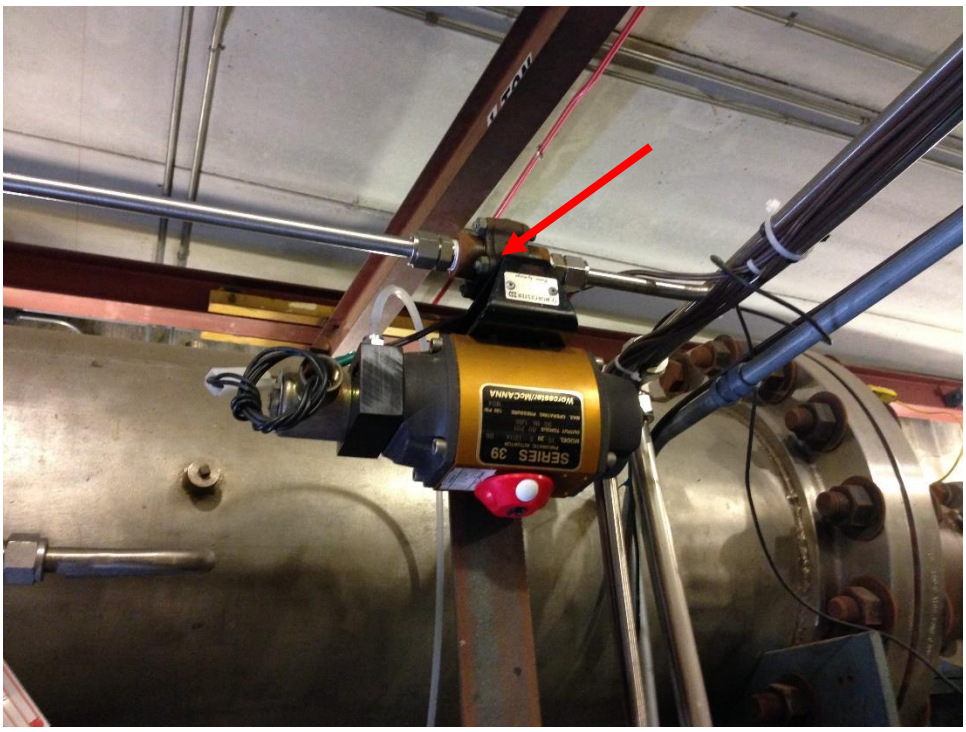

Helium Flow Valve (RM 127)

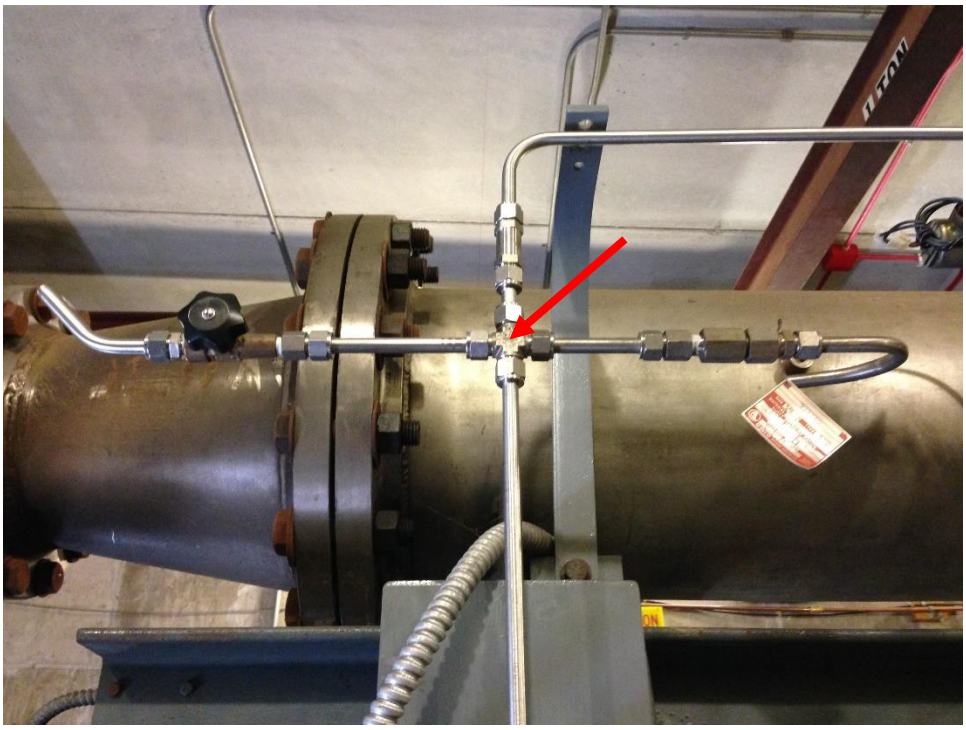

Helium Line, Run Tank Hand Valve (top of tank), and Burst Disc (RM 127)

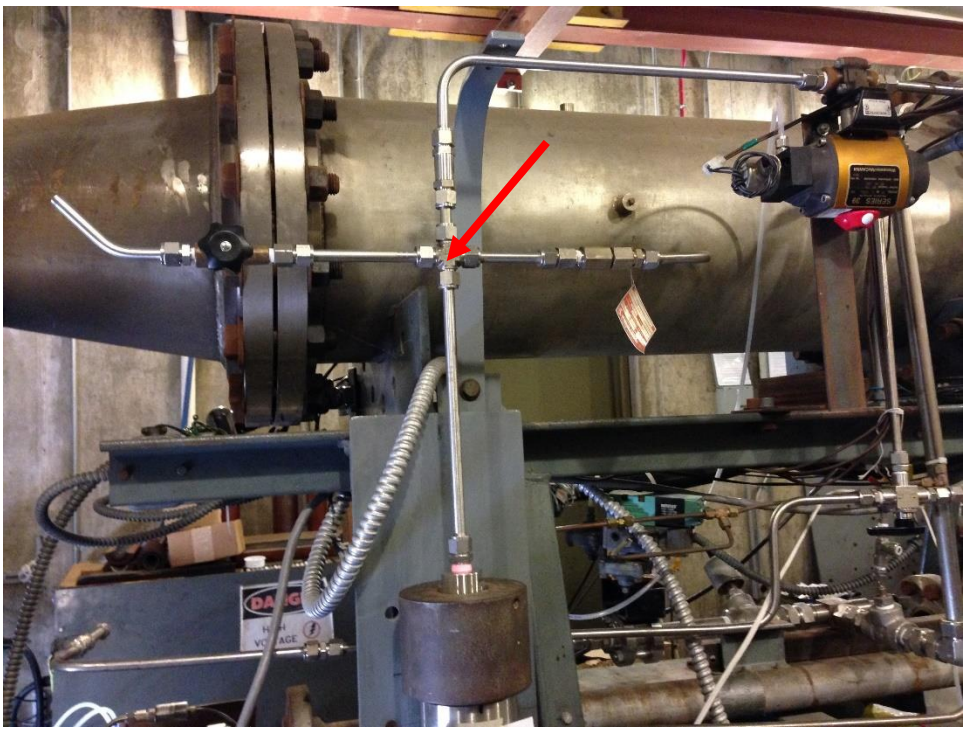

Helium Line, Run Tank Hand Valve (top of tank), and Burst Disc (RM 127)

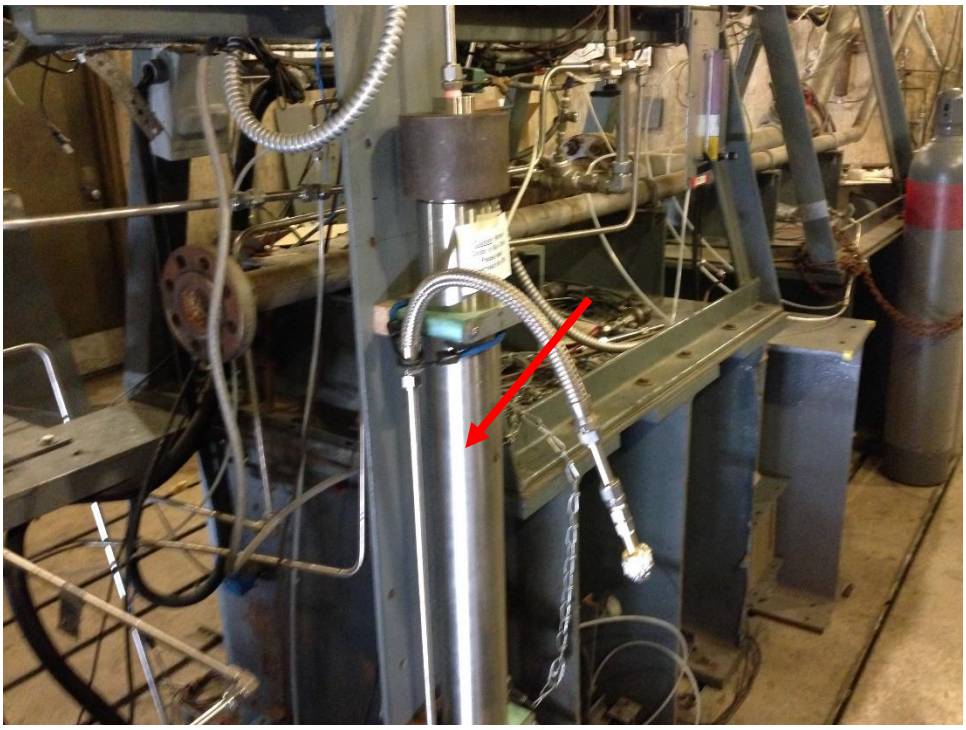

Nitrous Oxide Run Tank and Fill Line (RM 127)

Fill Line Assembly with Filter (RM 127)

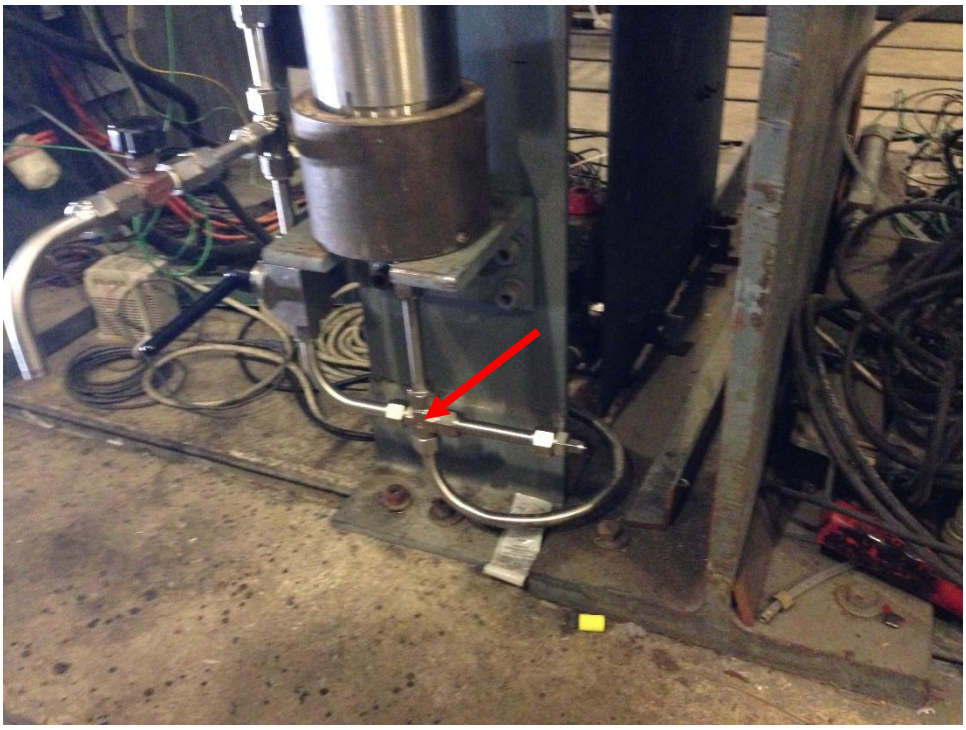

Tubing Junction at Bottom of Run Tank (RM 127)

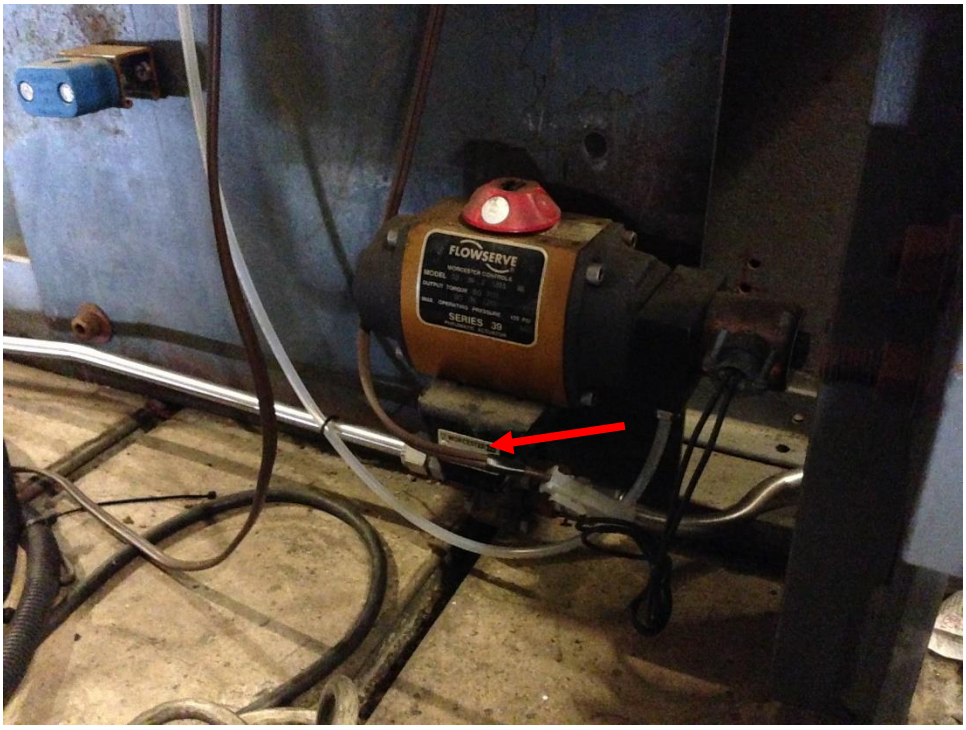

Nitrous Oxide Flow Valve (RM 127)

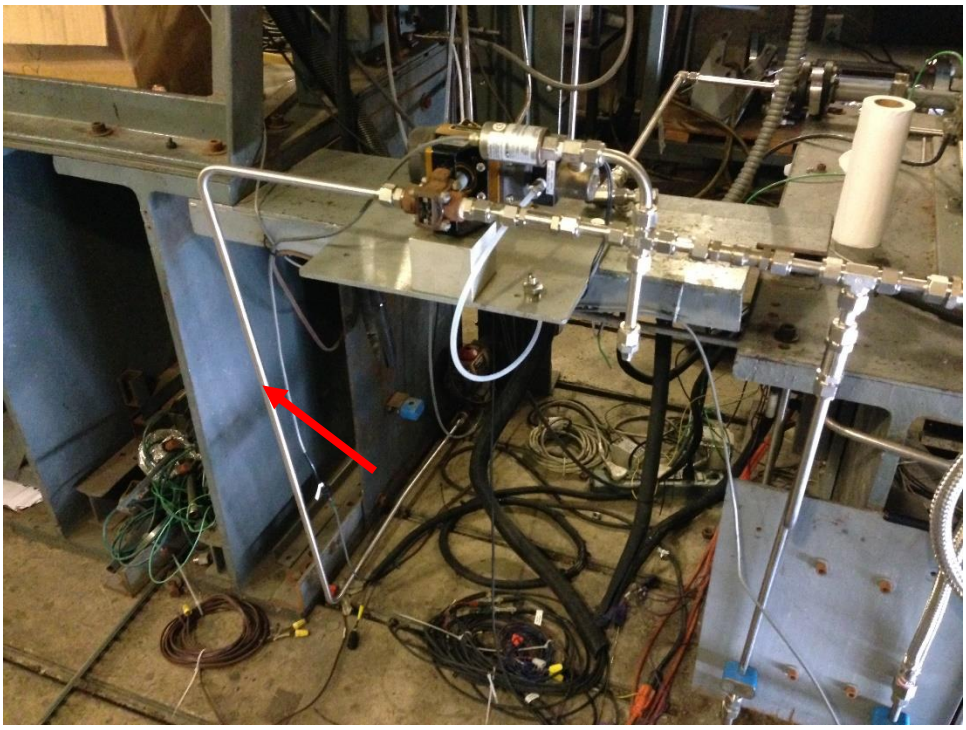

Nitrous Oxide Line (RM 127)

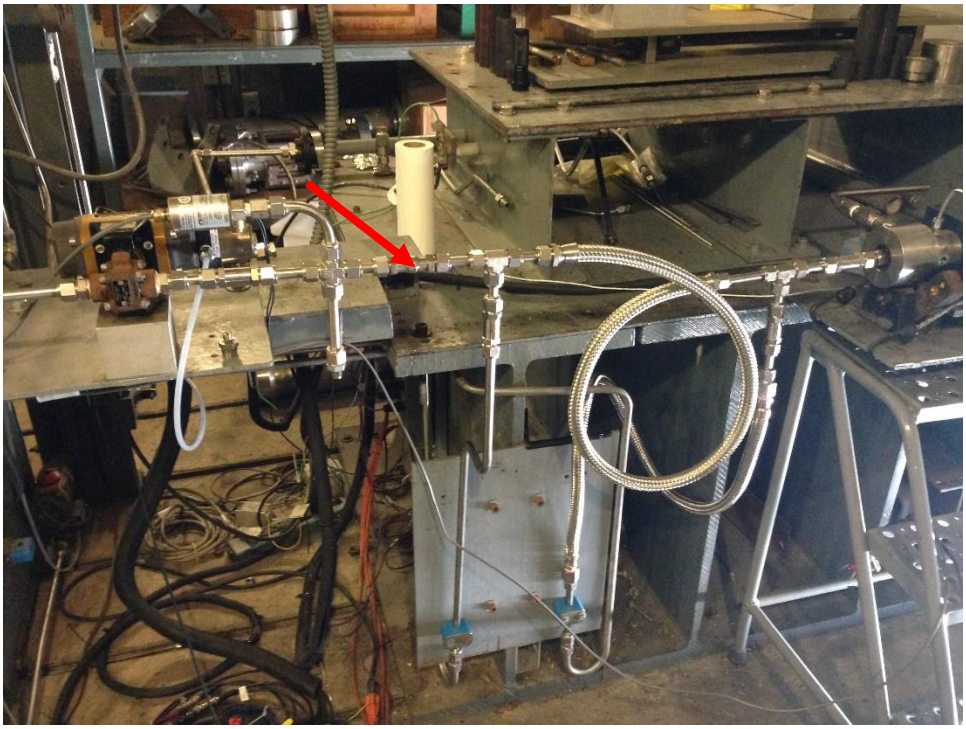

Nitrous Oxide Line with Orifice and Oxygen and Nitrogen entering (RM 127)

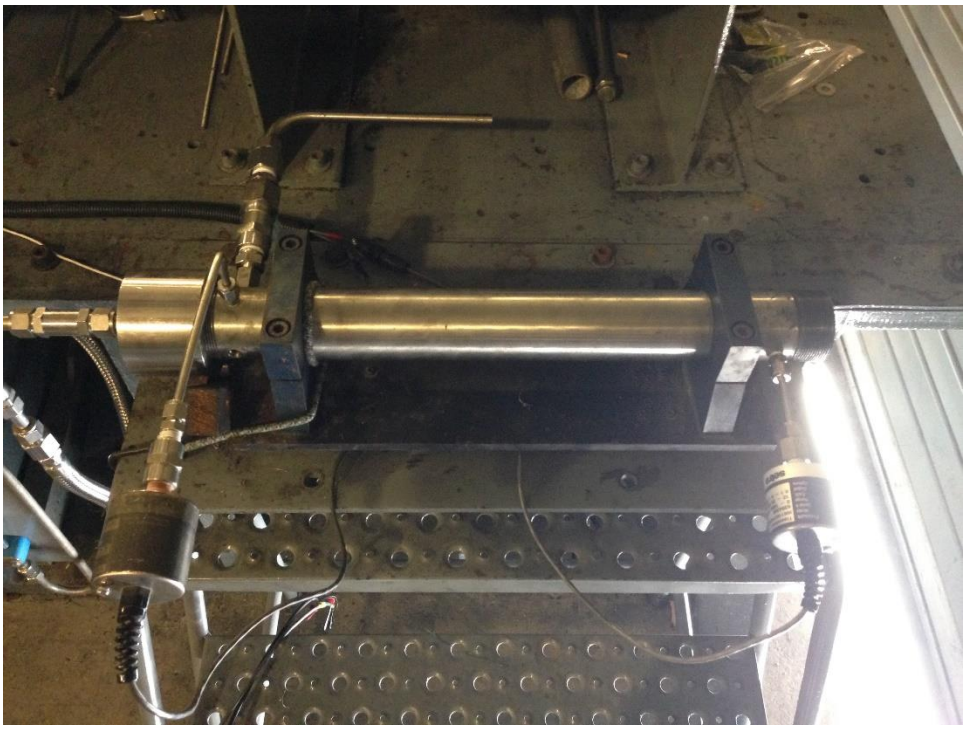

LGCP (RM 127)

Electrical:

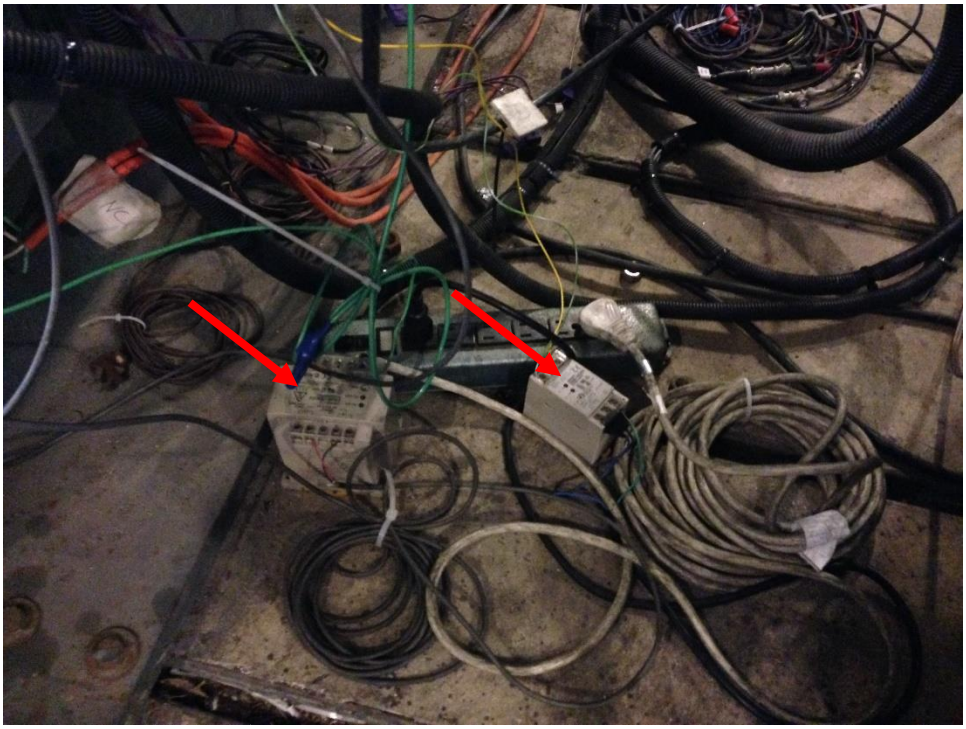

Power Supply for PTs, TCs, and LC (RM 127)

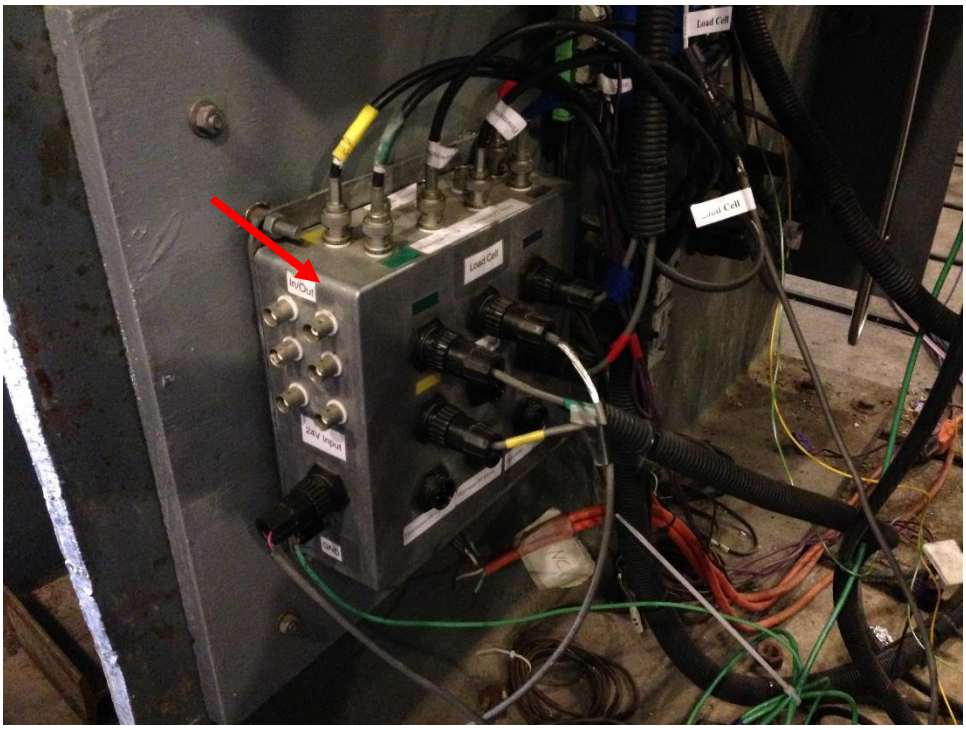

Panel for BNC Cables (RM 127)

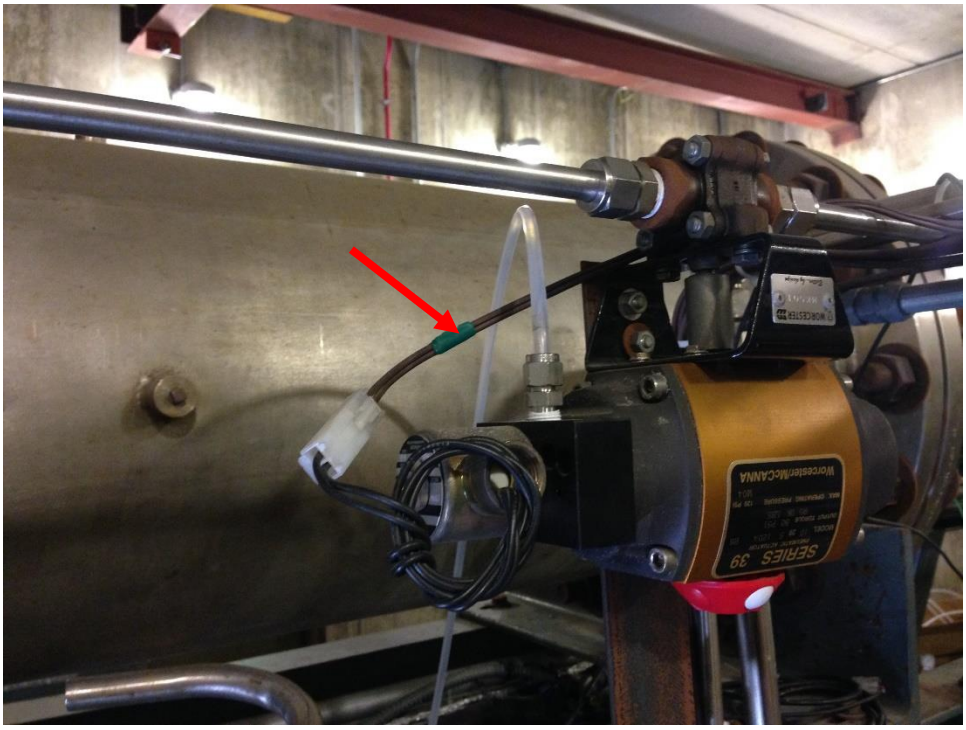

Green Cable for Helium Run Valve (RM 127)

Black Cable for N2O Flow Valve (RM 127)

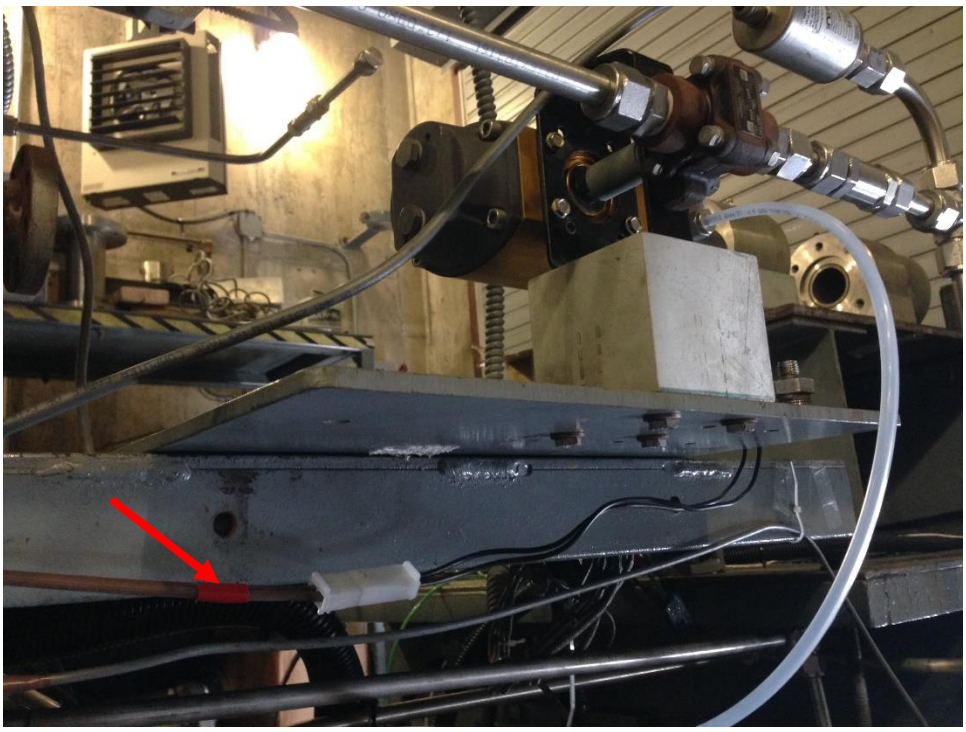
Red Cable for N2O Run Valve (RM 127)

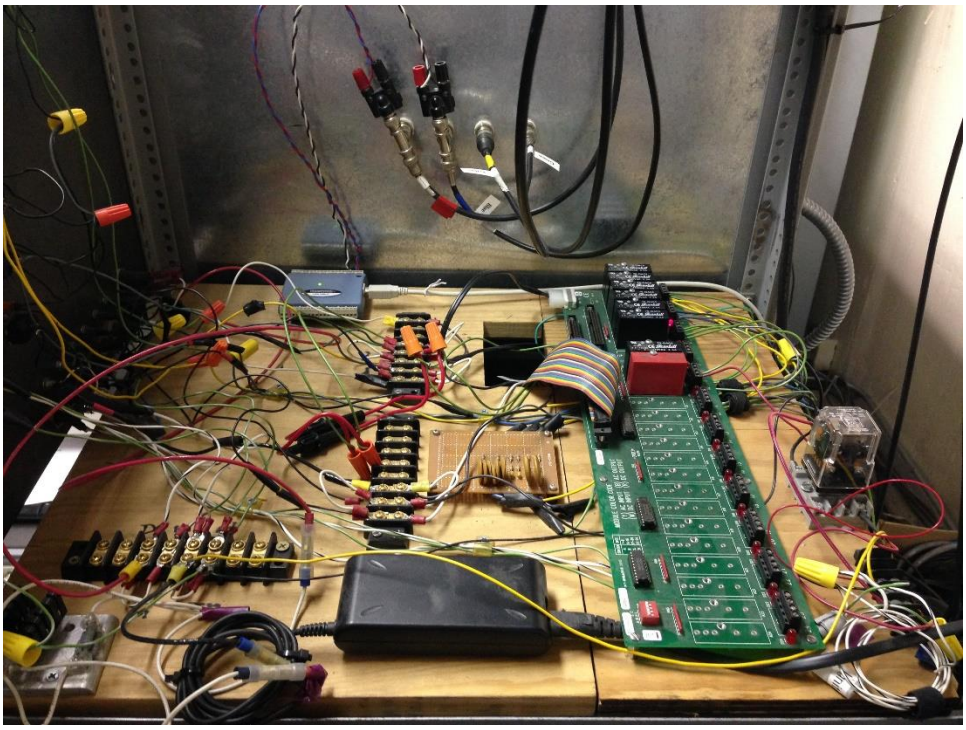

Relay Board (Control Room)

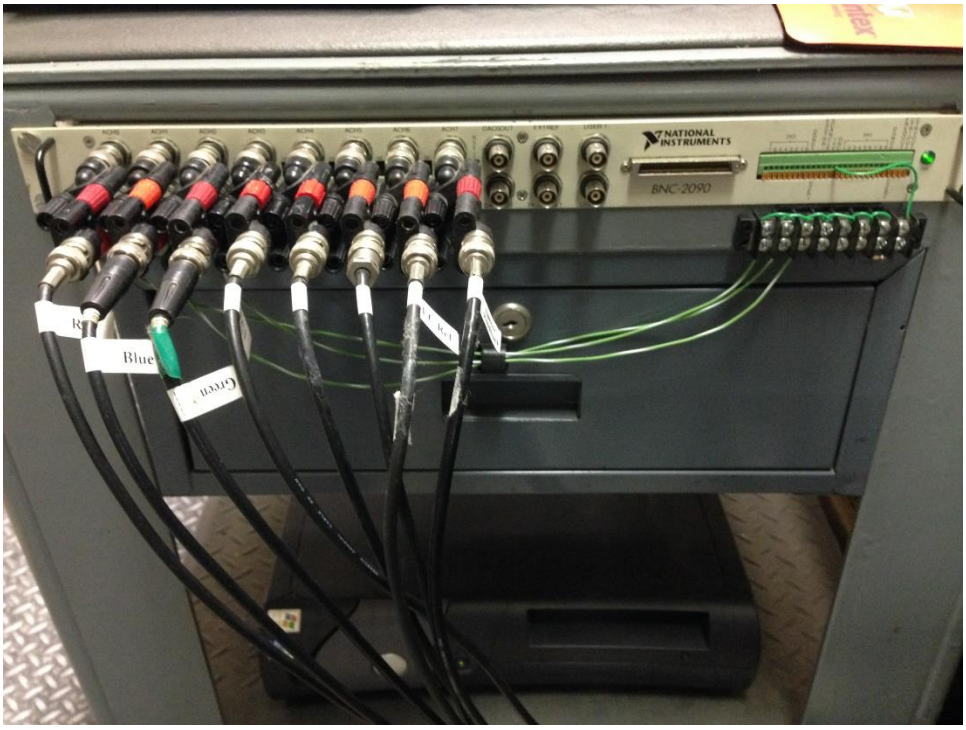

BNC Connections for DAQ Computer (Control Room)

Updates:

Pressure Transducer Digital Readout for Helium

- Regulator pressure can be wrong by as much as 150 psi. This readout gives a much more accurate number for the blowdown pressure from calibration of the pressure transducer.

Helium Bottle and Pressure Transducer for Digital Readout

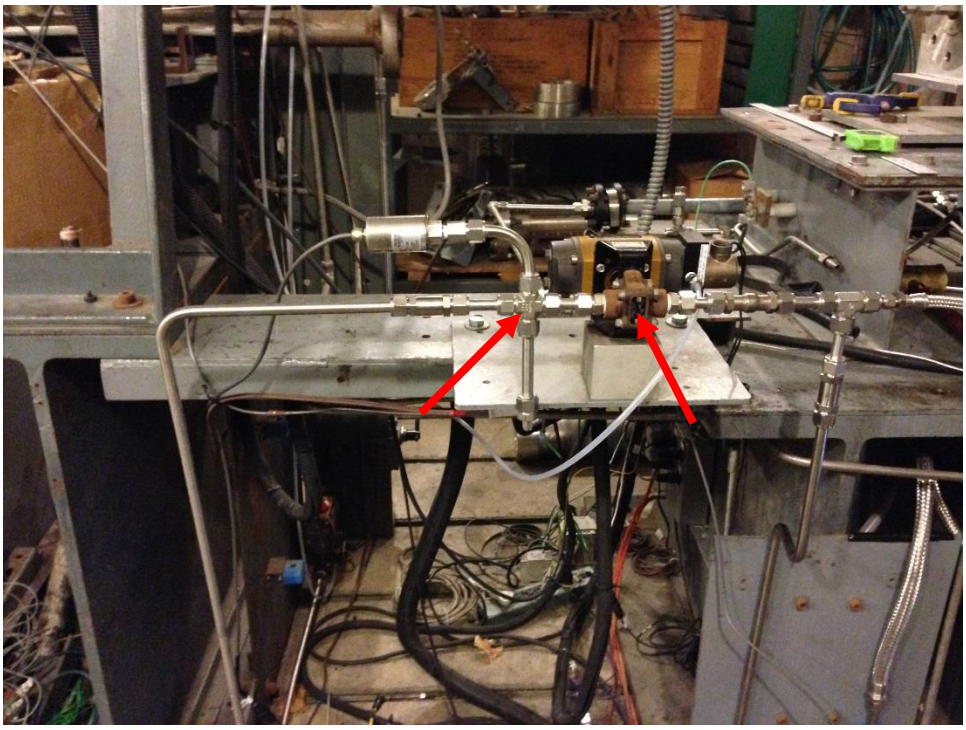

Rearranged nitrous oxide run valve and check valve/pressure transducer/thermocouple assembly.

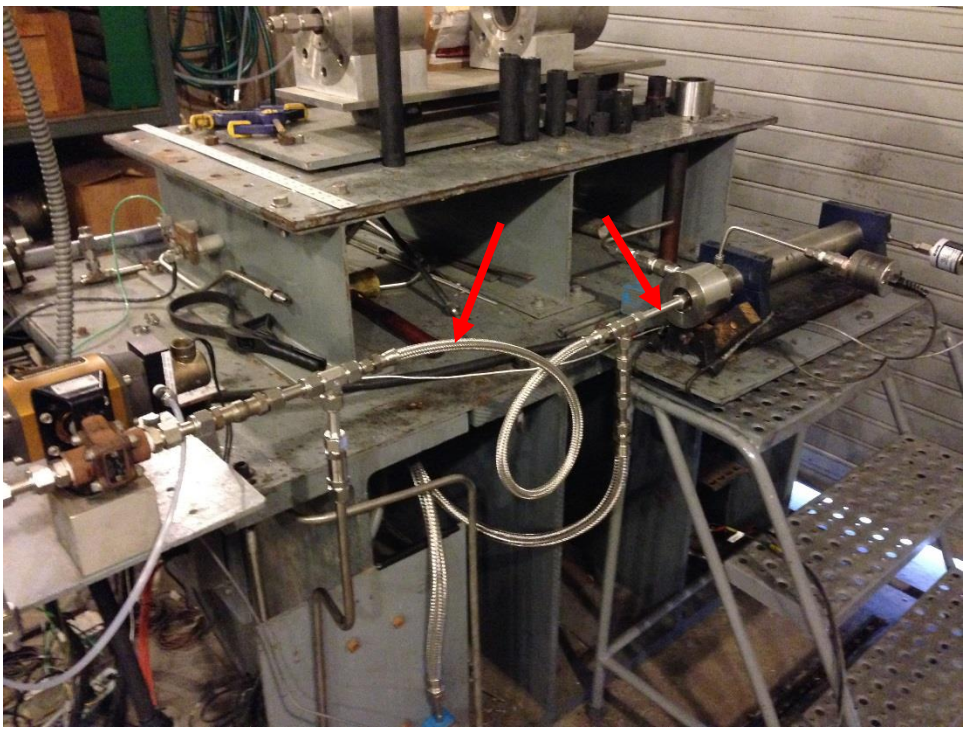

Installed smaller diameter oxidizer flex hose (1/4” diam. rather than 1/2” diam.) and removed check valve immediately before the injector.

- Check valve downstream of the flow control orifice could lead to the oxidizer feed driving pressure oscillations in the combustion chamber.

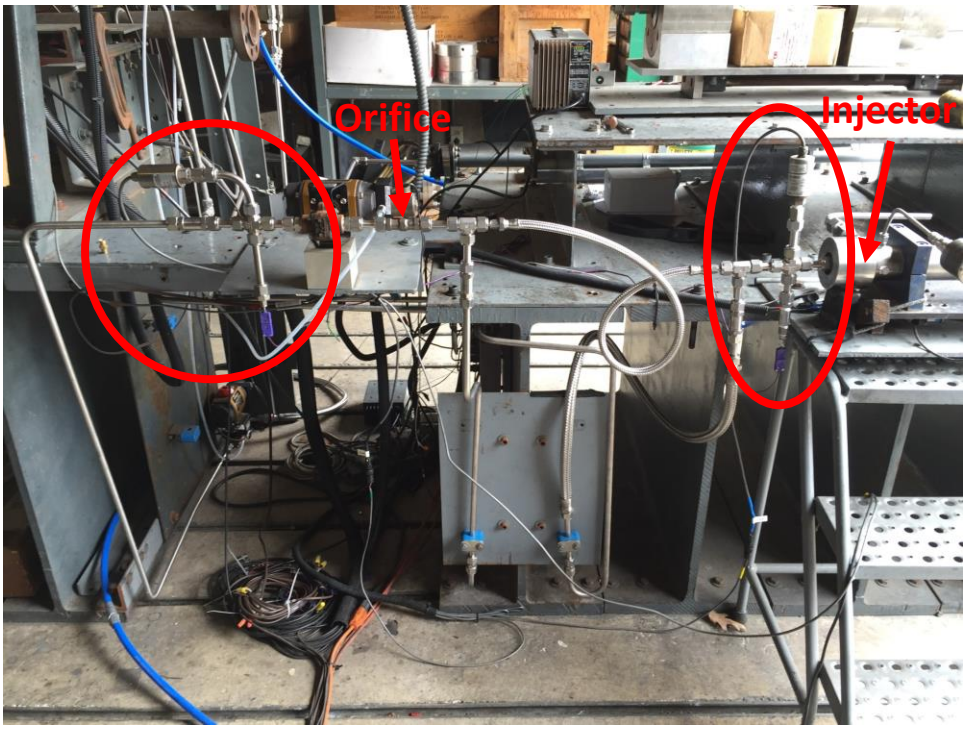

Added TC upstream of orifice and PT and TC before injector plate.

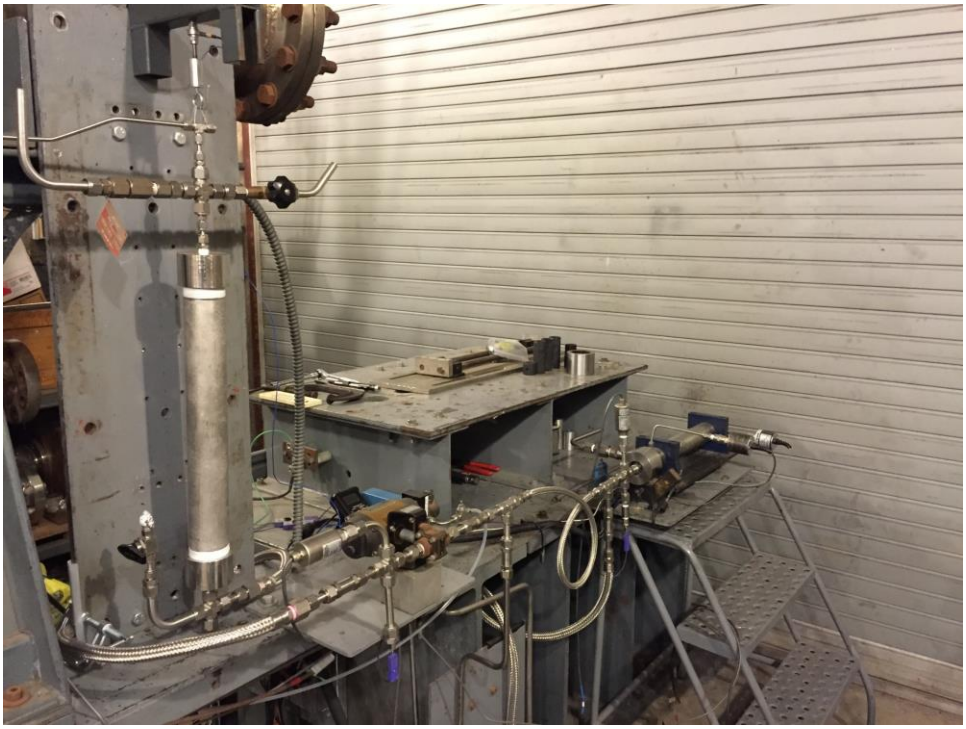
Run tank reconfigured. Small tank hanging from a tension load cell.

Helium line downsized to ¼” and routed to top of small run tank.

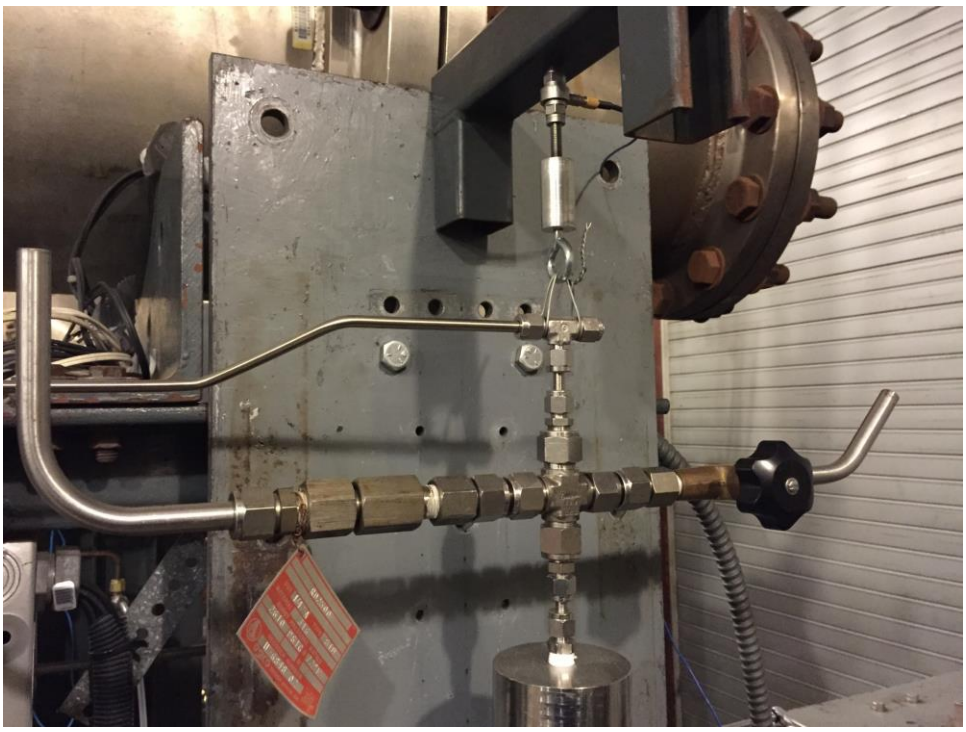
Helium inlet, hanging assembly with tension load cell, burst disc, and vent valve at the top of the small run tank.

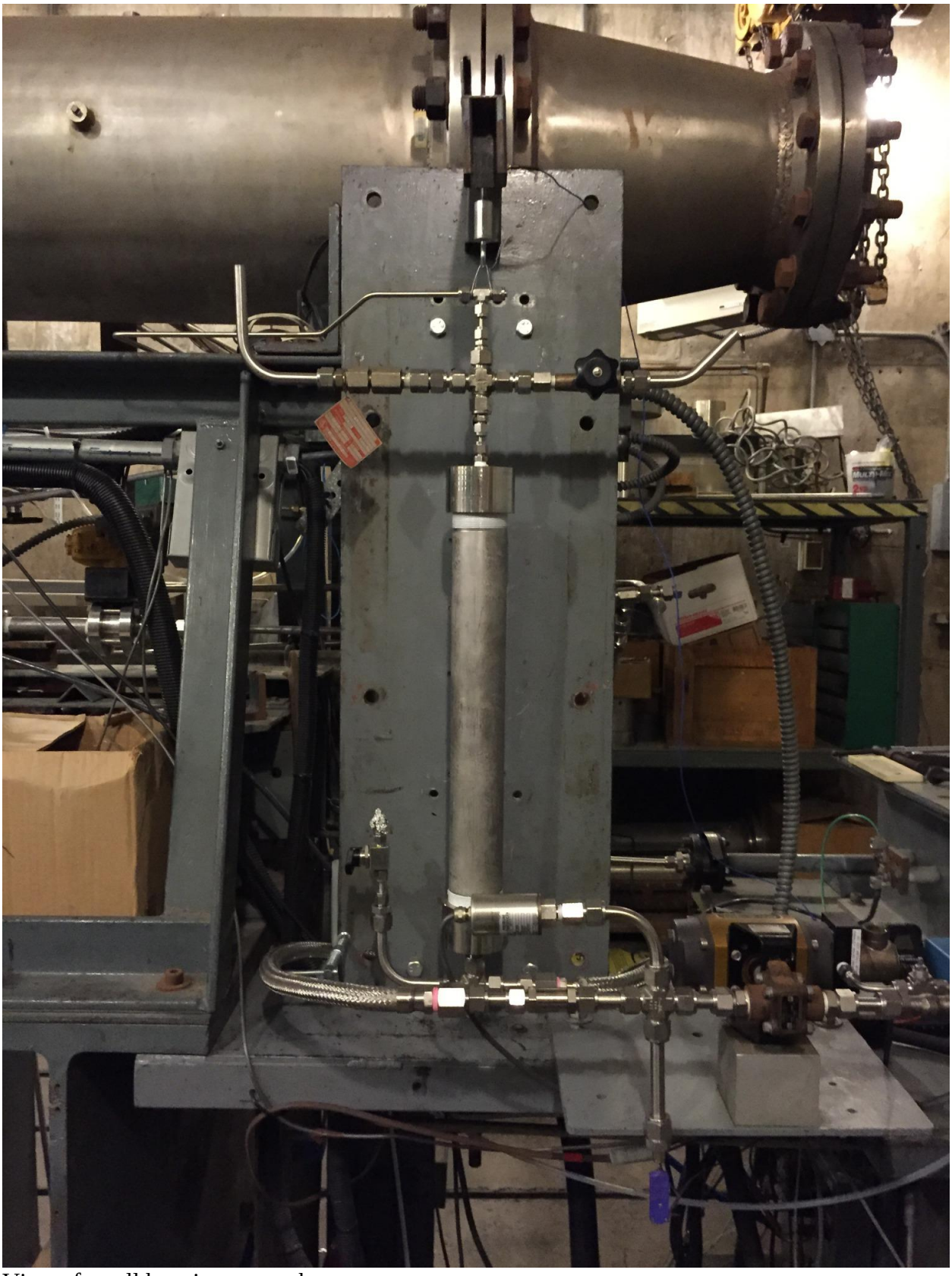

View of small hanging run tank.

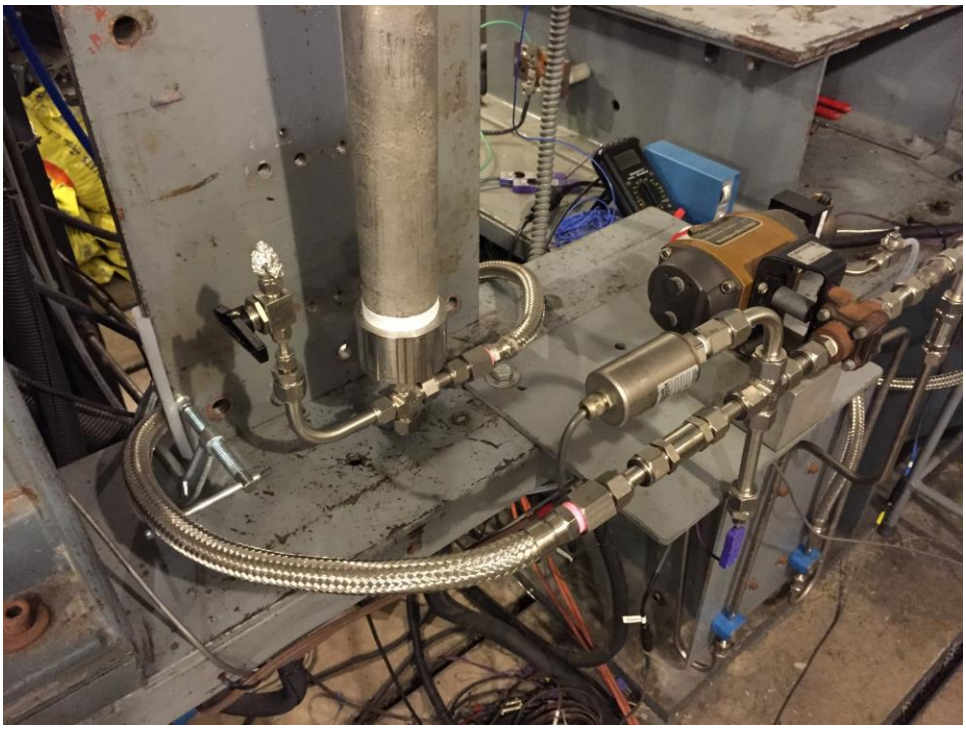

Nitrous oxide fill line assembly connection and flex hose to the nitrous oxide run valve. The nitrous oxide flow valve is no longer used.

Reconfigured fill line assembly.

APPENDIX O N_2O LGCP Motor Test Checklist

Nitrous Oxide Run Tank Filling Procedure:

- ❑ Open the test cell bay door.
- ❑ Turn on the overhead fan and place a box fan near the run tank.
- ❑ Bring the nitrous oxide fill bottle into the test cell and chain it to the test deck.
- ❑ Ensure that all valves to and from the run tank are closed.
- ❑ If the run tank is pressurized above the vapor pressure of nitrous oxide, manually toggle the helium flow valve to open, and then slowly vent the tank using the vent valve on the top of the tank. Once the vapor pressure has been reached, close both valves. Now the helium line and run tank are at the vapor pressure.
- ❑ Connect the fill bottle to the run tank using the fill line setup and ensure all valves in the fill line are closed.
- ❑ Slowly open the fill bottle.
- ❑ Slowly open the vent valve in the fill line. When liquid nitrous oxide is seen escaping, close the valve. The fill line should now be full of liquid. Do not place any body parts near or on the gas, liquid, or frost. Nitrous oxide gas, liquid, and frost is extremely cold.
- ❑ Slowly open the hand valve at the bottom of the run tank. The run tank should begin to fill if it was empty to start. If there was already some nitrous oxide in the tank, only a small amount may transfer.
- ❑ After several seconds, open the vent valve at the top of the run tank to allow nitrous oxide gas to vent from the top of the tank. This causes the tank pressure to drop and liquid nitrous oxide from the fill bottle to transfer into the run tank.

- ❑ Fill the nitrous oxide run tank until liquid is seen and heard escaping through the vent valve at the top of the tank. A dip tube sets the liquid level slightly below full to allow for liquid expansion with an increase in temperature.
- ❑ Once the run tank is full, close the vent valve at the top of the tank and the hand valve at the bottom of the tank. Close the fill bottle.
- ❑ Slowly open the vent valve in the fill line to clear the line of nitrous oxide.
- ❑ Observe the escaping nitrous oxide as it vents from the fill line setup. If the nitrous oxide is gaseous, the line will empty in one or two seconds and the fill bottle is empty. Replace the nitrous oxide fill bottle and add additional nitrous oxide to the run tank to ensure the desired amount of liquid is in the tank.
- ❑ Once nitrous oxide is completely vented from the fill line setup, close the vent valve.
- ❑ Disconnect the fill bottle from the run tank and remove the nitrous oxide fill bottle from the test cell.
- ❑ Disconnect the fill line setup and cover all open tubing.

Nitrous Oxide LGCP Hybrid Rocket Motor Test Setup Procedure:

- ❑ Turn on the overhead fan and place a box fan near the run tank.
- ❑ Setup a video camera and TV with a DVD recorder to record the motor firing.
- ❑ Title the DVD video display and set DVD to a new recording.
- ❑ Verify the shop air is connected to all remotely operated valves and greater than 90 psig in room 127 (_____ psig).
- ❑ Verify sufficient reserves of nitrogen, oxygen, and helium in bottles. Nitrous oxide should already be in the run tank following the fill procedure above.

- ❑ Turn on the power supply for the patch panel.
- ❑ Turn on the cold junction compensators for the E type thermocouples.
- ❑ Turn on the signal conditioner for the quartz force sensor and the multimeter for observing the output voltage.
- ❑ Ensure all signal cables are connected and turn on the data acquisition system.
- ❑ Verify sampling rate is 1 ks/s.
- ❑ Ensure all pressure transducers and thermocouples show appropriate baseline values on the data acquisition system.
- ❑ Ensure oxygen pintle on venturi is set to 2" (or full open).
- ❑ Ensure nitrogen purge line hand ball valve is aligned to LGCP.
- ❑ With the control board off, open the control program, "N2O LGCP Hybrid Control Rev_2.bas".
- ❑ Start the program.
- ❑ Turn on the control board.

Testing Procedure:

- ❑ Ensure all non-testing personnel are clear from the test cell and fenced-in area.
- ❑ Open nitrogen purge bottle and set regulator to amount specified on test data sheet (roughly 500-600 psig).
- ❑ Open reference pressure nitrogen bottle attached to oxygen regulator.
- ❑ Verify oxygen line hand valve and cluster hand valves with bottles are open (and hand valves leading to other systems are shut).
- ❑ Power on reference pressure digital readout.

- ❑ Slowly open oxygen bottle valves.
- ❑ Set oxygen regulator to value written on test data sheet (roughly 50 psig for oxygen ignition sequence).
- ❑ Plug in the digital readout for the helium pressure transducer.
- ❑ Open the helium bottle for pressurizing the run tank. Set the helium pressure below the vapor pressure, roughly 500 psig.
- ❑ Open the helium flow valve using the manual valve activation on the control program.
- ❑ Slowly increase the helium pressure to the desired amount for the test.
- ❑ Close the helium flow valve. This is the blowdown pressure. This step limits compression heating when pressurizing the nitrous oxide with helium.
- ❑ Secure the injector plug to the LGCP chamber.
- ❑ Announce "We will now be venting gases in room 127, all personnel stay clear".
- ❑ With the igniter, fuel grain, and graphite pieces removed, manually open the helium flow valve. Next, open the nitrous oxide run valve for roughly 2-3 seconds, or until liquid is seen venting through the chamber.
- ❑ Close the nitrous oxide run valve when liquid is observed leaving the injector plug. Then close the helium flow valve.
- ❑ Insert the fuel grain, post-combustion chamber, and nozzle plug into the chamber.
- ❑ Insert the graphite filler pieces, electric match, and injector plug into the chamber.
- ❑ Make an announcement for starting the test firing: "We will be conducting a motor firing in room 127. Please stand clear of the test cell and the fenced-in area."
- ❑ Connect igniter lines to electric match leads.
- ❑ Check ALL timing parameters.

❑ Re-check all regulators.

❑ Press “Record” on the DVD and start timer on title screen.

❑ Press “Record” on the data acquisition system.

❑ Use the control program to initiate the test.

**********TEST INITIATED**********

❑ If misfire occurs, stop using this portion of checklist and move onto the Misfire Procedure section.

**********TEST CONCLUDED**********

❑ Press “Stop” on DVD recorder and data acquisition systems.

❑ Check that all valves have shut.

❑ Replace block for load cell.

❑ Disassemble motor, remove fuel grain, and secure injector plug to motor chamber.

❑ If additional tests are to be completed, move to the New Test section.

❑ Announce “We will now be venting gases in room 127, all personnel stay clear”.

❑ Secure the injector plug to the LGCP chamber.

❑ With the igniter, fuel grain, and graphite pieces removed, manually open the helium flow valve. Next, open the nitrous oxide run valve.

❑ When liquid stops being visible, close the nitrous oxide run valve.

❑ Close the helium bottle.

❑ Manually open the nitrous oxide run valve. Allow the helium left in the run tank and lines to vent completely.

❑ Close the helium flow valve and the nitrous oxide run valve.

❑ Close oxygen bottles at the cluster.

❑ Using the manual mode of operation of the control program, open the oxygen run valve, followed by the oxygen flow valve, and allow the oxygen manifold to vent completely.

❑ Close the oxygen flow valve and the oxygen run valve.

❑ Close nitrogen bottle purge bottle.

❑ Using the manual mode of operation of the control program, open the nitrogen purge valve to allow nitrogen lines to vent.

❑ Close the nitrogen purge valve.

❑ Close and vent the nitrogen bottle and regulator being used for O2 pressure regulation.

❑ Check to ensure no back pressure in O2 manifold.

❑ Turn off the patch panel power supply and cold junction compensators.

❑ Turn off helium pressure digital readout and O2 reference pressure digital readout.

❑ Quit the N2O LGCP Hybrid Control Rev. 2 control program.

❑ Turn off the control board.

❑ Close shop air ball valve in the machine shop.

❑ Announce “Test completed in room 127”.

Misfire Procedure:

❑ Immediately turn off hybrid control board by turning key; this will start nitrogen flow and interrupt nitrous oxide and oxygen flow.

❑ Announce “Misfire has occurred in room 127, stay clear of the test cell and fenced in area until directed otherwise”.

❑ Continue nitrogen flow for at least 15 seconds.

❑ Continue recording event on outdoor camera.

- ❑ On the control program; restart and turn on manual mode and ensure all relays are in the shut position.
- ❑ Turn on control panel. Verify all flows have stopped and no smoldering is observed. If smoldering is observed, continue to purge the system using the manual control.
- ❑ Isolate oxygen by closing oxygen bottles at the cluster.
- ❑ Press “Stop” on the data acquisition system.
- ❑ Record time of misfire.
- ❑ Verify combustion has subsided via outdoor camera.
- ❑ After 10 minutes personnel may enter test chamber.
- ❑ Announce “Test completed in room 127”.
- ❑ Gather evidence and determine cause of problem.

New Test:

- ❑ Replace block for load cell.
- ❑ Disassemble motor.
- ❑ If next test is at a lower pressure vent necessary lines manually to reach nitrous oxide vapor pressure in the run tank.
- ❑ Follow run tank filling procedure.
- ❑ Follow testing procedure for next test.

APPENDIX P N_2O LGCP Motor Control Code

```
'*   NASA CubeSat Nitrous Oxide Hybrid Rocket Motor Control Program
'*   Version 2.0
'*   Date:  27-October-2014
'*   Author:  Nick Favorito
'*   Updated by:  Brendan McKnight

'*   Program Description:
'*      This program is based off of an earlier Indian Head Bi-Propellant Control Program
developed at the HPCL
'*       by Grant "Big Dad" Risha and Eric Boyer.
'*      It has been updated by Brendan McKnight to change program relay calls. Relays for the
oxygen flow, oxygen run, nitrogen purge,
'*       and igniter now match the board activation for the oxygen hybrid rocket motor control
program using LabView.
'*       The two programs can be run without changing relay positions or wiring. The tubing near
the motor must be swapped
'*       for the appropriate oxidizer. In addition, relay signals (0's or 1's) are flipped so that
"closed" condition corresponds to a closed valve.

#INCLUDE "CBW.BAS"           ' Mandatory INCLUDE file to access default
                        ' parameter values
#INCLUDE "WIN32API.INC"
'#INCLUDE "library test.bas"


DECLARE SUB MAINMENU ()
DECLARE SUB BOARDCONTROL (BoardNum%, PortName&, BitNum%, BitValue%)
DECLARE SUB INITIALCONFIG ()
DECLARE SUB MANUAL()
DECLARE SUB EVENTSELECT(A$, EVENTVAL AS STRING, BoardNum AS INTEGER,
PortName AS LONG, BitNum AS INTEGER, BitValue AS INTEGER)
DECLARE FUNCTION GetTickCount LIB "KERNEL32.DLL" ALIAS "GetTickCount" () AS
DWORD
DECLARE SUB TIMEDCONTROL()
DECLARE SUB SCRAM (whyscram AS INTEGER)

'-----------------------------------------------------------------------------------------
'-----------------------------------------------------------------------------------------


FUNCTION PBMAIN

DIM I AS INTEGER        'counter dummy variable
DIM BoardNum AS INTEGER
```

```
DIM PortName AS LONG
DIM BitNum AS INTEGER
DIM BitValue AS INTEGER
DIM Direction AS INTEGER
DIM CHOICE AS STRING
'configure ports for digital output
'  Parameters or cfDConfigPort (actual numeric values set in CBW.BAS):
'     BoardNum&   :the number used by CB.CFG to describe this board
'     PortNum&    :the output port
'     Direction&  :sets the port for input or output

   BoardNum = 0          ' Board number

   'Configure Port A
   PortName = FIRSTPORTA
   Direction = DIGITALOUT
   ULStat& = cbDConfigPort&(BoardNum, PortName, Direction)
   IF ULStat& <> 0 THEN EXIT FUNCTION

   'Configure Port B
   PortName = FIRSTPORTB
   Direction = DIGITALOUT
   ULStat& = cbDConfigPort&(BoardNum, PortName, Direction)
   IF ULStat& <> 0 THEN EXIT FUNCTION

   'For PortC, configure both low and high sections
   PortName = FIRSTPORTCH
   Direction = DIGITALOUT
   ULStat& = cbDConfigPort&(BoardNum, PortName, Direction)
   IF ULStat& <> 0 THEN EXIT FUNCTION
   PortName = FIRSTPORTCL
   Direction = DIGITALOUT
   ULStat& = cbDConfigPort&(BoardNum, PortName, Direction)
   IF ULStat& <> 0 THEN EXIT FUNCTION

   'Configure Initial Bit Configuration (close all except purge)
   CALL INITIALCONFIG ()
   CURSOR OFF
   CONSOLE SCREEN 25,80
   CALL MAINMENU

      WHILE CHOICE <> "Q" AND CHOICE <> "q"

      CHOICE = INKEY$
      LOCATE 1,1
      PRINT TIME$
```

```
      LOCATE 2,1
      PRINT DATE$
      IF CHOICE = "M" OR CHOICE = "m" THEN
         COLOR (7)
         CHOICE="Z"
         CALL MANUAL
      ELSEIF CHOICE = "R" OR CHOICE = "r" THEN
         COLOR (7)
         CHOICE="Z"
         CALL TIMEDCONTROL
      ELSEIF CHOICE = "O" OR CHOICE = "o" THEN
         COLOR (7)
         CHOICE="Z"
         CALL OPTIONS
      END IF


      IF GetTickCount()>4320000000 THEN
      LOCATE 20,0
      PRINT "The computer has been on for more than 50 days."
      PRINT "After 50 days this program may become unstable"
      PRINT "due to a fundamental Windows error."
      PRINT "Thank you Bill Gates."
      PRINT "Please reset the computer now, you may then continue."
      END IF

      LOOP
      SLEEP 0
END FUNCTION



'-------------------------------------------------------------------------------------------
'-------------------------------------------------------------------------------------------

SUB MAINMENU
'This subroutine prints the initial menu on the screen
COLOR (15)
      CLS
      PRINT : PRINT : PRINT : PRINT : PRINT : PRINT

      PRINT "          [][][][][][][][][][][][][][][][][][][][][][][][][][][][][]"
      PRINT "          []                                                    []"
      PRINT "          []            Navsea Hybrid                 []"
      PRINT "          []          Operation Main Menu             []"
      PRINT "          []                                                    []"
```

```
      PRINT "          []      (M)anual system test            []"
      PRINT "          []      (R)un sequencing routine        []"
      PRINT "          []      (O)ptions Menu                  []"
      PRINT "          []      (Q)uit                          []"
      PRINT "          []                                      []"
      PRINT "          []                                V1.0  []"
      PRINT "          [][][][][][][][][][][][][][][][][][][][][][][][][][][][][][][]"

      LOCATE 12, 28
      COLOR (14)
      PRINT "M"
      LOCATE 13, 28
      PRINT "R"
      LOCATE 14, 28
      PRINT "O"
      LOCATE 15, 28
      PRINT "Q"
      COLOR (7)

END SUB


'-------------------------------------------------------------------------------------------
'-------------------------------------------------------------------------------------------



SUB INITIALCONFIG ()
'This sub sets all outputs to an initial condition

DIM BoardNum AS INTEGER
DIM PortName AS LONG
DIM BitNum AS INTEGER
DIM BitValue AS INTEGER

   LOCAL I AS INTEGER
   BoardNum=0
   PortName=FIRSTPORTA

      'Set all relays to off, except purge
  FOR I=0 TO 23
      IF I=3 THEN
         'Turn on purge relay (purge is fail open, this closes the valve)
         BitNum=3
         BitValue=0
      CALL BOARDCONTROL (BoardNum, PortName, BitNum, BitValue)
```

```
      ELSE
         BitNum=I
         BitValue=1
         CALL BOARDCONTROL (BoardNum, PortName, BitNum, BitValue)
      END IF
  NEXT I



END SUB


'-------------------------------------------------------------------------------------------
'-------------------------------------------------------------------------------------------

SUB BOARDCONTROL (BoardNum%, PortName&, BitNum%, BitValue%)
'This sub controls each bit on each board
   ' declare revision level of Universal Library
   ULStat& = cbDeclareRevision(CURRENTREVNUM)
    IF ULStat& <> 0 THEN EXIT SUB

   ' Initiate error handling
   '  activating error handling will trap errors like
   '  bad channel numbers and non-configured conditions.
   '  Parameters:
   '    PRINTALL    :all warnings and errors encountered will be printed
   '    DONTSTOP    :if an error is encountered, the program will not stop,
   '                 errors must be handled locally
   ULStat& = cbErrHandling&(PRINTALL, DONTSTOP)
    IF ULStat& <> 0 THEN EXIT SUB

   ' If cbErrHandling% is set for STOPALL or STOPFATAL during the program
   ' design stage, Visual Basic will be unloaded when an error is encountered.
   ' We suggest trapping errors locally until the program is ready for compiling
   ' to avoid losing unsaved data during program design.  This can be done by
   ' setting cbErrHandling options as above and checking the value of ULStat%
   ' after a call to the library. If it is not equal to 0, an error has occurred.

   ' configure FIRSTPORTA for digital output
   '  Parameters:
   '    BoardNum&   :the number used by CB.CFG to describe this board
   '    PortNum&    :the output port
   '    Direction&  :sets the port for input or output

   ' write the value to FIRSTPORTA
   '  Parameters:
```

```
   '    BoardNum    :the number used by CB.CFG to describe this board
   '    PortNum%    :the output port
   '    DataValue%  :the value written to the port
   '  FIRSTPORTA should be used for the HPCL multiple port boards
   ULStat& = cbDBitOut&(BoardNum%, PortName&, BitNum%, BitValue%)
    IF ULStat& <> 0 THEN EXIT SUB

END SUB

'-----------------------------------------------------------------------------------------
'-----------------------------------------------------------------------------------------

SUB MANUAL
   CALL INITIALCONFIG ()


   LOCAL Flag1 AS INTEGER
   LOCAL Flag2 AS INTEGER
   LOCAL Flag3 AS INTEGER
   LOCAL Flag4 AS INTEGER
   LOCAL Flag5 AS INTEGER
   LOCAL Flag6 AS INTEGER
   LOCAL Flag7 AS INTEGER
   LOCAL Flag8 AS INTEGER



   DIM m1 AS DOUBLE            'slope of the pressure calibration curve
   DIM b1 AS DOUBLE           ' y-intercept of the pressure calibration curve
   DIM m2 AS DOUBLE            'slope of the pressure calibration curve
   DIM b2 AS DOUBLE           ' y-intercept of the pressure calibration curve

   CLS

   LOCATE 4, 53
   COLOR (4)
   PRINT "  OPEN"
   LOCATE 5, 53
   COLOR (4)
   PRINT "CLOSED"
   LOCATE 6, 53
   PRINT "CLOSED"
   LOCATE 7, 53
   PRINT "CLOSED"
   LOCATE 8, 53
   PRINT "CLOSED"
```

```
LOCATE 9, 53
PRINT "CLOSED"
LOCATE 10, 53
PRINT "CLOSED"
LOCATE 11, 53
PRINT "   OFF"



'Set initial settings as all off
FLAG1 = 0
FLAG2 = 0
FLAG3 = 0
FLAG4 = 0
FLAG5 = 0
FLAG6 = 0
FLAG7 = 0
FLAG8 = 0


A$="YUB"
' **********  SETTING DISPLAY SCREEN  **********


COLOR (10)
LOCATE 1,30
PRINT "Manual Valve Control"
COLOR (7)
LOCATE 3, 13
PRINT "Toggle        Device                Position"
LOCATE 4, 13
PRINT "  F1         N2 Purge"
LOCATE 5, 13
PRINT "  F2      Oxygen Flow Valve"
LOCATE 6, 13
PRINT "  F3       Oxygen Run Valve"
LOCATE 7, 13
PRINT "  F4    Oxygen Solenoid Valve"
LOCATE 8, 13
PRINT "  F5       N2O Flow Valve"
LOCATE 9, 13
PRINT "  F6       N2O Run Valve"
LOCATE 10, 13
PRINT "  F7       He Flow Valve"
LOCATE 11, 13
PRINT "  F8       Igniter Leads"
```

```
LOCATE 20, 8
COLOR (10)
PRINT "                    Type M to main menu."

OPEN "setup.txt" FOR INPUT AS #1
   INPUT #1, skip$
   INPUT #1,skip$,m1,b1  'Head end motor pressure transducer calibration
   INPUT #1,skip$,m2,b2  'Nozzle end motor pressure transducer calibration
CLOSE #1

COLOR (9)
LOCATE 15,0
PRINT "Chamber Pressure"
COLOR (9)
LOCATE 16,0
PRINT "PT Voltage"



A$="1"   'close N2 valve when starting

DO WHILE A$ <> "M" AND A$ <> "m"


'Trap function keys so they work like numbers...
'Convert F1 to "1", F2 to "2", etc.
'In PB, function keys return "extended" 2-byte code with value in
'the 2nd (right) byte, so need to isolate that.
'Then, value for F1=59, F2=60, etc. so subtract 58, convert back to string
'and strip leading space so it matches "1", "2", etc.
IF LEN(A$)=2 THEN                          'check for extended key
   KeyVal%=ASC(RIGHT$(A$,1))                    'get value of right byte
   IF (KeyVal% >= 59) AND (KeyVal% <= 66) THEN     'check for function key
      Fkeynum% = KeyVal% - 58                  'convert to equivalent number
      A$=TRIM$(STR$(Fkeynum%))                 'change back to string
   END IF
END IF

ULStat& = cbAIn&(1, 1, BIP10VOLTS, DataValue%)
ULStat& = cbToEngUnits&(1, BIP10VOLTS, DataValue%,EngUnits!)

COLOR (9)
```

```
   LOCATE 15,30
   B$ = FORMAT$( ((EngUnits!)*m1+b1),"#.0")
   PRINT B$
   LOCATE 16,30
   C$ = FORMAT$( EngUnits!,"#.000,")
   PRINT C$

'********************** Case Statement for Relay Activation (8 relays)
SELECT CASE A$

   CASE "1"     'Select Nitrogen Valve
   IF Flag1 = 1 THEN
     Flag1 = 0
     LOCATE 4, 53
     COLOR (10)
     PRINT "  OPEN"
     BoardNum%=0
     PortName&=FIRSTPORTA
     BitNum%=3
     BitValue%=1
   ELSE
     LOCATE 4, 53
     COLOR (4)
     PRINT "CLOSED"
     Flag1 = 1
     BoardNum%=0
     PortName&=FIRSTPORTA
     BitNum%=3
     BitValue%=0
   END IF

   CASE "2"    'Select Oxygen Valve
   IF Flag2 = 1 THEN
     Flag2 = 0
     LOCATE 5, 53
     COLOR (4)
     PRINT "CLOSED"
     BoardNum%=0
     PortName&=FIRSTPORTA
     BitNum%=0
     BitValue%=1
   ELSE
     LOCATE 5, 53
     COLOR (10)
     PRINT "  OPEN"
     COLOR (7)
```

```
  Flag2 = 1
  BoardNum%=0
  PortName&=FIRSTPORTA
  BitNum%=0
  BitValue%=0
END IF

CASE "3"     'Select O2 Run Valve
IF Flag3 = 1 THEN
  Flag3 = 0
  LOCATE 6, 53
  COLOR (4)
  PRINT "CLOSED"
  BoardNum%=0
  PortName&=FIRSTPORTA
  BitNum%=1
  BitValue%=1
ELSE
  LOCATE 6, 53
  COLOR (10)
  PRINT "  OPEN"
  COLOR (7)
  Flag3 = 1
  BoardNum%=0
  PortName&=FIRSTPORTA
  BitNum%=1
  BitValue%=0
END IF

CASE "4"     'Select O2 Solenoid Valve
IF Flag4 = 1 THEN
  Flag4 = 0
  LOCATE 7, 53
  COLOR (4)
  PRINT "CLOSED"
  BoardNum%=0
  PortName&=FIRSTPORTA
  BitNum%=23
  BitValue%=1
ELSE
  LOCATE 7, 53
  COLOR (10)
  PRINT "  OPEN"
  COLOR (7)
  Flag4 = 1
  BoardNum%=0
```

```
  PortName&=FIRSTPORTA
  BitNum%=23
  BitValue%=0
END IF


CASE "5"     'Select N2O Flow Valve
IF Flag5 = 1 THEN
  Flag5 = 0
  LOCATE 8, 53
  COLOR (4)
  PRINT "CLOSED"
  BoardNum%=0
  PortName&=FIRSTPORTA
  BitNum%=5
  BitValue%=1
ELSE
  LOCATE 8, 53
  COLOR (10)
  PRINT "  OPEN"
  COLOR (7)
  Flag5 = 1
  BoardNum%=0
  PortName&=FIRSTPORTA
  BitNum%=5
  BitValue%=0
END IF

CASE "6"     'Select N2O Run Valve
IF Flag6 = 1 THEN
  Flag6 = 0
  LOCATE 9, 53
  COLOR (4)
  PRINT "CLOSED"
  BoardNum%=0
  PortName&=FIRSTPORTA
  BitNum%=4
  BitValue%=1
ELSE
  LOCATE 9, 53
  COLOR (10)
  PRINT "  OPEN"
  COLOR (7)
  Flag6 = 1
  BoardNum%=0
  PortName&=FIRSTPORTA
```

```
  BitNum%=4
  BitValue%=0
END IF

CASE "7"     'Select He Flow Valve
IF Flag7 = 1 THEN
  Flag7 = 0
  LOCATE 10, 53
  COLOR (4)
  PRINT "CLOSED"
  BoardNum%=0
  PortName&=FIRSTPORTA
  BitNum%=2
  BitValue%=1
ELSE
  LOCATE 10, 53
  COLOR (10)
  PRINT "  OPEN"
  COLOR (7)
  Flag7 = 1
  BoardNum%=0
  PortName&=FIRSTPORTA
  BitNum%=2
  BitValue%=0
END IF

CASE "8"     'Select Igniter1
IF Flag8 = 1 THEN
  Flag8 = 0
  LOCATE 11, 53
  COLOR (4)
  PRINT "   OFF"
  BoardNum%=0
  PortName&=FIRSTPORTA
  BitNum%=8
  BitValue%=1
ELSE
  LOCATE 11, 53
  COLOR (10)
  PRINT "    ON"
  COLOR (7)
  Flag8 = 1
  BoardNum%=0
  PortName&=FIRSTPORTA
  BitNum%=8
  BitValue%=0
```

```
   END IF


   END SELECT
  '***** End of Case Statement for Relay Activation

   CALL BOARDCONTROL (BoardNum%, PortName&, BitNum%, BitValue%)

   A$ = INKEY$        'get any keypress
   SLEEP 0            'recommended in PB/CC manual to release CPU temporarily

   LOOP

   IF A$ = "M" OR A$ = "m" THEN       'If M is pressed return to main menu and activate initial
config
      CALL MAINMENU()
      CALL INITIALCONFIG ()
      EXIT SUB
   END IF


END SUB



'-------------------------------------------------------------------------------------------
'-------------------------------------------------------------------------------------------

SUB EVENTSELECT(A$, EVENTVAL AS STRING, BoardNum AS INTEGER, PortName AS
LONG, BitNum AS INTEGER, BitValue AS INTEGER)


   'A space is inserted before the number because the operation STR$() converts an integer to a
string, and inserts a space
    SELECT CASE A$
       CASE " 0"
          'This case is a place holder so that the event times have a point of reference for the test
start
      CASE " 6"
         EVENTVAL="Energize Igniter 1 Leads               "
         BoardNum=0
         PortName=FIRSTPORTA
         BitNum=8
         BitValue=0
      CASE " 7"
         EVENTVAL="De-energize Igniter 1 Leads            "
```

```
   BoardNum=0
   PortName=FIRSTPORTA
   BitNum=8
   BitValue=1
CASE " 15"
   EVENTVAL="Open N2 Purge Valve                "
   BoardNum=0
   PortName=FIRSTPORTA
   BitNum=3
   BitValue=1
CASE " 16"
   EVENTVAL="Close N2 Purge Valve               "
   BoardNum=0
   PortName=FIRSTPORTA
   BitNum=3
   BitValue=0
CASE " 5"
   EVENTVAL="Open O2 Flow Valve                 "
   BoardNum=0
   PortName=FIRSTPORTA
   BitNum=0
   BitValue=0
CASE " 11"
   EVENTVAL="Close O2 Flow Valve                "
   BoardNum=0
   PortName=FIRSTPORTA
   BitNum=0
   BitValue=1
CASE " 4"
   EVENTVAL="Open O2 Run Valve                  "
   BoardNum=0
   PortName=FIRSTPORTA
   BitNum=1
   BitValue=0
CASE " 10"
   EVENTVAL="Close O2 Run Valve                 "
   BoardNum=0
   PortName=FIRSTPORTA
   BitNum=1
   BitValue=1
CASE " 1"
   EVENTVAL="Open N2O Flow Valve                  "
   BoardNum=0
   PortName=FIRSTPORTA
   BitNum=5
   BitValue=0
```

```
CASE " 14"
   EVENTVAL="Close N2O Flow Valve                "
   BoardNum=0
   PortName=FIRSTPORTA
   BitNum=5
   BitValue=1
CASE " 2"
   EVENTVAL="Open He Flow Valve                  "
   BoardNum=0
   PortName=FIRSTPORTA
   BitNum=2
   BitValue=0
CASE " 13"
   EVENTVAL="Close He Flow Valve                 "
   BoardNum=0
   PortName=FIRSTPORTA
   BitNum=2
   BitValue=1
CASE " 3"
   EVENTVAL="Open O2 Solenoid Valve              "
   BoardNum=0
   PortName=FIRSTPORTA
   BitNum=23
   BitValue=0
CASE " 9"
   EVENTVAL="Close O2 Solenoid Valve             "
   BoardNum=0
   PortName=FIRSTPORTA
   BitNum=23
   BitValue=1
CASE " 8"
   EVENTVAL="Open N2O Run Valve                  "
   BoardNum=0
   PortName=FIRSTPORTA
   BitNum=4
   BitValue=0
CASE " 12"
   EVENTVAL="Close N2O Run Valve                 "
   BoardNum=0
   PortName=FIRSTPORTA
   BitNum=4
   BitValue=1
```

```
    END SELECT


END SUB

'-------------------------------------------------------------------------------------------
'-------------------------------------------------------------------------------------------


SUB TIMEDCONTROL ()

   DIM ENUM AS INTEGER
   ENUM = 16   'Number of events involved in test.
            'See sub EVENTSELECT for list of events.
            'If an event is added, then ENUM should be changed, the sub EVENTSELECT
            '  should be updated and the sub INITIALCONFIG should be updated.

   DIM SEQUENCE(0 TO ENUM) AS INTEGER
   DIM BOARDNUMA(1 TO ENUM) AS INTEGER
   DIM PORTNAMEA(1 TO ENUM) AS LONG
   DIM BITNUMA(1 TO ENUM) AS INTEGER
   DIM BITVALUEA(1 TO ENUM) AS INTEGER
   DIM EVENT(1 TO ENUM)AS STRING
   DIM ETIME(0 TO ENUM) AS DOUBLE
   DIM EORDER&(1 TO ENUM)
   DIM EventTime AS STRING
   DIM EVENTVAL AS STRING
   DIM BoardNum AS INTEGER
   DIM PortName AS LONG
   DIM BitNum AS INTEGER
   DIM BitValue AS INTEGER
   DIM I AS INTEGER
   DIM J AS INTEGER
   DIM LOAD AS STRING
   DIM oldtime AS DOUBLE
   DIM time(0 TO ENUM) AS DOUBLE
   DIM TEST#(1 TO ENUM)  'Use for debuging timeing problems
   DIM ScramNumber AS INTEGER    'this is the maximum number of times the pressure is
exceeded before the test is stopped
   DIM m1 AS DOUBLE             'slope of the pressure calibration curve
   DIM b1 AS DOUBLE             ' y-intercept of the pressure calibration curve
   DIM m2 AS DOUBLE             'slope of the pressure calibration curve
   DIM b2 AS DOUBLE             ' y-intercept of the pressure calibration curve
   DIM Voltagecrit(0 TO 1) AS DOUBLE
   DIM Pressurecrit(0) AS DOUBLE
```

```
   DIM scramcheck AS INTEGER
   DIM whyscram AS INTEGER

   CALL INITIALCONFIG()
    'Set timed events to a maximum time for sorting purposes
   FOR I = 1 TO ENUM
     ETIME(I) = 99999
   NEXT I

   'Set reference start time.  This also allows the program time to catch up and start all its threads
when
   'the test is actually begun.
   ETIME(0)=-1
   'Sequence is sorted with respect to ETIME so both arrays must have the same size.
Sequence(0) is a placeholder
   SEQUENCE(0)=0

   'Creates an array that will have values from 0 to 14 and will be sorted later to match increasing
event times.
   'Sequence(0) will always be the first event, and will be only a reference time.  No action will
be taken.
   FOR I=1 TO ENUM
      SEQUENCE(I) = I
   NEXT I

   CLS
   COLOR (7)
   PRINT : PRINT : PRINT
   PRINT "               COMPUTER ACTUATION SEQUENCING CONTROL SCREEN"
   PRINT "               ----------------------------------------"
   PRINT
   PRINT "       NOTE:  The event time accuracies are only within 50 milliseconds"
   PRINT
   PRINT
   PRINT
   INPUT LINE "   Press <L> to load times or <ENTER> to input actuation times (Q to quit):
";LOAD

      PRINT : PRINT




   'Load saved times
   'NOTE:  The file to be loaded must have a comma between each value to be read and a return
after each line
```

```
'including the last line.  Ensure that the cursor can go to the line below the last line of text.
'Skip$ is used to read the event as a dummy variable
IF LOAD = "Q" OR LOAD = "q" THEN
   CALL INITIALCONFIG
   FOR I = 1 TO ENUM
      ETIME(I) = 99999
   NEXT I
   COLOR 7
   CALL MAINMENU
   EXIT SUB
END IF


IF LOAD = "L" OR LOAD = "l" THEN
   CLS
   PRINT:PRINT
   PRINT      "  Type the name of the file to be loaded, including suffix,"
   PRINT:PRINT
   LINE INPUT "  or <ENTER> to load last run times: ";filename1$
   IF filename1$="" THEN
      filename1$="outputtimes.txt"
   END IF
   OPEN filename1$ FOR INPUT AS #1
   FOR I = 1 TO ENUM
      INPUT #1, skip$,ETIME(I)
   NEXT I
   CLOSE #1

'load times with manual control
ELSE
   CLS
   PRINT:PRINT
   PRINT "           Input times will be saved to outputtimes.txt"
   PRINT:PRINT
   PRINT "             Enter actuation times for the following: "
   PRINT:PRINT

  'Input Event Times manually
   FOR I = 1 TO ENUM
       A$=STR$(SEQUENCE(I))  'pick the case in EVENTSELECT to use
       CALL EVENTSELECT(A$, EVENTVAL, BoardNum, PortName, BitNum, BitValue)
'pass the values for each event
       PRINT "                 "; EVENTVAL;  'display the event currently to have a time entered
       LINE INPUT  EventTime                'enter the time for this event
       ETIME(I)= VAL(EventTime)               'change the input to a number
       EVENT(I) = EVENTVAL                    'store the event name to an array
```

```
      NEXT I

   END IF 'end loop for time file loading

   'save the manually input times to a file for later use by user
   OPEN "outputtimes.txt" FOR OUTPUT AS #1
   FOR I = 1 TO ENUM
      WRITE #1, EVENT(I), ETIME(I)
   NEXT I
   WRITE #1, TIME$
   WRITE #1, DATE$
   CLOSE #1

   CLS

  'Check events end after they are started, otherwise the error message is printed.
  'See Sub Eventselect to find what each ETIME corresponds to.
  'Also makes sure that there is oxidizer flow when ignigers are set off and
  'that purge starts after other valves are closed.

'   IF ETIME(1)>ETIME(7)OR ETIME(2)>ETIME(8) OR ETIME(3)>ETIME(4) OR
ETIME(9)>ETIME(10) OR ETIME(1)>ETIME(3) OR ETIME(2)>ETIME(3) OR
ETIME(4)>ETIME(9) OR ETIME(7)>ETIME(9) OR ETIME(8)>ETIME(9) OR
ETIME(5)>ETIME(6) THEN
'     PRINT:PRINT:PRINT:PRINT:PRINT
'     PRINT      "                          IMPORTANT!!!"
'     PRINT:PRINT:PRINT
'     INPUT LINE "          Possible Timing Error. Check on next screen. <ENTER>";check$
'   END IF


  'Sort Event Times and Sequencing case
   ARRAY SORT ETIME(), TAGARRAY SEQUENCE(), ASCEND

   'Set up timed events, bit values, and bit locations in order of activation
   FOR I=1 TO ENUM
      A$=STR$(SEQUENCE(I))
      'Call a a case select to creat arrays in the order of activation
      CALL EVENTSELECT(A$, EVENTVAL, BoardNum, PortName, BitNum, BitValue)
         EVENT(I) = EVENTVAL
         BOARDNUMA(I)=BoardNum
         PORTNAMEA(I)=PortName
         BITNUMA(I)=BitNum
         BITVALUEA(I)=BitValue
   NEXT I
```

```
   'Dispaly the sorted time
    CLS
    PRINT "              Events and times have been sorted as follows:"
    PRINT

    FOR I = 1 TO ENUM
       PRINT "                 "; EVENT(I); ETIME(I)
    NEXT I

    'Verify that the user wants to accepts all input values

    PRINT
    ANS$="Z"
    INPUT LINE "                  Is everything acceptable [Y/N] " ; ANS$

    'User check of times.  If Y then continue, if N then exit to main menu.  This ensures that the
program does
    'not get stuck in a loop inside of a loop inside of a loop, etc.


    IF ANS$ = "Y" THEN
       ELSE
       FOR I = 1 TO ENUM
          ETIME(I) = 99999
          NEXT I
          CALL MAINMENU
          EXIT SUB
    END IF


    'CLEAR SCREEN AND DISPLAY SEQUENCED DATA
    CLS
    PRINT "          Operation Sequence ARMED and Ready to Initiate"
    PRINT "          ---------------------------------------------"
    FOR I = 1 TO ENUM
       PRINT "                 "; EVENT(I); ETIME(I)
    NEXT I
   PRINT ""

    COLOR 29
    INPUT LINE"       ..... Hit <ENTER> to activate ignition sequence (Q to quit) ..... ";
LAUNCH$
    COLOR 7

    IF LAUNCH$ = "Q" OR LAUNCH$ = "q" THEN
```

```
      CALL INITIALCONFIG
      FOR I = 1 TO ENUM
         ETIME(I) = 99999
      NEXT I
      COLOR 7
      CALL MAINMENU
      EXIT SUB
   END IF

   LOCATE 16, 5
   COLOR (31)
   PRINT "              ... SYSTEM HAS BEEN ACTIVATED ...            "

   'give countdown
   SLEEP 1000
   FOR I = 3 TO 1 STEP -1
      BEEP '1000, 2        'SOUND not supported in PB/CC--use WinAPI call
      COLOR 11
      LOCATE 20 - I, 28: PRINT I; " SECOND(S)"
      SLEEP 1000         'stop for one second
   NEXT I


   ScramNumber=5   'This is the max number of data points allowed before the computer will
scram


  'Input the pressure transducer values and critical pressure values from the setup file

   OPEN "setup.txt" FOR INPUT AS #1
      INPUT #1, skip$
      INPUT #1,skip$,m1,b1  'Head end motor pressure transducer calibration
      INPUT #1,skip$,m2,b2  'Nozzle end motor pressure transducer calibration
      INPUT #1,skip$,Pressurecrit(0)
      INPUT #1,skip$,scramcheck
   CLOSE #1

   J=0

   Voltagecrit(0)=(Pressurecrit(0)-b1)/m1    'voltage that is the max allowed for the head end
chamber PT
   Voltagecrit(1)=(Pressurecrit(0)-b2)/m2    'voltage that is the max allowed for the aft end
chamber PT
   oldtime=GetTickCount()
```

```
   FOR I=1 TO ENUM
     time(I)=(ETIME(I))*1000+oldtime
   NEXT I

   LOCATE 20,0
   PRINT "PT Voltage" SPC(2) "Max Volt" SPC (3) "Counter"



   FOR I = 1 TO ENUM

      'keeps the program from moving on until the next event needs to start

      DO WHILE GetTickCount()<(time(I))  'temporarily stops program until the next event is
due to happen

         currenttime&=(GetTickCount()-oldtime)/1000
         LOCATE 1,0
         PRINT currenttime&                    'used to debug timing issues.  should not be used in
actual use to keep system fast
         LOCATE 2,0
         PRINT scramcheck


           'This checks the presure of one of the pressure transducers in the chamber
              'input the value from the I/O board
             ULStat& = cbAIn&(1, 0, BIP10VOLTS, DataValue%)
             ULStat& = cbToEngUnits&(1, BIP10VOLTS, DataValue%,EngUnits!)
              LOCATE 21,0
              PRINT EngUnits! SPC(5) Voltagecrit(0) SPC (5) J
              IF ULStat& <> 0 THEN EXIT SUB
                'If the pressure goes above the max value, then increment the number of bad points
              IF EngUnits! > Voltagecrit(0) THEN    'If the current voltage (pressure) is too high,
increment J
                 J=J+1
              ELSE
                 J=0   'if the pressure goes low again, reset the number of bad points
              END IF
               'If the pressure has been high for ScramNumber number of data points then
               'the test is stopped
              IF J=ScramNumber THEN    'If J gets to a preset number, consider the test failed
and go to scram
                   'This turns on and off the exit to scram conditions
                IF scramcheck=1 THEN
                   whyscram=1
                   CALL SCRAM(whyscram)
```

```
                    CALL INITIALCONFIG ()
                    EXIT SUB
                  END IF
                END IF

            'This checks the presure of the second pressure transducers in the chamber
                'input the value from the I/O board
               ULStat& = cbAIn&(1, 1, BIP10VOLTS, DataValue%)
               ULStat& = cbToEngUnits&(1, BIP10VOLTS, DataValue%,EngUnits!)
                LOCATE 22,0
                PRINT EngUnits! SPC(5) Voltagecrit(1) SPC (5) J
                IF ULStat& <> 0 THEN EXIT SUB
                 'If the pressure goes above the max value, then increment the number of bad points
                IF EngUnits! > Voltagecrit(1) THEN    'If the current voltage (pressure) is too high,
increment J
                   J=J+1
                ELSE
                   J=0   'if the pressure goes low again, reset the number of bad points
                END IF
                 'If the pressure has been high for ScramNumber number of data points then
                 'the test is stopped
                IF J=ScramNumber THEN    'If J gets to a preset number, consider the test failed
and go to scram
                     'This turns on and off the exit to scram conditions
                   IF scramcheck=1 THEN
                      whyscram=1
                      CALL SCRAM(whyscram)
                      CALL INITIALCONFIG ()
                      EXIT SUB
                   END IF
                END IF

          SLEEP 0    'This is recommended to temporarily release control of the computer

       LOOP

       CALL BOARDCONTROL (BOARDNUMA(I), PORTNAMEA(I), BITNUMA(I),
BITVALUEA(I))  'activate relay
       TEST#(I)=GetTickCount 'DEBUG TIMING ISSUES

       CALL EVENTDISPLAY(I)       'Use for debugging only.  This slows the system down

    NEXT I


   'DEBUG TIMING ISSUES
```

```
   SLEEP 4000
   CLS
   LOCATE 1,0
   PRINT "Precall time"
   LOCATE 1,15
   PRINT "Postcall time"
   LOCATE 1,30
   PRINT "Time Delay (ms)"
   LOCATE 1, 45

   FOR I=1 TO ENUM
      LOCATE I+2,0
      PRINT time(I)
      LOCATE I+2,15
      PRINT TEST#(I)
      LOCATE I+2, 30
      PRINT test#(I)-time(I)
   NEXT I

   LOCATE 22, 15
   COLOR 7
   INPUT LINE "....Hit <ENTER> to return to main menu...."; LAUNCH$
   LOCATE 26, 24
   COLOR 14
   CALL INITIALCONFIG
   FOR I = 1 TO ENUM
      ETIME(I) = 99999
   NEXT I
   COLOR 7
   CALL MAINMENU


END SUB


'-------------------------------------------------------------------------------------------
'-------------------------------------------------------------------------------------------

FUNCTION EVENTDISPLAY(BYVAL I AS LONG) AS LONG
'This function displays an X next to the event as it occurs during the computer controlled timing
events

COLOR (14)
LOCATE 1 * I + 2, 14: PRINT "X"; ""
LOCATE 1 + I, 1
```

```
END FUNCTION


'-------------------------------------------------------------------------------------------
'-------------------------------------------------------------------------------------------


SUB SCRAM (whyscram AS INTEGER)
   DIM BoardNum AS INTEGER
   DIM PortName AS LONG
   DIM BitNum AS INTEGER
   DIM BitValue AS INTEGER
   DIM whyscram1 AS STRING
   DIM I AS INTEGER

'Take the reason that the scram function was called and print out that corresponding reason
   IF whyscram=1 THEN whyscram1="Maximum chamber pressure exceeded."

   CLS
   PRINT
   PRINT
   PRINT
   PRINT
   PRINT
   PRINT
   PRINT
   PRINT
   PRINT
   PRINT SPC(35) "SCRAM!!!!!"
   PRINT
   PRINT
   PRINT
   PRINT, "Cause of Scram Condition:   " whyscram1
   PRINT
   PRINT
   PRINT
   PRINT, "Press <ENTER> to Reset System"

  'set all valves to "off" position for scram condition
  BitValue=0
  BoardNum=0
  FOR I=0 TO 23
      PortName=FIRSTPORTA
      BitNum=I
      CALL BOARDCONTROL (BoardNum, PortName, BitNum, BitValue)
  NEXT I
```

```
   INPUT LINE z$
   CALL MAINMENU()
END SUB

'-------------------------------------------------------------------------------------------
'-------------------------------------------------------------------------------------------


SUB OPTIONS()

   DIM PTtitle AS STRING
   DIM pt(1 TO 2) AS STRING
   DIM m(1 TO 2) AS DOUBLE
   DIM b(1 TO 2) AS DOUBLE
   DIM pcrittitle AS STRING
   DIM pcrit(1) AS STRING
   DIM Pressurecrit(1) AS DOUBLE
   DIM I AS INTEGER
   DIM J AS INTEGER
   DIM choice1 AS STRING
   DIM mtemp AS STRING
   DIM btemp AS STRING
   DIM scramcheck2 AS STRING
   DIM scramcheck1 AS STRING
   DIM scramcheck AS INTEGER
   DIM Pressurecrittemp AS STRING

   DIM timecheck(1) AS STRING
   DIM timecheckval (1) AS DOUBLE
   DIM timechecktemp AS STRING

     CURSOR OFF
   choice1="kick your nuts"

   DO WHILE choice1<>"Q"

   CLS

      PTtitle="Test Condition Calibration and Setup"
      pt(1)="Head-End Chamber Pressure Transducer"
      pt(2)="Nozzle-End Chamber Pressure Transducer"

      pcrit(1)="Chamber critical pressure"

      scramcheck1="Computer stops the test if errors are detected"
```

```
   OPEN "setup.txt" FOR INPUT AS #1
      INPUT #1, skip$
      FOR J=1 TO 2
         INPUT #1,skip$,m(J),b(J)
      NEXT J
      INPUT #1,skip$,Pressurecrit(1)
      INPUT #1,skip$,scramcheck
   CLOSE #1

   IF scramcheck=1 THEN scramcheck2="Y"
   IF scramcheck=0 THEN scramcheck2="N"

     PRINT SPC(15)PTtitle
     PRINT
     PRINT
     PRINT SPC(12) "Pressure Transducer                    Slope      Intercept"
     FOR J=1 TO 2
        PRINT SPC(4) J SPC(5) pt(J),m(J),b(J)
     NEXT J
     PRINT
     PRINT
     PRINT
     PRINT SPC(12) "Check for Overpressurization
     PRINT SPC(5) "A" SPC(6) pcrit(1) SPC(19) Pressurecrit(1)
     PRINT
     PRINT SPC(5) "S" SPC(6) scramcheck1 SPC(1) scramcheck2
     PRINT
     PRINT SPC(5) "Q" SPC(6) "Quit"
     PRINT
     PRINT

  INPUT LINE "     To change a value, press the corresponding number (letter): ";choice1

IF choice1="1" OR choice1="2" THEN
   I=VAL(choice1)
   INPUT LINE "     Enter new slope: " mtemp
   m(I)=VAL(mtemp)
   INPUT LINE "     Enter new offset: " btemp
   b(I)=VAL(btemp)
END IF

IF choice1="A" THEN
   INPUT LINE "     Enter new critical pressure: " Pressurecrittemp
   Pressurecrit(1)=VAL(Pressurecrittemp)
END IF
```

```
   IF choice1="B" THEN
      INPUT LINE "     Enter new check time value: " timechecktemp
      timecheckval(1)=VAL(timechecktemp)
   END IF

   IF choice1="S" AND scramcheck=0 THEN
      scramcheck=1         'use automatic computer scram checking
      ELSE
      IF choice1="S" AND scramcheck=1 THEN
      scramcheck=0         'do not use automatic computer scram checking
      END IF
   END IF

   OPEN "setup.txt" FOR OUTPUT AS #2
      WRITE #2, PTtitle
      FOR J=1 TO 2
         WRITE #2,pt(J),m(J),b(J)
      NEXT J
      WRITE #2,pcrit(1),Pressurecrit(1)
      WRITE #2,scramcheck1,scramcheck
   CLOSE #2


   LOOP
   CALL MAINMENU()

END SUB


'-------------------------------------------------------------------------------------------
'-------------------------------------------------------------------------------------------
```

APPENDIX Q Example Output Timing

```
"Open N2O Flow Valve                ",4
"Open He Flow Valve                ",1
"Open O2 Solenoid Valve             ",0
"Open O2 Run Valve                 ",1.1
"Open O2 Flow Valve                ",1.2
"Energize Igniter 1 Leads          ",6.4
"De-energize Igniter 1 Leads        ",6.7
"Open N2O Run Valve                 ",6.3
"Close O2 Solenoid Valve            ",.1
"Close O2 Run Valve                ",6.61
"Close O2 Flow Valve               ",6.6
"Close N2O Run Valve                ",13.6
"Close He Flow Valve               ",13.61
"Close N2O Flow Valve               ",13.62
"Open N2 Purge Valve               ",13.4
"Close N2 Purge Valve              ",50
"17:38:24"
"12-16-2014"
```

APPENDIX R Nitrous Oxide Mass Flow Rate Calibration Attempts

The use of a 0.035” converging/diverging orifice for control of the oxidizer mass flow rate resulted in many problems. Characterizing the mass flow rate of nitrous oxide through the orifice for the LGCP hybrid rocket motor test series proved to be extremely difficult. A large number of steps were taken to address the problems that were observed and resulted in the final method discussed in the body of this thesis. The following sections will describe each calibration method, the problems that were discovered, and how they were to be addressed. The methods are described in the order that they were attempted to show the thought process and iterations used to arrive at the final method.

R.1 Initial Calibration Method

R.1.1 Setup

- Large nitrous oxide run tank with loosened green plastic support clamps
- 500 lb compression load cell between tank cap and support plate (slightly off center due to tubing connections at the bottom of the tank)
- Orifice vented to atmosphere

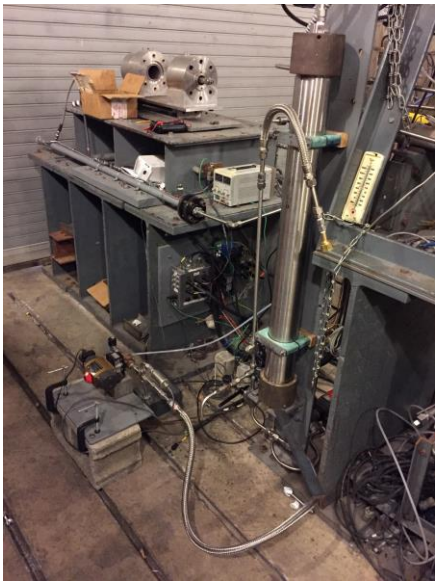

R.1.2 Procedure

- Calibrate load cell before and after each flow test
- 60 second flow test at 800 psig, 1000 psig, and 1200 psig
- Measure change in tank mass
- Use change in tank mass and flow duration to find mass flow rate

R.1.3 Results

- Inconsistent mass flow rate results
- Further calibration tests of the load cell found inconsistency depending on how the tank was resting on the button of the load cell
    - Potential for side loading

R.1.4 Adjustments for Next Attempt

- Replace green plastic clamps with a loose chain (decrease sliding friction)
- Place load cell directly under cross fitting at the bottom of the tank to center the weight on the load cell button

R.2 Second Calibration Method

R.2.1 Setup

- Large nitrous oxide run tank with chain lightly wrapped around
- 500 lb compression load cell between cross fitting at the bottom of the run tank and an I-beam underneath the support plate
- Orifice vented to atmosphere

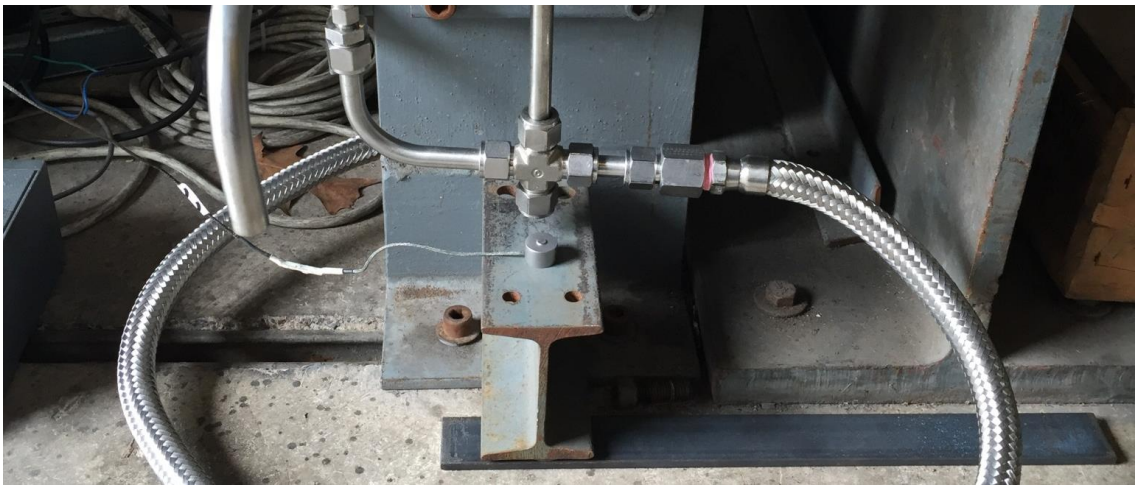

R.2.2 Procedure

- Calibrate load cell before and after each flow test
- 60 second flow test at 800 psig, 1000 psig, and 1200 psig
- Measure change in tank mass
- Use change in tank mass and flow duration to find mass flow rate

R.2.3 Results

- Self-consistent mass flow rate results, but significantly higher values than initial method
- Further testing and comparisons with the initial method revealed strong sensitivity to temperature (lower temperature nitrous oxide results in higher mass flow rate)

R.2.4 Adjustments for Next Attempt

- Attempt to temperature control the nitrous oxide with copper coil around the run tank
- Add a thermocouple prior to the orifice

R.3 Third Calibration Method

R.3.1 Setup

- Large nitrous oxide run tank with chain lightly wrapped around
- 500 lb compression load cell between cross fitting at the bottom of the run tank and an I-beam underneath the support plate
- Orifice vented to atmosphere
- Copper coil wrapped around the run tank with insulation and duct tape around the outside
- Run hot/cold water through tubing to temperature condition the nitrous oxide
- Added a thermocouple prior to the orifice

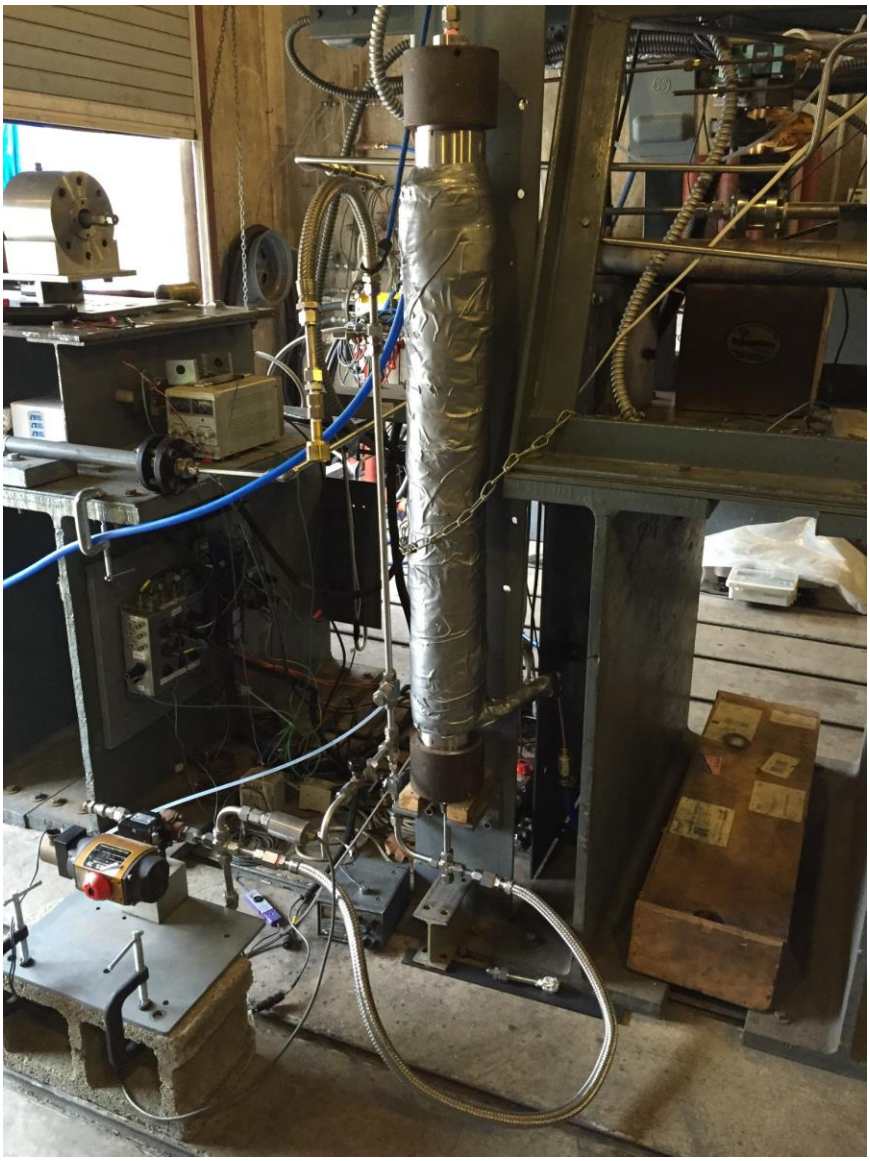

R.3.2 Procedure

- Set tank temperature by adjusting hot/cold tubing
- Calibrate load cell before and after each flow test
- 60 second flow test at 800 psig, 1000 psig, and 1200 psig
- Measure change in tank mass
- Use change in tank mass and flow duration to find mass flow rate

R.3.3 Results

- Difficulty establishing a constant nitrous oxide temperature during the long duration flow
- Changing temperature will result in changing instantaneous mass flow rates

R.3.4 Adjustments for Next Attempt

- Setup as if going to run an actual motor firing
- Add a pressure transducer and thermocouple prior to injector plate
- Add needle valve to the nozzle assembly to maintain chamber pressure

R.4 Fourth Calibration Method

R.4.1 Setup

- Large nitrous oxide run tank with chain lightly wrapped around
- 500 lb compression load cell between cross fitting at the bottom of the run tank and an I-beam underneath the support plate
- Copper coil wrapped around the run tank with insulation and duct tape around the outside
- Run hot/cold water through tubing to temperature condition the nitrous oxide
- Added a pressure transducer and thermocouple prior to injector plate
- Added a needle valve to nozzle assembly to maintain chamber pressure

R.4.2 Procedure

- Set tank temperature by adjusting hot/cold water flow rates through the coil
- Calibrated load cell before and after each flow test
- 60 second flow test at 800 psig, 1000 psig, and 1200 psig
- Measure change in tank mass
- Use change in tank mass and flow duration to find mass flow rate
- Adjust needle valve to maintain 200 psig in the chamber

R.4.3 Results

- Needle valve helps with consistency in the mass flow rate measurement
- Temperature control still unsteady

R.4.4 Adjustments for Next Attempt

- Setup a small run tank (< 50 lb) on vertical guide rails with PTFE-lined sleeve bearing carriages

R.5 Fifth Calibration Method

R.5.1 Setup

- Small nitrous oxide run tank on sliding platform with guide rails and PTFE-lined sleeve bearing carriages
- 50 lb compression load cell between sliding platform and stationary block
- Continue using needle valve

R.5.2 Procedure

- Calibrated load cell before and after each flow test
- 15 second flow test at 800 psig, 1000 psig, and 1200 psig
- Measure change in tank mass
- Use change in tank mass and flow duration to find mass flow rate

R.5.3 Results

- Inconsistency with baseline load cell reading

R.5.4 Adjustments for Next Attempt

- Use ball bearing slider for next test

R.6 Sixth Calibration Method

R.6.1 Setup

- Small nitrous oxide run tank on a sliding platform with ball bearing sliders
- 50 lb compression load cell between sliding platform and stationary block
- Continue using needle valve

R.6.2 Procedure

- Calibrated load cell before and after each flow test
- 15 second flow test at 800 psig, 1000 psig, and 1200 psig
- Measure change in tank mass
- Use change in tank mass and flow duration to find mass flow rate

R.6.3 Results

- Inconsistency in baseline load cell reading

R.6.4 Adjustments for Next Attempt

- Suspend run tank

R.7 Seventh Calibration Method

R.7.1 Setup

- Small nitrous oxide run tank suspended from tension quartz force sensor
- Continue using needle valve

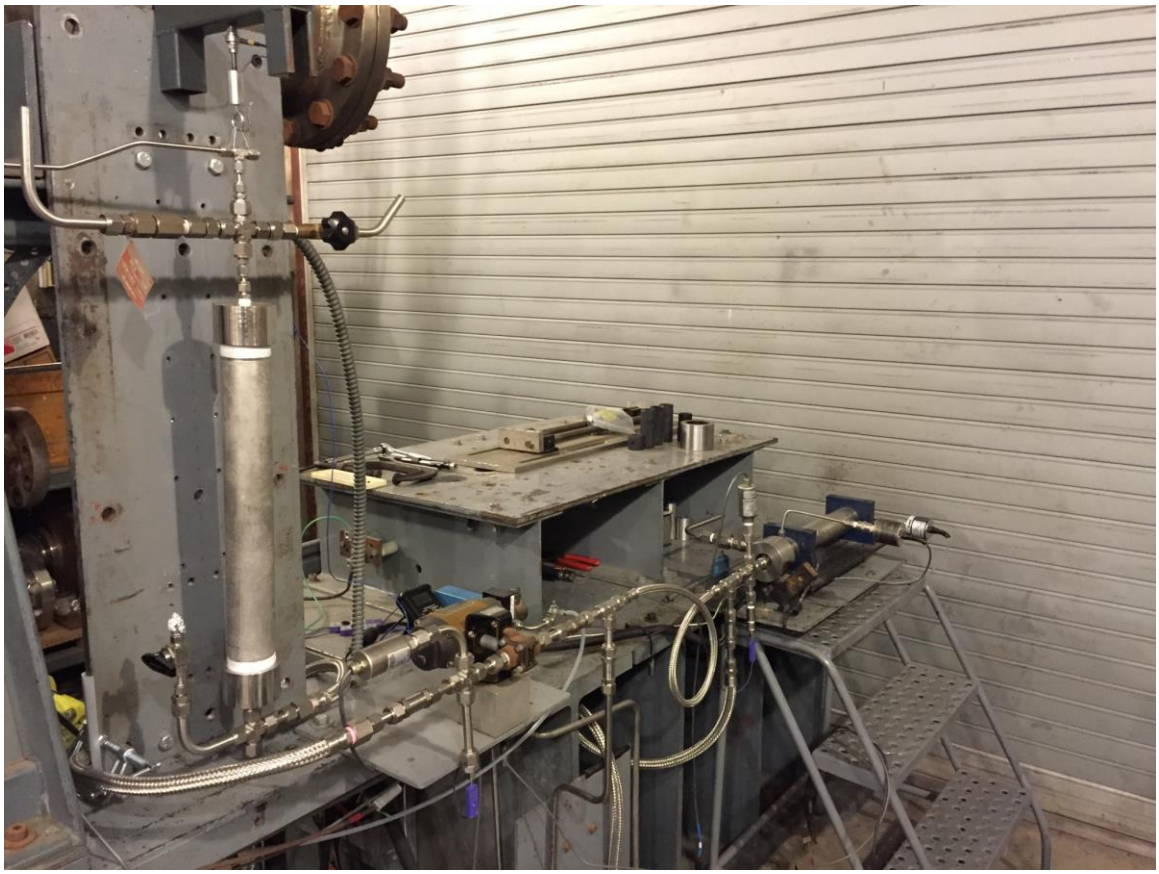

R.7.2 Procedure

- Calibrated load cell before and after each flow test
- 10 second flow test at 800 psig, 1000 psig, and 1200 psig
- Measure change in tank mass
- Use change in tank mass and flow duration to find mass flow rate

R.7.3 Results

- Consistent readings for a given temperature
- All tests must be run at a known temperature and the orifice must be calibrated using the above procedure at that temperature
- Variation from the calibrated temperature will cause error in the mass flow rate value
- If the temperature changes by more than a couple degrees Celsius, recalibrate at that temperature for that test condition